Biodegradable Microspheres for Controlled Drug/Cell Delivery and Tissue Engineering

A DISSERTATION SUBMITTED TO

THE UNIVERSITY OF OXFORD

FOR THE DEGREE OF

DOCTOR OF PHILOSOPHY

BY

HAO ZHANG B.Sc and B.A

ST HUGH'S COLLEGE

HILARY TERM 2012

DEPARTMENT OF MATERIALS

Abstract

Biodegradable Microspheres for Controlled Drug/Cell Delivery and Tissue Engineering

D.Phil Thesis — Hao Zhang

Hilary Term 2012 — St Hugh's College

The synthetic biodegradable polymer poly(lactide-co-glycolide) (PLGA) has been widely explored as substrate biomaterials for controlled drug delivery and tissue engineering. ECM component heparin and bone mineral hydroxyapatite (HA) are attractive biomaterials which can functionalize the PLGA surface to improve cell cell response and to bring in the dual growth factor delivery, because heparin and HA both can improve cell responses and bind with various proteins.

To combine the osteoconductivity of HA and the controlled drug release of PLGA microspheres, HA coated PLGA microspheres were developed by a 3 hour rapid HA precipitation on the PLGA microsphere surface. Effects of various fabrication parameters on microsphere and HA coating morphology were evaluated. This core-shell composite worked as a dual drug delivery device and demonstrated better cell cell response than PLGA microspheres without HA coating.

Three different methods, including osmogen, extractable porogen and gas-foaming porogen, were evaluated to fabricate porous microspheres as injectable cell scaffolds in the tissue engineering. The gas-foaming method produced covered porous PLGA microspheres, on which a skin layer covered all the surface pores. The skin layer was hydrolysed by NaOH to control the surface porosity. The modified open porous microspheres have large continued surface areas between pores, which provided more continued areas for cell adhesion. The porous microspheres with controllable surface porosity and large surface continuity between pores could be novel injectable cell scaffolds.

Heparin was immobilized on the open porous PLGA microspheres by a facile layer-by-layer assemble to combine the advantages of porous structure and the protein binding from heparin. The heparin-coated porous microspheres promoted cell adhesion, spreading, proliferation and osteogenic differentiation. Growth factor-like protein lactoferrin was immobilized on the heparin coated porous microspheres, which further enhanced MG-63 proliferation and osteogenic differentiation. The heparin-coated porous microspheres are promising multi-functional devices for controlled drug delivery and injectable cell delivery.

Preface

The work presented in this thesis was conducted by the author in the Department of Materials and Nuffield Department of Orthopaedics, Rheumatology and Musculoskeletal Sciences, University of Oxford between October 2007 and June 2011 supervised by Dr. Jan T Czernuszka, Dr. Zhidao Xia, and Dr. Sarah Franklin. No part of this thesis has been submitted or accepted for any other degree at this university or elsewhere.

Various parts of this work are in preparation for patents and publications, and have been presented at conferences as follows:

1. H Zhang, S Franklin, Z Xia, J Czernuszka. Hydroxyapatite coated PLGA microspheres for dual drug delivery and their cell cell response (manuscript in preparation)

2. H Zhang, S Franklin, Z Xia, J Czernuszka. Comparisons of osmogen, extractable porogen and gas-foaming methods to fabricate porous microspheres (manuscript in preparation)

3. H Zhang, S Franklin, Z Xia, J Czernuszka. Heparin coated porous microspheres as growth factor delivery devices and injectable cell scaffolds (manuscript in preparation)

4. H Zhang, S Franklin, Z Xia, J Czernuszka. Heparin coated porous microspheres for controlled drug and cell delivery. GRIBOI 2011 The 21st Interdisciplinary Research Conference on Injectable Osteoarticular Biomaterials and Bone Augmentation Procedures (Boston, USA 2011) (oral presentation)

5. H Zhang, Z Xia, J Czernuszka Cell response of hydroxyapatite coated PLGA microspheres 2nd Marie Curie Cutting Edge Practical Training Course (Aachen, Germany 2009

Acknowledge

I sincerely acknowledge the following support which helped me overcome many challenges during my overseas study and made my life enjoyable in Oxford.

My supervisor, Dr Jan Czernuszka, for his wisdom, guidance, patience and support throughout my DPhil study.

My supervisor, Dr. Zhidao Xia, for his guidance and advices in the design of cell work and the patent application.

My supervisor, Dr. Sarah Franklin, for her kind support in the final cell experiment and great help in the thesis corrections.

St Hugh's College (2008 Wei Lun Scholarship), China Oxford Scholarship Fund (2008 Honorary Award), Oxford University (2009 Overseas Research Scholarship) are acknowledged for the funding support.

Prof. Dr. Roland Bodmeier of Freie Universität Berlin is appreciated for the approval of research collaboration and German Academic Exchange Service (2009 DAAD visiting Scholarship) is acknowledged for funding the collaboration at Freie Universität Berlin in 2008-2009.

All members in the Oxford Biomaterials groups are appreciated for their useful discussions and help: Qingguo, Grame, Robin, Gary, Asma, Jenni, Zamri, Qi, Xuan and et al. The Polymer group members Matthew and Vincent are also thanked for the help and discussions.

I would like to thank all my friends Jun, Meng, Susan, Fenny in Oxford and elsewhere for their support and encouragements.

Finally, I would like to thank my family, my Mum Qin Zhang and Dad Xiancheng Zhang, my grandmother Yuxiu Jin for their unconditional love, encouragements, and support throughout my 4 year study in Oxford. My girlfriend, Tiantian Jia, is also thanked for her love, support and help.

Thank you all for helping me to fulfill my dream!

Contents

Abbreviation and glossary of terms

ACP	amorphous calcium phosphate
AL	alendronate
α-MEM	α minimal essential medium
ANOVA	analysis of variance
ALP	alkaline phosphatase
α-TCP	α -tricalcium phosphate
ATR-IR	attenuated total reflection infrared spectroscopy
bFGF	basic fibroblast growth factor
BMP	bone morphogenetic protein
BP	bisphosphonate
BSA	bovine serum albumin
β-TCP	β -tricalcium phosphate
°C	degree Centigrade
CCT	cell culture plate
CO2	carbon dioxide
CTAB	cetyltrimethylammonium bromide
DCM	dichloromethane
DCPA	dicalcium phosphate
DCPD	brushite
DDS	drug delivery systems
DNA	deoxyribonucleic acid
DSS	dioctyl sodium sulfosuccinate
ECM	extracellular matrix
EDX	energy-dispersive X-ray spectroscopy
EGF	epidermal growth factor
ELISA	enzyme-linked immunosorbent assay
FBS	fetal bovine serum
FDA	Food and Drug Administration
FGF	Fibroblast growth factor
FWHM	full width at half height
GAG	glycosaminoglycan
HA	hydroxyapatite
HAS	human serum albumin
HLB	hydrophilic & lipophilic balance
H2O	water
H2O2	hydroperoxide
HPLG	hydroxyapatite coated PLGA
hMSC	human mesenchymal stem cell
IGF-1	insulin-like growth factor
IL-1β	Interleukin 1 beta

kV	kilovolt
L	litre
LbL assemble	layer-by-layer assemble, a repeated sequentially deposition process of oppositely charged polycationic and polyanionic polymers
M	molar
MS	microspheres
mg	milligram
mins	minutes
ml	millilitre
mm	millmetre
mM	millimolar
mN	micronewton
mRNA	messenger RNA
NaOH	sodium hydroxide
ng	nanogram
NH4HCO3	ammonium bicarbonate
nm	nanometre
nM	nanomolar
OA	osteoarthritis
OCP	octacalcium phosphate
O/O	oil-in-oil single emulsion method to fabricate polymer microspheres
Osmogens	Highly water-soluble pore-forming components inducing the osmotic pressure gradient to create pores on microspheres
O/W	oil-in-water simple emulsion method to fabricate polymer microspheres
PBS	phosphate buffered saline
PCR	polymerase chain reaction
PDAF	platelet-derived angiogenesis factor
PDEGF	platelet-derived endothelial growth factor
PDGF	platelet derived growth factor
PEG	polyethylene glycol
PGA	poly(glycolide)
PLA	poly(lactide)
PLGA	poly(lactide-co-glycolide)
Porogens	Pore-forming components in making porous microspheres
PVA	polyvinylalcohol
RA	rheumatoid arthritis
RFU	relative fluorescent unit
rpm	run per minture
SBF	stimulated body fluid

SDS	sodium dodecyl sulfate
SEM	scanning electron microscopy
S/O/W	solid-oil-water double emulsification method to fabricate polymer microspheres
TGA	thermogravimetric analysis
TGF-β	transforming growth factor-β
TM	trade mark
VEGF	vascular endothelial growth factor
µg	microgram
µl	microlitre
µm	micrometre
µM	micromolar
u	unit
U.K.	United Kingdom
U.S.A.	United States of America
VMC	vancomycin hydrochloride
v/v	volume/volume
W/O/W	water-in-oil-in-water method to fabricate polymer microspheres

1. Chapter 1: Literature review

1.1. Introduction

Bone is a connective and highly vascularised tissue [1, 2]. The aging population and the limitations of the existing bone disease treatments have created large clinical needs for break-through therapies from bone tissue engineering [3] and for more sophisticated drug delivery devices [4]. Bone tissue engineering is a promising approach to fabricate biological substrates as alternatives to autografts and allografts for bone regeneration [3]. Controlled drug delivery can be combined with tissue engineering to mimic the natural release of growth factors from extracellular matrix (ECM) to promote the regenerative process. It can also be utilized independently in healing various bone diseases to reduce systemic drug toxicity and improve treatment efficiency [4, 5].

Based on relatively good cell response and biodegradability, synthetic biodegradable polymers, especially poly(lactide-co-glycolide) (PLGA) have been extensively evaluated as substrate biomaterials (nano/microspheres or scaffolds) for controlled drug delivery and tissue engineering [6]. ECM component heparin has specific binding with various proteins such as BMP-2 and bFGF, and hence has been utilized as surface coating biomaterials to bind growth factors [7-9] and to regulate cell functions [10, 11].

Poorly crystallized hydroxyapatite (HA) is also an attractive biomaterial to functionalize the substrates for better bone cell response due to its chemically

similarirty to bone mineral and osteoconductivity [12-14]. HA can enhance bone targeted attachment, and promote osteoblastic cell proliferation and differentiation [15, 16]

The main focuses of this thesis are therefore on the applications of synthetic biodegradable polymer as localized and injectable drug/cell delivery devices for bone tissue engineering. Heparin and HA were both introduced on the PLGA microspheres individually to regulate the cell response of PLGA.

This chapter expands the concepts of basic bone diseases, bone tissue engineering and localized drug delivery. The biomaterials used in localized drug delivery, approaches to fabricate microspheres and surface modification techniques are also reviewed in this chapter.

Musculoskeletal diseases, such as osteoporosis and arthritis, are on the rise due to an ageing population. Bone surgerys followed by systematically oral or parenteral administrations of antibiotics, pain killers and anti-inflamation drugs are the conventional therapies for bone fractures, late-stage osteoporosis and arthritis. However, the routine use of drugs for these postoperative complications is not ideal due to the lack of specific drug targeting and systematic administrations, coupled with severe side effects. Therefore, localized drug delivery devices attract great interests for healing bone diseases, because they can be deposited on the implant surfaces for localized release of drugs and can improve the long-term biocompatible fixation of implant by using biocompatible materials. Due to the disadvantages of currently bone

graft materials, bone tissue engineering is a new promising alternative to autografts and allografts to provide constant engineered biological substitutes for healing bone diseases. Biodegradable microspheres (MS) have been rapidly developed in recent years as localized drug delivery devices and bone tissue engineering materials for cell therapy. The review outlines the basic scientific background and present progress in the uses of biodegradable MS as controlled drug and cell delivery devices in bone tissue engineering.

1.2. **Bone physiology and bone diseases**

1.2.1. Bone physiology

Bones are connective tissues, mainly comprised of inorganic components (bone minerals), organic components (collagens and fibrous proteins) and four types of bone cells embedded in the mineralized organic matrix (Table 1.1) [2].

Table 1.1 Composition of bovine cortical bone [17]

Component	**Percentage by weight (%)**
Water	9.1
Inorganic mineral	68.8
Organic (collagen)	19.5
Other organic components	2.6

The four kinds of bone cells play important roles in metabolic balance between old bone dissolution and new bone formation (Table 1.2). The basis of most bone diseases can be traced to the aberrant behaviour of cellular components in bone metabolism, such as the osteoporosis induced from the imbalance between the osteoblast and osteoclast [18]. In the adult, the majority of bones do not undergo bone formation and

resorption at any given time, and these inactive surfaces in adult skeleton are lined by bone lining cells.

Table 1.2 Functions of main bone cells

Cell types	**Functions**
Osteoblast	Mononucleate bone-forming cell that synthesizes the bone matrix and participates in bone mineralization [18-20]
Osteoclast	Responsible for bone resorption including polarization and formation of new membrane domains, HA dissolution, degradation of organic matrix, removal of degradation products [19, 21-23]
Bone lining cell	Inactive osteoblast works as the nutritional and metabolic support of osteocytes, and initiation of osteoclast rdesorption [24]
Osteocyte	The most abundant and fully differentiated cells in bone, arising from osteoblasts and contained within spaces called lacunae. They are formed when the bone formation front moves on, leaving some osteoblasts encapsulated in mineralized tissue [25]

1.2.2. Bone minerals

The process of bone formation starts by the action of osteoblasts, which synthesize and release collagen matrix. Bone minerals is formed by calcium phosphate, referred to a poorly crystalline and carbonate-substituted apatite $Ca_{10}(PO_4)_x(CO3)_{(9-1.5x)}(OH)_2$, stoichiometrically similar to hydroxyapatite (HA)-$Ca_{10}(PO_4)_6(OH)_2$. The carbonate content ranges between 4% and 8%, varying with age. The bone apatite is the materials that gives bones their rigidity and amounts to 65-75% of the total bone mass. There are two distinct features of biological bone apatite: the small dimensions and

low crystallinity, which contribute to the special features of bone material, such as non-stoichiometric composition, inner crystalline disorder and the presence of carbonate ions in the crystal lattice [26, 27]. As the most similar material to the bone apatite, HA is the most used calcium phosphate in implant fabrications or as a target for bone therapeutics [19, 26]. Ceramic made of HA can form a strong bond with the bone and favour bone formation.

1.2.3. Main bone metabolism diseases

1.2.3.1. Osteoporosis

Osteoporosis is characterized by bone loss and microstructural deterioration in bone tissue, which results in skeletal fragility and an increased risk of bone fractures. The disease is usually divided into two categories: primary osteoporosis or postmenopausal osteoporosis; and secondary osteoporosis or age-related osteoporosis [28]. Postmenopausal osteoporosis is associated with menopause or oestrogen deficiency and characterized by accelerated trabecular bone resorption. The estimates of the total cost of osteoporotic fractures in the United States is in the region of $10–20 billion annually [29]. The bone loss in osteoporosis is caused by an imbalance between the bone formation from osteoblasts and the bone resorption from osteoclasts. Osteoclasts resorb bone to release calcium, phosphate and other ions for homeostasis and to initiate the structural remodelling which adapts skeletal architecture to mechanical loads. Most conditions leading to osteoporosis are associated with increased osteoclastic bone resorption in postmenopausal women [18].

The primary preventive modality for postmenopausal osteoporosis is hormone replacement therapy, and oestrogen appears to be the best option at this time. The most common administration route of oestrogen is oral without interruption for about 6 years or more. Current doses of oestrogen may induce side effects, leading to non-compliance and loss of efficacy. Therefore, to overcome the problem of non-compliance due to the side effects of oestrogen and the difficulty in taking the medication in prolonged therapy, an alternative approach is to formulate a low-dose estradiol and progesterone combination for about 1 year long prolonged drug delivery using biodegradable biocompatible polymers. The application of subcutaneous implants to deliver estradiol continuously for up to 1 year for treatment or prevention of osteoporosis has been officially available in Great Britain since 1981 [18].

Sometimes, a reduction in bone formation could also lead to inadequate bone replacement during remodelling and to gradual bone loss. As these cellular activities are readily modulated by protein-based endogenous signalling mechanisms, proteins are the ideal therapeutic agents for alleviating such cellular behaviours [30]. For example, bone morphogenetic proteins (BMP), one of the most important growth factors with potential for bone regeneration, are widely used to promote bone formation.

Besides protein therapy and hormone replacement therapy, bisphosphonate (BP) is another class of compounds widely used for the management of disorders of osteoporosis. Oral BP has become the most widely used drug in the treatment of osteoporosis for reducing the risk of new fractures. BP inhibits osteoclast formation

and induces apoptosis of mature osteoclasts, but they affect the proliferation and function of osteoblast cells as well. Some experts caution that the benefits of prolonged use of BP must be carefully weighed against the potential negative effects of over suppression of bone metabolism. Therefore, the localized drug delivery of BP becomes more desirable for healing osteoporosis [31].

1.2.3.2. Osteoarthritis

Rheumatoid arthritis and osteoarthritis (OA) are two main kinds of arthritis, the progressive destruction disease of particular cartilage. OA is the most common type of arthritis which can develop from inflammatory arthritis or local diseases such as mechanical injury. OA is often considered as the inevitable consequence of ageing [32], with few effective therapies other than the eventual surgical replacement of the arthritic joint. For example, total joint arthroplasty by using bone grafts or substitutes is a widely used therapy with marked pain relief and functional improvement. However, due to the limitations of bone grafts and substitutes, such as insufficient amounts and immune rejection, bone tissue engineering emerged as a potential alternative therapeutic process to treat severely injured patients with minimally invasive surgery.

1.2.3.3. Rheumatoid arthritis

Rheumatoid arthritis (RA) is a chronic, systemic inflammatory disease characterized by chronic inflammation and loss of joint function[33, 34]. RA targets synovial joints and series of extra-articular manifestations will occur with RA to cause significant

morbidity. It is the most common type of inflammatory arthritis, and the second most common joint disease seen in clinical practice [35]. The Arthritis Research Council estimates that approximately 0.5-1% of the adult population has RA in UK [35].

When RA develops into a non-reversible condition by destructive changes and synovial inflammation in an intact joint, surgery is recommended to replace the destroyed joint with implants. In order to solve the problem of long-term implant fixation to bone, HA and tricalcium phosphate coating on the prostheses is used [36]. HA exhibits good properties as a biomaterial, such as cell response, bioactivity, osteoconductivity, and can encourage bone growth along its surface when placed in the vicinity of viable bone or differentiated bone-forming cells. BMP also has been utilized to enhance the attachment of prostheses to bone [37, 38]. Even though HA coated prostheses are used in orthopaedic surgery, postoperative infections are still a problem. Deeper infections are very serious and the removal and re-implantation of prostheses are required. Drug delivery systems for long-term localized release of antibiotics and BMP from the HA coating could be very promising for curing postoperative infections and improving prostheses fixation.

1.3. **Bone tissue engineering**

Current bone disease therapies, such as major bone grafts, have many limitations especially in large bone defects and injuries. Bone tissue engineering has become a promising approach to fabricate tissues as alternatives to autografts and allografts for bone regeneration and substitution. Bone tissue engineering utilizes the combination of cells, biodegradable scaffolds, and bioactive molecules (such as growth factors) to

recapitulate natural processes of bone tissue regeneration and development to fabricate new functional tissues, rather than just artificial implants (Figure 1.1) [3].

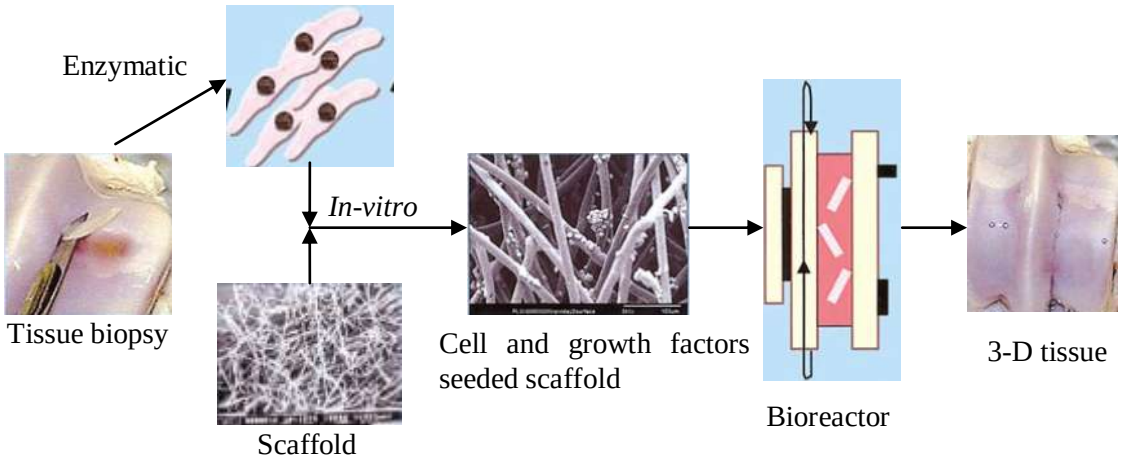

Figure 1.1 Tissue engineering strategy ([3])

Growth factors are cytokines secreted by cells to work as intracellular signalling molecules [3]. Growth factors can stimulate or prevent cellular adhesion, proliferation, migration and differentiation. In the bone tissue engineering strategy, sustained supply of growth factors in a effectual concentration is one of the key steps to promote bone regeneration *in vitro* [3, 39]. The sustained supply of growth factors can be achieved by optimally designed drug delivery systems.

1.4. **Drug delivery systems**

Drug delivery systems (DDS) are devices to administer drugs by controlled release rate in the body or directly to specific disordered tissues in a pre-designed time period]. The goal of effective DDS is to reduce systemic drug toxicity, improve treatment efficiency, enhance drug targeting, protect sensitive drugs from hazardous environment, and extend efficacious time to reduce drug administration frequency [5]. To design sophisticated DDS, the drug administration route, the drug carriers, and the

drug targets are all of great importance. Localized drug delivery system is one kind of DDS designed to deliver medications to specifically targeted parts of the body to regulate a drug's access rate locally [4, 5].

1.4.1. Localized drug delivery for bone diseases

Routine treatment of excessive joint pain and fractures are the surgical treatment with bone grafts and implants However, these are associated with many postoperative problems, such as infections, associated tissue pain, looseness between bone and implants. Problems with systemic administration of antibiotics and anti-inflammatory drugs by oral or intravenous delivery include lack of targeting and systemic toxicity for these postoperative complications. Localized drug delivery systems can reduce systemic toxicity and increase the effectiveness of therapy. Localized delivery of antibiotics has been successfully used to cure or reduce the risk of infections during orthopaedic surgery [40]. Natural or synthetic biodegradable materials, such as polymers or ceramics have been proposed as bone fillers or cements, or coating materials for metal implants to locally deliver antibiotics [41-43].

1.4.2. Localized growth factor delivery for bone diseases

Besides antibiotics and other small pharmaceutical molecules, growth factors are also required to be locally delivered to specific bone sites to improve the long-term fixation of bone and implants [36] and facilitate bone repair [44]. Bone repair is a complex biological process regulated by bone cells, the extracellular matrix and various proteins such BMP and basic fibroblast growth factor (bFGF) [30]. The

origins of most bone diseases can be traced to aberrant cellular activities governed by the protein-based endogenous signalling mechanisms [45]. Hence proteins, especially growth factors, are promising potential therapeutic molecules to activate and regulate various cellular functions for bone repair.

Results of systemic administration of growth factors are often unpredictable, due to their short biological half life, lack of long term stability, tissue specificity, and potential dose-dependent carcinogenicity [3]. Therefore, the preferred carrier of growth factors needs primarily act as a local regulator to control doses and kinetics of released growth factors, in order to increase their potential retention time at therapeutic concentration levels. Moreover, osteoconductive and osteoinductive properties, biodegradability, adequate mechanical strength and low toxicity are essential for the design of growth factor carriers [6, 46, 47]. The simultaneous delivery of two growth factors with transplanted bone marrow stromal cells has been confirmed to enhance significant bone formation [48]. There are many different approaches of growth factor delivery for bone repair (Figure 1.2).

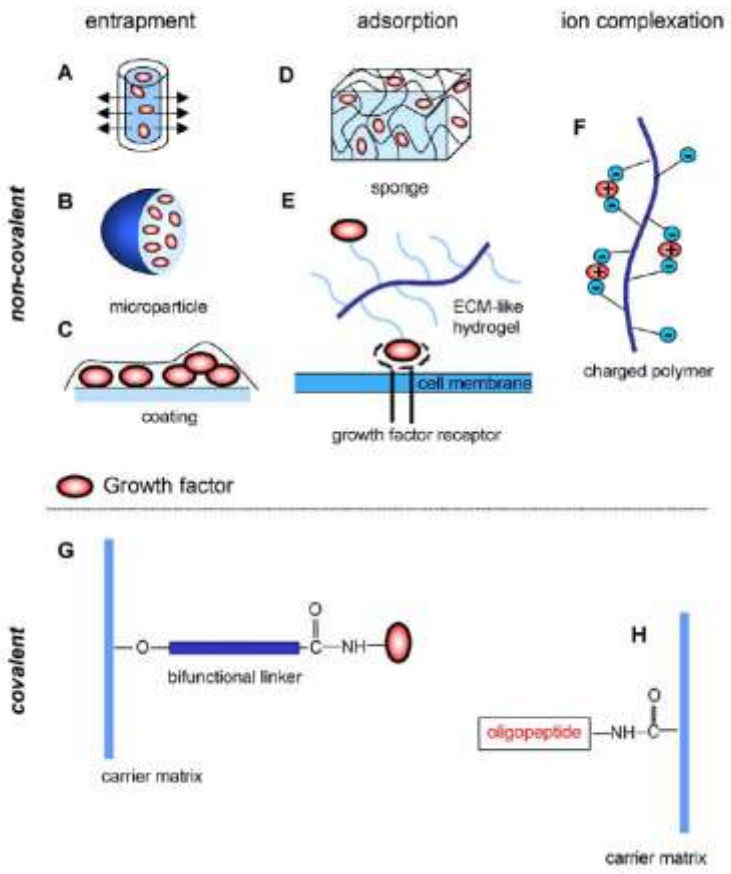

Figure 1.2 Different growth factor delivery systems ([6])

Biodegradable MS can physically encapsulate growth factors (Figure 1.3 B) and release them by the drug diffusion and polymer degradation [6]. Bone mineral HA can used as carriers for various growth factors for bone therapeutic targeting due to the physically adsorption (Figure 1.3 D) and strong ionic binding of proteins (Figure 1.3 F) [49]. Heparin, a sulphated glycosaminoglycan, has also been used for controlled delivery of growth factors due to the ionic complexation with growth factors [7-9].

1.4.3. Biomaterials used in bone drug delivery

Many synthetic materials have been explored to locally release antibiotics to heal the infected bone tissue, or to deliver proteins to improve long-term implant fixation to

bone and diseased bone tissue regeneration. Calcium phosphates including HA, and biodegradable polymers, especially PLGA, have been widely used in bone drug delivery systems separately [50, 51]. However, there are still many obvious limits for these current systems.

Biodegradable polymers can control the drug release profiles by altering their degradation properties through changing their composition, molecular weight, formulation etc. But most of them are not osteoconductive and not easily integrated with bone tissue after application [52]. The acidic micro-environments induced by polymer biodegradations (hydrolysis of ester linkages) are harmful for protein stability [53-55].

HA is widely used as a bone substitute material due to its good cell response and osteoconductivity, resulting from its similarity to the mineral component of bone [12-14, 49]. HA can enhance the bone targeted attachment, proliferation of osteoblastic cells and promote bone regeneration. Moreover, HA beads and cements, porous HA blocks [56, 57] and HA coating on metal implants [15, 16] have been investigated as carriers of various drugs, such as antibiotics and growth factors. Nevertheless, drug release may be too fast and a sustained drug release in a controlled manner is difficult to achieve by only utilizing HA [15, 16].

Among all the investigated materials, biocompatible composites could be seen as a future direction of development because they combine the advantages of biodegradable polymers and bone-like calcium phosphate. It could be a good method

to combine HA with biodegradable polymer to design novel bone targeted drug delivery devices HA-coated PLGA (HPLG) MS [58]. HA coated biodegradable polymer implants or drug delivery devices (microspheres or nanospheres) can combines the osteoconductivity and pH buffer capability from HA with the drug delivery function of biodegradable polymer.

1.5. **PLGA MS for controlled drug delivery**

1.5.1. Characterisations of PLGA copolymer

The use of natural polymers, such as bovine serum albumin (BSA), human serum albumin (HSA), collagen, gelatin, and haemoglobin, for drug delivery is limited due to their higher costs [59]. Amongst used synthetic biodegradable polymers, Food and Drug Administration (FDA) approved poly(glycolide) (PGA), poly(lactide) (PLA), especially their copolymer PLGA (Figure 1.3), have received much attention due to their favourable properties such as good cell response, biodegradability, and surfficient mechanical strength.

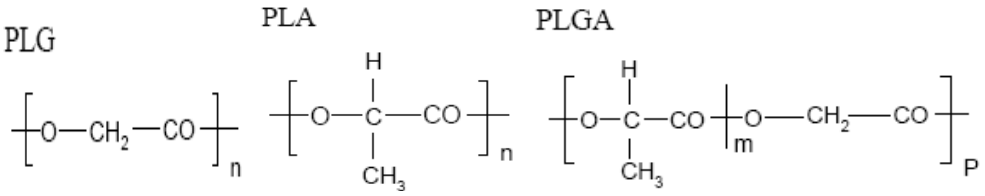

Figure 1.3 Chemical structure of polyester PLA, PLG, and their copolymer PLGA [2].

1.5.1.1. Physical-chemical properties of PLGA

Physical properties such as the molecular weight and the polydispersity index affect the mechanical strength of the polymer, its ability to be formulated as a drug delivery

device, its biodegradation rate and hydrolysis rate. The mechanical strength, swelling behavior, capacity to undergo hydrolysis, and subsequently the biodegradation rate are directly influenced by the crystallinity of the PLGA polymer. The resultant crystallinity of the PLGA copolymer is dependent on the type and the molar ratio of the individual monomer components (lactide and glycolide) in the copolymer chain [59, 60].

1.5.1.2. Cell response of PLGA

When exposed to physiological conditions, PLGA is degraded by random hydrolysis and can also be broken down by particular enzymes, especially those with esterase activity [53-55]. The degradation product, glycolic acid, is not toxic and it can enter the tricarboxylic acid cycle after which it is excreted as water and carbon dioxide and a part of the glycolic acid is also excreted in urine [61]. Similarly, PLA and PLGA can be degraded by hydrolysis of ester linkages into low molecular weight molecules that can either be metabolized or cleared through the renal system.

The evaluation of the cell response of implantable delivery systems requires an understanding of the inflammatory and healing responses of the implantable materials [62]. The sequence tissue responses to implantations of a microsphere drug delivery system are illustrated in Table 1.3and Figure 1.4.

Table 1.3 The sequence tissue responses to implantations (modified from [63]).

Tissue response	Involved cells
Injury	Injection, Implantation
Acute inflammation	Polymorphonuclear leukocytes
Chronic inflammation	Monocytes and lymphocytes
Form granulation tissue	Fibroblasts and new blood capillaries
Foreign body reaction	Macrophages and foreign body giant cells at the material-tissue interface
Fibrosis	Fibrous capsule

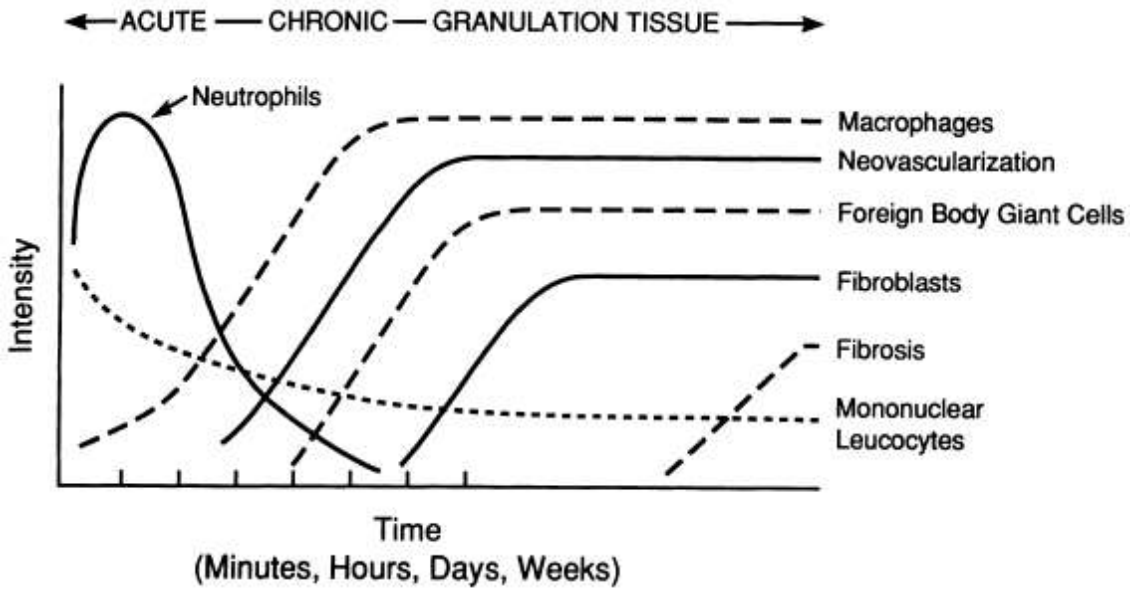

Figure 1.4 The temporal variation of tissue responses to implanted biodegradable MS ([63]).

Many studies examining cell response characteristics of PLGA biomaterials have suggested that PLGA is compatible with bone tissue [64]. However, there still remain some concerns of PLGA compatibility [65], as evidenced by inflammation and formation of fibrovascular tissue around implanted PLA [66]. In particular, the hydrophobic nature of the polymer may drive denaturation of extracellular matrix

proteins that readily adsorb to the material [67, 68], which could contribute to the inflammatory response.

1.5.1.3. Biodegradation of PLGA

It is generally considered that the mechanism of degradation of aliphatic polyesters is a hydrolytic mechanism. In aqueous environments, PLA, PGA, and PLGA are insoluble but degrade hydrolytically [69-72]. Hydrolysis, pH sensitive, occurs as ester linkages of the molecules are randomly cleaved to form carboxylic acid and hydroxyl chain ends following the reaction (from [73]):

$$R\text{-}COO\text{-}R' + H_2O \rightarrow RCOOH + R'OH$$

Generally, the polymer erosion can be classified into two mechanisms, namely surface and bulk erosion [2, 59] (Figure 1.5). PLGA are bulk erosion polymers, where the water penetration is faster and the degradation and erosion affect all the polymer bulk [2].

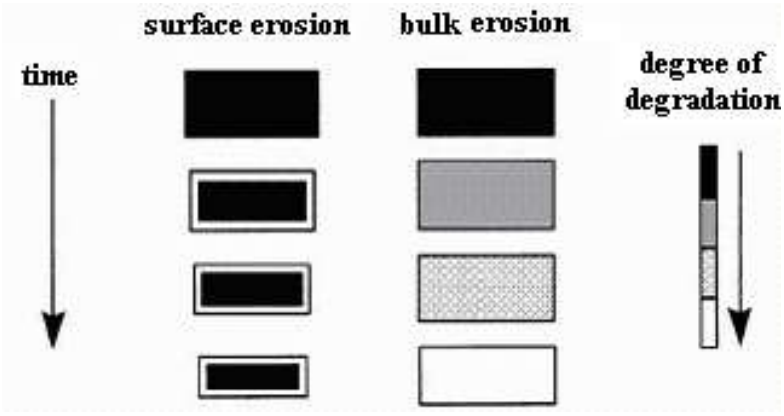

Figure 1.5 Schematic illustration of the changes that a polymer matrix undergoes during the surface erosion and bulk erosion ([2]).

Some scientists have also proposed a three-phase mechanism for the PLGA biodegradation [63]: Firstly, it is the random chain scission process. The molecular

weight of the polymer decreases significantly, but no appreciable weight loss and no soluble monomer products formed. In the middle phase, a decrease in molecular weight accompanied by rapid loss of mass and soluble oligomeric and monomer products are formed. Finally, soluble monomer products formed from soluble oligomeric fragments. The phase is that of complete polymer solubilization. There are many factors, such as chemical composition, porosity, morphology and ect, which can affect the biodegradation rate [63].

Generally, biodegradation times of polylactides range from 18-24 months for poly(L-lactide), to 12-16 months for poly(D,L-lactide), and between 150 days and 50-60 days for poly(D,L-lactide-co-glycolide) with varying copolymer ratios [74]. Figure 1.6 shows the influences of *in vivo* biodegradation rate resulted from the molar ratio of the lactic and glycolic acids in the polymer chain [63]. The fastest rate of degradation occurs with the 50:50 copolymers. As the glycolic acid content decreases, the rate of polymer degradation decreases [74].

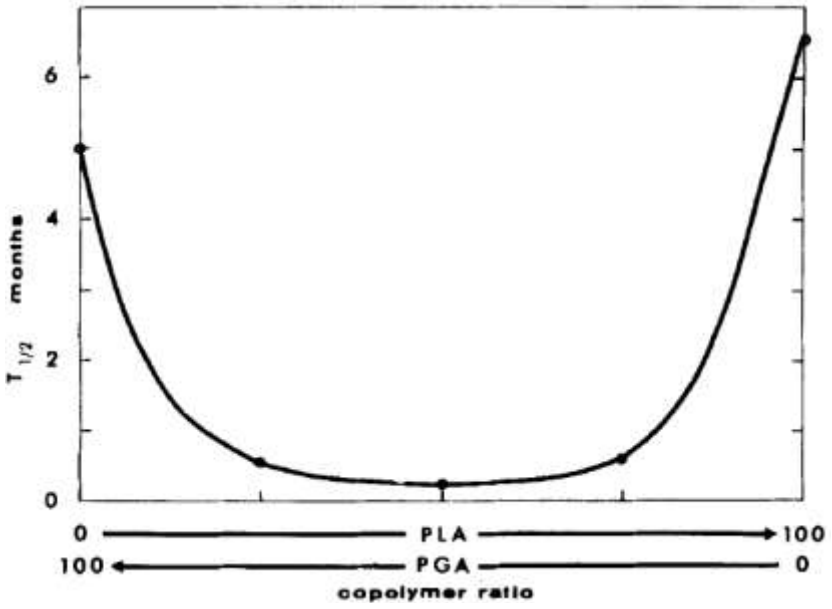

Figure 1.6 Half-life of various ratios of PLGA copolymers implanted in rat intramuscular tissues ([74]).

1.5.2. Fabrication techniques of PLGA MS for drug delivery

Although there are various microencapsulation techniques to fabricate PLGA MS for drug delivery, the following requirements are essential for every technique [59]: the stability and biological activity of the drug should not be adversely affected; the size of microsphere should be no bigger than 250 μm and ideally smaller than 125 μm; the drug encapsulation efficiency should be higher than 40%; the microsphere quality and the drug release profile should be reproducible within specified limits; the MS should be produced as a free flowing powder and should not exhibit aggregation or adherence. Solvent evaporation and emulsion method is one of the most widely used technologies fulfilling the above requirements to fabricate PLGA MS. Some widely used solvent evaporation and emulsion methods are introduced here.

1.5.2.1. Singe emulsion method

In principle, this oil-in-water method, usually abbreviated as O/W emulsion, is to emulsify the organic phase containing the polymer (O) in an aqueous phase that contains a stabilizing agent (W). The evaporation of the organic solvent then hardens the microdroplets to generate microspheres [75]. The major disadvantage of the O/W emulsification method is the poor encapsulation efficiencies of moderately water-soluble and water-soluble drugs [59, 76, 77]. In order to increase the encapsulation of the hydrophilic drugs, an oil-in-oil (O/O) emulsion method was developed where the continuum phase is formed by an organic liquid such as a mineral oil [76].

1.5.2.2. Double or multiple emulsions methods (W/O/W and S/O/W)

The is a water-in-oil-in-water (W/O/W) method and is best suited to encapsulated

water-soluble drugs like peptides, proteins, and vaccines, unlike the o/w method which is ideal for water-insoluble drugs like steroids [59, 76]. Although the extraction or evaporation of solvent methods are simple, there are several variables that have to be adjusted to optimize the properties of the obtained nano- and microparticles, such as solvents, surfactants, concentration of the PLA-based polymer, stirring rate, amount of aqueous Phase, and the amount of polymer dissolved in the organic phase [78].

In order to avoid the water-organic solvent interface during the first emulsion, a solid-oil-water (S/O/W) emulsification method is utilized as an alternative to the double emulsion, which is excellent in terms of the protein integrity because solid-state proteins are stable in an organic solvent [79].

1.5.3. Drug release mechanism of PLGA MS

Nano/MS fabricated by biodegradable polymers mostly exhibited triphasic drug release profiles including an initial burst release, drug diffusion and sustained release governed by polymer degradation [54, 80]. The first phase of burst drug release is governed by the rapid release of drugs adsorbed on the microsphere surface or drugs physically encapsulated in the microsphere near the surface. The second phase of drug release is characterised as the swelling of PLGA copolymer due to the inward diffusion of water, which dissolves the encapsulated drugs and enable them to diffuse outward through the polymer barrier in a low dose. The third phase of drug release occurs when the erosion and degradation of polymers begin. As PLGA copolymer is a bulk erosion polymer not a surface erosion polymer, the water penetration is fast and

the degradation affect all the polymer bulk [2]. Therefore, all encapsulated drugs will be dissolved by water and diffuse out quickly in this phase.

1.6. **Injectable porous PLGA MS for cell culture and delivery**

Besides the conventional nonporous MS for drug or growth factor delivery, PLGA copolymer can also be used to fabricate porous MS for multi-functional applications in tissue engineering and regenerative medicine, such as cell carriers for injectable cell therapy, transplantable substrates for cell expansion, three-dimension (3D) cell culture and inhalation drug delivery devices.

1.6.1. Porous MS as injectable scaffold for cell therapy

The current strategies of tissue engineering have utilized autologous stem cells in combination with biodegradable scaffolds and bioactive molecules to restore damaged tissues [81]. In order to repair complex-shape tissue bulks where self-regeneration is difficult, injectable scaffold is proposed to transplant cells and delivery growth factors to improve cell proliferation and differentiation in tissue defects with minimal invasive surgery [82]. Injectable cell delivery scaffold can be used for *in vitro* culture and expansion of cells in the bioreactor, followed by injecting the cells-carriers constructs by needles into disordered tissues to help them repair and regeneration. Porous MS can be used as injectable cell microcarriers to mimic the ECM. Most cells need to adhere to a solid ECM to fulfil cellular functions. The native ECM provides a physical substrate with specific ligands for cell adhesion and migration. Cell proliferation and differentiation are also regulated by the growth factors in the ECM.

Conventional scaffolds in tissue engineering mimic the natural ECM to support cell growing to specific tissues for transplantation [3], [83]. However, for complex-shaped tissue repair, injectable porous PLGA MS are more suitable as injectable cell scaffolds than big conventional scaffolds for an accurate fit with minimally surgical interference [84-86].

Osteoblasts and other progenitors of osteogenic cells have been reported to proliferate on microcarriers *in vitro* and *in vivo* [87]. With large surface to area volume ratios, injectable porous microcarriers can achieve rapidly cell growth and expansion with lower cost and more space-saving manner. Moreover, the sheer stress in the bioreactor can enhance the differentiation of osteogenic cells on microcarriers, as the stress mimic the real bone environment where the stress is expected for bone tissues [88].

Since human bone and cartilage cells are on average 10-20 μm in diameter before seeding and the ideal injectable cell microcarriers should be smaller than 200 μm in order to pass through the syringes needles [89], the ideal porous MS for injectable cell delivery are expected to be 40-200 μm in diameter with pore sizes around 10-40μm.

1.6.2. Porous MS as transplantable substrates for cell expansion

Porous MS can also be used as microcarriers to speed the expansion of many cell types and for large scale viral vaccine production [90, 91]. Compared with onventionally static culture systems using T-flasks and tissue culture Petri dishes, the large surface area of microcarriers makes the expansion and analyses of a large amount of cells possible in a relatively small space with high time and labour

efficiency. For example, 1g of Cytodex™ 1 microspheres can provide a surface area of 4400 cm^2 as large as approximately fifty-eight 75 cm^2 culture flasks [92]. Porous MS have even larger surface areas than the commercially available microcarriers due to the more porous structure and higher porosity. Therefore Porous MS are expected to work as microcarriers for cell expansion to facilitate bulk-culture and delivery stem cells, especially embryonic stem cells, for regenerative medicine [93, 94].

Moreover, culturing cells on transplantable substrates, such as microcarriers and porous MS, can provide cell aggregates directly for clinical appliaciton to avoid repeated trypsinization, which is often used to harvest *in vitro* expanded cell for transplantation in the current cell culture methods [88]. The cell interactions with the ECM will be hindered by the repeated trypsinization, which may reduce the cell viability and limit the therapeutic efficacy [95].

However, commercially available microcarriers are only confirmed for cell culture not for clinical applications. Biodegradable polymers are already confirmed for clinical applications as drug delivery devices and implants [50, 51]. Hence porous MS made of biodegradable polymer are promising multi-functional microcarriers combining the cell expansion with cell transplantation [96].

1.6.3. Porous MS for inhalation drug delivery devices

Besides working as injectable cell carriers and cell expansion platforms, biodegradable porous MS can also be used as long acting inhalation drug delivery systems due to the adjustable sustained release, low density and aerodynamic

diameters but large geometric diameters [97-101]. However, as the porous MS for inhalation drug delivery need be small than 10μm in diameter [102] for better aerodynamic performance, the following sections focus mainly on the large porous MS (40-200 μm in diameter) for cell culture and delivery.

1.6.4. Effects of MS structure and surface properties for cell delivery

Similar to the porosity requirements of scaffolds in tissue engineering, the injectable cell carriers must also posses an open porous structure with interconnected geometry in order to allow cell in-growth and exchange of nutrients, gases, and metabolic waste from cells [89, 103]. Their interconnected porous structure also provides large surface areas and higher buoyancy to improve cell adhesion and growth. The porosity and interconnectivity are especially important for bone cells, because high rates of mass transfer are required during the bone regeneration [104].

Moreover, both the chemical and topographic properties of the substrate surface can affect the cellular functions, such as adhesion, migration, proliferation and differentiation [105, 106]. Chemical properties, such as surface charges and hydrophilicity, can affect cell adhesion and the ECM protein interactions with the substrates, in turn, which will regulate the protein-based endogenous signalling and modulate other cellular functions [30].

Topographic properties, such as the surface roughness and porosity, have been reported regulating osteogenic cell migration and differentiation [105]. Improved surface roughness can facilitate cell migration to the substrate surface, because the

rough surface can lock up the fibrin matrix secreted by the cells to prevent cells detaching during migration. The rough surface can also guild osteogenic cell to present like more differentiated osteoblast with reduced cell numbers, increased protein and alkaline phosphatase activity [105].

1.6.5. Fabrication techniques of porous PLGA MS

There are various methods derived from the techniques used in fabrication of porous scaffolds to fabricate porous PLGA MS in the Water/Oil/Water ($W_1/O/W_2$) or O/W emulsion process. These methods can be classified by the use of different pore-forming components (porogens), such as osmogens [99, 107-109], extractable porogens [7, 101, 107], and gas-foaming salts [100, 110, 111].

Osmogens, highly water-soluble porogens (e.g. salt, cyclodextrins and sucrose) presented in the internal phase, attracts water from the external phase to penetrate along the osmotic pressure gradient to create pores [99, 107-109].

Certain materials, which have relatively higher solubility than PLGA both in water and the oil phase, can be used as the extractable porogens, e.g. pluronics, glycerol monooleate, polyethylene glycol (PEG) and fatty acid salts. Extractable porogens, mixed with PLGA in the oil phase, can be extracted by the external water phase to form pores during the PLGA hardening process [7, 101, 107].

Gas-foaming salts, such as ammonium bicarbonate and hydrogen peroxide, work as effervescent porogens to generate gas bubbles by decomposition in the polymer oil

phase to create well inter-connected pores [100, 110, 111].

1.7. **Heparin coating for protein delivery and tissue engineering**

The hydrophobic nature of PLGA polymer inhibits the cellular adhesion and drive denaturation of extracellular matrix proteins [67, 68], so the surface of PLGA MS, both nonporous or porous, have been modified by NaOH [112], heparin [7], amine [113] and carbonate apatite [114] to improve biocompatibility. As heparin and HA (bone-like apatite) have another functions to bind and release growth factors by ionic interactions [7-9, 49], the following sections will discuss the fabrication techniques and applications of heparin or HA coating on biodegradable polymer MS.

1.7.1. Controlled growth factors delivery by heparin

Among various ECM components, heparin is a negatively charged glycosaminoglycan (GAG) (Figure 1.7) on the cell membrane and ECM which can bind specifically with various angiogenic growth factors and transforming growth factor-β [115, 116].

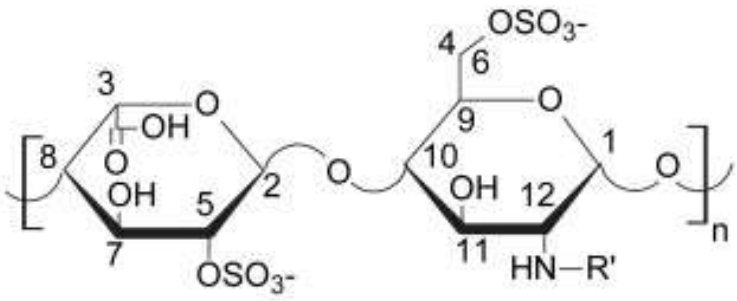

Figure 1.7 Heparin chemical structure [117]

As the -OSO_3- groups of heparin have specific ionic interactions with the lysine and

arginine groups of the growth factors, heparin can bind growth factors non-covalently. Later, the bound growth factors can be sustained release from heparin by diffusion [117]. The growth factor stability can also be improved as the heparin binding protects them from thermal denaturation and enzymatic digestion [118]. Moreover, heparin can form complexes with growth factor receptors on cells to enhance cytokine signalling [117], and mitogenic activity [119]. Therefore, heparin and heparan sulfate have been immobilized on the surface of various materials for controlled release of growth factors, such as alginate [8] and PLGA [11].

1.7.2. Cell responses to heparin

Heparin can interact with various protein receptors and proteins, such as fibronectin regulating cell adhesion, bFGF affecting proliferation, and BMP modulating osteogenic differentiation [10, 11, 120, 121]. Therefore, heparin has been immobilized onto various biomaterials to govern heparin-binding growth factor activity, which, in turn, is expected to influence cell functions. For examples, heparin functionalized gels were reported facilitating human mesenchymal stem cell (hMSC) adhesion, spreading, and proliferation, and osteogenic differentiation [11]. Fibroblast adhesion was also reported to be improved by the chitosan/heparin complex surface [122].

1.7.3. Techniques for heparin coating

Due to above applications in growth factors delivery and tissue engineering, various techniques have been reported to immobilize heparin on the substrate surface [123, 124]. Based on the different immobilization mechanisms for heparin coating, these

techniques can be classified as covalent chemical methods [7-9] and noncovalent methods [117, 125-127].

The covalent chemical methods include covalent conjugation [7-9], copolymerization [10] and photopolymerization [117] The covalent conjugation is one of the most widely used approaches to incorporate heparin on biomaterials, such as collagen scaffolds, PLGA scaffolds and PLGA microspheres [7-9, 119]. The substrates were conjugated with primary amine groups at first, and then the carboxylic groups of heparin were covalently conjugated with the surface-exposed amine groups using 1-ethyl-3-(3-dimethylaminopropyl) carbodiimidehydrochloride and N-hydroxysuccinimide .

In comparison, the noncovalent methods are more facile and cost-saving, including electrostatic binding [128], hydrogen bonding [129] and ionic interactions [125-127]. The hydrogen bonding method is a facile method to conjugate heparin with the Pluronic F127 polymer. Among the ionic interactions methods, layer-by-layer (LbL) assemble is the most promising approach mimicing the natural polyelectrolyte assembly within ECM [130] which will be highlighted in the following section.

1.7.4. LbL assembly of polyelectrolyte multilayers for heparin coating

LbL assemble is a repeated sequentially deposition process of oppositely charged polycationic and polyanionic polymers onto a substrate by the ionic interactions [124]. Compared with the covalent chemical methods and other noncovalent approaches, the LbL assemble is a facile method to construct nano-scale bioactive 3D or 2D thin

polyelectrolyte films on substrate surface [104]. As heparin is an anionic glycosaminoglycan and chitosan is a cationic polysaccharide, heparin and chitosan have been sequentially deposited onto various substrates, including polycaprolactone [131] and PLA [132], to modulate cellular adhesion and to delivery bioactive molecules by the LbL assemble.

1.8. **HA coating on polymer MS for bone tissue engineering**

1.8.1. Bone minerals

HA (Figure 1.8) is stoichiometrically similar to bone minerals, which are poorly crystalline, calcium-deficient apatites with small crystal size. The unit cell of bone apatites with dimensions of a = 0.943 nm and c = 0.688 nm can be arranged and grown along the c-axis to form a needle-like morphology. Bone apatites are parallel to each other and the collagen fibres in organic matrix with average length of 50 nm, width of 28 nm and thickness of 2-5 nm [26, 133-135]. They can form laminated composites with nano-structured architecture and complex hierarchical structure. This provides bone superior rigidity and mechanical strength. Furthermore, the proper combination of bone apatites with organic elements such as collagens makes bone durable but not brittle.

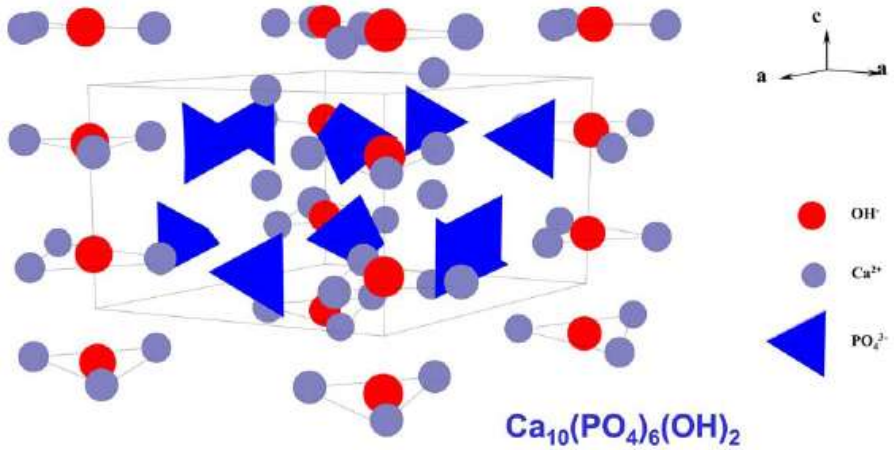

Figure 1.8 The hexagonal lattice structure of stoichiometric HA (from [26])

1.8.2. Kinetics for HA precipitation in supersaturated solution

HA is the crystalline and the most thermodynamically stable phase in calcium phosphates. Normal HA and its related calcium phosphates can be precipitated from supersaturated solution of calcium and phosphate. The precipitation of calcium phosphates is a very complicated crystal chemistry reaction involving many phases (Table 1.4).

Table 1.4 Main phases of calcium phosphate (from [136, 137])

Phase	Abbreviation	Formula	Structure	Ca/P ratio
Amorphous calcium phosphate	ACP	n/v	Irregular	1.3-1.67
Brushite	DCPD	$CaHPO_4.2H_2O$	Monoclinic	1.00
Dicalcium phosphate	DCPA	$CaHPO_4$	Triclinic	1.00
Octacalcium phosphate	OCP	$Ca_8H_2(PO4)_6.5H_2O$	Triclinic	1.33
α -Tricalcium phosphate	α-TCP	$Ca_3(PO4)_2(OH)_2$	Monoclinic	1.50
β -Tricalcium phosphate	β-TCP	$Ca_3(PO_4)_2(OH)_2$	Rhombohedral	1.50
Hydroxyapatite	HA	$Ca_{10}(PO_4)_6(OH)_2$	Hexagonal	1.67

Precursor phases such as DCPD and OCP are firstly formed, subsequently dissolved when the precipitation reaction proceeds, and finally transformed to HA. DCPA and β-TCP can also possibly participate as precursor phase in the precipitation of HA [138-141]. Four main phases, ACP, DCPD, OCP and HA, are formed preferentially when calcium phosphates are precipitated from an aqueous solution. The bone biomineralisation is regarded to start from the formation of ACP and then transform into OCP, which finally evolves to carbonated HA [140, 141].

As both Ca^{2+} and PO_4^{3-} ions participate the extensive complexation reactions resulting in the co-existence of various charged and uncharged species, such as Ca^{2+}, PO_4^{3-}, HPO_4^{2-}, $H_2PO_4^-$, $CaPO_4^-$, $CaHPO_4$, $CaH_2PO_4^+$ and $CaOH^+$, the calcium phosphate precipitation is extremely complex [138, 142, 143]. Various chemical equilibria exist and influence the formation of HA and its related calcium phosphates during the HA precipitation. For a certain phase precipitation, supersaturation is the thermodynamic driving force and given by the equations:

$$\Delta G = -RT \ln \beta \quad \text{- Equation 1.1}$$

where ΔG is the Gibbs free energy for nucleation, R = gas constant, T = absolute temperature, β = supersaturation;

$$\beta = (IP/K)^{1/\nu} \quad \text{- Equation 1.2}$$

where IP = ionic product, K = solubility product, ν = number of ions in salt formula.

For HA, K is 2.35×10^{-59}, ν is 9, and IP = $[Ca^{2+}]^5[PO_4^{3-}]^3[OH^-]$. The formation of HA is always preceded by the formation of precursor phases [140, 144]. Homogeneous (or spontaneous) precipitation and heterogeneous (or seeded) precipitation are two kinds

of reactions for HA precipitation from aqueous solution. For homogeneous HA precipitation, there are two stages of the HA crystallization in the solution: nucleation and the nuclein growth to macroscopic dimensions. For heterogeneous HA precipitation, the nucleating seeds (such as DCPD, TCP, OCP, HA, etc) need to be introduced into the stable supersaturated solution of HA. HA crystals can subsequently grow directly on the surface of the seed materials [144]. In bone tissue, the growth of HA by the biomineralisation process is also through the heterogeneous precipitation involving more than 200 different acidic proteins acting as templates, nucleins and inhibitors for the epitaxial growth of nanocrystal apatite anchoring on the collagen [145].

1.8.3. Methods for HA coating on polymeric materials

As biodegradable polymers are normally sensitive to heat, the convenient coating methods for ceramics and metals under high temperatures are not suitable for biodegradable polymers [136, 146, 147]. There are numerous methods to coat HA and its related calcium phosphates on substrates at low temperatures [136, 146, 147]. The most frequently used techniques to coat polymer substrates are the Kokubo biomimetic process using stimulated body fluid (SBF) [[148, 149] and the constant composition precipitation method [58]. The biomimetic process is to immerse substrates at the physiological condition (37^{o}C and pH 7.4) into SBF, which has ion concentrations similar to those of human blood plasma, and exchange SBF every day for 7-21 days [150, 151]. As the constant composition precipitation method can achieve complete HA coating on polymer substrates in 24 hour- much faster than the biomimetic method, it is more suitable for biodegradable polymers which may

undergo degradations and erosions during the long time biomimetic process [58]. Therefore, the constant composition precipitation method is further discussed in the following sections. The HA coating on PLGA polymers can be used for growth factor delivery due to its ionic binding to various growth factor. The drugs can also be co-precipitated during the HA precipitation process [152]. In principle, all methods of binding drugs on or co-precipitation drugs in calcium phosphate [153, 154] can be used to load drugs on HA coating on PLGA polymers by the constant composition precipitation.

1.8.4. The constant composition precipitation method

The constant composition method was originally developed to investigate the precipitation process of calcium phosphates [161, [155-160]. The seed materials were firstly added to a stable supersaturated solution of calcium phosphate at the required pH. The concentrations of lattice ions were monitored and maintained by the simulation addition of reagent solutions containing calcium, phosphate, and hydroxide ions. Once the calcium phosphate precipitated on the seed materials, pH and the calcium concentration of the solution decreased, which would trigger the reagent addition until the pH and the calcium concentration rose back.

High temperature and acidic or basic environment can accelerate the degradation of drug loaded biodegradable MS, which will result in more intial drug leakage and burst. The process time of HA coating on drug loaded biodegradable MS should also be short to avoid drug leakages. Therefore, a modified constant composition method is developed within our group to coat HA on the surfaces of drug encapsulated PLGA

MS instead of the conventional Kokubo biomimetic process at the physiological condition (37^{o}C and pH 7.4). Our modified constant composition method is a 3 hour low-temperature process and easy to control the HA coating thickness by reaction time [58] (Figure 1.9).

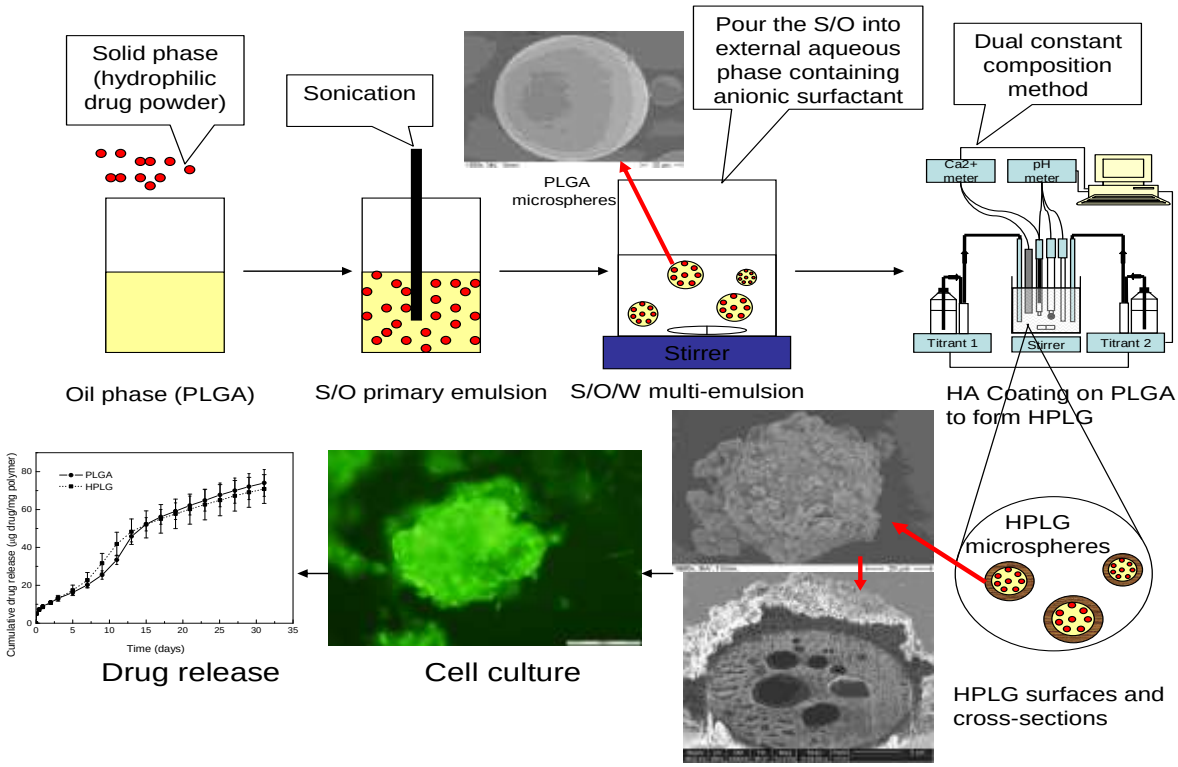

Figure 1.9 The modified constant composition technique (revised from [58])

The modified constant composition method is an easily computer controllable method, and the quick coating can be achieved by maintaining the high supersaturation in the biological conditions, pH around 7.4 and at 37^{o}C. The fast HA precipitation process can minimize the encapsulated drug leakage and the denaturation of sensitive drugs. Furthermore, HA coated PLGA MS (HPLG MS) were shown to have pH-buffer capability to prevent the pH drop of solution induced by PLGA degradation during the dug release period [58] (Figure 1.10). For conventional PLGA MS without HA coating, the pH of drug release solution (PBS) decreased from 7.4 to approximately

6.2 in 30 days (Figure 1.10) because of the acidic fragments produced by the PLGA degradation [73]. In contrast, the solution pH drop was significantly inhibited in the presence of HA coating on HPLG MS (only slightly droped from 7.4 to 7.1). This is presumably because the HA coating neutralised the acidic fragments from PLGA degradation [161]. The HA function of preventing pH drop can inhibit the further autocatalysis degradation of PLGA, prolong the drug release period [162] and protect growth factors from acidic micro-environment induced by PLGA degradation [53-55].

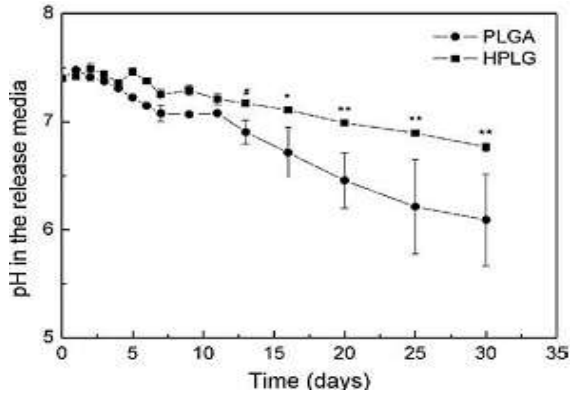

Figure 1.10 pH changes of the PBS medium incubated with drug loaded PLGA and HPLG MS. Data are means ± S.D. (n=3). *, P<0.01 and **, P<0.001 ([58])

1.8.5. Preconditions for the constant composition technique- negatively charged PLGA MS

Before using the constant composition method to coat HA on drug encapsulated polymer MS, a high negatively charged surfaces are needed as the seed materials to selectively precipitate HA. Negatively charged sites on the polymer surface have the function of providing nucleation sites for HA overgrowth, by attracting Ca^{2+} ion accumulation due to inonic interaction. The negatively charged surfaces can be formed by anionic surfactants which act as both the stabilizing agent during the microencapsulation and the functional sites for the nucleation and growth of HA crystals on PLGA MS surface. It was the calcium ion adsorption and the ion

complexation with the negative charged group initiated the apatite nucleation in a supersaturated condition.

However, the most widely used surfactant in nano/microsphere fabrications is polyvinylalcohol (PVA) which cannot produce a highly negative surface charge to the PLGA MS. In principle, -COOH and -OH groups on the PLGA could dissociate partially to form a negatively charged polymer surface, which could accumulate calcium ions through electrostatic forces and hydrogen bonding [151]. Nevertheless, the capability of -COOH and -OH to induce HA coating is very weak [163, 164] compared with $-H_2PO_4$ [165], $-SO_3$ [166], and –SiOH [167]. Tanahashi *et al* [165] has carried out a systemic study to investigate the effects of various functional groups on apatite formation by the Kokubo biomimetic method. The growth rate of apatite decreased in the order $PO_4H_2 > COOH >> CONH_2 \approx OH > NH_2 >> CH_3 \approx 0$. Anionic surfactants with strong negative groups are particularly attractive alternatives for PVA. The amphiphilic nature of these surfactants enables them strongly adhere to the particles surface by anchoring the hydrophobic tail into the polymer and leaving the polar or ionic head protruding from the surface. The anionic surfactants acted as both the stabilizing agent during the microencapsulation and the functional sites for the nucleation and growth of HA crystals on PLGA MS surface.

1.8.6. Effects of surfactants in the constant composition technique

The nano/microsphere morphology and stability of the suspension are dependent on the surfactant hydrophilic & lipophilic balance (HLB) number and negative charge dispersed on the nano/microsphere surfaces. Various surfactants have been used in

making nano/MS by water-in-oil-in-water (W/O/W) (Table 1.5) or solid-in-oil-water (S/O/W) emulsification methods (Table 1.6).

Table 1.5 Comparisons of different surfactants for making PLGA nanospheres by W/O/W method (refined from [29, 168])

Surfactants	Types	Toxic	HLB	PLGA(mg) : surfactant solution(ml)	Particle sizes (nm)	Zeta potential (mV)	After 64 day in water	
							Particle sizes (nm)	Zeta potential (mV)
SDS	Anionic	Y	40	50:25	182.4	-105.3	202.3	-113.3
SDS	Anionic	Y	40	50:50	159.2	-58.4	159.8	-72.7
Sodium cholate	Anionic	N	53.6	50:25	120.6	-59.6	156.5	-42.6
Poloxamer 188	Non-ionic	N	29	30:25	132.0	-17.6	134.3	-4.6
CTAB	Cationic	N	7.4	50:25	204.8	74.8	205.4	80.8
Taurine	Alphlic	N	17.5	50:25	137.1	-25.1	135.7	-31.4

Table 1.6 Comparisons of different surfactants for making PLGA MS by W/O/W and S/O/W methods (refined from [168])

Surfactants	Types	Toxic	HLB	Particle size (μm)		Zeta potential (mV)		Drug encapsulation efficiency		HA coating(%) [a]
				W/O/W	S/O/W	W/O/W	S/O/W	W/O/W	S/O/W	
SDS	anionic	Y	40	40.2±5.2	16.4±0.8	-83.5±2.7	-69.9±1.5	4.0%	40.6%	22.60
DSS	anionic	N	32	46.6±4.5	4.7±0.2	-74.0±1.0	-66.6±0.6	37%	61.0%	54.28
CTAB	cationic	N	7.4	32.2±3.5	23.1±1.1	60.6±0.2	42.4±2.5	12%	32.0%	N/A
PVA	nonionic	N	18	51.9±3.8	23.4±1.3	-31.0±1.4	-17.7±1.5	5.3%	35.3%	N/A

[a] determined by the remaining weight after TGA measurement (30-800 ^{o}C)

Sodium dodecyl sulphate (SDS) [58], normally used in household products, and dioctyl sodium sulfosuccinate (DSS) [168], FDA-confirmed material, are currently being investigated for inducing HA coating on PLGA MS for drug delivery (Figure 1.11) [168]. The negative charged groups of sulfate ($-OSO_3^-$, SDS) and sulfonate ($-SO_3^-$, DSS) were in the ionized states and attracted calcium ions more easily than the $–SO_3H$ and $–OSO_3H$, which needed to be dissociated to interact with Ca^{2+} [166]. Compared with the hydrolysed PLGA MS, which have –COOH group, and PLGA MS with PVA as surfactant containing –OH groups, the coating of HA on negatively charged PLGA MS with SDS or DSS as surfactant are more successful [168], consistent with previous studies [163-165].

In additions, SDS is not confirmed by FDA for clinical application but DSS has been confirmed for applications in drugs [169] and vaccine delivery [155-160]. Compared with SDS, DSS does not readily form large micelles in aqueous solution due to a bulky hydrophobic structure and limited water solubility (Figure 1.11) [168].

SDS

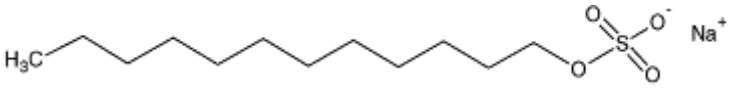

DSS

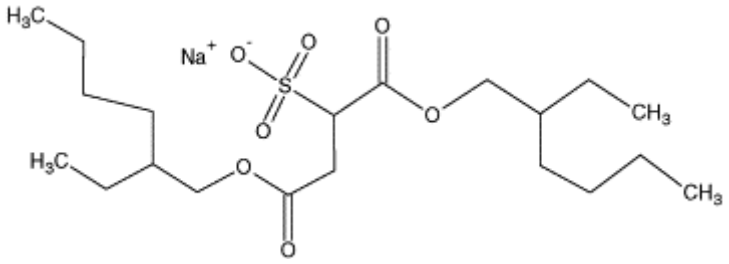

Figure 1.11 Chemical structures of SDS and DSS

1.8.7. Fabrication techniques of negatively charged PLGA MS

The S/O/W [58] emulsification method is utilized to make negatively charged PLGA

MS due to improved drug stability compared with the conventional W/O/W method [170]. The utilization of controlled drug delivery devices requires controllable dosage released as a function of time. In the S/O/W emulsification technique, this function and the MS morphology can be adjusted by various fabrication parameters, such as polymer matrix properties (composition, molecular weight), drug types, sonication/homogenization speed and time, oil: aqueous phase ratio, surfactants types and etc. The effects of these parameters on MS morphology and HA coating are discussed in the following sections.

1.8.7.1. Effects of PLGA composition on MS morphology

The structure of the PLGA monomers (Figure 1.12) indicates that the lactide, which has two extra methyl groups, is more hydrophobic than the glycolide. Thus, the polymer that contains a higher fraction of lactide is relatively more hydrophobic and should precipitate out of an aqueous environment at a faster rate than those containing higher fractions of glycolide.

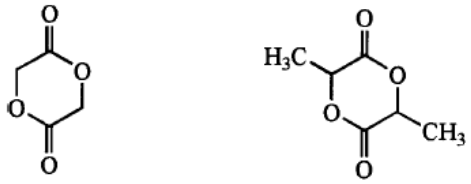

Figure 1.12 Structures of glycolide and lactide

Furthermore, at the same stirring rate in the S/O/W emulsion process, a polymer that precipitates at a faster rate is likely to be composed of bigger size MS. Therefore, using PLGA with higher fraction of lactide, such as 85:15 PLGA, tends to form bigger MS at the same fabrication condition.

1.8.7.2. Effects of internal oil: aqueous phase ratio on MS morphology

The microsphere size is partly controlled by the extraction rate of dichloromethane (DCM) into the aqueous phase and the evaporation rate of DCM from the aqueous phase. With a high aqueous phase ratio, more DCM will be extracted to the aqueous phase in a short time and evaporate quickly after transferring the oil phase to the aqueous phase. The results in faster precipitation of the microdroplets, which will finally result in bigger hardened MS [29].

1.8.7.3. Effects of surfactant concentration on MS morphology

At high surfactant concentration, smaller microdroplets will be well stabilized by the emulsifier, and the tendency for microdroplets to coalesce to form bigger droplets is very low. Xu *et al* [168] reported that microsphere sizes decreased from 34.9 to 12.1 μm with an increase of surfactant SDS concentration from 0.1% to 2%. Some MS aggregated when using 0.1% SDS, probably because the SDS concentration is too low to stabilize the microdroplets and some coalescence occurred.

1.8.7.4. Effects of the infiltration pressure of the aqueous solution on MS morphology

In the S/O/W method, leakages of hydrophilic drugs usually happen when transferring the S/O emulsion into the aqueous solution, where the hydrophilic drugs will diffuse through the polymer/organic phases into the aqueous solution. Salt, such as NaCl and KCl, have been used to improve the infiltration pressure of the external aqueous solution to suppress the drug migration [171]. However, when adding NaCl into the

external aqueous phase with SDS or DSS as the surfactant to reduce the drug leakages, PLGA microdroplets aggregated immediately [168]. This is presumable because NaCl changed the [Na^+] balance in the aqueous phase and inhibited the ionization of DSS and SDS. In aqueous solution there is one ionization balance: SDS ↔ $C_{12}H_{25}S0_4^-$ + Na^+ and only 30% SDS can be ionized to act as surfactant [172]. $C_{12}H_{25}S0_4^-$ is the real functional group of SDS. When adding NaCl which is almost completely ionized in water, [Na^+] will be increased and hence inhibit SDS ionization. Therefore the application NaCl or KCl to inhibit drug leakage is greatly dependent on the surfactants in the external aqueous solution.

1.9. **Summary**

The review outlines basic knowledge and technologies related localized bone drug delivery devices with to HA coating and porous MS as injectable cell scaffolds. It also includes main bone diseases and their therapies, various properties of PLGA, the fabrication techniques of conventional PLGA MS for drug delivery and porous PLGA MS for injectable cell therapy, heparin coating methods and their applications, HA properties and methods for HA coating, and fabrication parameters of negatively charged PLGA MS. HA coated PLGA MS have very promising clinical applications because these composite materials can mimic the natural hard tissue and deliver the therapeutic to special sites in the bone system. By introducing porous structure and surface modification by bioactive molecules such as heparin, porous PLGA MS can be utilized as multi functional devices for drug delivering injectable cell scaffolds.

In the rests ot the thesis, Chapter 2 developes a rapid HA coating method for PLGA

microspheres by using a FDA approved anionic surfactant dioctyl sodium sulfosuccinate, which introduced high negative charges on the microsphere to induce HA precipitation. Various fabrication parameters were investigated for their effects on microsphere morphology and HA coating. The HA coated PLGA microspheres worked as dual drug delivery devices by encapsulating antibiotics inside the polymer core and binding proteins on the outside HA shell. The HA coating enhanced cell adhesion and proliferation.

Chapter 3 investigates three different approaches, including osmogen, extractable porogen and gas-foaming porogen, to fabricate porous microspheres for injectable cell delivery. Covered porous microspheres (all surface pores covered by a thin skin layer) were fabricated by a modified ammonium bicarbonate gas-foaming method. NaOH surface modification can turn the covered porous microspheres into open porous microspheres, and control the open pore size and porosity on the microsphere surface by hydrolysing the skin layer. The porous microspheres with controllable surface porosity are desirable microcarriers as injectable scaffolds for cell delivery.

In Chapter 4, heparin was immobilized on the above open porous PLGA microspheres by a lay-by-layer assemble process to fabricate drug delivering injectable cell scaffolds. Heparin coated porous microspheres improved cell adhesion, viability, proliferation, spreading and osteogenic differentiation measured by an increased alkaline phosphatase (ALP) activity over 16 days.

Chapter 5 and Chapter 6 present a summary conclusion of the entire thesis and

directions for future work.

2. Chapter 2: HA coated microspheres for localized dual drug delivery

2.1. Introduction

Poly(lactic-co-glycolic acid) copolymer microspheres (PLGA MS) are one of the most widely used biodegradable polymer carriers in the controlled delivery of drug molecules, due to their good cell response, controllable biodegradability, flexibility in fabrications, high drug loading efficiency and controllable drug release profile [50, 51]. The delivered drugs can be small chemical molecules, DNA and proteins [53]. As the apatite stoichiometric similar to the bone mineral, hydroxyaptite $Ca_{10}(PO_4)_6(OH)_2$ (HA) is often used as a substitute material in orthopaedic and dentistry implants. HA can also be used as drug delivery devices for various cytokines and proteins with bone therapeutic targeting, and as filling materials for chromatographic protein separations due to its strong binding and release of various proteins [49].

Antibiotic loaded PLGA MS with HA nanocrystal coating (HPLG MS) have been developed in our group to combine the advantages of controlled release from PLGA MS and osteoconductivity from HA [58]. A modified constant composition method [173] was used to grow continuous HA nanocrystals on negatively charged PLGA MS surface in 3 hours. The method is much quicker than the traditional Kokubo biomimetic method which requires 7-21 days to grow HA on polymer [148, 149]. The biomimetic method requires pre-hydrolysis of the polymer, immersing the polymer into simulated body fluid (SBF) which has ion concentrations similar to those of human blood plasma, and exchanging the SBF every day at physiological temperature

37^{o}C and pH at 7.4 [150, 151]. Although the modified constant composition method [58] is much quicker, a toxic anionic surfactant- sodium dodecyl sulfate (SDS) (Figure 1.11) was required in the solid-in-oil-in-water (S/O/W) emulsion method [53-55] to fabricate PLGA MS with high negative surface charge. Therefore, non-toxic anionic surfactants suitable for applications in the human body are needed to prepare negatively charged PLGA MS and the resultant HPLG MS.

In this study, an FDA approved anionic surfactant- dioctyl sodium sulfosuccinate (DSS) (Figure 1.11) was investigated as an alternative substrate to fabricate negatively charged PLGA MS and its ability to induce rapid HA coating by the modified constant composition method. DSS has already been used as an inactive ingredient in licensed injectable products [169] and as a surfactant to prepare anionic microparticles for vaccine delivery [155-160]. Various formulation parameters such as DSS concentration, HA coating time, polymer type and drug type have been also evaluated when using DSS as the surfactant.

Bisphosphonates (BP) are a class of drugs used clinically for the treatment of bone loss [174, 175]. Due to the poor metabolic adsorption, side effects of over suppression of bone metabolism and strong target binding to HA [174, 175], localized BP delivery is a very promising application of the HPLG MS. Thus, alendronate (AL), one type of BP was investigated as the model drug alongside the antibiotic, vancomycin hydrochloride (VMC) (Figure 2.1) to fabricate HPLG MS.

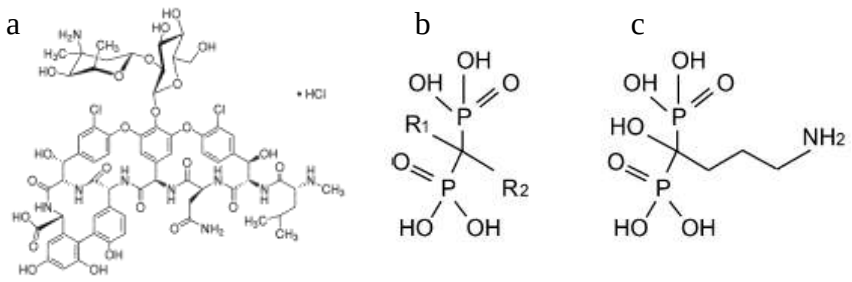

Figure 2.1 Chemical structures of (a) vancomycin, (b) general structure of bisphosphonates and (c) alendronate [176]

Proteins are very susceptible to proteolytic degradation which results in low loading efficiency and decreased bioactivity when encapsulated into PLGA MS for localized delivery [53-55]. Therefore, the HA coating on HPLG MS was evaluated as a substrate for the binding and sustained release of model protein- lysozyme. The HA coating can also buffer the pH decrease induced by later PLGA degradation [162]. The cell response study of this new HPLG system was primarily investigated by the initial attachment and spreading of 2T3 mouse osteoblasts.

2.2. **Materials and Methods**

2.2.1. Materials

PLGA copolymer (50:50 PLGA, Mw 50K, viscosity 0.55 dL/g; 85:15 PLGA, Mw 92.5K, viscosity 0.64dL/g; both with ester-end) was supplied by Birmingham Polymers Inc. (AL, USA). Vancomycin hydrochloride (VMC), alendronate (AL), sodium dodecyl sulfate (SDS), dioctyl sodium sulfosuccinate (DSS), dichloromethane (DCM) and lysozyme were all purchased from Sigma (Dorset, UK). Commercial HA (Captal®60-1) is supplied by Plasma Biotal, UK. Calcium nitrate, potassium chloride, potassium hydroxide, and potassium dihydrogen phosphate were all provided by BDH

(Poole, UK). PBS and αMEM culture medium were from BioWhittaker (Lonza Wokingham, UK).

2.2.2. Fabrication of PLGA MS with different formulation parameters

Drug loaded PLGA MS were prepared by the modified solid-in-oil-in-water (S/O/W) method [53] using anionic surfactants SDS or DSS (Figure 2.2). 50mg drug powders (VMC or AL) (solid phase) were dispersed in 2 ml DCM (oil phase) with 200 mg PLGA (50:50 or 85:15 PLGA) by sonication (Kerry ultrasonics Ltd., UK) at 100W for 1 minute (10 second working and 10 second rest) in an ice-water bath. The s/o dispersion was homogenized in 10 ml 1% (v/v) SDS or DSS solutions (different concentration at 1%, 0.5% or 0.2% (v/v) at 6500 rpm using a Turrax IKA T18 basic homogenizer (IKA works Inc., USA) at room temperature for 30 second. The S/O/W emulsion was subsequently re-emulsified in the extra 90 ml SDS or DSS solutions and stirred for 3 hours to evaporate the organic solvent DCM. The resultant PLGA MS were harvested by centrifugation at 3000 rpm (Heraeus Labfuge 200, Germany) and washed three times with distilled water.

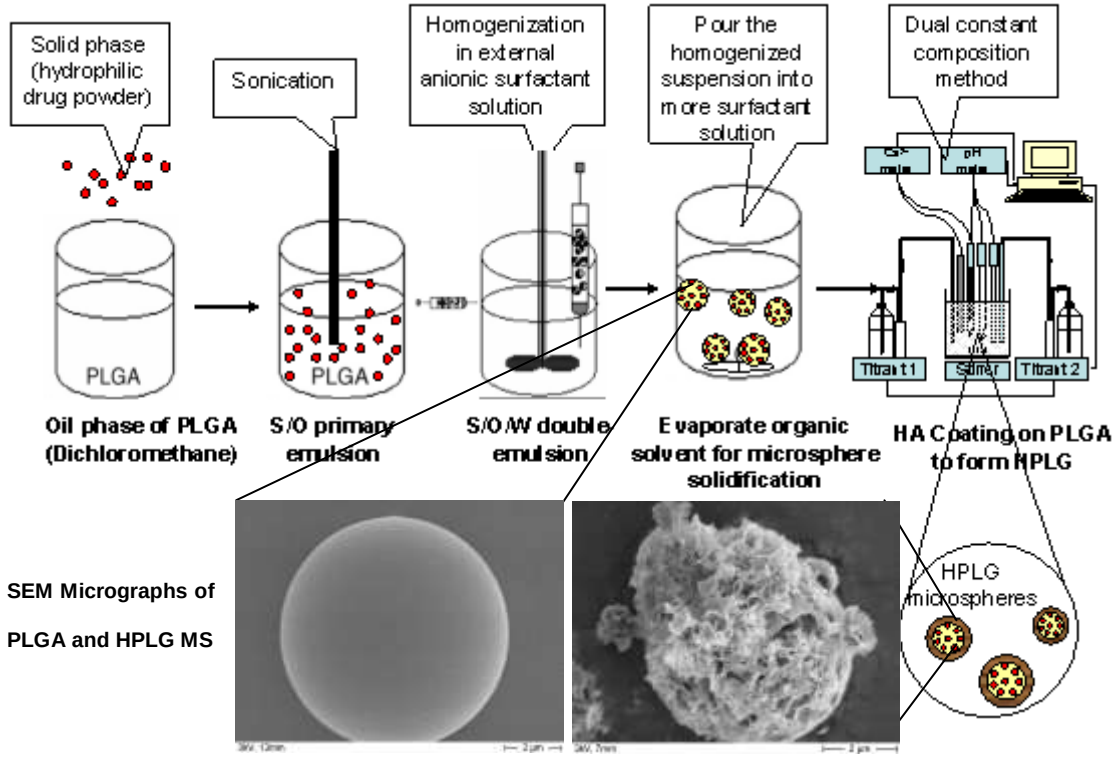

Figure 2.2 A schematic diagram of PLGA MS fabrication by the S/O/W method and HA coating by the constant composition method

2.2.3. HA coating on drug loaded PLGA microsphere

HPLG MS were prepared by the recently developed dual constant composition method [177]. The analytic grade chemicals, 2.362g $Ca(NO_3)_2.4H_20$ (M_w=236.2g M^{-1}), 1.361g KH_2PO_4 (M_w=136.09g M^{-1}), 0.561g KOH (M_w=56.11g M^{-1}) and 10.11g KNO_3 (M_w=101.1g M^{-1}) were individually dissolved into 100ml of ultra-pure water to form 0.1M solutions of $Ca(NO_3)_2$ (pH 6.29), KH_2PO_4 (pH 4.56), and KOH (pH 12.67), and 1M KNO_3 (pH 6.46). A working solution supersaturated with respect to calcium phosphate and two concentrated titrants were prepared with the compositions in Table 2.1. The working solution with Ca/P molar ratio of 1.67 (the stoichiometric Ca/P ration of HA) was prepared by mixing 10 ml of 1M KNO_3, 2.5 ml of 0.1M $Ca(NO_3)_2$,

and 1.5 ml of 0.1M KH_2PO_4 into 80 ml water. KOH was added to adjust the pH to the required value 7.4 and water was added to dilute the final working solution to 100 ml. Calcium titrant was prepared by mixing 2.5 ml of 0.1M $Ca(NO_3)_2$, 1 ml of 1M KNO_3, and 6.5 ml water. Additionally, phosphate titrant preparation consisted of mixing 1.5 ml of 0.1M KH_2PO_4, 1 ml of 1M KNO_3 and 5 ml of 0.1M KOH with 2.5 ml water.

Table 2.1 Composition of the working and titrant solutions

Solutions	**$Ca(NO_3)_2$ (mM)**	**KH_2PO_4 (mM)**	**KNO_3 (mM)**	**KOH (mM)**	**pH**
Working solution	2.5	1.5	100	10	7.4
Calcium titrant	25	0	100	0	5.53
Phosphate titrant	0	15	100	50	12.16

For the HA coating process, a freshly prepared PLGA MS with negative surface charge were suspended in 80 ml distilled water before adding 10 ml 1M KNO_3 and 2.5 ml 0.1M $Ca(NO_3)_2$ at 37^{o}C. After stirring for 10 minute to allow the Ca^{2+} to attach to the microsphere surface, 1.5 ml of 0.1M KH_2PO_4 was added to form the supersaturated working solution to induce the precipitation of hydroxyapatite. After another10min incubation, 0.1M KOH was added drop by drop to increase the pH to the required value of 7.4. A radiometer PHM85 pH meter and a radiometer ION85 ion analyzer were connected to a computer for automatic monitoring. pH was measured with Radiometer GK2401 combined with glass pH electrodes, which were stabilized by standard buffer solutions (pH4 and pH7 at 37 ^{o}C). The onset of HA precipitation around PLGA MS resulted in a drop of pH which triggered the simultaneous addition of two titrants from the two autoburettes (Radiometer ABU91 Triburete) to maintain the concentration of lattice ions constant (Figure 2.2). After 1.5 or 3 hours, the HPLG

MS were collected by centrifugation, washed three times with distilled water, and freeze-dried (MicroModulyo, EC Apparatus Inc., USA).

2.2.4. Adsorption of model proteins onto the HA coating

5mg freeze dried HPLG MS were immersed in a tube of 1.5ml 1×PBS solution containing 500 µg/ml model protein, lysozyme, at 37^{o}C for 4 hours. In order to avoid the system error of lysozyme absorbed on the tube, the tube was washed by the same 500µg/ml lysozyme PBS solution before the test. The MS were then harvested by centrifugation, washed with distilled water and freeze dried for microcharacterization. The amount of lysozyme in the supernatant was measured by BCA protein assay (Pierce, IL). Three parallel experiments were carried and results were presented as means and standard deviations. The protein loading efficiency was calculated as:

$$\text{Efficiency} = 1 - Ls/Lt \quad \text{- Equation 2.1}$$

Where *Ls* is the lysozyme content in supernatant after adsorption and *Lt* is the total lysozyme content.

2.2.5. Microcharacterization of HA coated MS

2.2.5.1. Scanning electron microscopy

Morphological characteristics of MS were examined by scanning electron microscopy (SEM; JEOL JSM 840F) at an accelerating voltage of 3 kV. To reduce charging effects, the samples were coated with platinum on Cressington sputter coater HR208 with MTM-20 thickness controller (Watford, UK). The average MS size were calculated by using image analysis software Image J (Public Domain, National Institute of Health, USA) to analyze the SEM micrographs of over 20 MS. HA crystal

size and other sample sizes on the SEM images were all analyzed by Image J too.

2.2.5.2. Surface charge measurement

The surface charges on PLGA and HPLG MS were examined by measuring their zeta-potentials in distilled water on a Zetasizer Nano (Malvern Instruments Ltd., UK). The MS were suspended in 10 ml water by vortex to form stable dilute suspensions, and then they were injected into the U shape clear dispersible zeta cell. The measurements were carried out at 25 ^{o}C, 2.00 mm position, with attenuator 8-11. Three replicates were conducted for each sample, and for each replicate 30 zeta runs were recorded. The zeta-potential in aqueous systems is not a size dependent parameter according to manufactures' guide, and the most important thing is that the suspension should be stable during measurement. To produce a stable suspension, thorough vortex before measurement was carried out.

2.2.5.3. X-ray diffraction

X-ray diffraction (XRD) analysis is a mean of characterising crystallographic properties of powder materials, such as crystal size, phase and texture. A monochromatic X-ray beam generated from the source was applied on the sample at specific angles, and the diffracted intensity of the X-rays of specific lattice planes of the crystals was then collected. XRD patterns were obtained on a Siemens D5000 diffractometer operated at 40 kV and 40mA with Cu *Ka* radiation in the 2θ range of 5-60^{o}. X'Pert HighScore software was used to obtain the values for the Bragg angle and the associated peak full width at half maximum peak intensity (FWHM). Assuming there is no broadening due to lattice strain and a Gaussian-type line profile to the peak,

the crystallite thickness (t) in the [002] direction was calculated by the Scherrer equation:

$$t = \frac{k\lambda}{B\cos\theta} \quad \text{-- Equation 2.2}$$

Where k is a constant and assumed to be 0.89, λ is the wavelength of the X-ray (0.15418 nm for Cu radiation), B is full width at half height (FWHM) modified by removing broadening due to instrumental effects, and θ is the Bragg angle of the (002) peaks. The crystallite thickness is an average size measured in the direction perpendicular to the surface of the specimen.

2.2.5.4. Attenuated total reflection infrared spectroscopy

Attenuated total reflection infrared (ATR-IR) spectroscopy was performed on the freeze dried sample powders on a Perkin-Elmer Spectrum 2000 Explorer FTIR spectrometer (Spectrum 2000, Perkin Elmer Ltd., UK). ATR-IT is used to determine the chemical bonds of a material and their state of vibration (bending, stretching, or contracting). The absorbance of the infrared light by specific bonds at specific wavelengths (wavenumbers) is measured against a background spectrum. 15 scans over the range of 500-1800 cm^{-1} were performed at a resolution of 2 cm^{-1} with the background scan subtracted. As the extinction ratio values of the carbonate band at 1420 cm^{-1}(E_{1420}) and the phosphate band at about 563 cm^{-1}(E_{563}) is linearly related to the carbonate percentage of HA, the carbonate percentage in of HA was calculated by the following equation with an accuracy of ±5% [178]:

$$CO_3^{2-} \text{ weight content in HA} = 17.4\ E_{1420} / E_{563} + 0.4 \quad \text{-Equation 2.3}$$

2.2.5.5. Raman spectroscopy

The formation of hydroxyapatite on HPLG MS surface was also investigated with a Raman Station 400F Spectrometer (Perkin Elmer Ltd., UK). The Raman spectra were obtained by accumulating 60 scans with a resolution of 4 cm^{-1} in the spectral range of 200–1150 cm^{-1}.

2.2.5.6. Energy-dispersive X-ray spectroscopy

Energy-dispersive X-ray spectroscopy **(**EDX) was carried out using environmental scanning electron microscopy (ESEM; Zeiss's EVO LS 15) with an INCA EDX at 10 kV to analyze the MS surface element and Ca/P ratio of the HA coating.

2.2.5.7. Thermogravimetric analysis

Thermogravimetric analysis (TGA) of PLGA and HPLG MS was performed on a Pyris 1 TGA thermal analyser (Perkin Elmer, UK) to measure HA coating content. Samples of about 5 mg were heated in a platinum crucible from 30 to 400^{o}C at 10^{o}C/min under the air flow (20ml/min). The resultant particles were collected for SEM micrograph to analyze the morphology.

2.2.6. Model drug - VMC encapsulation efficiency

VMC, a large antibiotic molecule (3.2 x 2.2 nm) used in treating osteomyelitis, was studied as a model drug encapsulated in the HPLG MS for controlled release. The drug content in HPLG MS and encapsulation efficiency were measured after extraction of the drug from the MS. 20 mg VMC loaded MS were dissolved in 2 ml dichloromethane and subsequently 5 ml of PBS was added. The mixture was vortexed

at 2500 rpm for 1 min and then for a further 2 hours at 1000 rpm at room temperature. VMC had a stable light absorption at 280nm [179, 180]. After centrifugation at 10,000rpm, the VMC content in the supernatant was analyzed by a UV/Vis spectrophotometer (JASCO V-570, Tokyo, Japan) at a wavelength of 280 nm with PBS as reference. Drug content was determined by comparison with a standard curve of VMC solutions in PBS with concentration between 0.001 to 0.1 mg/ml. Three experiments were conducted concurrently and results were presented as means and standard deviations from the three replicates.

The drug encapsulation efficiency is calculated as follows:

$$\text{Encapsulation efficiency} = Da / Dt \qquad \text{- Equation 2.4}$$

Where *Da* is the actual drug encapsulated in MS and *Dt* is the initially total drug used in the fabrication.

2.2.7. *In-vitro* drug release

In-vitro VMC release from HPLG MS was performed in a Haake SWB25 shaking bath (Karlsruhe, Germany) at 80 rpm and 37^{o}C. 20mg of drug-loaded MS were enclosed in dialysis membrane (Sigma, Dorset, UK) with 1 ml of PBS (pH 7.4) and then incubated in a conical flask containing 10 ml PBS. The apparatus was incubated in the shaking bath and the PBS was changed completely at each measurement interval. The amount of VMC released at certain set times was determined by UV/Vis spectroscopy at 280 nm (with PBS as reference).

2.2.8. The degradation analysis of PLGA MS

The degradation analysis of PLGA MS was performed by dispersing blank 85:15 PLGA MS in 10 ml medium of PBS (pH 7.4) at a Haake SWB25 shaking bath (Karlsruhe, Germany) at 80 rpm and 37 ^{o}C. After 21 days, the PLGA MS were collected by centrifugation and freeze dried for morphology analysis by SEM.

2.2.9. Cell culture

2T3 mice osteoblasts were kindly provided by the Botnar Research Centre (Oxford, UK). Cells were cultured in alpha modified Eagles medium (α-MEM) supplemented with 10% foetal Bovine serum (FBS) (MB Meldrum Ltd., Buckinghamshire, UK), penicillin 100U/Ml and streptomycin 100ug/ml(final concentration). Cell culture was conducted in T75 flasks (Falcon, BD biosciences, UK) using a humidified incubator (Heraeus instruments 6000) gassed with 5% CO_2 in air at 37^{o}C. The culture medium was replaced with fresh α-MEM containing 10% FBS every 3 days. Once the cells have grown to 70-80% confluency, the T75 flasks were rinsed twice by 10 ml of PBS, and then incubated in 5 ml of trypsin/EDTA solutions to detach the cells. 5 ml of 10% FBS solution was added to quench the trypsinisation reaction. Cells were centrifuged at 1000 rpm for 5 mins and finally dispersed in fresh α-MEM with 10% FBS. 20µl cell suspension was collected for counting cell numbers by the disposable counting chambers (Fast Read 102, ISL, Paignton, UK). The cells were then transferred to new flasks for subculture or experiments on MS samples.

10 mg freshly prepared drug-free PLGA MS and HPLG microsphere were sterilized by γ-radiation and dispersed in 500 µl α-MEM with 10% FBS. 50µl of the dispersion

(1mg of samples) was added into each well of 96-well cell culture plate (CCT). 1×10^5cells were gently added onto the MS in each well (1×10^5cells/well). The cells were fed with 250µl α-MEM with 10% FBS for each well. Cells seeded on the plate surface were used as the control.

2.2.10. Cell seeding efficiency and cell proliferation

Cell seeding efficiency and cell proliferation was evaluated using the Alamar Blue™ assay (BioSource Europe, Belgium). Alamar Blue™ assay kit contains a solution of REDOX indicator, which is a non-toxic indicator for viable cells. It can both fluoresce and change colour upon chemical reduction due to the normal cellular metabolism. The allows for the determination of viable cell number relative to the control group with known cell numbers. At certain time scales (day 1 and 3 after seeding), cell culture medium was replaced with fresh serum-free α-MEM containing 5% Alamar blue (BioSource Europe, Nivelles, Belgium) and incubated at 37 °C for 2 hours. The relative fluorescent units of cell-degraded Alamar blue was measured on a SPECTRAmax GEMINI microplate spectrofluorimeter (Molecular Devices, Berks, UK) at an excitation wavelength of 530 nm and an emission wavelength 590 nm, with a cut-off at 570 nm. The amount of absorbance is proportional to the number of viable cells and corresponds to the cells metabolic activity.

2.2.11. Statistical analysis

Experiments were repeated three times and results were presented as means and standard deviations. Results of cell proliferation were evaluated by one way analysis

of variance (ANOVA) in combination with Fisher's test and were considered as statistically significant at $p < 0.05$.

2.3. **Results**

2.3.1. HA coated microspheres (MS) fabricated by different parameters

2.3.1.1. Effect of anionic surfactant on MS morphology and HA coating

The MS morphology and surface charge are dependent on the characters of surfactant in the external water phase of the S/O/W emulsion process. SDS emulsified MS were shown smooth surface with some PLGA segments adsorped on the surface (Figure 2.3a, b). Compared with SDS, which is normally used in household products, FDA approved anionic surfactant DSS made the 85:15 PLGA MS much smaller (average size 6.2±3.1 μm) than those emulsified by SDS (21.1 ± 8.7 μm) (both with model drug VMC loaded) (Figure 2.3). This indicates that DSS has stronger emulsification ability than SDS. DSS emulsified PLGA MS were also shown smooth surface without any pores (Figure 2.3d).

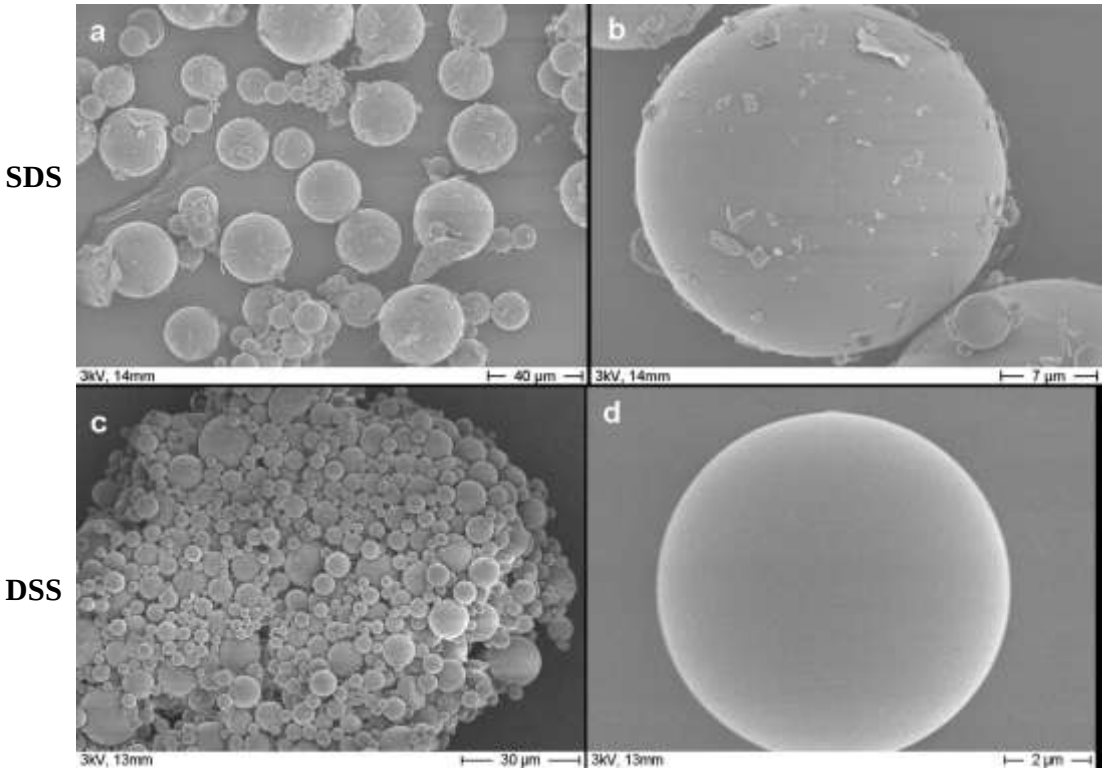

Figure 2.3 SEM micrographs of PLGA MS made by different anionic surfactants 1% SDS (a, b), 1% DSS (c, d). DSS has stronger emulsification ability than SDS which reduced the MS size from 21.1 ± 8.7 µm to 6.2±3.1 µm.

The zetal potential of PLGA MS emulsified by SDS and DSS were quite similar (Figure 2.4) and suggested that the particles were both highly negatively charged. These high negative charges may result from the functional groups of sulfate ($-OSO_3^-$, SDS) and sulfonate ($-SO_3^-$, DSS) absorbed on the PLGA microdroplets' surfaces during the external emulsion process. In contrast, the surface charge of PLGA MS, emulsified by the most widely used nonionic surfactant PVA, were at only -17.7 ± 1.5 mV in the S/O/W method [51].

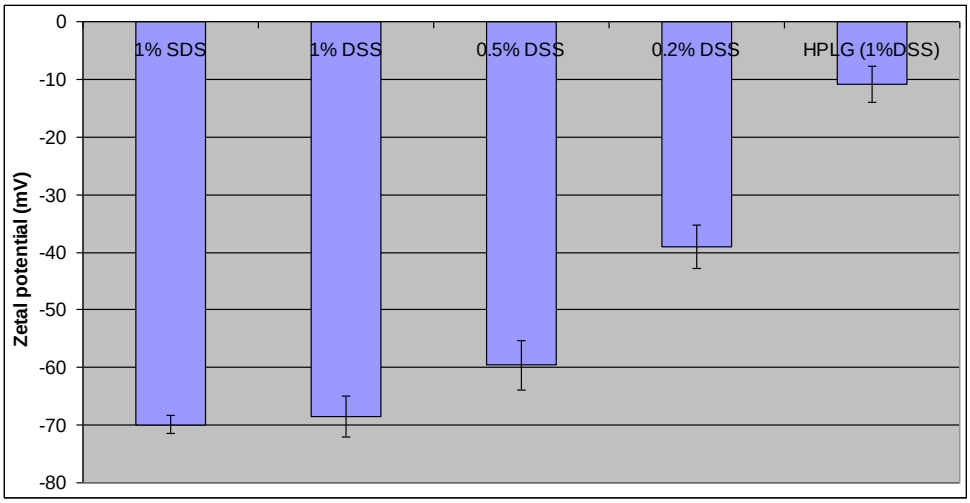

Figure 2.4 Zetal potential of PLGA MS emulsified by 1% SDS and DSS with varying concentrations, and HPLG MS emulsified by 1% DSS. Zetal potential dropped with decreasing DSS concentration and after HA coating.

The above PLGA MS were treated by the constant composition method to grow HA nanocrystals based on the following equation:

$$10\ Ca(NO_3)_2 + 6\ KH_2PO_4 + 2\ H_2O \rightarrow Ca_{10}(PO_4)_6(OH)_2 + 6\ KNO_3 + 14\ HNO_3$$

- Equation 2.5

The precipitation of HA decreased the pH which triggered the addition of calcium and phosphate titrants from 2 autoburettes to raise the pH back to 7.4 to maintain the reaction solution at a constant high supersaturation with fixed Ca/P ratio 1.67 with respect to HA [173].

After 3 hour reaction in the constant composition process, the SEM images (Figure 2.5) indicated the MS were both coated successfully with continuous nanocrystallites on the microsphere surface, which exhibited a porous structure of plate-like crystals at the nanometer scale (averaging 20-30 nm in diameter and 80-200 nm in length),

similar to the native bone tissue and bio-inspired mineral grown in SBF [181]. The HA crystals on MS emulsified by DSS exhibited smaller plate sizes than those on MS emulsified by SDS. The zeta potential of PLGA MS emulsified by 1% DSS decreased from -68.5 ± 3.5 mV to -10.9 ± 3.1 mV after growing HA crystal on the surface (Figure 2.4).

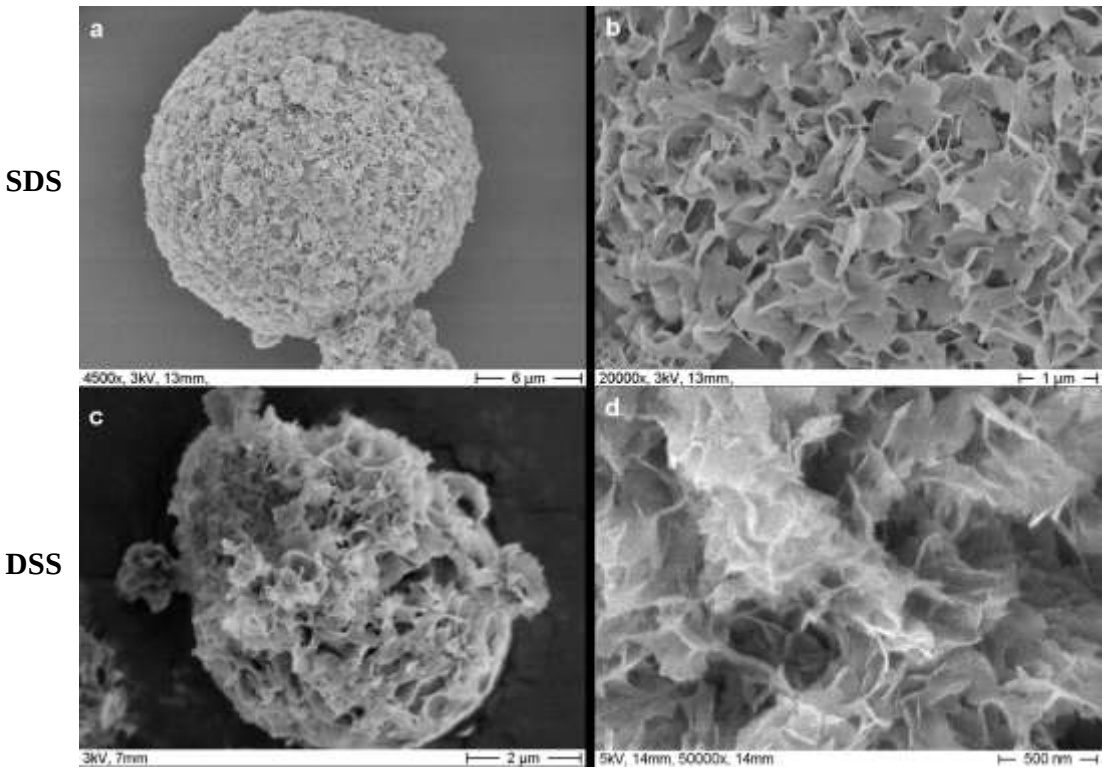

Figure 2.5 SEM micrographs of HA nanocrystals grown on PLGA MS emulsified in (a, b) 1% SDS and (c, d) 1% DSS by the constant composition method

2.3.1.2. Effect of DSS concentration on MS morphology and HA coating

Decreasing DSS concentration from 1% to 0.2%, 85:15 PLGA MS average sizes increased from 6.2±3.1 µm to 18.9±10.2 µm (Figure 2.6) and Zetal potential decreased from -68.5± 3.5 mV to -39.1± 3.8 mV (Figure 2.4). The size variations of PLGA MS emulsified by 0.2% DSS also became wider (Figure 2.6a), showing the surfactant did not emulsify the microdroplets homogenously. The potentially could be

due to the insufficient DSS molecules to disperse PLGA microdroplets and stop them forming bigger droplets in the external emulsification procedure. All MS still possessed a smooth surface.

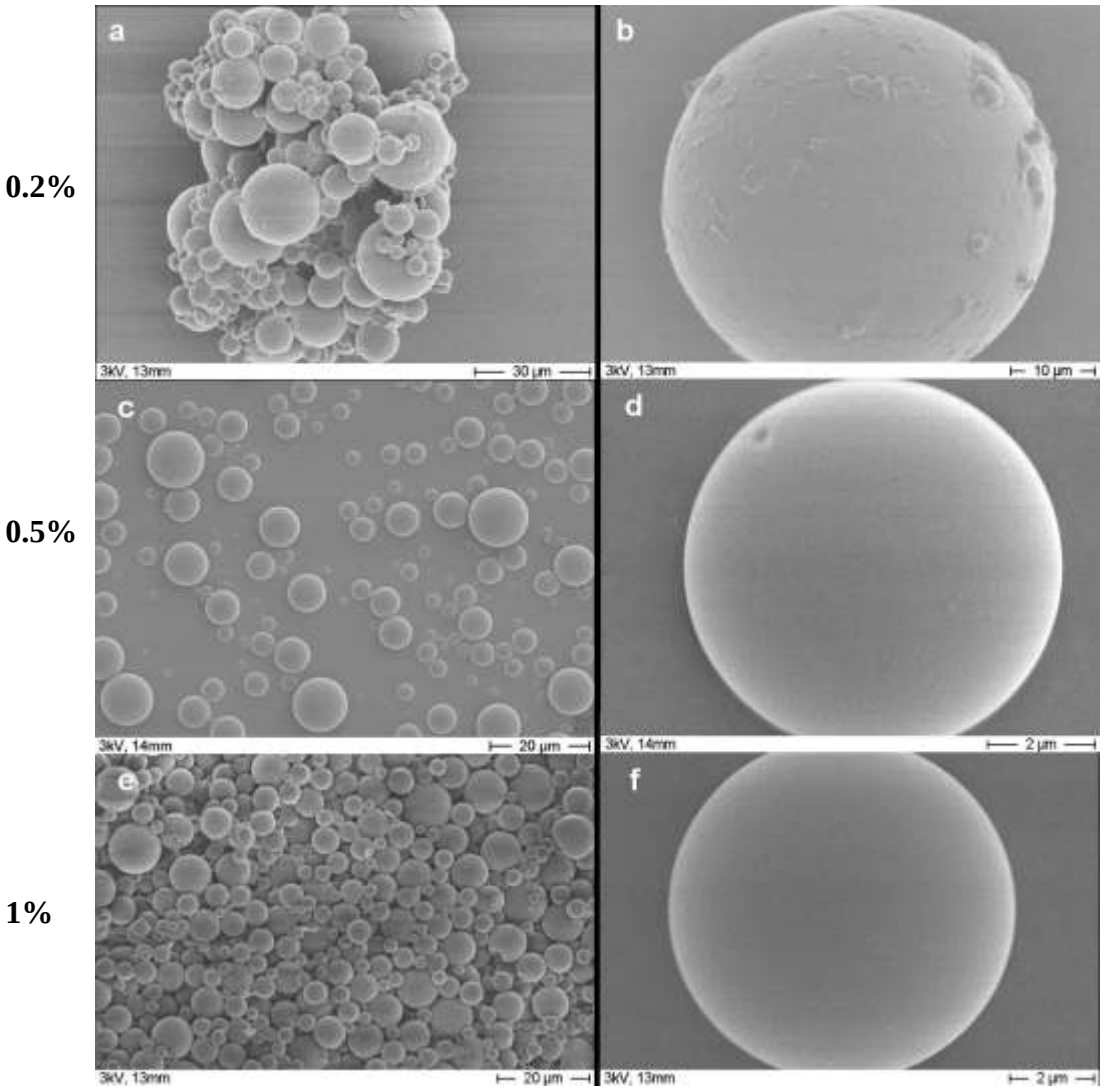

Figure 2.6 SEM micrographs of PLGA MS emulsified by different DSS concentrations: 0.2% (a, b), 0.5% (c, d), and 1% (e, f). Microsphere size decreased with increasing the surfactant concentration.

The ability of varying DSS concentration to induce HA nanocrystals in the constant composition method was also evaluated (Figure 2.7). PLGA MS emulsified by 0.2% DSS induced non-continuous HA coating with islanded HA plate-like nanocrystals (Figure 2.7a, b). The was in accordance with the previous assumption that a low DSS

concentrations could not provide enough polar functional groups $-SO_3^-$ of DSS to cover the whole PLGA MS. The further confirmed the ionized $-SO_3^-$ worked as the nucleation sites on MS surface to capture Ca^{2+} ion accumulation for HA overgrowth [58].

0.5% DSS had already acquired the emulsification ability to distribute PLGA MS homogenously (Figure 2.6c) and enough negative surface charge to induce continuous plate-like HA crystals on MS (Figure 2.7c, d). PLGA MS emulsified by 1% DSS were smaller in size (Figure 2.6e, f), had higher negative surface charges (Figure 2.4), and induced thicker HA coating with larger crystals (Figure 2.7e, f). The indicated the thickness and crystal size of HA coating in the constant composition method increased with more polar functional groups $-SO_3^-$ of DSS absorbed on MS surface.

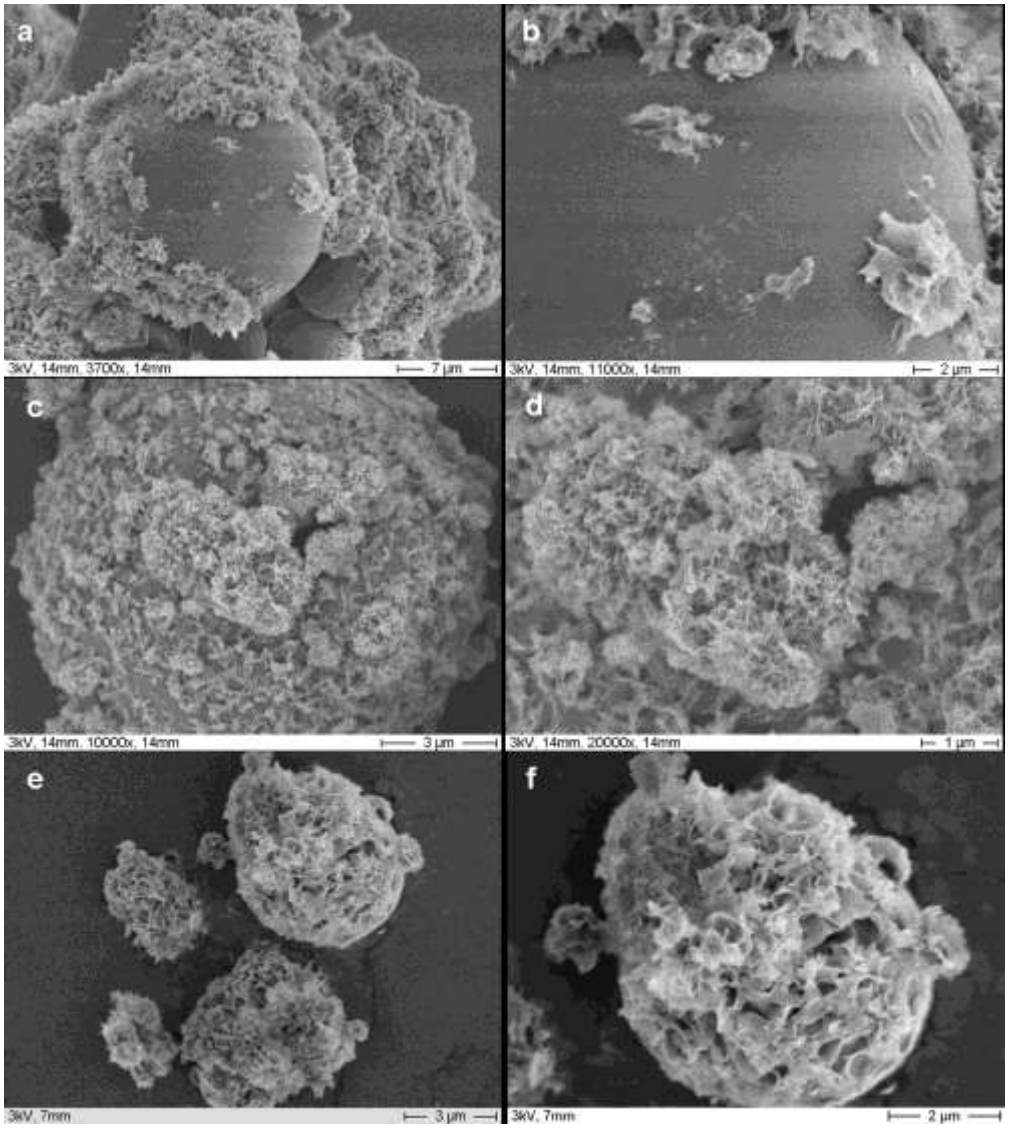

Figure 2.7 SEM micrographs of nanocrystals grown on PLGA MS emulsified by different DSS concentrations 0.2% (a, b), 0.5% (c, d), and 1% (e, f). PLGA MS emulsified by 0.2% DSS failed in inducing continuous and complete HA coating.

2.3.1.3. Effect of HA coating time on the morphology of HA coating

After 1.5h HA coating in the constant composition process, the PLGA MS (emulsified by 0.5% DSS) exhibited scattered, isolated, and small plate-like nanocrystal (Figure 2.8a, b) on its surface suggesting the heterogeneous nucleation of HA. The size of these scattered nanocrystal varied from 100 to 600nm (Figure 2.8b). The large crystals of approximately 600 nm were composed of aggregated small plate-like nanocrystal.

After 3 hour HA coating, continuous large plate-like nanocrystal with big crystal clusters (Figure 2.8c, d) grew on PLGA MS. The result was in accordance with HA crystals grown on PLGA MS emulsified by 1% DSS after 1, 3 and 6 hour reactions [58].

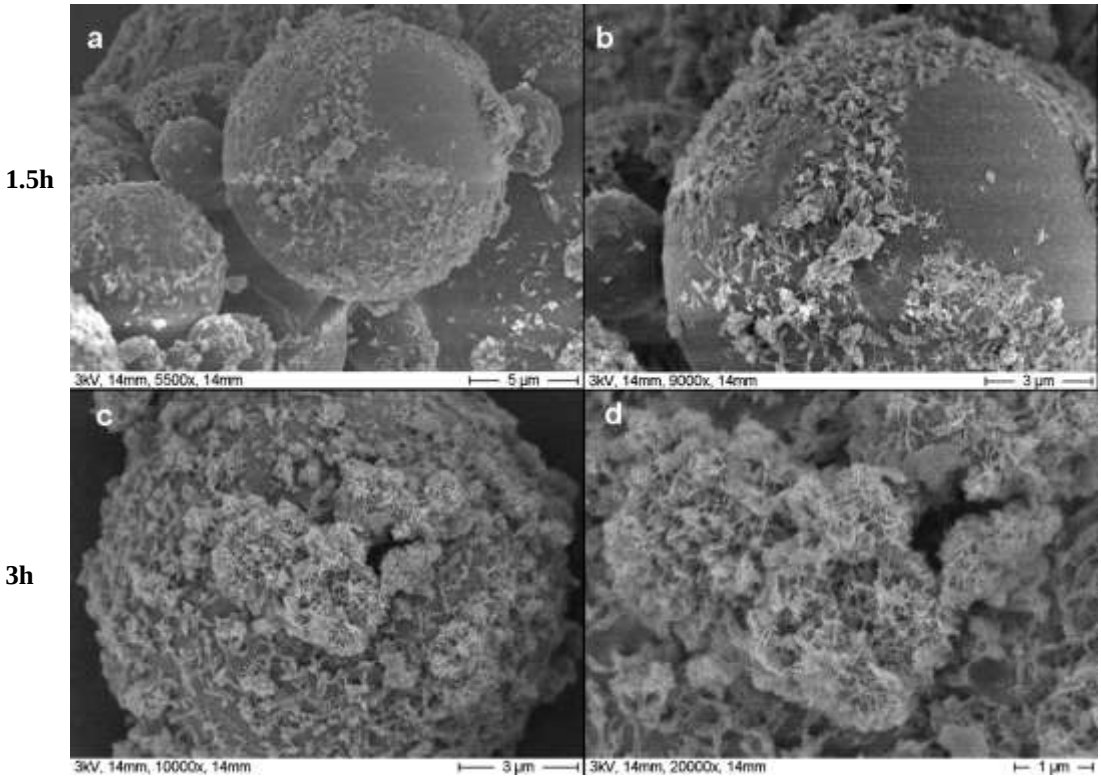

Figure 2.8 SEM micrographs of HA nanocrystals grown on PLGA MS after (a, b) 1.5 hour and (c, d) 3 hour reaction in the constant composition process

2.3.1.4. Effect of PLGA type on MS morphology and HA coating

At the same fabrication condition using 1% DSS, 50:50 PLGA (viscosity 0.55 dL/g) were also used to investigate the effects of PLGA copolymer type on MS morphology and HA crystal coating. The SEM observations (Figure 2.9) showed MS made of 50:50 PLGA had smaller size (average 3.1 µm) than those made of 85:15 PLGA (average 6.2µm).

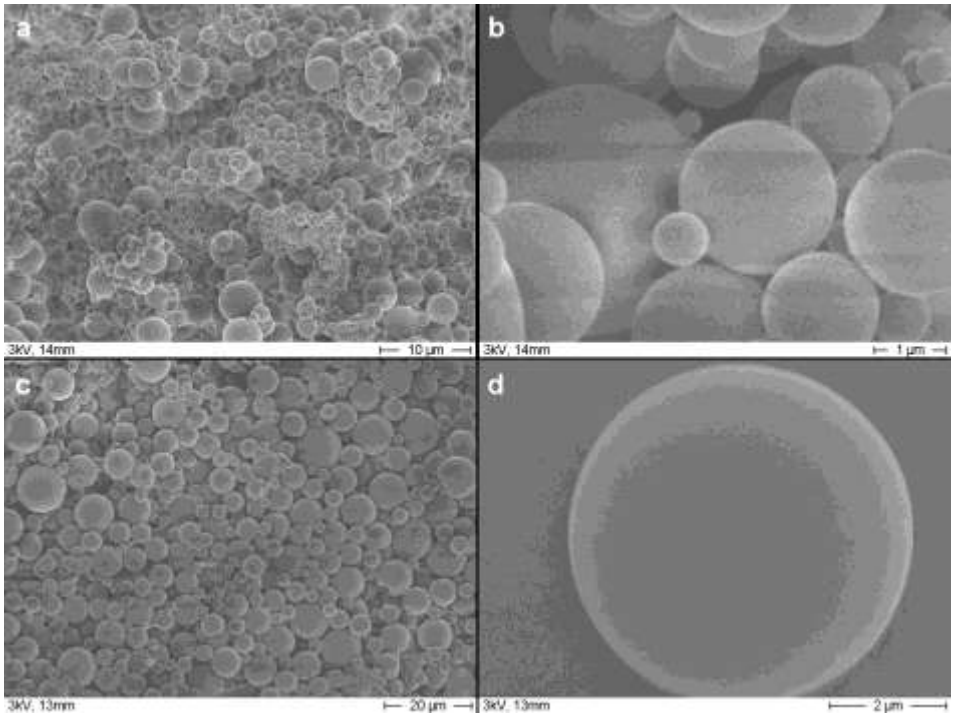

Figure 2.9 SEM micrographs of (a, b) 50:50 PLGA and (c, d) 85:15 PLGA MS. MS made of PLGA with more lactide precipitated faster to form large particles.

After 3 hour HA coating in the constant composition process, 50:50 PLGA MS were successfully coated with the same plate-like HA nanocrystals as those on 85:15 PLGA, but there were many microsphere aggregates (Figure 2.10). HA nanocrystals grew on not only single microsphere surface (Figure 2.10c, d), but also on the surface of big and irregular microsphere aggregates (Figure 2.10a, b).

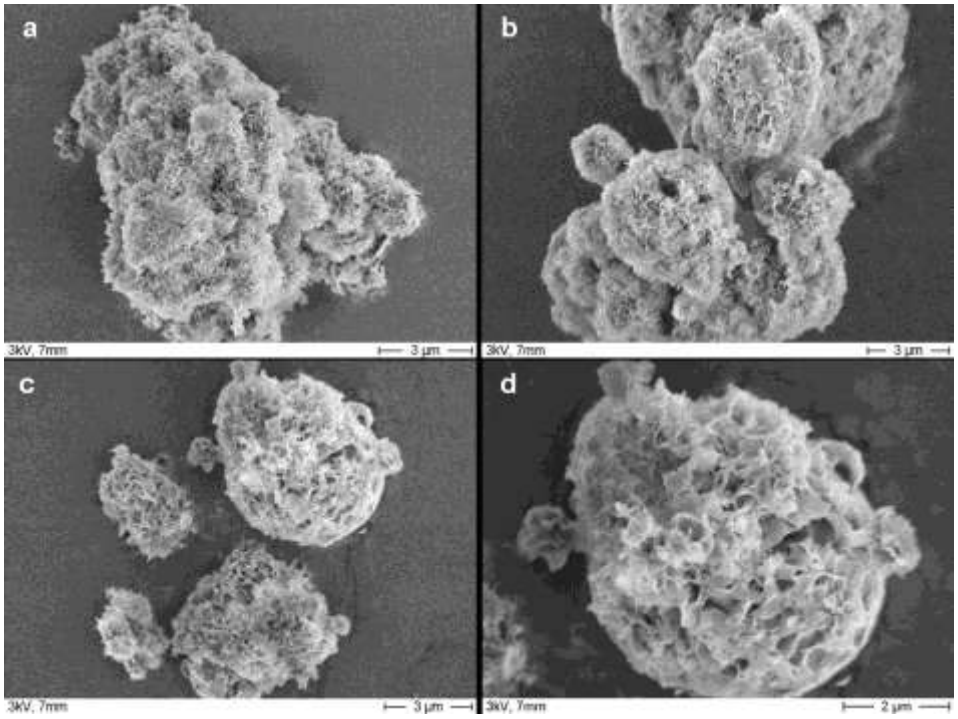

Figure 2.10 SEM micrographs of HA crystal coated (a, b) 50:50 PLGA and (c, d) 85:15 PLGA MS. HA crystals can grow on substrate independent of the substrate shape and size.

2.3.1.5. Effect of drug type on MS morphology and HA coating

Beside the model drug vancomycin (VMC), anti-bone loss drug - alendronate (AL), with strong HA binding ability (Figure 2.1), were also evaluated to fabricate HPLG MS. AL loaded MS (4.8 ±2.3 µm) were smilar in sizt to VMC loaded MS (6.2±3.1 µm). Both MS showed a typical smooth surface (Figure 2.11).

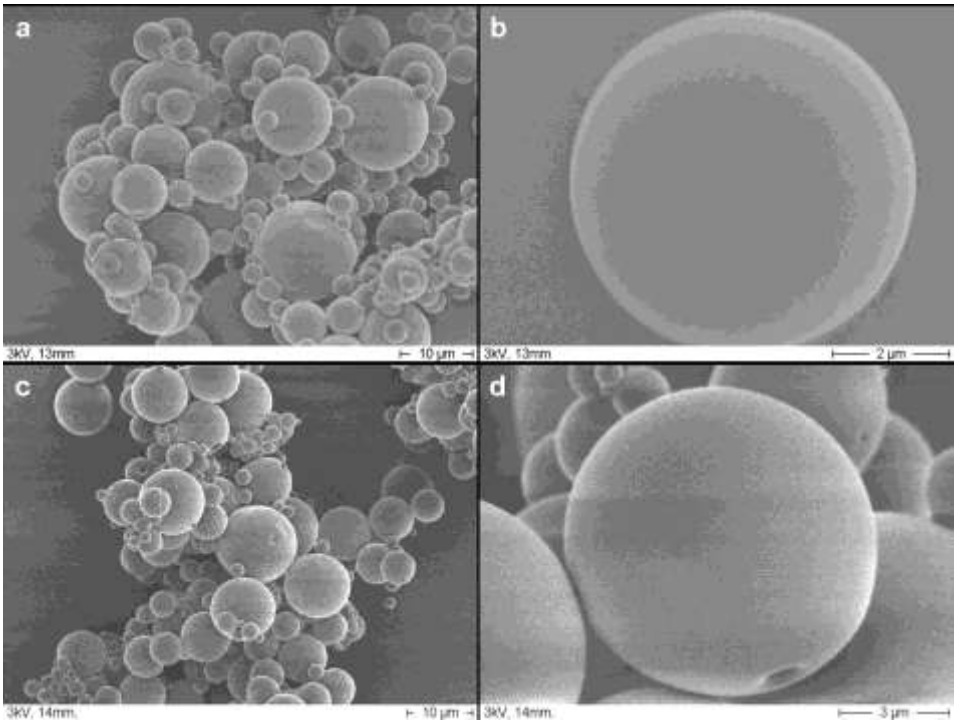

Figure 2.11 SEM micrographs of (a, b) VMC and (c, d) AL loaded 85:15 PLGA MS emulsified by 1% DSS. All MS showed smooth surface.

However, after 3 hour HA coating in the constant composition process, no HA crystals grew on AL loaded MS (Figure 2.12c, d), while VMC loaded MS were completely coated with continuous plate-like HA crystals (Figure 2.12a, b). SEM image in high magnification (Figure 2.12d) showed isolated amorphous Ca-P globules scattered on the surface of some AL loaded MS. The diameter of these globules varied from 60 to 300 nm.

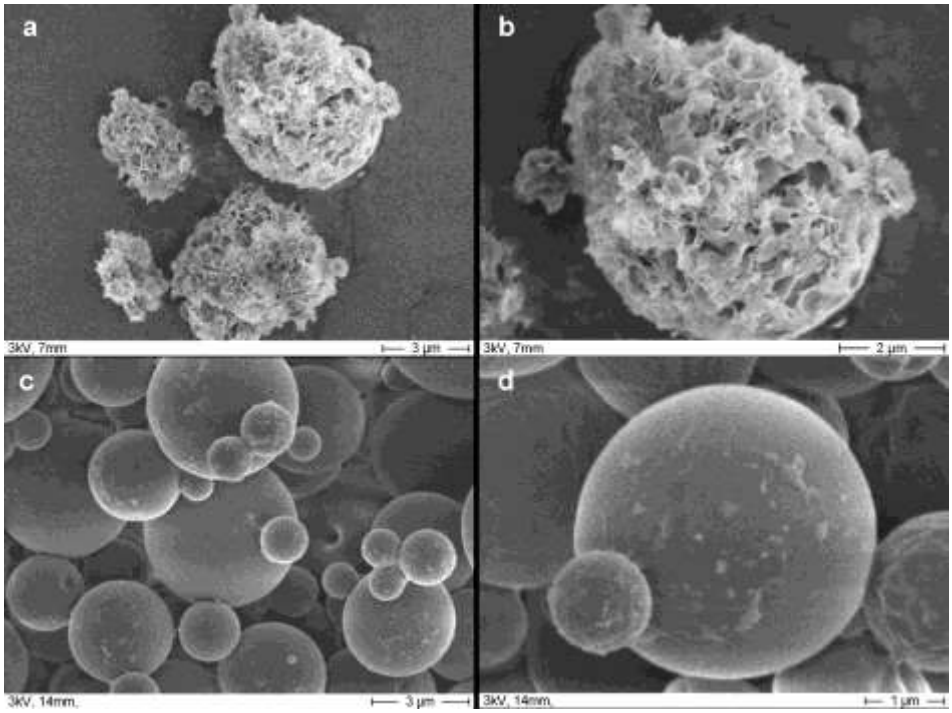

Figure 2.12 SEM micrographs of (a, b) VMC and (c, d) AL loaded MS after 3 hour HA coating process. No HA crystals grew on AL loaded MS.

As the bisphosphonates can bind strongly to hydroxyapatite crystals and inhibit their formation and dissolution [182], it was speculated that a small amount of AL may leak during the 3 hour HA coating process, which inhibited the HA nanocrystal formation.

2.3.2. Model proteins - lysozyme loading efficiency

As several growth factors, such as fibroblast growth factor-2, bone morphogenic proteins, and transforming growth factor β are all basic proteins, lysozyme (isoelectric point 11.1, Ms 14,600 Da, basic protein), which is positively charged (2.53 mV) at physiologic pH 7.4 [183], was used as model protein for evaluating the binding ability of HA coating on HPLG MS. After 4 hour incubation of HPLG MS in the 1.5ml 500 µg/ml 1×PBS solution of lysozyme, the unabsorbed protein content in the PBS

supernatant was measured by comparison with a lysozyme standard curve (Figure 2.13) produced using the BCA assay. The standard curve was measured by the absorbance at a wavelength of 562 nm for lysozyme with known concentration. 73.0±0.3% (547.5±2.25 μg) lysozyme remained in the 1.5ml 1×PBS solution after 4 hour incubation, so the lysozyme adsorption efficiency of HA coating was 27.0±0.3% (202.5±2.25 μg lysozyme on 5 mg HPLG MS). This demonstrates the efficacy and potential of the HA coating shell of HPLG MS to act as a drug delivering matrix.

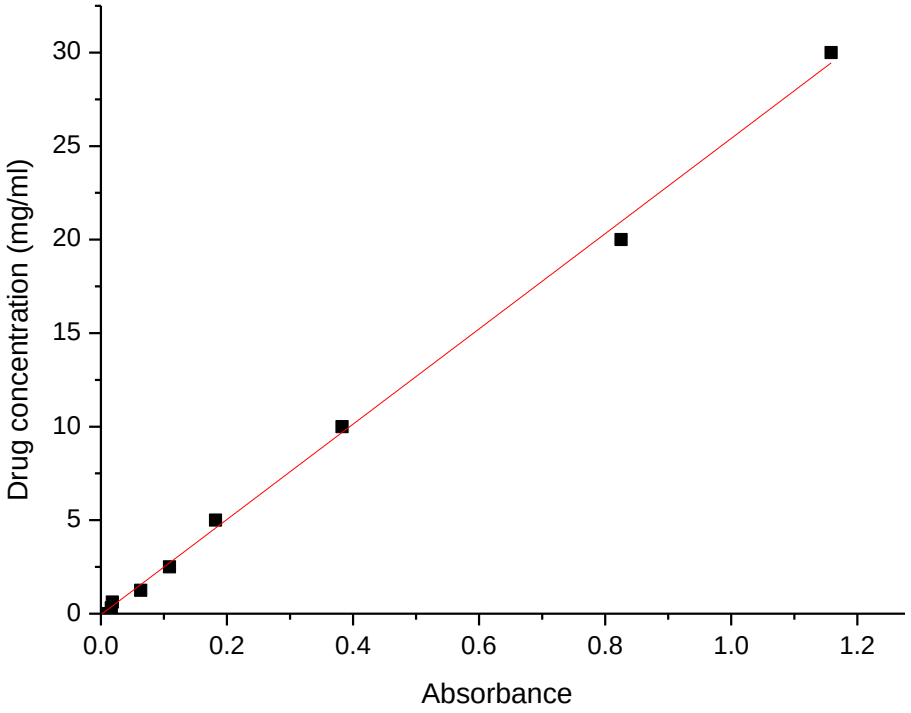

Figure 2.13 Standard Curve for Lysozyme concentration by BCA assay

Lysozyme concentration = 25.466*Absorbance $_{Lysozyme}$ - 0.0538, R^2 = 0.9981
-Equation 2.6

Similar results were reported by Jongpaiboonkit *et al.* [49] who tested the BSA and cytochrome adsorption of mineral coated PLGA MS made in mSBF.

2.3.3. Microcharacterization of MS and HA coating

2.3.3.1. XRD analysis

85:15 PLGA and HPLG MS (1% DSS as surfactant and 3h HA coating) were used for the following analysis. The characteristic diffraction peaks of commercial HA corresponding to the 002, 210, 211, 202, 310, 222, 213 and 411 reflections, can be easily distinguished in the XRD pattern of the composite MS- HPLG MS (marked with * at Figure 2.14). A strong 002 peak is observed at 26.7 corresponding to crystalline HA belonging to the hexagonal symmetry. The average crystal thickness on [002] of the precipitated HA on HPLG (DSS) MS were calculated to be 32.7 nm (Position at 26.7^{o}2θ and FWHM 0.2676^{o}2θ) from the Scherrer equation (Equation 2.2), thicker than the 25.1 nm of HA precipitated using SDS as surfactant [58]. This corresponded to the crystallite dimensions measured by the SEM micrographs (Figure 2.5). The broadening of 211 and 300 peaks are typical of calcium-deficient apatite with a low crystallinity [31]. Model protein lysozyme adsorbed HPLG MS exhibited no significant difference in the diffraction patterns.

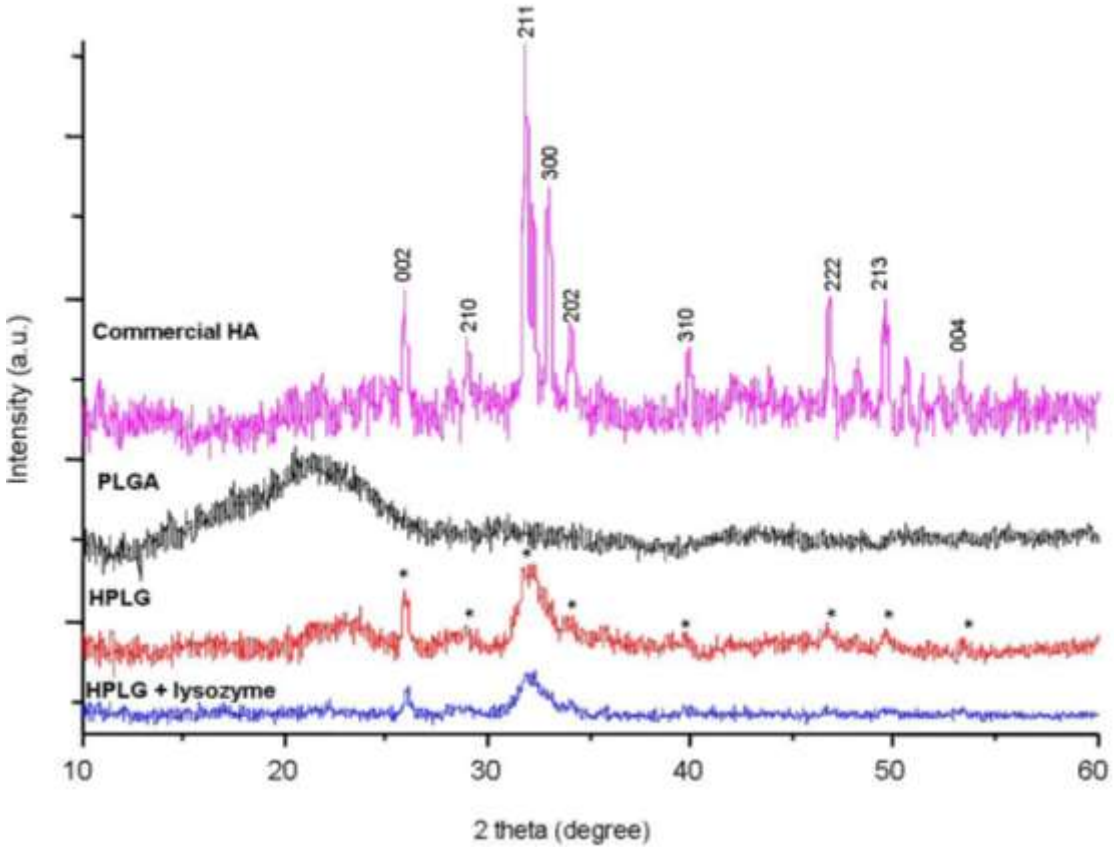

Figure 2.14 XRD patterns of commercial HA, PLGA, HPLG and lysozyme absorbed HPLG MS. HPLG MS exhibited characteristic diffraction peaks of calcium-deficient apatite (marked with *) and no significant change elicited after adsorbing lysozyme.

2.3.3.2. ATR-IR analysis

The ATR-IR analysis confirmed the chemical composition of the HA phase on HPLG MS and detected the lysozyme bound on the HA coating layer. The characteristic adsorption bands of phosphate at 563, 601, 960, 1027 and 1080 cm^{-1}, which are not present in PLGA MS, were found in the spectrum of HPLG MS (Figure 2.15). The 960 cm^{-1} band is due to v_1 symmetric stretching vibration. The twin band at 563 and 601 cm^{-1} corresponds to the v_4 O-P-O bending vibration and the single one at 1027 cm^{-1} corresponds to the $v3$ asymmetric P-O stretching. These bending and stretching modes of the P-O group elicited the crystalline nature of the HA coating on HPLG

MS [9]. The band at 870 and one broad band at 1420 cm^{-1} corresponds to the v_2 and v_3 stretching mode of CO_3^{2-} respectively [184]. PLGA was characterized by the bands at 1457 and 1750 cm^{-1}. All these peaks indicated that the HA coating on HPLG MS was Ca-deficient carbonated hydroxyapatite. Based on the Equation 2.3 (Page 68), the CO_3 weight content in HA coating was 5.89%, within the range of 4-8% seen in the biological bone apatite [26, 27]. The ATR-IR spectrum also shows amide bands at 1530 cm^{-1} corresponding to the 40% C-N stretching coupled with 60% N-H bending in amide II, and at 1650 cm^{-1} due to the C=O stretching in amide I group [185], which confirmed the presence of lysozyme bound to the HA coating surface.

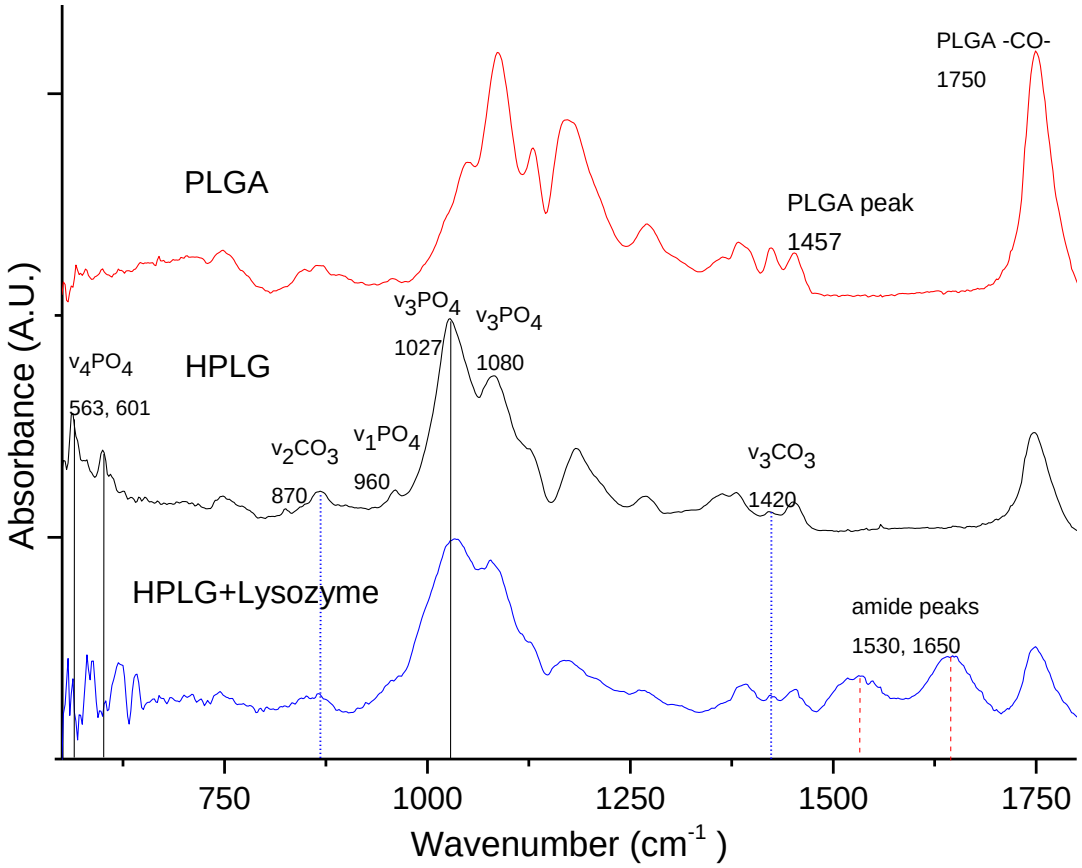

Figure 2.15 ATR-IR spectra of PLGA, HPLG, and lysozyme absorbed HPLG (HPLG + Lysozyme) MS. The characteristic absorptions of P-O and CO_3^{2-} groups indicated the Ca-deficient carbonated apatitic structure of the HA coating. Amide bands confirmed the lysozyme bound to the HA coating.

2.3.3.3. Raman analysis

Raman spectra further confirmed the chemical nature of the HA coating. Compared with the Raman spectrum of blank PLGA MS [186], the P-O symmetric stretching of PO_4^{3-} groups at 960cm^{-1} in the Raman spectrum of HPLG MS (Figure 2.16), is a representative indication of crystalline hydroxyapatite [187]. The peak at 875, 1044, 1130 cm^{-1} corresponds to C-COO stretching, C-CH_3 stretching and CH_2 asymmetric rocking of lactic acid in PLGA respectively [186]. As the ratio of the distinct HA specific band (960 cm^{-1}) to the PLGA specific band (875 cm^{-1}) was 0.42, which presents the amount of HA formed on HPLG MS [188], the HA coating content can

be thus calculated at approximately 29.6% of the total HPLG MS.

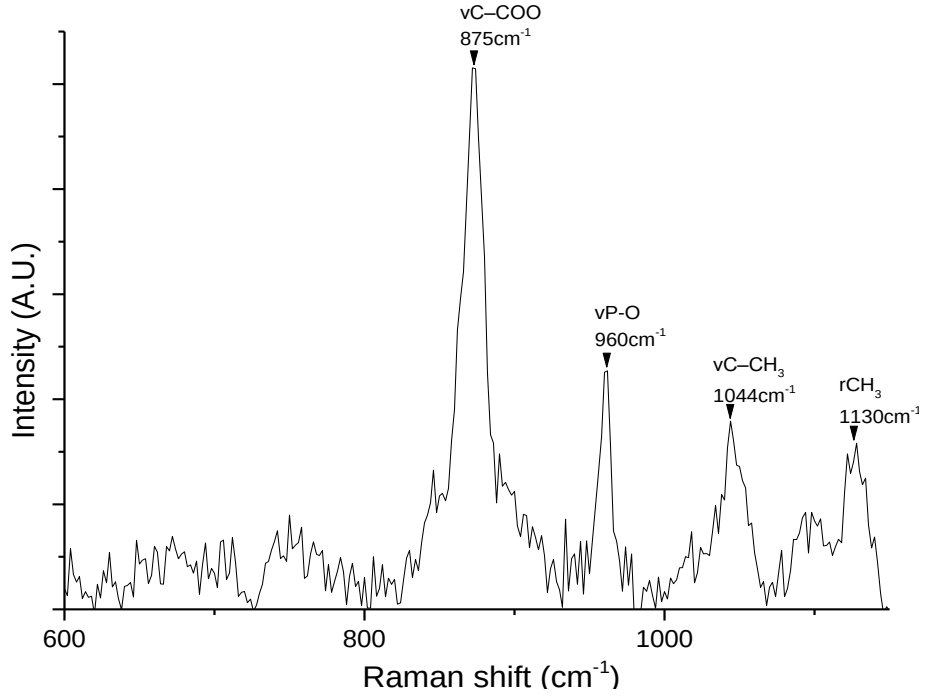

Figure 2.16 Raman spectrums of HPLG MS. The characteristic band of P-O at 960 cm^{-1} demonstrated the crystalline nature of the HA coating.

2.3.3.4. EDX analysis

The EDX analysis reveales that the Ca:P ratio of plate-like nanocrystal coating on HPLG MS (Figure 2.17). Strong signals of calcium and phosphorus were detected and the Ca/P ratio was calculated as 1.56±0.09, lower than that of stoichiometric hydroxyapatite (1.67). This result corroborated the findings of XRD and ATR-IR analysis that the nanocrystal coating was Ca-deficient hydroxyapatite.

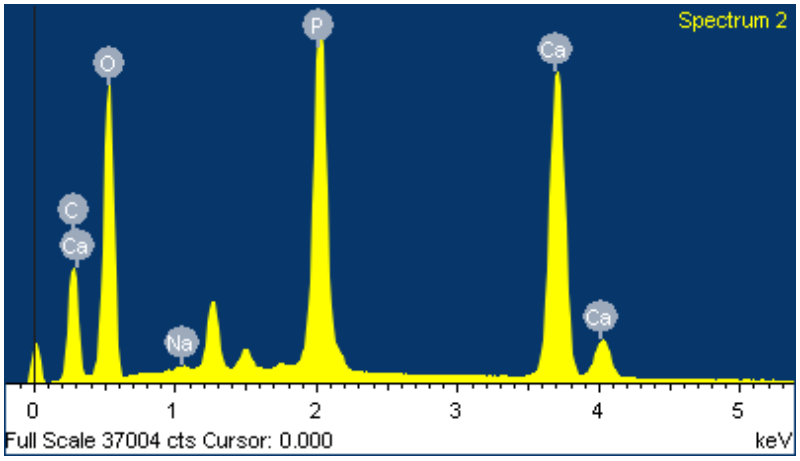

Figure 2.17 EDX spectrum of the nanocrystal coating on HPLG MS. The Ca/P ratio was 1.56±0.09 corresponding to Ca-deficient hydroxyapatite.

2.3.3.5. TGA analysis

For both PLGA and HPLG MS, the TGA curve (Figure 2.18) exhibited slight weight losses between 30-200^{o}C corresponding to the loss of water. Significant weight losses occurred in the range of 200-350^{o}C, which resulted from the thermal decomposition of PLGA polymer. There was almost no change in the individual weights between 350-400^{o}C. Only 5.23% materials remained for PLGA MS which were the organic carbon wastes of PLGA after burning. 28.16% materials remained for HPLG MS which are believed to be the mixture of HA crystal coating and organic carbon wastes. The HA crystal coating was stable at temperatures up to 400^{o}C. Therefore, the actual HA coating content was 22.93% (=28.16% - 5.23%) of the HPLG MS (with 1% DSS as surfactant and 3 hour HA coating), which is much higher than that on HPLG MS with SDS as surfactant [58]. The actual weight content of HA (22.93%) is a little lower than the calculated ratio (29.6%) from the Raman spectrum (Figure 2.16).

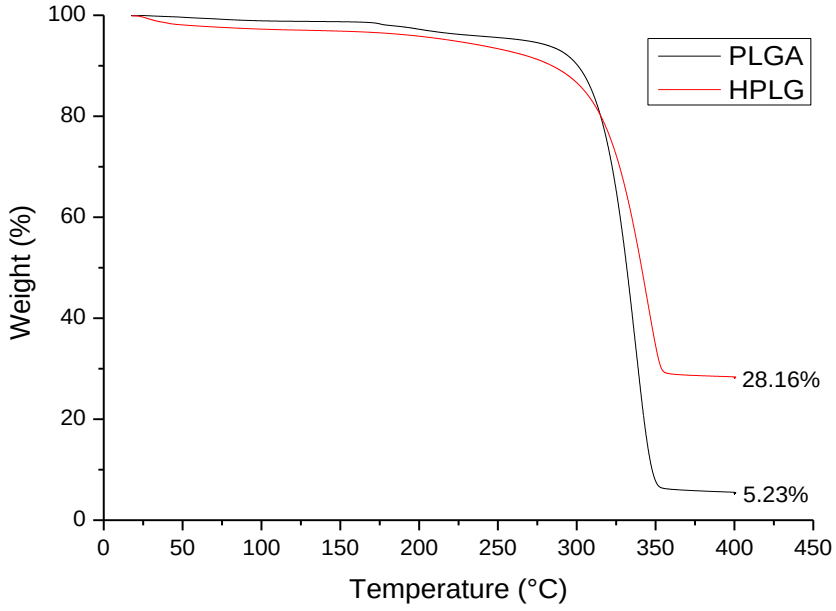

Figure 2.18 TGA curves of PLGA and HPLG MS weight loss. Remained materials were 5.23% for PLGA MS and 28.16% for HPLG MS.

After TGA measurement, the plate-like HA nanocrystal coating (100-600 nm) transformed to a hollow shell made of agglomerated small nanocrystal globules (smaller than 100 nm), while the PLGA core almost completely burned off (Figure 2.19). This further demonstrated the core-shell structure of HPLG MS fabricated by the constant composition precipitation method with DSS as surfactant.

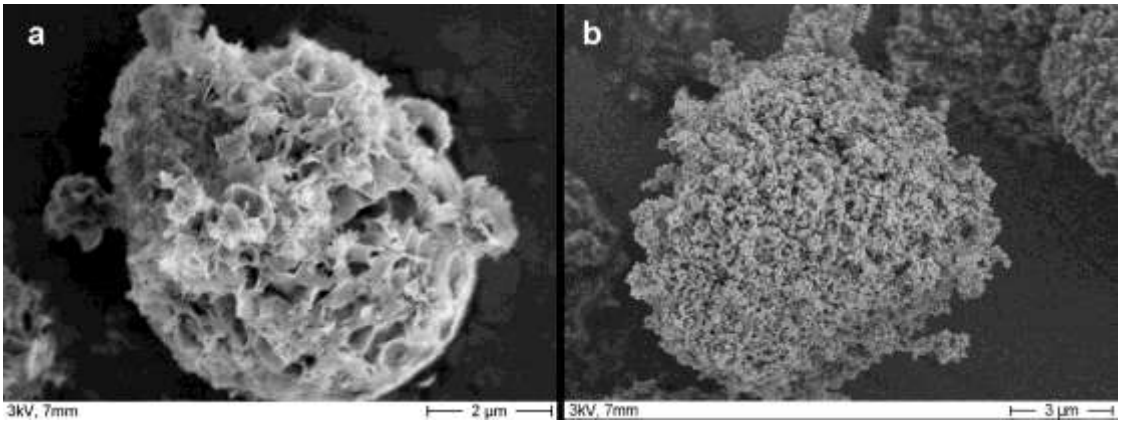

Figure 2.19 SEM micrographs of HPLG MS (a) before and (b) after TGA analysis up to 400^{o}C. The confirmed the core-shell structure of HPLG MS.

2.3.4. Model drug- VMC encapsulation efficiency

Besides the protein binding and delivery ability of the HA coating shell, the HPLG MS also acquired multi-drug delivery functions by the internal PLGA microsphere core. The hydrophilic antibiotic, VMC was investigated as a model drug encapsulated inside HPLG microsphere core by the S/O/W method. VMC has a stable light absorption at 280 nm (Figure 2.20), therefore the VMC content was determined by comparing the absorption of VMC solution (unknown concentration) at 280 nm with the standard curve (Figure 2.21). The standard curve was ploted by the 280 nm UV-VIS absorption of VMC solution (with known concentration) against the concentration.

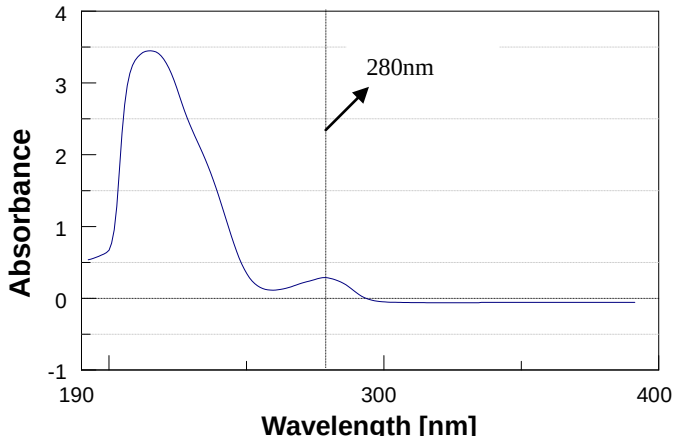

Figure 2.20 UV-VIS spectrometry of 0.1 mg/ml VMC with characteristic maximum absorbance at the wavelength of 280nm

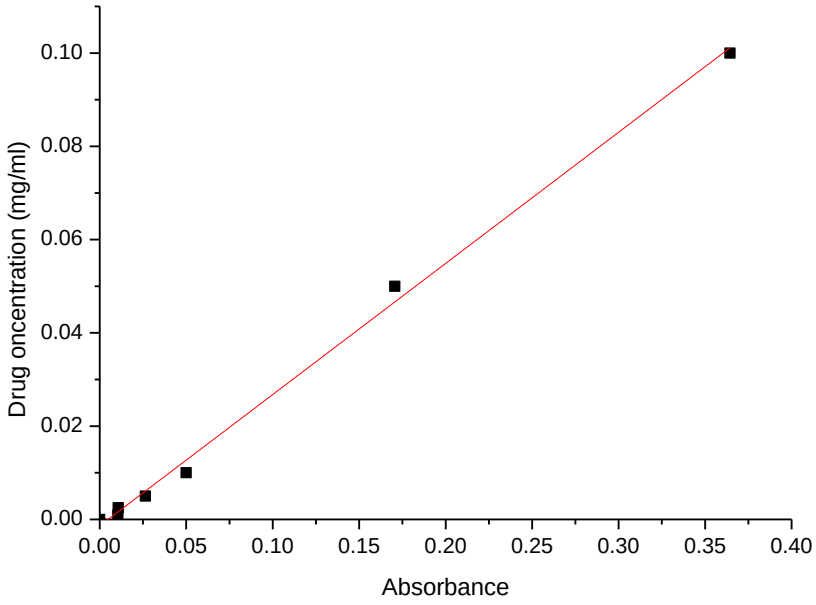

Figure 2.21 Standard Curve for VMC with concentration between 0.001 to 0.1 mg/ml in 1×PBS

Concentration = 0.2812*Absorbance$_{VMC}$ - 0.0013, R^2=0.9972 - Equation 2.7

According to the standard curve (Figure 2.21) and Equation 2.7, the encapsulation efficiency of VMC in HPLG MS was 60.9±2.7%, which is significant higher than the amoxicillin encapsulation efficiency 40.6±2.9% in HPLG MS emulsified by SDS [58].

2.3.5. *In-vitro* drug release

Since the VMC encapsulation efficiency in HPLG MS was 60.9±2.7%, when using 50 mg drug with 200 mg PLGA, the drug weight content in HPLG MS was 9.4% (drug/HPLG), taking into account the 22.6% HA content in HPLG MS. The cumulative release of VMC (Figure 2.22) exhibited a typical tri-phase release profile similar to those of other biodegradable polymer based drug delivery devices [54, 58, 80]. A small burst release at the first 24h was followed by a second plateau phase with a slow drug release for about 7 days. The third stage was a decelerated drug release,

starting from Day 8 and lasting until Day 21.

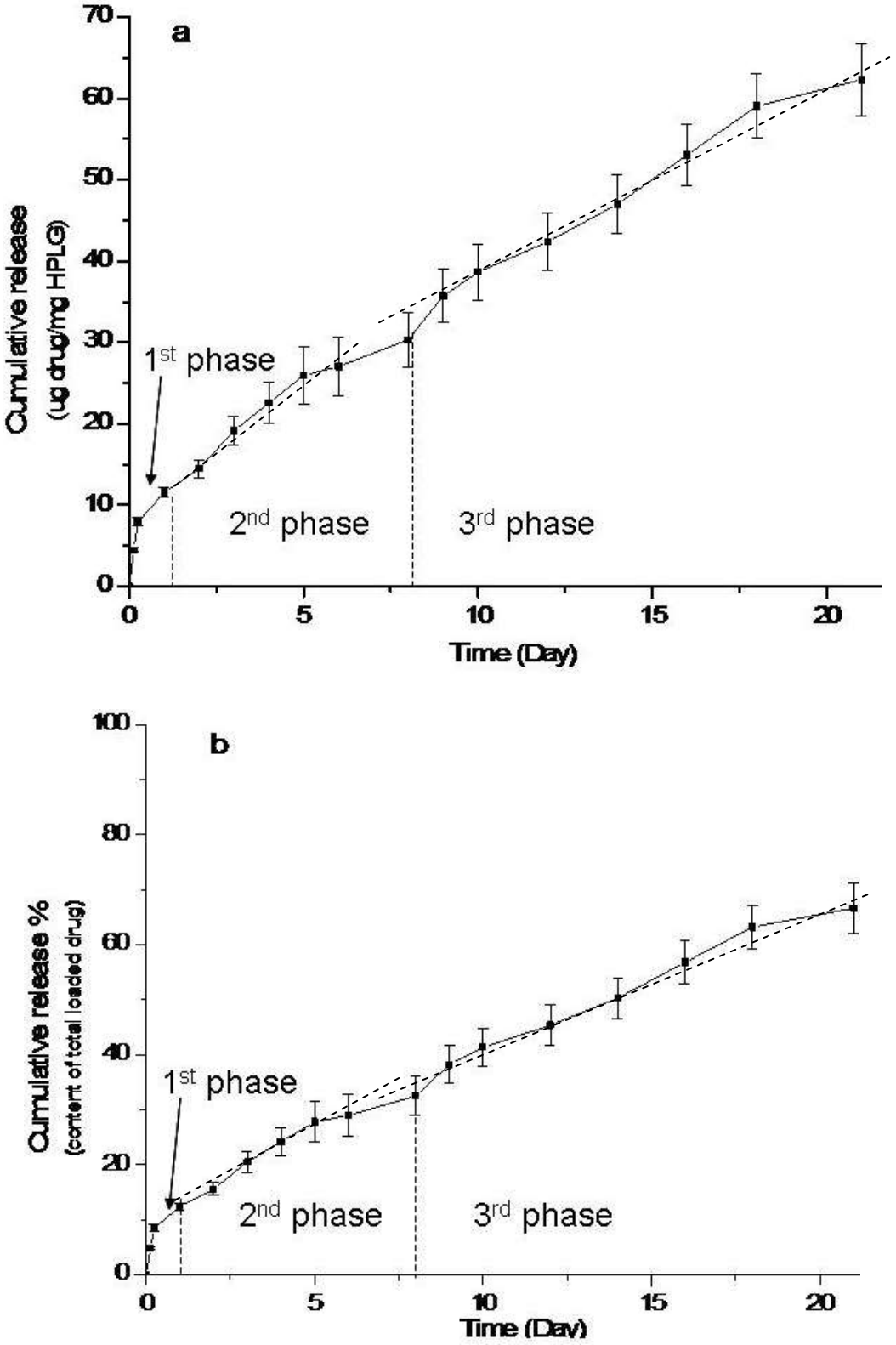

Figure 2.22 Cumulative release of VMC (a) weigh content, drug/HPLG (ug/mg) and (b) released ratio of total loaded drug (%) from HPLG MS in PBS (pH7.4). Data are means ± S.D. (n = 3).

2.3.6. The morphology of PLGA MS after degradation

The morphology of PLGA MS after 21 days in PBS (pH 7.4, 37^{o}C, the same solution used for *in-vitro* drug release) (Figure 2.23), reveales that PLGA polymer had already undergone bulk degradation, which caused 100-200 nm holes on the MS surface and inside the matrix.

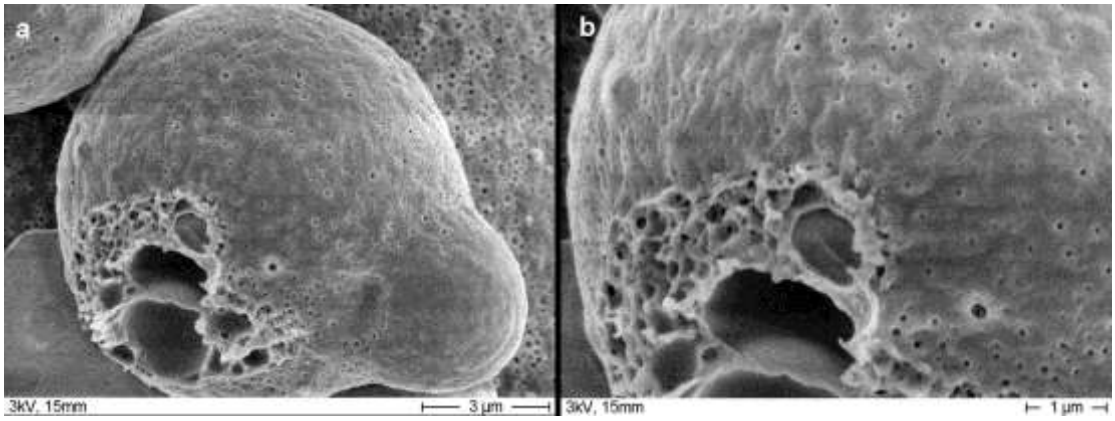

Figure 2.23 SEM micrographs of PLGA MS (a) low magnification (b) high magnification after 21 days in PBS (pH 7.4). Nano-size holes (about 100-200 nm) on the surface and inside walls indicated the bulk degradation of PLGA [2, 63].

2.3.7. Cell adhesion efficiency and cell proliferation

As the viable cell number is linear proportional to the absorbance in Alamar Blue^{TM} assay, the cell adhesion and proliferation on PLGA and HPLG MS, which is characterized by the viable cell number, were evaluated by directly comparing the relative fluorescence. This assay reveales that a similar proportion of viable cells attached on the tissue culture plate surface (Control group) and HPLG MS, both significantly more than those on PLGA MS, all 24 hour after seeding (Figure 2.24). This indicates HPLA MS has better cell affinity than PLGA MS, and can achieve similar cell adhesion efficiency as the tissue culture plate.

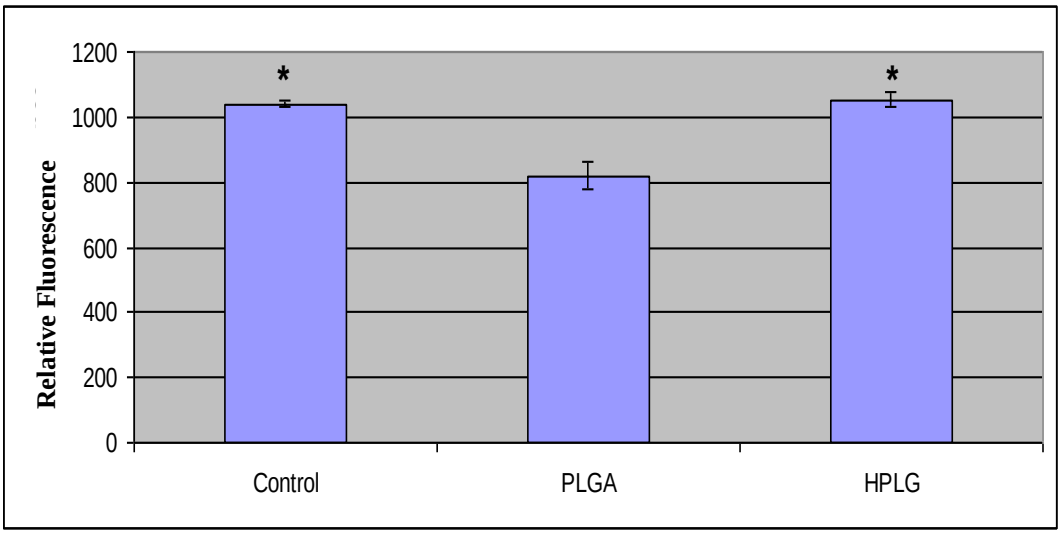

Figure 2.24 Relative fluorescence using Alamar Blue™ assay of 2T3 mice osteoblasts after 24 hour in culture on Control (culture plate surface), blank PLGA MS and HPLG MS (* significant increase compared with PLGA MS $p < 0.01$). This indicates the HA coating facilitated the cell attachment on HPLG MS compared with PLGA MS.

After 3 days in culture, HPLG MS enhanced the number of viable cells with a 1.7 fold increase compared to PLGA MS (Figure 2.25). These results confirmed that the HA coating on HPLG MS stimulated osteoblast cell adhesion and proliferation as reported by others [14, 189, 190].

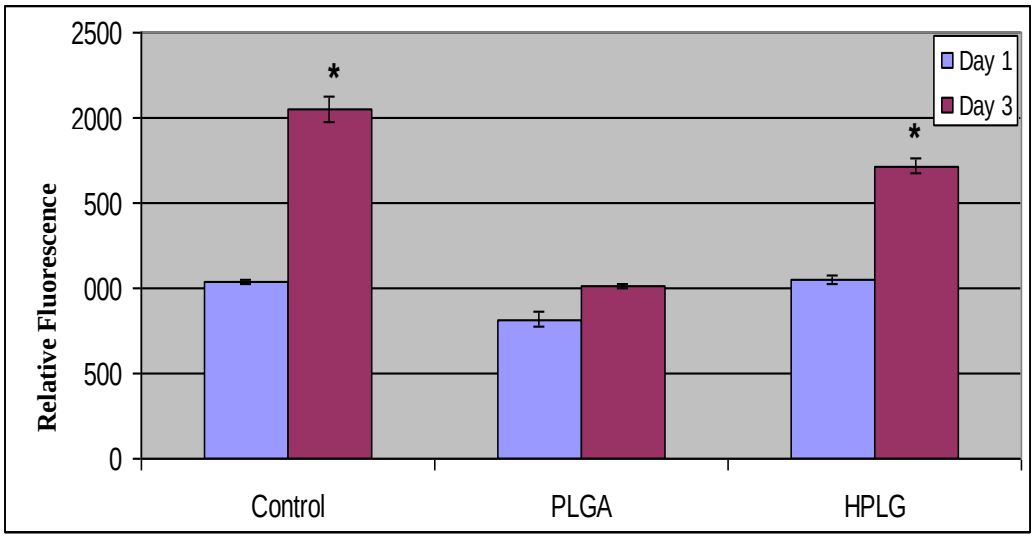

Figure 2.25 Relative fluorescence using Alamar Blue™ assay of 2T3 mice osteoblasts after 1 and 3 days in culture on Control (culture plate surface), blank PLGA MS and HPLG MS (* significant increase compared with PLGA MS at Day 3 $p < 0.01$). The HA coating further increased the number of viable cells on HPLG MS than PLGA MS.

2.4. **Discussion**

2.4.1. Use of FDA approved DSS in the constant composition method for HA precipitation on PLGA MS

In order to avoid high temperature damage and to induce a complete coating on a complex surface, the Kokubo biomimetic method is most widely used to grow HA on polymers [150, 151, 191, 192]. However, this biomimetic method is unsuitable for drug loaded biodegradable polymer devices, because the long time immersion (7-21 days) in simulated body fluid (pH 7.4 and 37 ^{o}C) will result in a high percentage of drug leakage and polymer degradation, demonstrated on (Figure 2.22) and (Figure 2.23) respectively. Therefore, a rapid HA coating technique, named as modified constant composition precipitation, has been recently developed in our group by using anionic surfactant SDS [58].

The constant composition method was first used to coat HA on phosphorus-containing polymers [193]. As the growth of HA on the foreigner substrates is a heterogeneous process [194], thus abundant negatively charged groups on a substrate surface are required to work as nucleation sites to decrease the free energy barrier for inducing HA nucleation and growth in the constant composition method [195-197]. The ionized groups $-(OSO_3)^-$ of SDS worked as both the stabilizing agent during the microencapsulation and the functional sites for the nucleation and growth of HA crystals in the modified constant composition precipitation [58]. SDS is widely used in cleaning and hygiene products but not approved by the FDA for clinical use, therefore the current study modified this HA coating technique by using a FDA approved surfactant DSS [155-160] instead of the SDS.

The successful growth of plate-like HA crystals on PLGA MS emulsified by DSS (Figure 2.5c, d), confirmed that indeed the $-(SO_3)^-$ of DSS can work as nucleation sites as the $-(OSO_3)^-$ of SDS (Figure 2.5a, b), to attract Ca^{2+} and to induce continuous HA crystal growth [58]. The high negative zeta potential of DSS emulsified MS (Figure 2.4) mainly came from the $-(SO_3)^-$ of DSS, which protruded from the microsphere surface as stabilizing agent during the s/o/w emulsion. Based on other reports of HA nucleation on polymer [58, 198-200], the underlying mechanism was concluded as a heterogeneous nucleation for the HA coating on DSS emulsified PLGA MS. The HA growth process was demonstrated in Figure 2.26. After adding KNO_3 and $Ca(NO_3)_2$ at 37°C with stirring for 10 minute, the electrostatic interactions between $-(SO_3)^-$ and Ca^{2+} initially induced adsorption and accumulation of Ca^{2+} on the polymer surface (Figure 2.26).. Then KH_2PO_4 and KOH were added to form HA specific supersaturated working solution. The pH of the supersaturated working solution was relatively stable in the first 10 minute after adjusting the start pH to 7.4 by KOH. The 10 minute is the induction time as reported in other constant composition processes [193, 198, 201]. In this 10 minute, it is hypothesized that a diffuse layer of PO_4^{3-} and OH^- gathered around Ca^{2+} accumulated microsphere surface, and in turn enhanced the supersaturation levels specific for HA locally in the working solution. This circular reaction might finally signal the onset of HA nucleation at these sites (Figure 2.26). Then the pH of the working solution started to decrease at a relatively slow speed (around pH 0.03 per 2 second), which triggered the addition of titrants, so the pH would rise back to 7.4 to maintain supersaturation specific for HA. The induction time reflects the time needed for the formation of stable supercritical nuclei on the substrate (Figure 2.26), which in turn indicates the capability of different

surface functional group to induce apatite formation [198]. After 3 hour addition of titrants, the islanded HA supercritical nuclei grew to large nanocrystal and connected with each other to form continuous coating to cover the whole MS (Figure 2.26). Therefore, in this modified fast constant composition process, abundant negatively charged functional groups are required to form supercritical nuclei to grow continuous HA nanocrystal coating on the substrate surface.

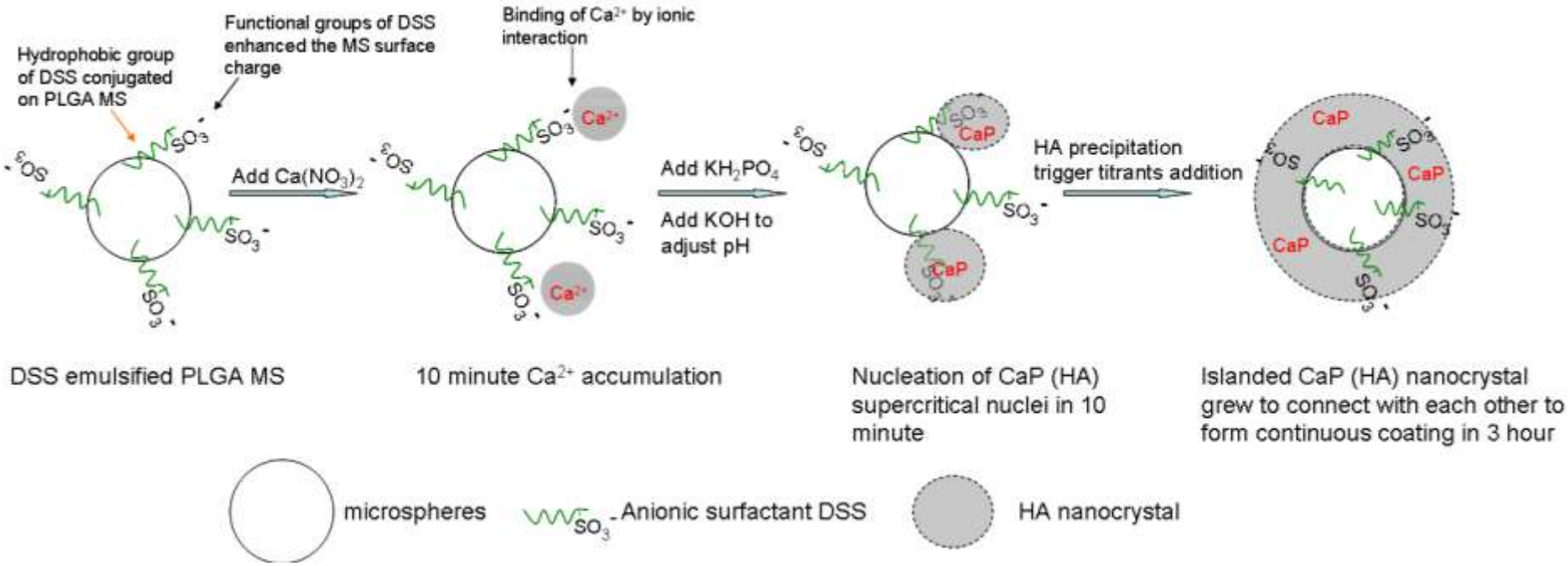

Figure 2.26 Chemical schematics of HA growth on negatively charged microspheres (MS) emulsified by DSS

The incomplete and islanded HA nanocrystals on PLGA MS using low concentration DSS (0.2%, Figure 2.7a, b), confirmed the requirements of abundant negatively charged groups on the substrate surface to grow continuous HA crystal coating. 0.5% (v/v) DSS is sufficient to provide the necessary negatively charged groups for continuous HA coating (Figure 2.7c, d). In accordance with the HA coating on MS using SDS [58], a 3 hour reaction is still needed for continuous HA coating in the constant composition process, while the 1.5 hour reaction only induced isolated plate-like nanocrystal (Figure 2.8). The indicated that after the attraction of Ca^{2+} and the heterogeneous nucleation on the negative charged surface, the constant composition method needs sufficient time (at least 3 hour in this case) to grow HA nanocrystals large enough to reach their nearest neighbour nucleation sites to form continuous crystal coating.

2.4.2. Effects of various formulation parameters on HA coating

2.4.2.1. The type of PLGA substrate

The structures of the two monomers in PLGA copolymer (Figure 1.12) indicate that the lactide, which has two extra methyl groups, is more hydrophobic than the glycolide. Thus, the 85:15 PLGA that contains a higher fraction of lactide is relatively more hydrophobic and precipitates out of an aqueous environment at a faster rate to form bigger size microdroplets (Figure 2.9), compared to the 50:50 PLGA which contains higher fractions of glycolide.

These much smaller 50:50 PLGA MS (Figure 2.9a, b) aggregated easily in the supersaturated working solution during the constant composition HA coating,

however, the HA nanocrystals still grew successfully and covered completely the single microsphere surfaces and yielded large irregular microsphere aggregates (Figure 2.10 and Figure 2.27). This implies that the HA crystals can grow on substrate irrespective of their size and morphology in the constant composition process, therefore this rapid HA coating method can be applied to virtually any substrate with high negatively charged surface. Similar microsphere aggregates were reported when growing HA on MS in the modified SBF for 7 days [29]. One possible reason for this aggregation may be that there are fewer negatively charged $-(SO_3)^-$ groups of DSS surfactant on the surfaces of smaller 50:50 PLGA MS, which are easily neutralised by adsorbing Ca^{2+} during the initial accumulation of the HA coating process, compared with bigger 85:15 PLGA MS (Figure 2.27). Moreover, the small particles are easily affected by the electrostatic interactions which induces the MS aggregation to reduce the free surface energy prior to the HA nucleation.

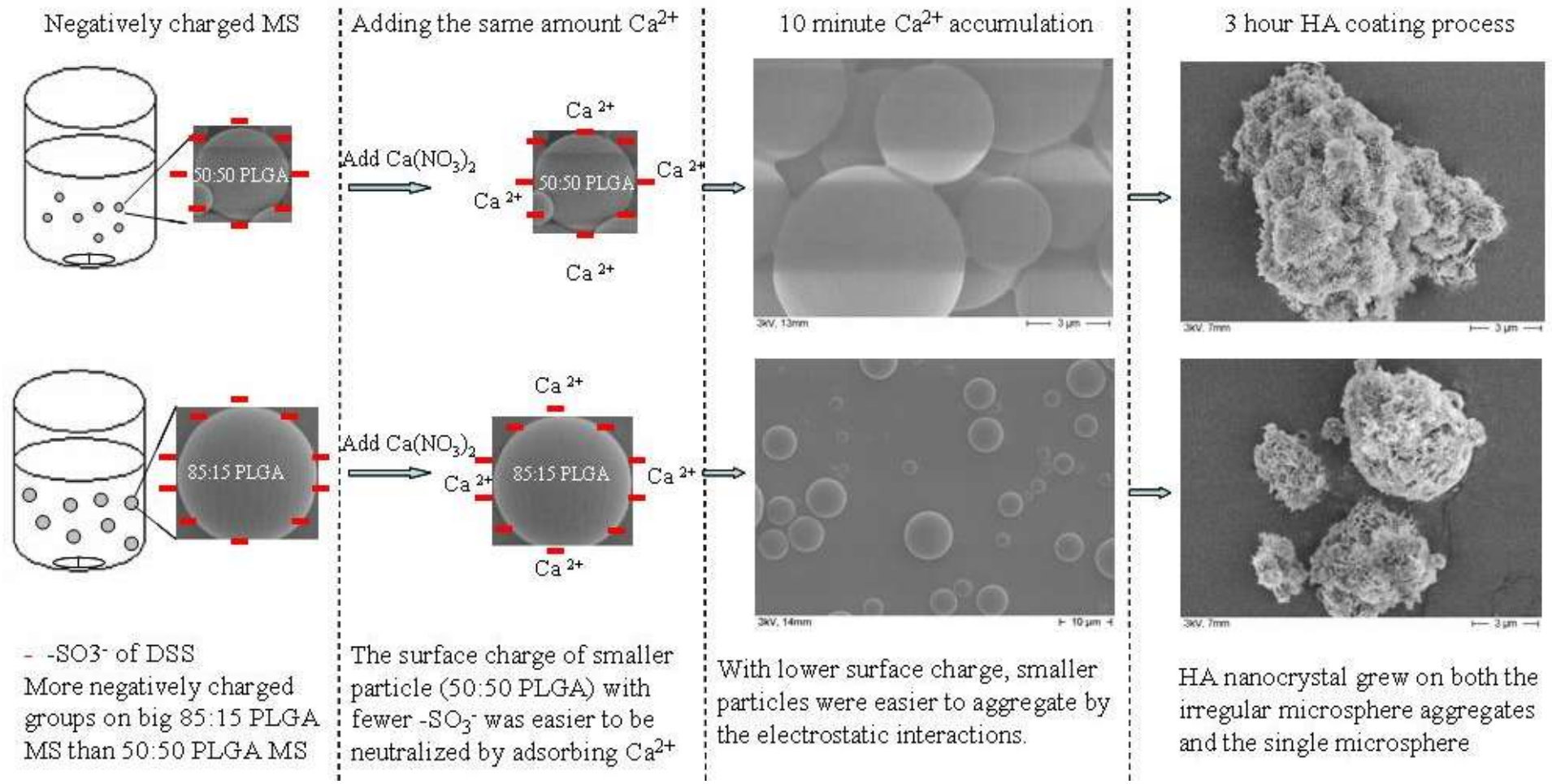

Figure 2.27 Schematic diagrams of small MS (50:50PLGA) aggregation during the HA crystal growth.

2.4.2.2. Influence of loaded drug

Bisphosphonates have been used to prevent soft tissue calcification because they can bind strongly to hydroxyapatite crystals and inhibit their formation and dissolution [182]. Therefore, even though only a very small dose of AL (around 4.8%, assuming the release profile of AL similar to VMC (Figure 2.22) as they are both water-soluable small molecules) leaked during the HA coating process, this AL inhibited the direct synthesis of polycrystalline HA (Figure 2.12). Boanini *et al*. [176] also reported amorphous globules presented when synthesising HA in the presence of AL. The finding highlights the effects of drug leakage during the HA coating process, and suggests that this constant composition technique is unsuitable for the MS encapsulated with drug inhibiting HA formation. The bisphosphonates may be loaded onto the HPLG MS after completing the HA coating, as the same method used for the model protein lysozyme, to form a multi-drug delivery device. Enhanced drug release has been reported by adsorbing AL on HA nanocrystals encapsulated inside PLGA MS [23].

2.4.3. Characterizations of HA coating

Most bone minerals are formed as a poorly crystalline 4-8% carbonate-substituted hydroxyapatite [26, 27]. XRD patterns of HPLG MS (Figure 2.14) reveales the HA coating was calcium-deficient hydroxyapatite with a low crystallinity as seen in bone mineral. In accordance with the BSA incorporated HA coating on PLGA fibres [202], XRD patterns exhibit no significant change after adsorbing lysozyme on HPLG MS. As the bone mineral crystal contains 4-8% carbonate, the modified constant composition method was conducted in air condition in order to introduce CO_2 into the

precipitated HA crystals. This is different from the original constant composition method requiring the nitrogen atmosphere [194] to prevent introduce CO_2. ATR-IR spectra (Figure 2.15) confirms the HA coating as Ca-deficient 5.89% carbonated hydroxyapatite, indicating the modified constant composition can precipitate HA crystals very similar to bone mineral. Raman (Figure 2.16) and EDX (Figure 2.17) analysis further confirmed the structure of HA coating with Ca/P ratio 1.56±0.09 corresponding to Ca-deficient hydroxyapatite. TGA analysis (Figure 2.18) confirmed the HA coating content of 22.93% (w/w), which corresponded to the calculated ratio from the Raman spectrum (Figure 2.16). The resultant SEM micrographs after TGA analysis (Figure 2.19) demonstrated the core-shell (organic polymer- inorganic HA crystal) structure of HPLG MS. The core-shell structure can make HPLG MS an effective multi-drug carriers by encapsulating the drug inside the polymer core [51] or adsorbing protein onto the HA coating shell [49]. Furthermore, the HA coating shell was reported with a pH buffer capability preventing the drop in pH induced by PLGA degradation [58]. This will be another significant advantage for the HPLG MS besides their combination of bioactivity with multi-drug delivery.

2.4.4. Model protein binding

ATR-IR spectra (Figure 2.15) demonstrated the presence of lysozyme bound to the HA coating, indicating that the HA coating was capable of efficiently binding soluble biological molecules via ionic interaction between the surface charges of HA and proteins [49]. Lee *et al.* reported lysozymes can be effectively loaded onto and released from the calcium phosphate cement scaffolds for up to more than one month [183]. The facile protein-adsorption loading process can also avoid the disadvantages

of low loading efficiency and decreased bioactivity in the conventional microencapsulation methods for growth factor delivery [53-55]. With appropriate lysozyme loading efficiency of 27.0±0.3% after 4 hour immersion, the HPLG MS will be very promising carriers for multi protein binding and sustained release.

2.4.5. Model drug release

A typical tri-phase release profile was exhibited for model drug vancomycin encapsulated in HPLG MS. In the first burst stage, a small dose of VMC (about 4.5 μg drug/mg HPLG, which accounted for 4.8% of the total drug encapsulated) was released in the first 3 hours. The indicated that there would be a small drug leakage during the same time scale- 3 hour in the constant composition HA coating process. As AL is also hydrophilic small molecule drug, the AL leakage in the 3 hour constant composition process is speculated similar to VMV. Since AL can inhibit HA formation and dissolution [182] it is speculated AL leakage that inhibited the HA nanocrystal precipitation on AL encapsulated PLGA MS (Figure 2.12). After 24h of the first burst, 12.4% of the encapsulated drug was released, much lower than those of MS fabricated by the w/o/w methods [53]. The initial burst was believed to be due to the rapid release of the drug absorbed and encapsulated near the microsphere surface [57]. The s/o/w method made the drug distribute in the polymer matrix as separated solid particles, which prevented drugs dissolving in the water phase. This reduced the drug amount distributed near the microsphere surface and thus resulted in a lower initial burst.

The second relatively slow release phase is caused by the slow swelling of PLGA due

to inward diffusion of water for approximately 7 days. The VMC drug encapsulated inside the PLGA matrix also dissolved in the water and diffused out in a low dose.

The third phase was caused by the release of approximately 2.3 ug drug/mg HPLG (~2.5% of the total encapsulated drug), which was governed by the hydrolytic degradation of PLGA polymer [71]. The degradation occurred as ester bonds of PLGA polymer were cleaved to create carboxylic acid and hydroxyl chain, which resulted in the mass loss, pH drop and easier water diffusion [72]. PLGA are bulk erosion polymers, where the water penetration and erosion affect all the polymer bulk for over 30 days [1, 62]. VMC is a hydrophilic antibiotic similar to amoxicillin which has a low adsorption on HA [15], it is therefore concluded that the HA coating will make no significant difference on the VMC release from HPLG MS, similar to amoxicillin release from PLGA and HPLG MS [57]. Therefore, all the above properties of the PLGA polymer led to the decelerated drug release lasting from Day 6 to 21 on HPLG MS. The cumulative drug release after 21 days was 62.3 ug drug/mg HPLG, corresponding to 66.6% of total encapsulated drug.

In contrast, as AL has much stronger bind with HA than VMS [176], the outer shell HA coating is speculated to have a great effect on prolonging the AL release. If AL is encapsulated inside PLGA MS, its leakage can inhibit HA formation on PLGA MS to form HPLG MS [176, 182]. Therefore, AL can only be adsorbed onto the outer shell HA formed on HPLG MS in advance to form dual-drug delivery device (VMC inside PLGA core and AL on the outer shell HA). Shi et al has reported bisphosphate additives adsorbed on HA for long-term release [42]

After 21 days incubated in PBS for drug release (pH 7.4, 37^{o}C), the smooth surface of PLGA MS (Figure 2.3) became porous with 100-200nm holes on the surface and inside matrix (Figure 2.23). The is consistent with that PLGA is a bulk erosion polymer [1], for which the degradation occurs simultaneously both at the surface and inside the bulk structure.

These holes will accelerate the water diffuse rate and encapsulated drug release. This indicates that the Kokubo biomimetic HA coating technique, which requires the pre-hydrolysis and immersion of samples in SBF for 7-21 days [147, 148, 150, 151], were not suitable for biodegradable polymer that will degrade in SBF. The finding also highlights the advantage of the constant composition technique which induces fast HA coating in just 3 hours.

2.4.6. Increased cell adhesion and proliferation

HPLG MS exhibited good cell adhesion, comparable to that seen on the culture plate surface designed for cell culture (Control) (Figure 2.24). Like most biodegradable polymers, PLGA is FDA approved for clinical applications, but is not osteoconductive or osteoinductive [51]. The hydrophobic nature of PLGA also inhibits the cell adhesion [66, 67]. Therefore, it was concluded that the similarity to the bone minerals of HA coating and the increased surface porosity by the HA nanocrystal [203-205], caused the improved cell adherence for HPLG MS [25]. The HA coating further facilitated the osteoblast cells proliferation after 3 days culture (Figure 2.25) in agreement with other studies [13, 189, 190]. All these findings demonstrated the HA coating enhanced the cell response of PLGA MS and introduced osteoconductive properties to this drug delivery device.

2.5. **Summary**

A bone-like carbonated hydroxyapatite (HA) nanocrystal with calcium-deficient and low crystallinity was successfully precepitated on drug loaded PLGA microsphere surface by a modified constant composition method in 3 hours in physiological conditions. The FDA approved surfactant DSS, instead of the previous toxic surfactant SDS, was used as both the stabilizing agent in the microsphere emulsion and the functional agent to provide negatively charged surface for the nucleation of HA. The modified constant composition method introduced CO_3^{2-} into the HA nanocrystal coating, and can coat negatively charged substrates irrespective of their size and surface morphology. With the S/O/W method, the drug entrapment efficiency was over 60% and only 4.8% drug leaked during the 3 hour HA coating. However, some leaked drugs, such as bisphosphonates, can still inhibit the HA nucleation. The vancomycin encapsulated inside the polymer core exhibited a typically triphasic *in vitro* release lasting over 21 days. The HA coating shell can work as a carrier to adsorb lysozyme for sustained release, and also improve the osteoblast cell attachment and viability significantly. The HA coated PLGA microsphere could be a promising localized drug delivery device combining osteoconductivity with controlled multi-drug delivery.

3. Chapter 3: Porous microspheres with controllable porous structure for injectable cell delivery

3.1. Introduction

Bone-like hydroxyapatite (HA) nanocrystals coated poly(lactic-co-glycolic acid) (PLGA) microspheres (MS) have been successfully fabricated, with all FDA approved materials, as a multi-drug delivery device. Nevertheless, one single HA coated PLGA (HPLG) MS (average 3-9 μm in diameter) is too small for cell adhesion and subsequent migration [104, 206]. HPLG MS have to accumulate together to form big aggregations for cell adhesion, but these aggregations are not stable in dynamic aqueous solution. Therefore, HPLG microspheres are only suitable for multi-drug delivery but not for cell delivery, if not increasing the microsphere size.

Compared with conventional scaffolds used in tissue engineering to support cell growth to specific tissues for transplantation, an injectable cell carrier is more desirable to deliver cells to repair complex-shaped tissue *in vivo*, and easier to be handled for an accurate fit with minimal surgical interference [83-85]. Conventional scaffolds are primarily used for implantation which requires open surgery. Biodegradable porous MS have recently become an attractive choice as injectable cell carriers, as they can combine drug delivery with three-dimensional (3D) cell culture as injectable scaffolds. Their interconnected porous structure can facilitate nutrient transport, and provide large surface area and higher buoyancy to improve cell adhesion and growth [88, 102].

Since suspended human bone and cartilage cells are on average 10 μm in diameter before seeding and the ideal injectable cell carriers should be smaller than 200μm in order to pass though the syringe needles [88], the ideal porous microsphere for injectable cell delivery should be 80-150 μm in diameter with pore sizes around 10-20μm.

The work in this chapter compares three different methods to fabricate the ideal injectable cell carriers designed as above, these including osmogen (KCl) [106], extractable porogen (Pluronic F127) [6, 100, 106] and gas-foaming porogen (ammonium bicarbonate) [99, 109, 110]. Osmogen are highly water-soluble pore-forming components, which can induce the osmotic pressure gradient inside the oil droplets to create pores by extracting water into the oil droplets (as demonstrated in Figure 3.1) [6, 100, 106].

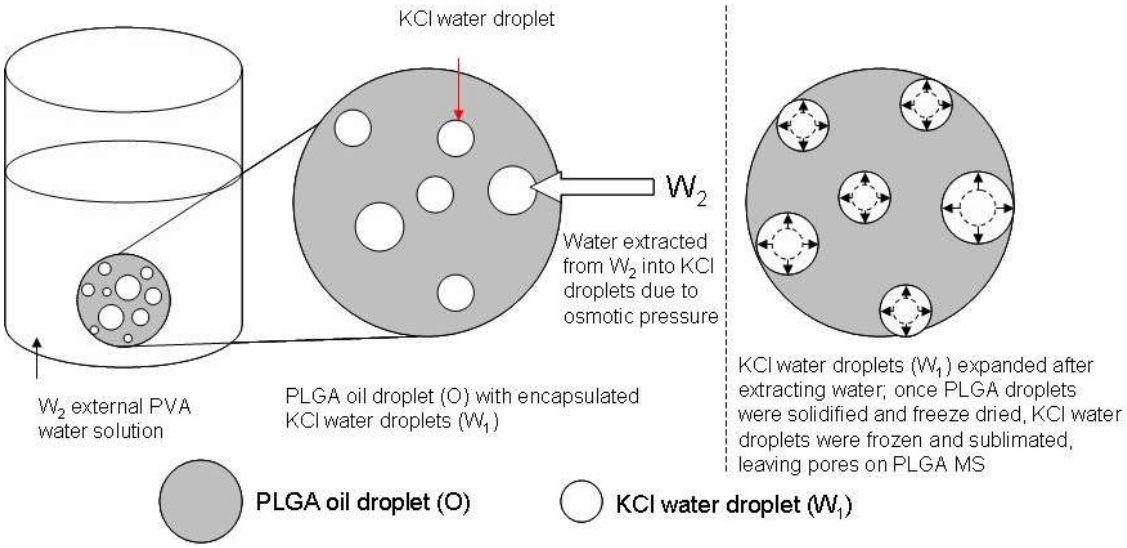

Figure 3.1 Schematic diagrams of pore formation on PLGA droplets by osmogen KCl

For extractable porogen method, pores can be formed in PLGA droplets by washing away water-soluble polymer Pluronic F127, which was dissovled and mixed with PLGA in DCM (as demonstrated in Figure 3.2) [6, 100, 106].

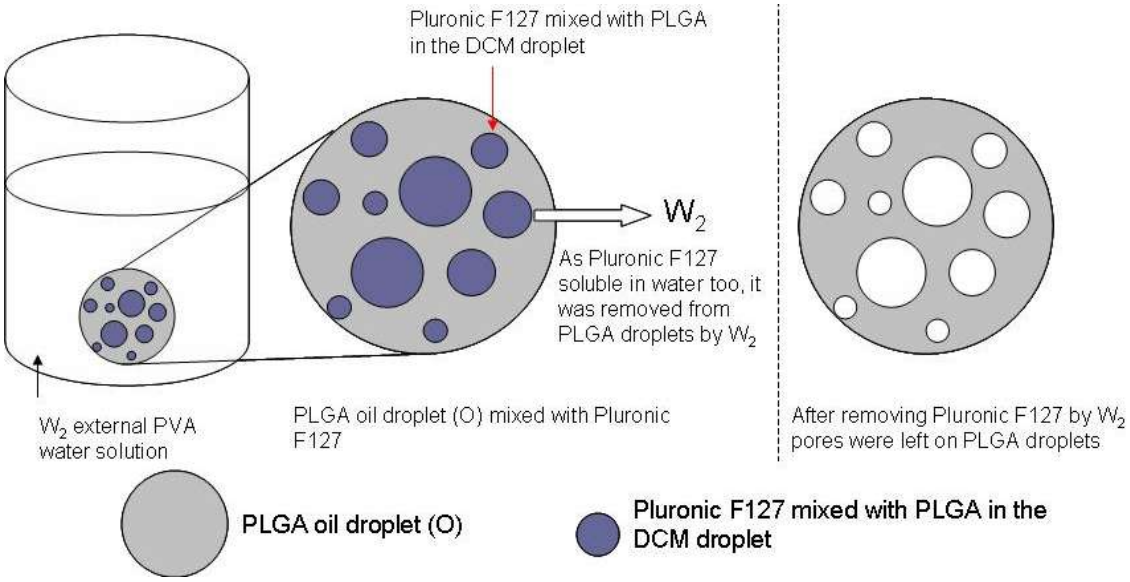

Figure 3.2 Schematic diagrams of pore formation on PLGA droplets by extractable porogen Pluronic F127

In the gas-foaming porogen method, porogen NH_4HCO_3 water droplets were firstly encapsulated inside PLGA oil droplets. Pores can be then created in PLGA droplets by decomposing NH_4HCO_3 into NH_3 and CO_2 using high speed homogenization (as demonstrated in Figure 3.3) [99, 109, 110].

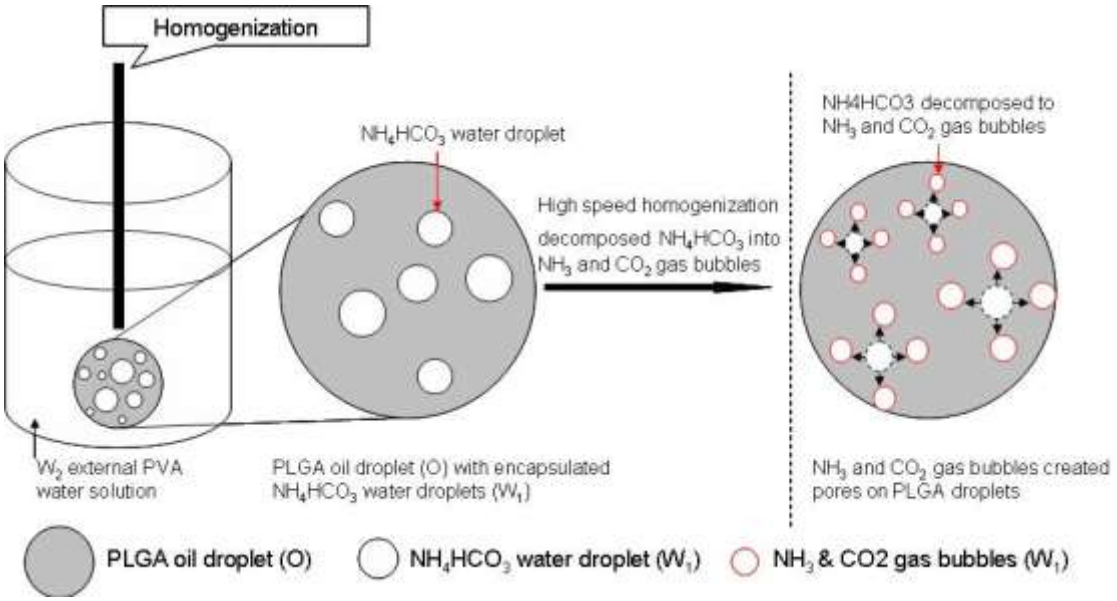

Figure 3.3 Schematic diagrams of pore formation on PLGA droplets by NH_4HCO_3 gas foaming method

Formulation parameters of the three methods were investigated and optimized to fabricate the biodegradable porous PLGA MS with average size of 80-150μm and pore sizes of approximately 10-20μm [114, 115]. Covered and partially covered porous PLGA MS with ideal sizes and porous were fabricated using NH_4HCO_3 based gas foaming $W_1/O/W_2$ double emulsion method. Surface treatments with selected solutions including NaOH, ethanol and acetone were evaluated to control the surface open pore size and ratio. These porous MS with adjustable open pore size are of great potential as injectable cell carriers combining the cellular functions and sustainable drug release.

3.2. **Materials and Methods**

3.2.1. Materials

PLGA copolymer (50:50 PLGA, Mw 50K, inherent viscosity 0.55 dL/g; 75:25 PLGA, Mw 76K, inherent viscosity of 0.57 dL/g; and 85:15 PLGA, Mw 92.5K, inherent viscosity 0.64dL/g; all ester-ended) were supplied by Birmingham Polymers Inc. (AL, USA). Poly vinyl alcohol (PVA) (average Mw 31,000-50,000, 98-99% hydrolysed dioctyl), dioctyl sodium sulfosuccinate (DSS), and dichloromethane (DCM), were obtained from Sigma (UK). Pluronic F127 [(PEG)99(PPG)69(PEG)99] (Mw 12,600) was provided by BASF (Germany). Polyethylene glycol (PEG 2000MW) was purchased from Polysciences, Inc (USA). Potassium chloride and sodium hydroxide were provided by BDH (Poole, UK).

3.2.2. Fabrication of conventional nonporous MS

As the control group, conventional nonporous MS were fabricated by the O/W single emulsion method, to enable morphological comparison with porous MS. 150 mg 75:15 PLGA in 1.5 ml dichloromethane (DCM) were emulsified in 100 ml 2% (w/v) PVA solution under 700 rpm stirring. After 3h evaporation of the DCM, the solidified MS were washed 3 times by distilled water, separated by centrifugation and freeze dried for 12 hours.

3.2.3. Fabrication of porous MS by osmogen KCl

Osmogen KCl based salt leaching method was used to fabricate porous microparticles by the $W_1/O/W_2$ double emulsion methods derived from our research collaborators [106]. The The first aqueous phase (W_1) of 100mg KCl in 1 ml water was emulsified in 4ml dichloromethane of 300 mg 75:15 PLGA (oil phase) by probe sonication for 30 seconds in an ice bath to obtain the primary W_1/O emulsion. This was immediately poured into 800 ml external 0.5% w/v PVA solution. 500µl of the new $W_1/O/W_2$ emulsion was collected by pipette to examine the PLGA droplet morphology using optical microscopy. The rest of the $W_1/O/W_2$ emulsion was stirred for 3 hours to evaporate the DCM. The hardened MS were collected by centrifugation, washed with 200 ml deionized water and then re-dispersed in 1000 ml deionized water stirring for 24 hours to remove the remaining KCl.

3.2.4. Effects of formulation parameters on MS morphology in the osmogen method

3.2.4.1. Freeze dry and air dry

The above resultant porous MS were separated from water by wet-sieving, using 50μm stainless steel test sieves, and freeze dried for 12 hours or desiccator dried for 48 hours.

3.2.4.2. KCl concentration

In order to make big pores, excess KCl 900 mg was dispersed in 1 ml water to form the first aqueous phase (W1). The solubility of KCl in water at room temperature is 340 mg/ml, therefore 900 mg KCl in 1ml water forms turbid supersaturated solution with non-dissolved KCl particles. The rest conditions and steps were the same as those in 3.2.3 and the resultant MS were freeze dried.

3.2.4.3. Nonionic surfactant and anionic surfactant

Besides nonionic surfactant PVA, anionic surfactant DSS (0.5% w/v) was also used as the external solution (W_2) to fabricate KCl-leaching MS with a negatively charged surface. The effect of salt on the DSS solution was investigated separately as well. After placing 0.5% (w/v) PVA, 0.1%, 0.5% and 1% DSS solution in 5 separate vessels, certain amounts of KCl (0.04%) were added into the 5 solutions under the observation of optical microscopy.

3.2.5. Fabrication of porous MS by extractable porogens

The extractable porogen method was investigated as an alternative to fabricate porous

MS [207]. 300mg 75:25 PLGA were mixed with Pluronic F127 (700mg dissolved in 3ml DCM) as the internal oil phase, which was subsequently homogenized in 100ml of 0.5% (w/v) PVA solution at 6500 rpm using a Turrax IKA T18 basic homogenizer (IKA works Inc., USA) for 90 seconds. The O/W emulsion was then stirred for 3 hours to evaporate the organic solvent DCM. The resultant MS were centrifuged, extensively washed by deionized water to remove Pluronic F 127, and freeze dried.

3.2.6. Effects of formulation parameters on MS morphology in the extractable porogen method

3.2.6.1. Nonionic surfactant and anionic surfactant

Anionic surfactant DSS (0.5% w/v) was also evaluated as the external solution (W_2) instead of PVA. A mixture of 300mg PLGA and 700mg Pluronic F 127 in 3ml DCM was homogenized in 100ml of 0.5% DSS solution at 6500 rpm for 90 seconds and 500µl of the resultant O/W emulsion was collected for observation by optical microscopy. The remaining emulsion was stirred for 3 hours to obtain the solid MS, which was washed and freeze dried.

3.2.6.2. Higher homogenization speed

The homogenization speed was increased from 6500 rpm to 24,000 rpm to evaluate the effects on microsphere morphology while the other conditions were constant using DSS as the surfactant.

3.2.6.3. Pluronic F127: PLGA ratio

The Pluronic F127: PLGA ratio was changed from 700:300 to 700:150 while keeping

the other conditions constant with DSS as the surfactant.

3.2.6.4. PLGA composition

Besides 75:25PLGA, 300 mg 50:50PLGA was blended with 700 mg Pluronic F 127 to fabricate MS. DSS was used as the surfactant.

3.2.6.5. Different extractable porogen- PEG

Instead of Pluronic F127, polyethylene glycol (PEG) was also explored as the extractable porogen to fabricate MS. 50 mg PEG and 200 mg 75:25PLGA in 2 ml DCM was homogenized in 100ml of 0.5% DSS solution at 6500 rpm for 90s and then stirred for 3h. The resulting MS were washed and freeze dried.

3.2.7. Fabrication of porous MS by gas foaming porogen NH_4HCO_3

NH_4HCO_3 based gas foaming method was explored to fabricate porous MS using the $W_1/O/W_2$ double emulsion methods [109]. Schematic diagrams of the procedure are demonstrated in (Figure 3.4). 2.5ml of 1% (w/v) NH_4HCO_3 (W_1) was homogenized in 8ml DCM of various weights of PLGA (O) at 6,000 rpm for 3 minutes, and then stirred in the external 200ml 0.1% (w/v) PVA (W_2) for 3 hours under the observation of optical microscopy. The MS formed were centrifuged, washed 3 times with distilled water and freeze dried.

A control group of MS without the NH_4HCO_3 solution (W_1) or homogenization was fabricated too: 1.6% (w/v) 75:25 PLGA of 8ml DCM was stirred in 200ml 0.1% (w/v) PVA (W_2) for 3 hours to evaporate DCM. Thre resultant hardened MS were

centrifuged, washed by distilled water and freeze dried.

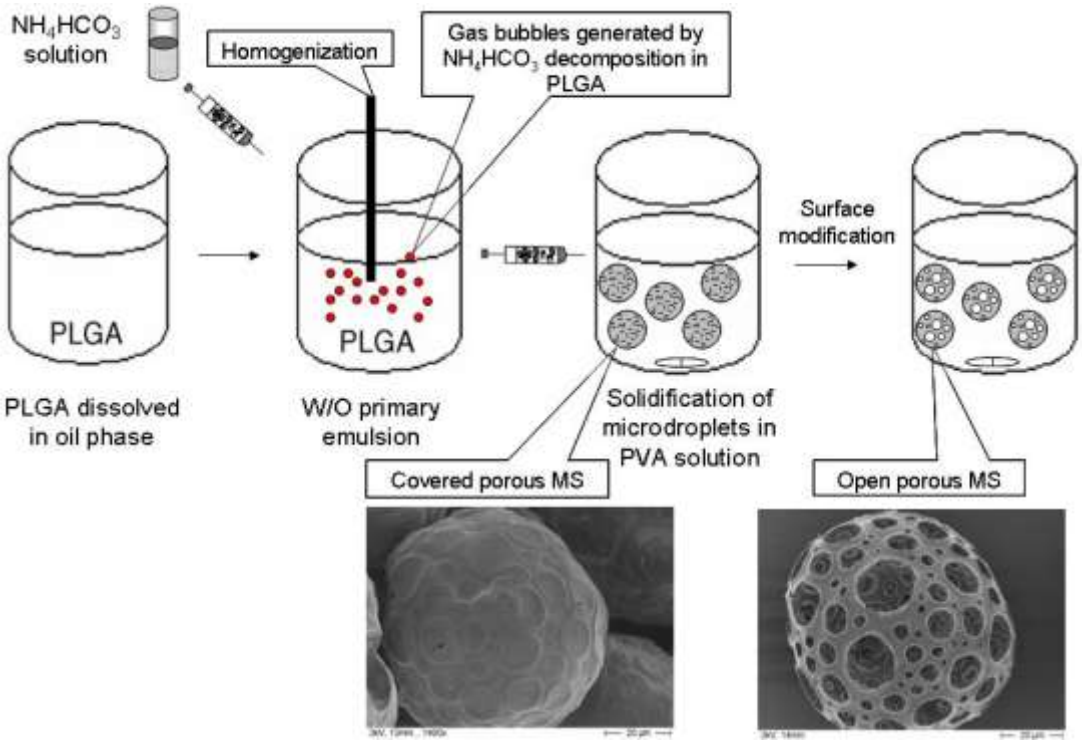

Figure 3.4 Schematic diagrams of covered and open porous MS fabrication process.

3.2.8. Effects of formulation parameters on MS morphology in the gas porogen method

3.2.8.1. PLGA concentrations

Various amounts of 75:25PLGA (1.6, 2.5, 3.8, and 6.2% (w/v) of 8ml DCM) were used to fabricate MS by the above procedure.

3.2.8.2. NH_4HCO_3 concentrations

NH_4HCO_3 concentration was increased from 1% to 2% or 4% (w/w) to explore their effects on the microsphere morphology. Keeping the NH_4HCO_3 concentration at 1%, the effects of NH_4HCO_3 amount (2.5 and 5 ml) were also evaluated.

3.2.8.3. PLGA composition

50:50PLGA and 85:15PLGA were further used instead of 75:25PLGA to fabricate the MS.

3.2.8.4. O: W2 ratio

The oil: external surfactant phase (O: W2) ratio was changed from 8:200 to 8:100, 8:400 or 8:800 to investigate their effects on MS morphology.

3.2.9. Characterization of the skin layer covering the pores on MS

The source of a skin layer covering the pores on the covered porous MS was analyzed by attenuated total reflection infrared (ATR-IR) spectroscopy. ATR-IR was performed on the sample powders on a Perkin-Elmer Spectrum 2000 Explorer FTIR spectrometer (Spectrum 2000, Perkin Elmer Ltd., UK). The absorbance of the infrared light by specific bonds at specific wave lengths (wave numbers) was measured against a background spectrum. 15 scans over the range of 500-1800 cm^{-1} were performed at a resolution of 2 cm^{-1} with the background scan subtracted

3.2.10. Surface modifications to clean skin layers on covered porous MS

Covered porous MS made by the extractable and gas foaming porogens were further modified by various solutions to control the surface open pore size and porosity (Figure 3.4). Microspheres were immersed in varying concentrations of NaOH solution, a mixture of NaOH with either ethanol (50%, 25% or 10%) or 1% DSS, or 25% (w/v) acetone individually. The surface treated MS were thoroughly washed with

distilled water later to remove any remaining solution, freeze dried and observed by SEM. Covered porous MS made by various PLGA concentrations and compositions, were modified by NaOH solution to compare the morphology differences. The incubation time of MS in NaOH solution was also investigated to optimize the best treatment to control the pore size and porosity.

3.2.11. Microcharacterization of covered and open porous MS

3.2.11.1. Scanning electron microscopy

The surface and cross-section morphology of MS were examined by scanning electron microscopy (SEM; JEOL JSM 840F) at an accelerating voltage of 3 kV. All MS were freeze dried and mounted on alumina stubs with double sided carbon tapes. The MS were then pre-coated with 3 nm platinum by the Cressington Sputter Coater HR208 with MTM-20 thickness controller (Watford, UK). The average microsphere size, surface open pore size and porosity of the total surface were calculated by using Image J (Public Domain, National Institute of Health, USA) to analyze the SEM micrographs of approximately 20 MS and 10 pores on each microsphere. The open pore porosity was calculated as Equation 3.1

$$\text{Open pore porosity} = \frac{Surface\ areas\ of\ all\ open\ pores\ \ on\ one\ microsphere}{Surface\ area\ of\ the\ whole\ microsphere}$$

-Equation 3.1

3.2.11.2. Particle size measurement

The particle size and distribution of MS were examined by a Malvern Mastersizer X (Malvern Instruments, UK). Microspheres were dispersed in the deionized water and

sonicated for 5min before the test. The mean particle size represents the volume mean diameter of the MS from three test batches of MS.

3.2.11.3. Surface charge measurement

The surface charges of MS were examined by measuring their zeta-potentials in deionized water at 25°C on Zetasizer Nano (Malvern Instruments Ltd., UK). The samples were dispersed into deionized water to form stable dilute suspensions by vortex in order to provide the low ionic strength for performing the measurements, therefore making the surface charge measurements more accurate. Three replication experiments, each one containing 30 zeta measurements, were conducted for every sample.

3.3. **Results**

3.3.1. Conventional MS

Conventional MS fabricated by the O/W single emulsion method without any porogens presented typical sphere structures (Figure 3.5a). The high magnification image of one single microsphere exhibited the smooth and nonporous surface (Figure 3.5b).

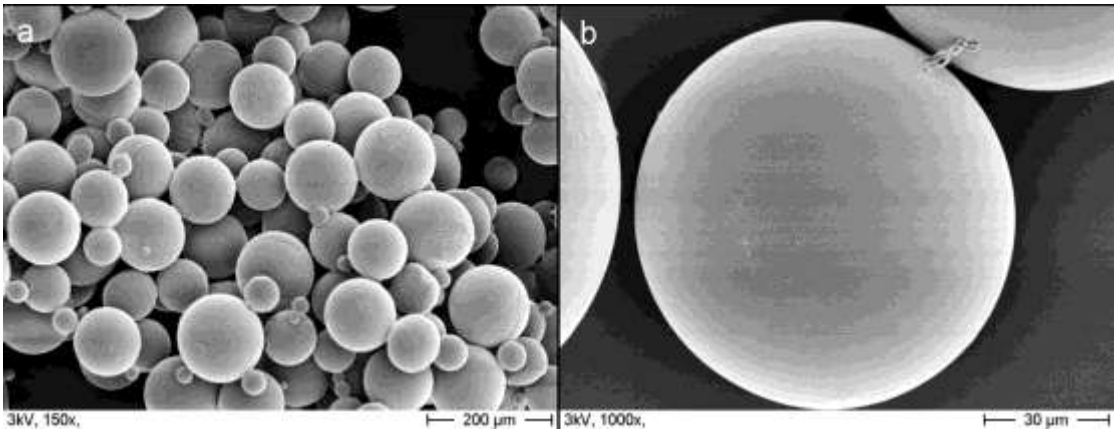

Figure 3.5 SEM micrographs of conventional PLGA nonporous MS: (a) gross and (b) single morphology. MS exhibited typical smooth and nonporous surface.

3.3.2. Porous MS fabricated by osmogen KCl

Images in Figure 3.6 demonstrate that pores were generated immediately on the PLGA oil droplets after pouring the primary W_1/O emulsion into the external surfactant PVA solution. Some PLGA droplets looked unhardened after 5 minute emulsion in the PVA solution (Figure 3.6b).

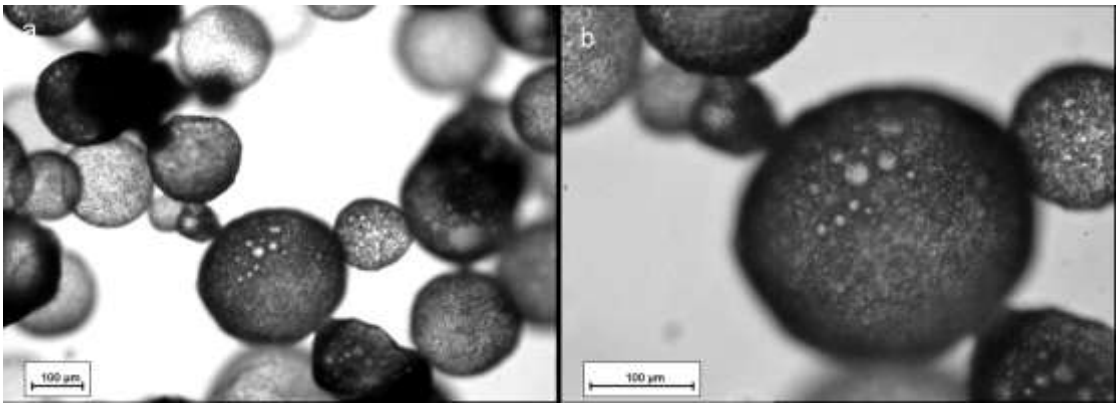

Figure 3.6 Optical micrographs of KCl-leaching PLGA microdroplets after 5 minute emulsion in PVA solution at (a) gross and (b) single morphology. Pores were identified on the PLGA droplets which were caused by water penetration due to the osmotic pressure.

3.3.3. Effects of fabrication parameters on MS morphology in the osmogen method

3.3.3.1. Effects of freeze dry and air dry on MS morphology

The osmogen KCl leaching method is derived from the previous report [106] from our research collaborators, which air dried the MS in a desiccator for 48 hour. In order to investigate the influences of freeze drying and air drying on microsphere structures, the PLGA microdroplets in Figure 3.6 were stirred in the PVA solution for 3h to obtain hardened MS after evaporating DCM, re-dispersed in 1000ml deionized water to wash excess salt, and freeze dried or desiccator dried. Most freeze dried MS exhibited rough and porous surfaces with pores in the range of 0.5-6 μm (Figure 3.7) compared with the conventional nonporous MS (Figure 3.5), which is consistent with the previous report [106]. In contrast, the air dried microparticles with broad size distribution and even some oval shapes (Figure 3.7 c) were more likely to collapse than those freeze dried. Their surfaces were also rougher with pores about 2-15 μm (Figure 3.7 d).

Freeze dry

Air dry

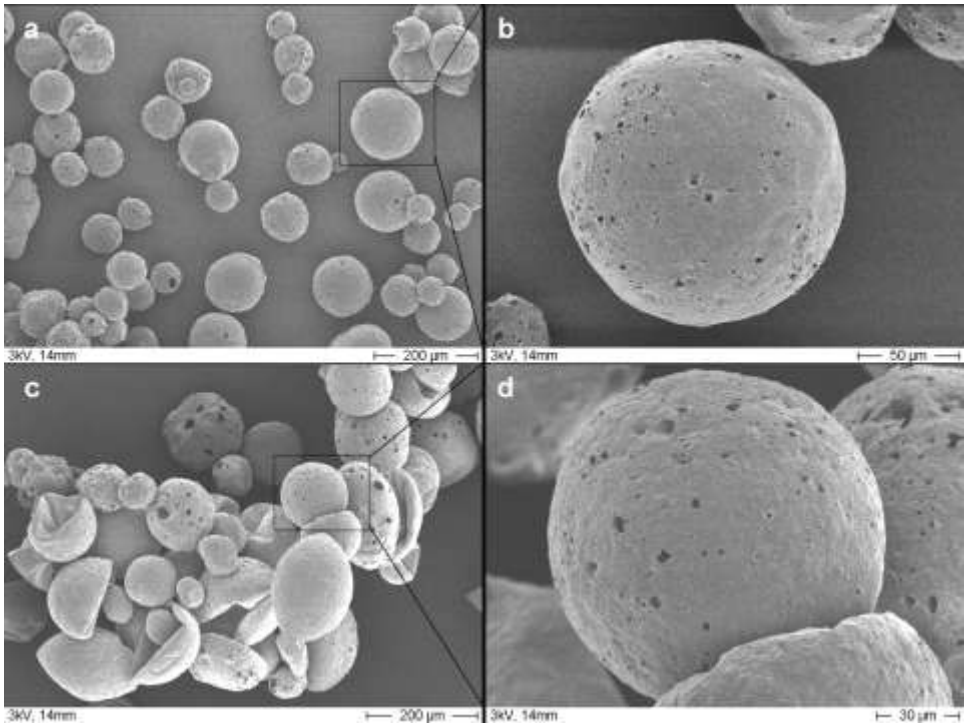

Figure 3.7 SEM micrographs of KCl-leaching porous MS made by (a, b) freeze dry and (c, d) air dry. Air dried MS were more likely to collapse than those freeze dried.

3.3.3.2. Effects of KCl concentration on MS morphology

After increasing the osmogen KCl concentration from 100 mg to 900mg in 1ml water (W_1), the MS became larger than 400 µm with pores between 1-9 µm in diameter (Figure 3.8). This indicates that the microsphere size can be greatly increased by increasing the internal salt concentration; however this is not the case for the surface pores. The solubility of KCl in water is 340 mg/ml at room temperature, hence there were KCl particles in the internal phase (W_1), some of which were still entrapped in the PLGA matrix without dissolving in the external solution (Figure 3.8).

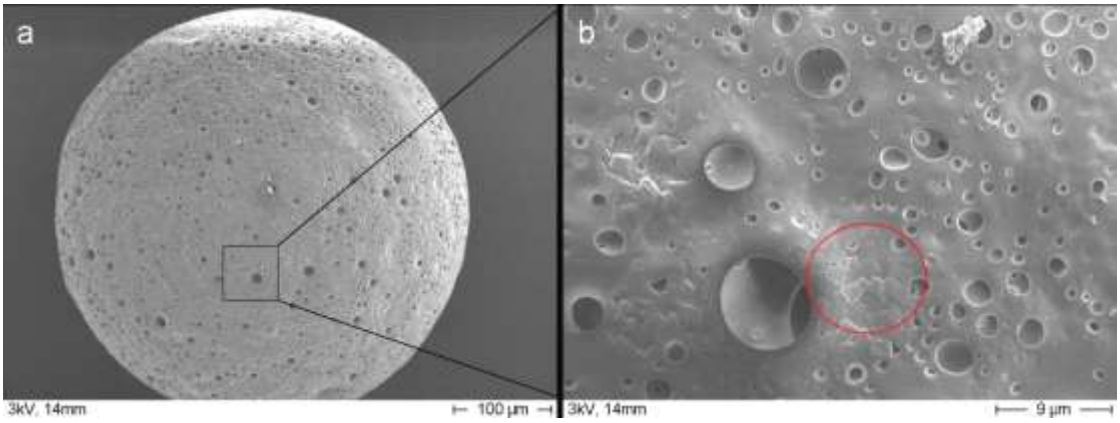

Figure 3.8 SEM micrographs of 900 mg KCl leaching porous MS: (a) single and (b) surface morphology. Non-resolved salt particles are marked by the red circle. Microsphere size increased with increasing salt concentration.

3.3.3.3. Effects of anionic surfactants on MS morphology

When changing the external surfactant solution from nonionic PVA to anionic DSS, large aggregations of PLGA oil droplets with branches stretching on the surface (Figure 3.9a) appeared immediately after pouring the primary W_1/O emulsion into the external solution. Even after 3h emulsion, the hardened MS still aggregated together (Figure 3.9b). It is hypothesized that KCl inhibited the surfactant DSS function to emulsify and stabilize the droplets.

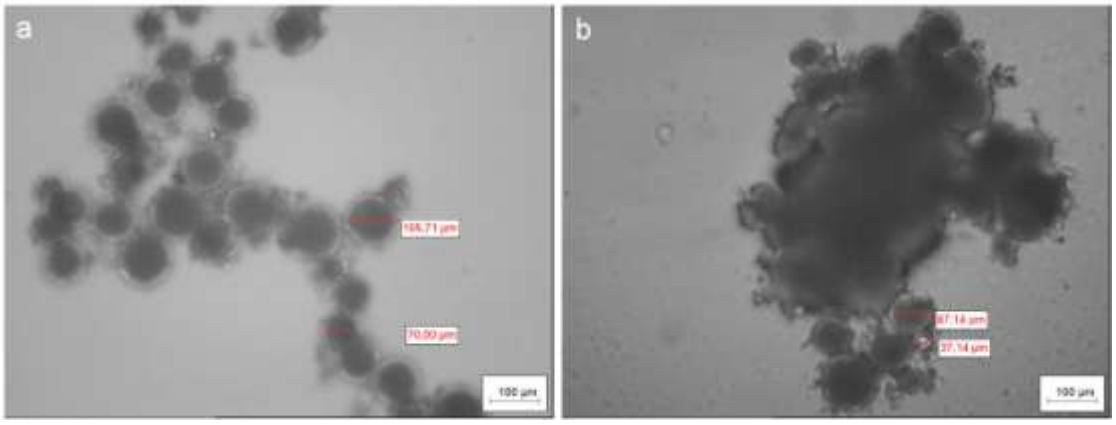

Figure 3.9 Optical micrographs of KCl- leaching microdroplets aggregations after (a) 5mins and (b) 3h emulsion in DSS solution. Microdroplets aggregated when changing the surfactant from PVA to DSS.

3.3.3.4. Effects of KCl on DSS dissolution

The above hypothesis was confirmed by showing that 0.04% KCl made the 0.5% DSS solution become cloudy with micelles of approximately 17-54 µm in diameter being formed, while the 0.5% PVA solution was still clear and thereby not affected by the 0.04% KCl (Figure 3.10a, b). After adding the same amount of KCl, smaller micelles ranging from 10-24 µm in diameter appeared in the 0.1% DSS solution (Figure 3.10c), and bigger micelles of approximately 157 µm in diameter were present in the 1% DSS solution (Figure 3.10d). The micelle size increased with increasing DSS concentration, indicating the micelles were precipitated DSS.

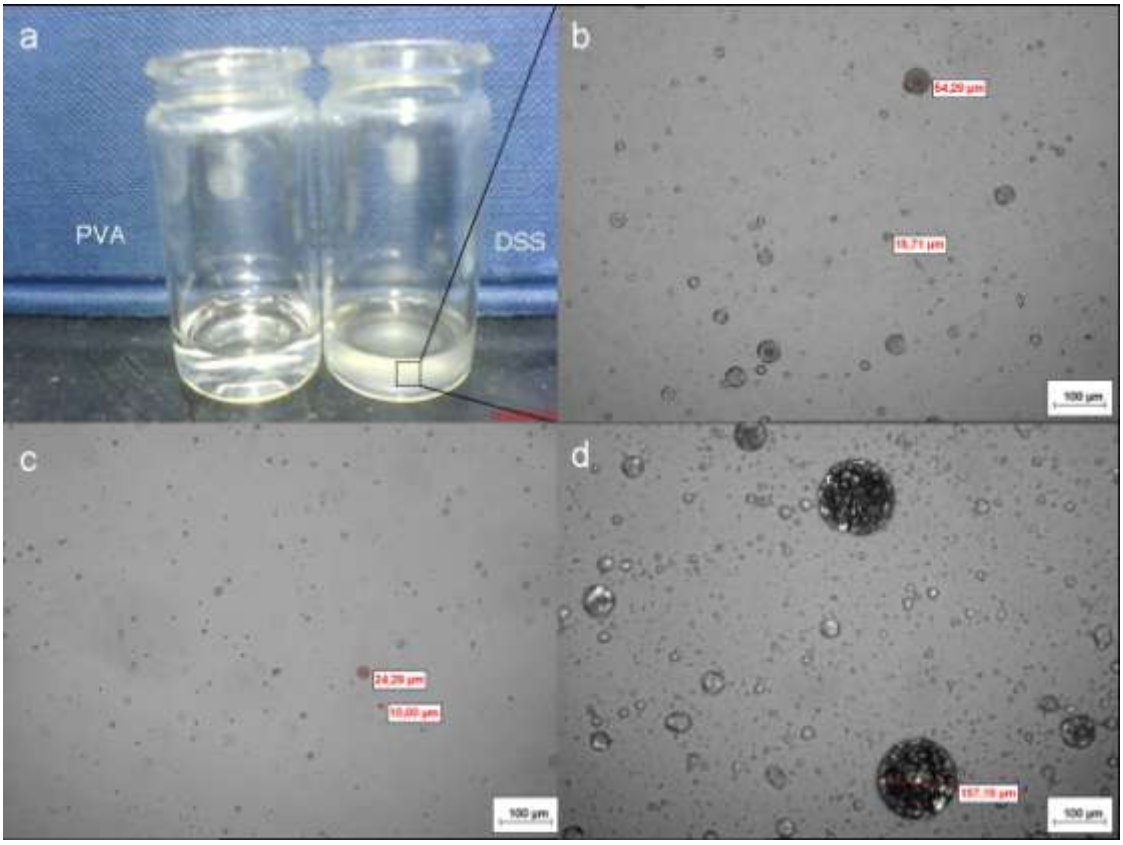

Figure 3.10 (a) Images of 0.5% PVA and 0.5% DSS solution after adding 15 mg KCl. Optical micrographs of 15mg KCl effects on (b) 0.5%, (c) 0.1% and (d) 1% DSS solution. Big DSS micelles precipitated after increasing the DSS concentration to 1%.

3.3.4. Porous MS fabricated by extractable porogens

No obvious pores were identified on the PLGA droplets fabricated by the extractable

porogen-Pluronic F127 method (Figure 3.11) compared with those made by the osmogen (Figure 3.6). SEM images of these hardened PLGA MS (Figure 3.12a, b) further confirmed that only some MS were porous with well distributed pores (average 3.5μm) on the surface.

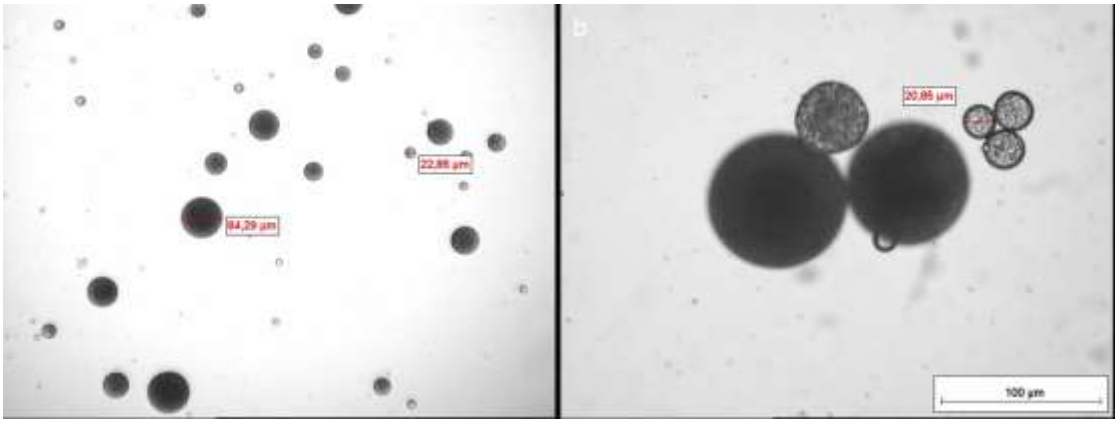

Figure 3.11 Optical micrographs of Pluronic F127-leaching PLGA microdroplets after 5min emulsification in PVA solution at (a) low and (b) high magnification. No pores exhibited on PLGA droplets.

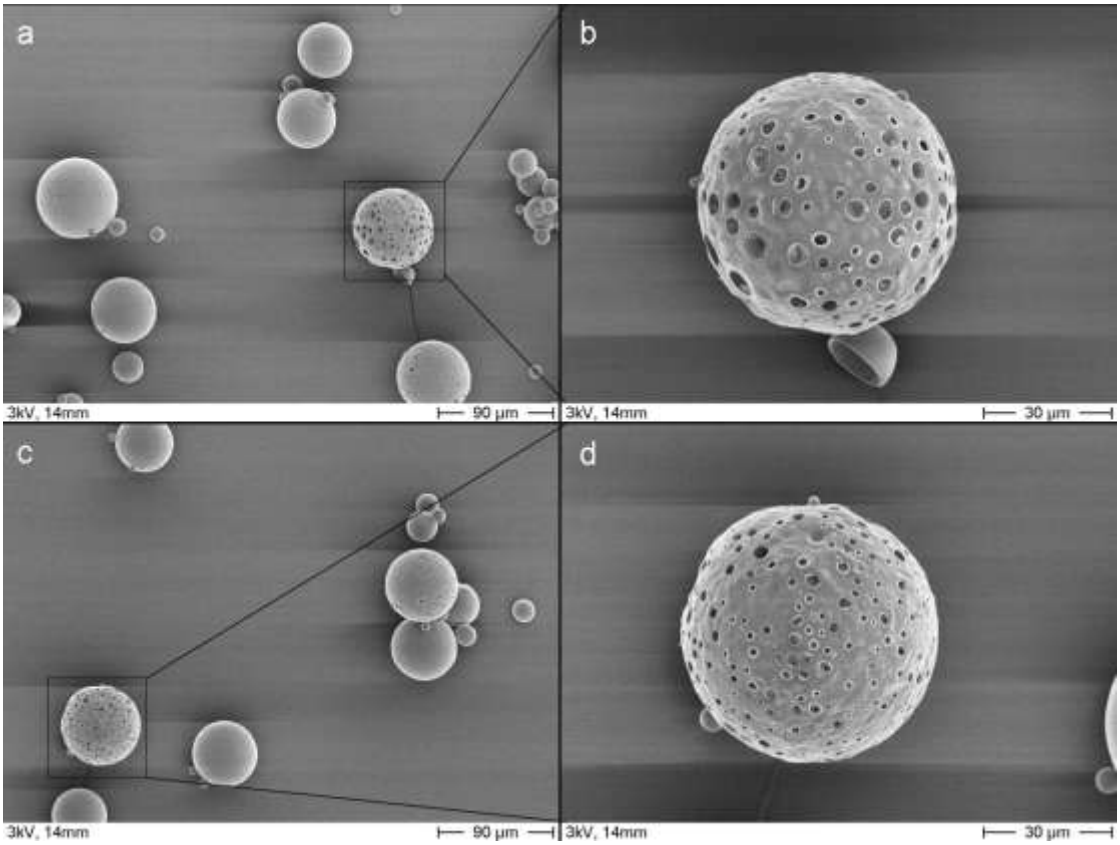

Figure 3.12 SEM micrographs of Pluronic F127-leaching porous MS emulsified by: (a, b) PVA and (c, d) DSS. Only some MS showed well distributed pores on the surface. Pluronic F127 did not inhibit DSS emulsion function.

3.3.5. Effects of fabrication parameters on MS morphology in the extractable porogen method

3.3.5.1. Effects of anionic surfactants on MS morphology

No droplet aggregation occurred after changing the external surfactant solution from PVA to DSS, and only part of the resultant MS exhibited well distributed pores on the surface (Figure 3.12c, d). This highlights the fact that the extractable porogen Pluronic F127 did not inhibit the anionic surfactant DSS compared with the osmogen KCl. The pores on the MS emulsified by DSS (average 2 µm) were similar to those using PVA as the external surfactant (average 3.5 µm).

3.3.5.2. Effects of homogenization speed on MS morphology

In order to distribute porogen Pluronic F127 more homogeneously in PLGA droplets to generate pores on every microsphere, a higher homogenization speed of 24,000 rpm was applied instead of 6500 rpm to make the O/W emulsion. However, most of the resultant MS were still nonporous (Figure 3.13a) although the average microsphere size decreased from 60μm (Figure 3.12a) to 8μm.

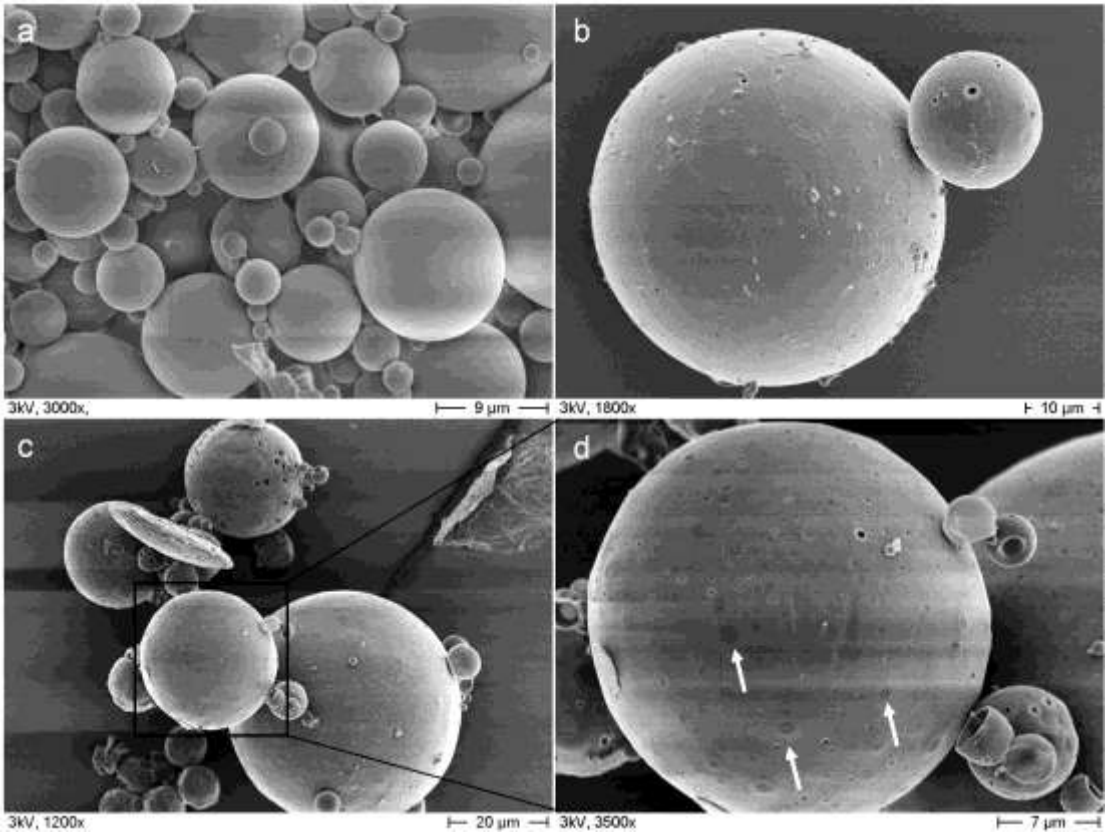

Figure 3.13 SEM micrographs of Pluronic F127-leaching porous MS fabricated at (a) higher homogenization speed 24k rpm, (b) higher F127:75 PLGA ratio (700:150), and (c, d) 50:50 PLGA instead of 75:25 PLGA. (d) Pores covered by a thin skin layer are marked by white arrows. Most MS were still nonporous.

3.3.5.3. Effects of Pluronic F127: PLGA ratio on MS morphology

Increasing the porogen Pluronic F127: PLGA ratio from 700:300 to 700:150 did not generate more pores on the MS (Figure 3.13b), although higher Pluronic F127: PLGA ratio increased the chance of distributing more Pluronic F127 onto each PLGA droplet

to induce more pores.

3.3.5.4. Effects of different PLGA composition on MS morphology

50:50PLGA has lower viscosity (0.55 dL/g) than 75:25PLGA (0.57 dL/g), which makes 50:50PLGA more likely to be mixed homogeneously with porogen Pluronic F127 in the primary oil emulsion to generate more homogeneously distributed pores. Nevertheless, most MS made of 50:50PLGA were still nonporous (Figure 3.13c). The high magnification image (Figure 3.13d) of the single microsphere demonstrated that there were many pores covered by a thin skin layer on the microsphere surface.

3.3.5.5. Effects of different extractable porogen on MS morphology

Another extractable porogen, PEG, was investigated as the alternative of Pluronic F127 to fabricate porous MS. The MS did not aggregate (Figure 3.14a), indicating that PEG did not inhibit DSS emulsion function as Pluronic F127.

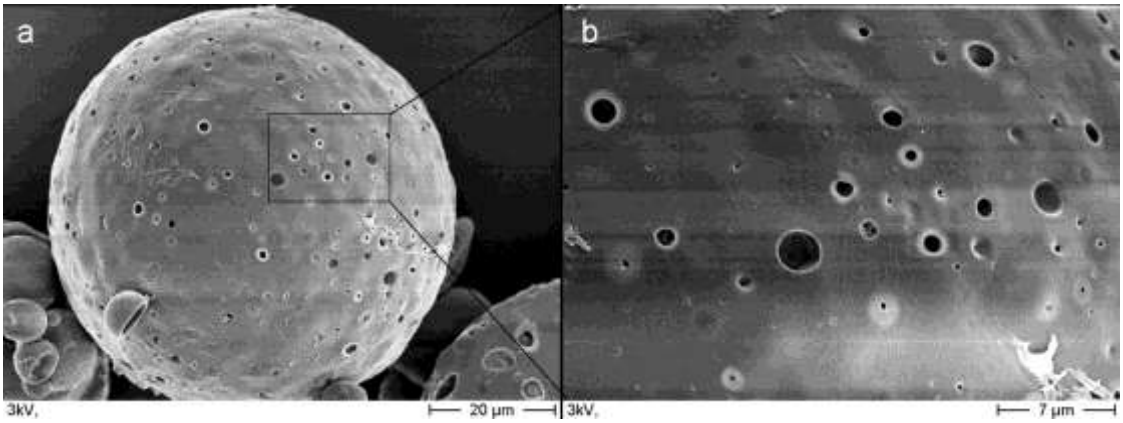

Figure 3.14 SEM micrographs of PEG-leaching porous MS. Most MS were porous with pore size arranging from 0.5-3 µm.

Most MS made by PEG were porous with small pores ranging from 0.5-3 µm (Figure 3.14a, b). This indicates that PEG was more homogeneously distributed in PLGA droplets than Pluronic F127.

3.3.6. Porous MS fabricated by gas foaming porogen NH_4HCO_3

After pouring the primary W_1/O emulsion into the external surfactant PVA solution, obvious gas bubbles appeared in the PLGA droplets using the gas forming porogen NH_4HCO_3 (Figure 3.15a, b). These are different compared to the PLGA droplets formed during the pore-forming process using osmogen (Figure 3.6) or the extractable porogens (Figure 3.11). These gas bubbles enlarged the PLGA droplet size (Figure 3.15b), consistent with Kim *et al.*'s report [109]. After 3 hour, most organic solvent DCM in the PLGA droplets evaporated, which resulted in the solidification of PLGA droplets to become porous MS (Figure 3.15c). The SEM micrograph (Figure 3.15d) of resultant MS further confirmed the presence of larger pores (average 10 μm in diameter) scattered on the MS surface, but some pores were partially covered by a thin skin layer.

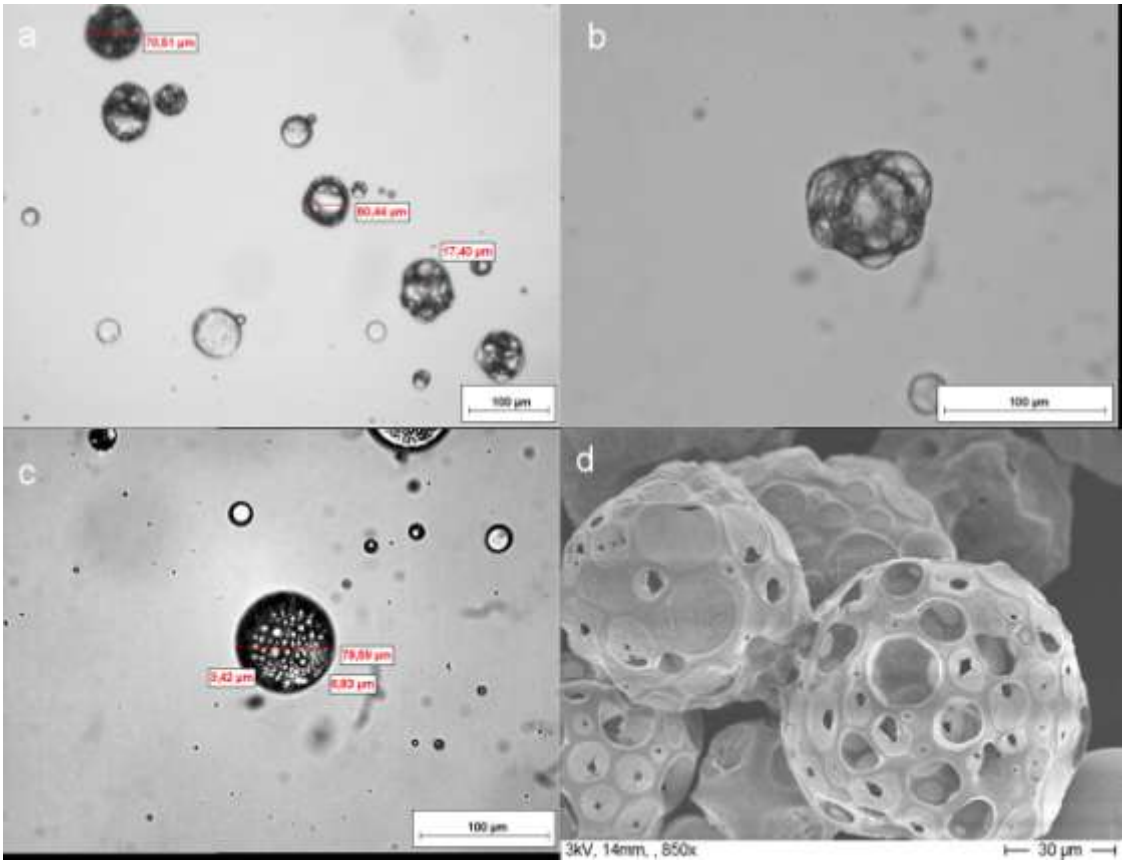

Figure 3.15 Optical micrographs of gas foamed PLGA droplets after pouring the primary W_1/O emulsion into the external PVA solution for (a, b) 5min, (c) 3h; and (d) SEM micrograph of resultant hardened MS. Gas bubbles were generated from the internal NH_4HCO_3 water phase in the PLGA droplets. Hardened PLGA MS exhibited big pores (average 10µm) with some pores partially covered by a skin layer.

The function of NH_4HCO_3 in generating pores on MS was further confirmed by MS fabricated in the same conditions but without NH_4HCO_3 or homogenization (Figure 3.16). Microspheres, without NH_4HCO_3 or homogenization (Figure 3.16), exhibited a smooth surface similar to the conventional MS (Figure 3.5), and were bigger in diameter (200-270 µm) than those made with NH_4HCO_3 (45-80 µm) (Figure 3.15).

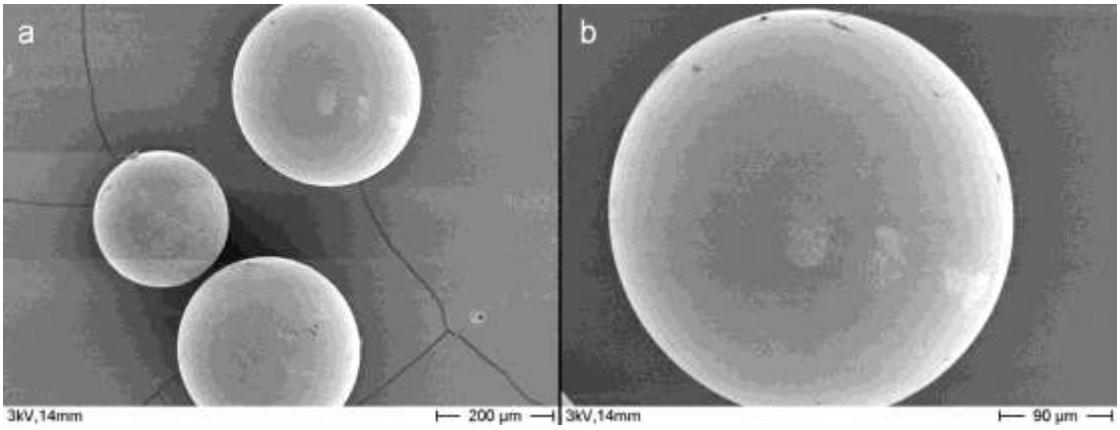

Figure 3.16 SEM micrographs of MS fabricated at the same condition without NH_4HCO_3 or homogenization. MS exhibited smooth surface as the conventional MS and bigger sizes (200-270µm) than those made with NH_4HCO_3.

3.3.7. Effects of fabrication parameters on MS morphology in the gas foaming method

Various parameters of the gas forming based $W_1/O/W_2$ double emulsion method were investigated to control the surface pore size and porosity of the porous MS.

3.3.7.1. Effect of PLGA concentration on MS morphology

There were more pores covered partially by a thin skin layer (Figure 3.17b) on the MS using 2.5% (w/v of 8ml DCM) PLGA than those made by 1.6% PLGA (Figure 3.17a), although the skin layer covered on some pores were particially broken (Figure 3.17b). The average open pore size (pores not covered by the skin layer or the holes on the skin layer) decreased from 10µm to 8µm, and the open pore porosity (surface areas of open pores/surface area of MS) decreased from 30% to 28% (Figure 3.18).

A similar trend was seen when increasing the PLGA concentration further to 3.8% (Figure 3.17c). When the PLGA concentration is increased, there is an increase in

microsphere size (Figure 3.17) along with a decrease in open pore size and porosity (Figure 3.18).

With further increase of the PLGA concentration to 6.2%, the average microsphere sizes increased greatly to over 150μm, almost double than those made of 3.8% PLGA (Figure 3.17d), while the average open pore sizes and ratio decreased to 5μm and 22% respectively (Figure 3.18). As the pores were too small, there was no obvious skin layer on the pores.

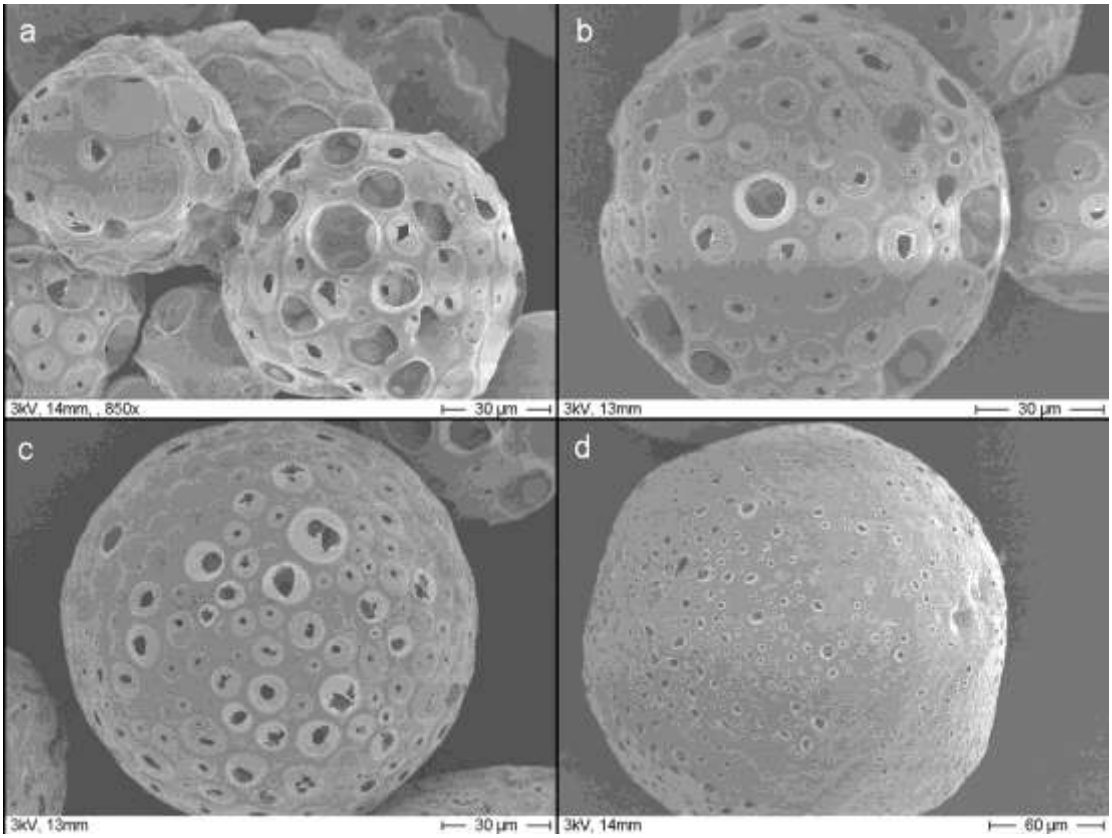

Figure 3.17 SEM micrographs of gas foamed porous MS made at different 75:15PLGA concentration (w/v of 8ml DCM) (a) 1.6%, (b) 2.5%, (c) 3.8%, and (d) 6.2%. The surface open pore sizes and ratio of the total surface area decreased with increasing PLGA concentration.

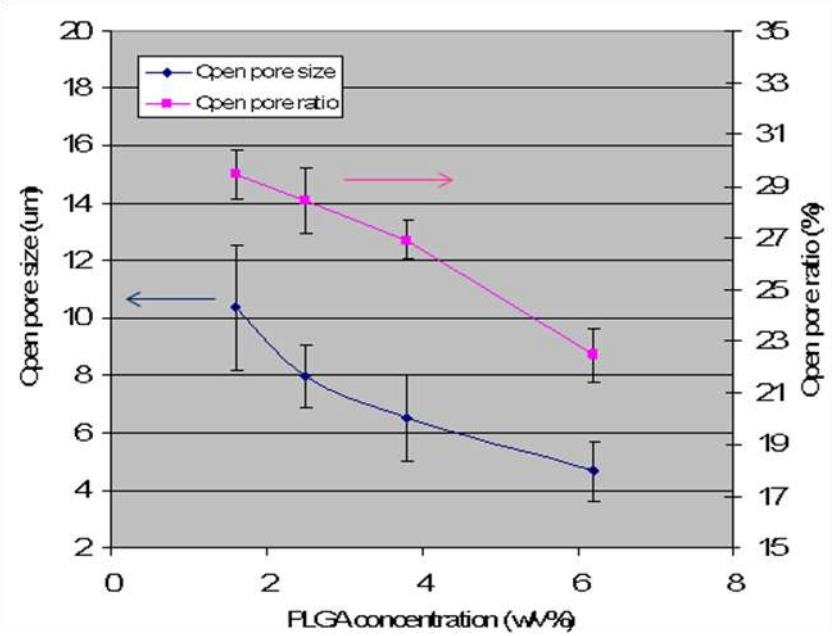

Figure 3.18 The surface open pore size (μm) ● and ratio (%) ■ of the total MS surface area decreased with increasing PLGA concentration (w/v) in DCM from 1.6 to 6.3%.

3.3.7.2. Effect of NH_4HCO_3 concentration on MS morphology

Using a PLGA concentration of 1.6% (w/v), increasing the NH_4HCO_3 concentration from 1% to 4% made the recovered PLGA mass lose the sphere structure and collapse to become porous sponges (Figure 3.19).

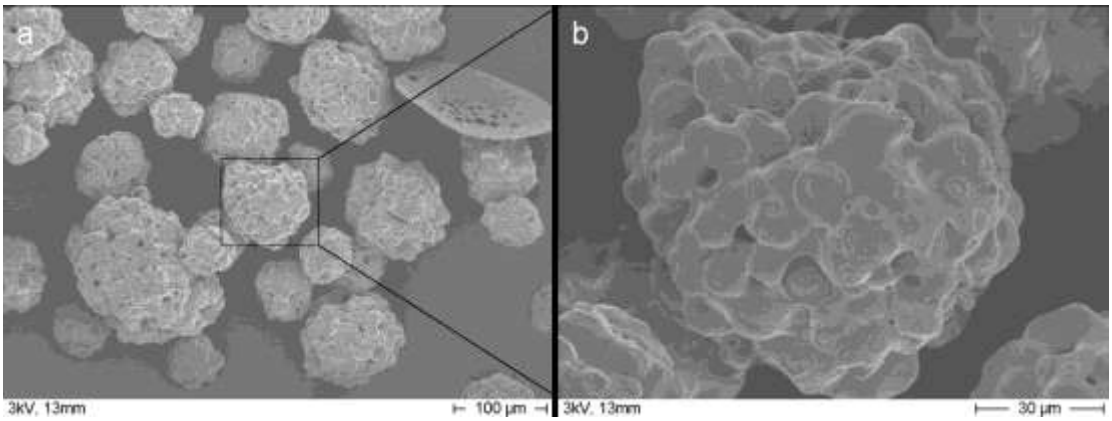

Figure 3.19 SEM micrographs of gas foamed porous MS (1.6% PLGA) collapsed when increasing NH_4HCO_3 concentration to 4%: (a) gross and (b) single morphology. MS collapsed to porous sponges.

When the NH_4HCO_3 concentration was kept at 4%, the microsphere collapse occurred

at higher PLGA concentration (3.8%) (Figure 3.20a), but some resultant PLGA microparticles appeared more spherical (Figure 3.20b) than those made at 1.6% PLGA (Figure 3.19b). Although the resultant PLGA mass was no longer a microsphere but a porous sponge-like microparticle, the surface pores caused by the effervescence of NH_4HCO_3 were still covered by a skin layer (Figure 3.20c, d) similar to the skin layer in previous covered porous MS (Figure 3.17).

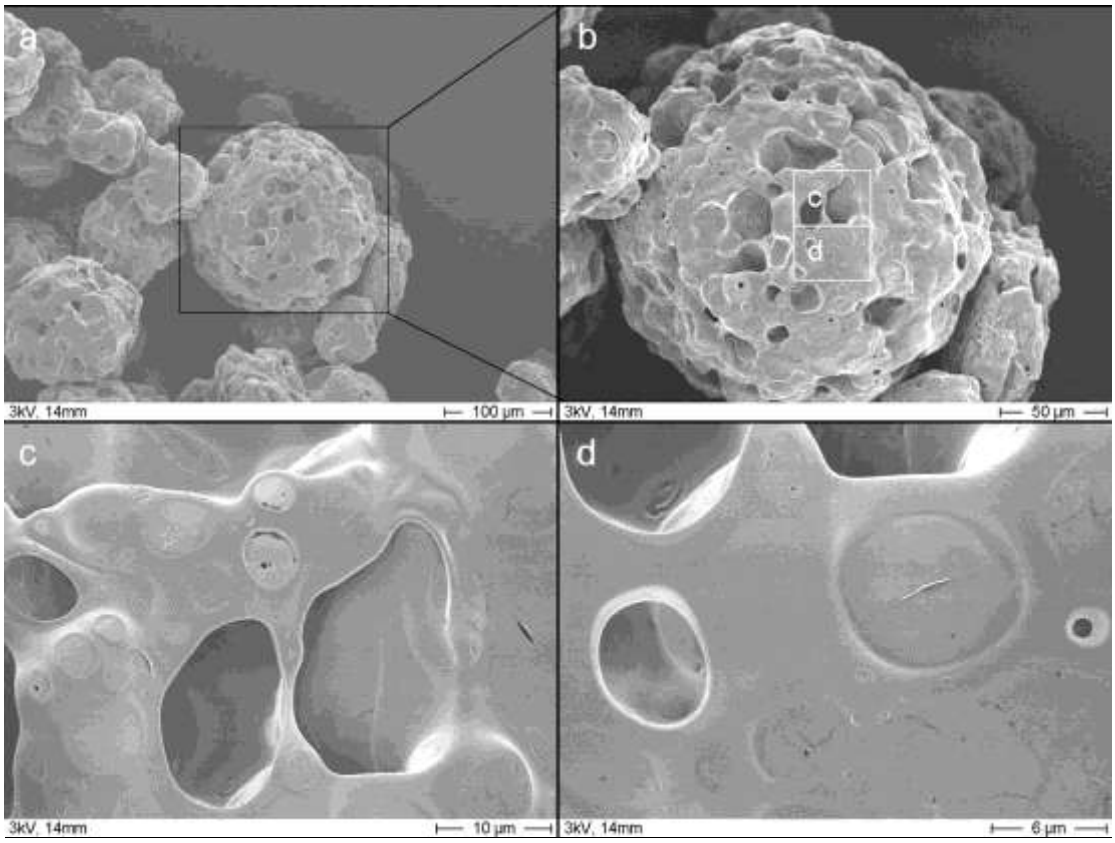

Figure 3.20 SEM micrographs of gas foamed porous MS (3.8% PLGA) collapsed when increasing NH_4HCO_3 concentration to 4%: (a) gross and (b) single morphology: (c) surface of destroyed sphere structure and d) some pores were still covered.

When the NH_4HCO_3 concentration was decreased to 2% (w/v of 2.5 ml water) and the PLGA concentration was 3.8%, the recovered PLGA mass were still sponge-like microparticles (Figure 3.21a, b). When keeping the NH_4HCO_3 concentration at 1% but increasing the NH_4HCO_3 volume from 2.5ml to 5ml, the recovered PLGA mass

became even bigger sponge-like particles (Figure 3.21c, d) than those using 2.5 ml with a 2% NH_4HCO_3 concentration (Figure 3.21a, b).

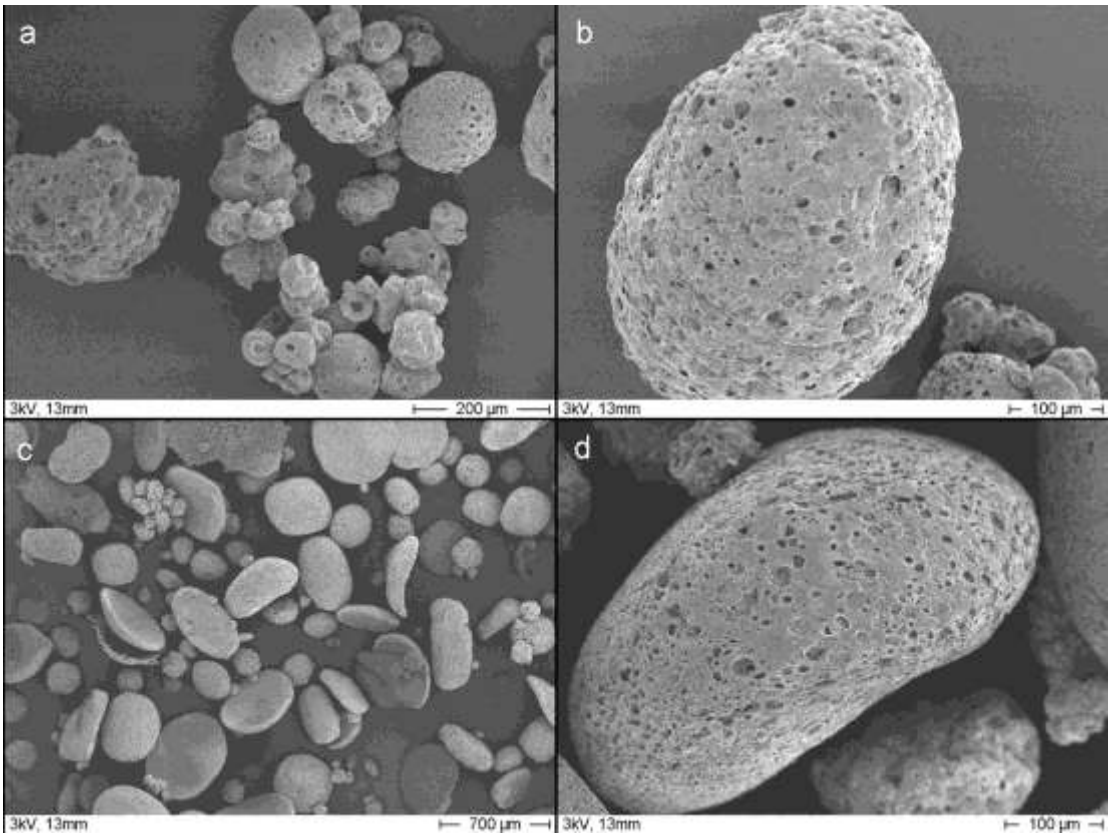

Figure 3.21 SEM micrographs of gas foamed porous MS(3.8% PLGA) collapsed when (a, b) decreasing NH_4HCO_3 concentration to 2%, and (c, d) increasing the 1% NH_4HCO_3 volume to 5ml. MS collapsed to sponge-like microparticles.

3.3.7.3. Effect of PLGA composition on MS morphology

When NH_4HCO_3 concentration was 1% (w/v of 2.5ml water), MS made by 1.6% 50:50 PLGA (lactide: glycolide=50:50) had more open porous pores, the surface skin layer of which was broken (Figure 3.22a), than those using 75:15 PLGA (Figure 3.17a). In contrast, there were a thicker skin layer and fewer open porous pores on the surface of MS made with 1.6% 85:15 PLGA (Figure 3.22b).

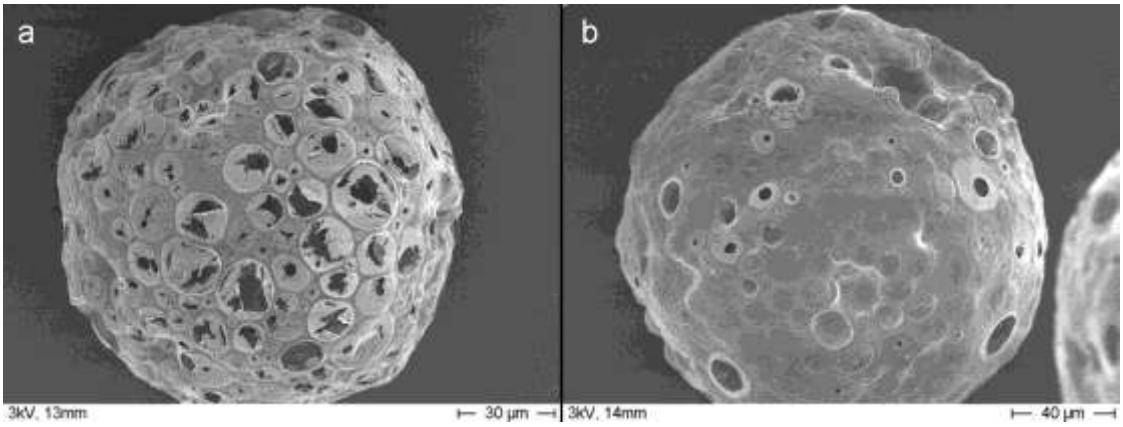

Figure 3.22 SEM micrographs of gas foamed porous MS made by (a) 50:50 PLGA and (b) 85:15PLGA. More skin layers were broken to form open pores on MS made by 50:50 PLGA than those using 85:15 PLGA.

3.3.7.4. Effect of the external solution volume on MS morphology

When using 2.5 ml 1% NH_4HCO_3 (W_1) and 8 ml DCM of 1.6% 75:15 PLGA (O), almost all surface pores were completely covered by a skin layer with an increase in the external PVA solution volume (W_2) from 200ml to 400ml, namely O:W_2=8:400 (Figure 3.23a).

The cross section image of the resultant covered porous microsphere (Figure 3.23b) demonstrated that there were interconnected holes (around 6-12 µm) inside the microsphere and the skin layer was thinner than 2 µm.

With a higher W_2 volume of 800ml (O: W_2=8:800), there were some pores covered by a very thick skin layer on the microsphere surface (Figure 3.23c, d), indicating that the gas bubbles made by the effervescence of NH_4HCO_3 were blocked in the solidificated periphery of the MS deeply. The gas bubbles only created the protruded surface parts but could not break the thick and dense periphery layer.

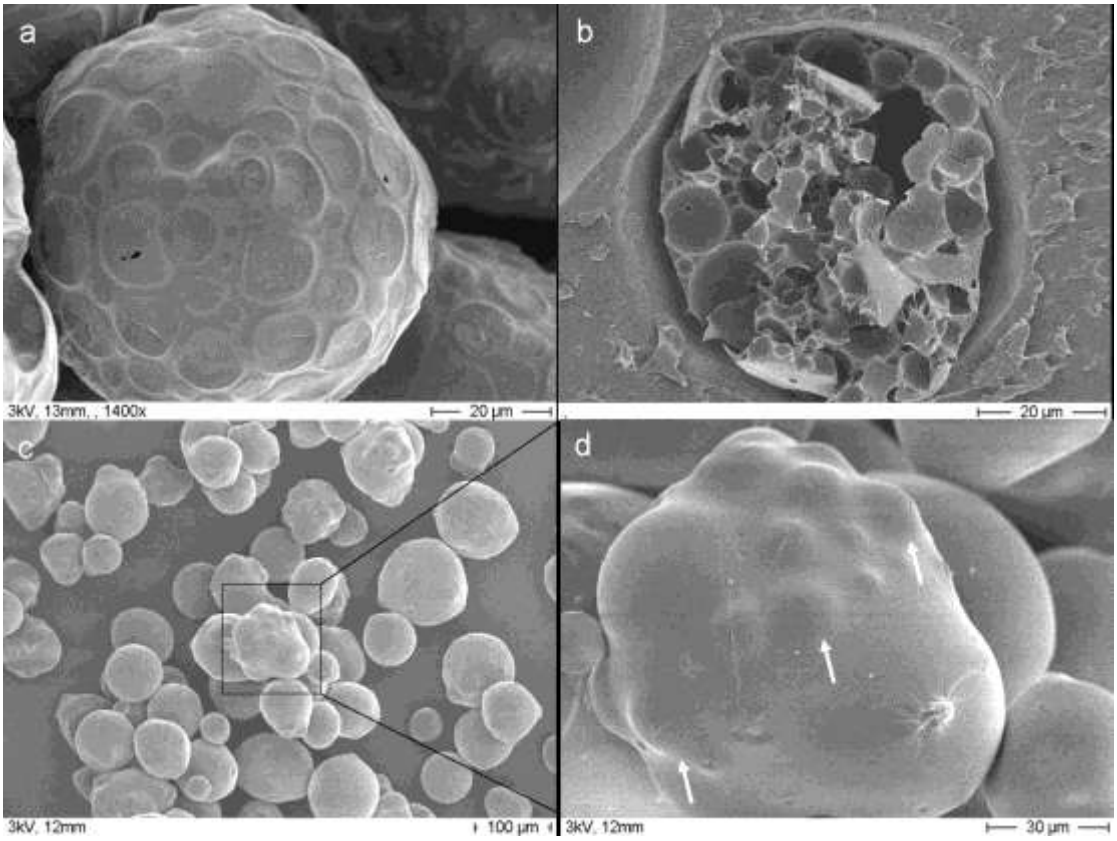

Figure 3.23 SEM micrographs of gas foamed porous MS made at different O: W2 ratio: (a, b) 8: 400 and (c, d) 8:800. (b) Cross sectional area of MS made at O: W2 ratio 8:400; (d) single morphology of microsphere made at O: W2 ratio 8:800 with protruded parts marked by white arrows.

With O:W_2 at 8:800 and a NH_4HCO_3 concentration of 4%, the recovered PLGA mass was not made up of sponge-like microparticles as shown on Figure 3.19, but were covered porous MS(Figure 3.24a, b). The gas bubbles still could not break the dense periphery layer of the MS, but there were obvious pores (Figure 3.24b) rather than protruded parts (Figure 3.23d) on the microsphere surface. All these pores were covered by a thicker and denser skin layer (Figure 3.24b) than those using 1% NH_4HCO_3 and 200 ml external solution (W_2) (Figure 3.17a).

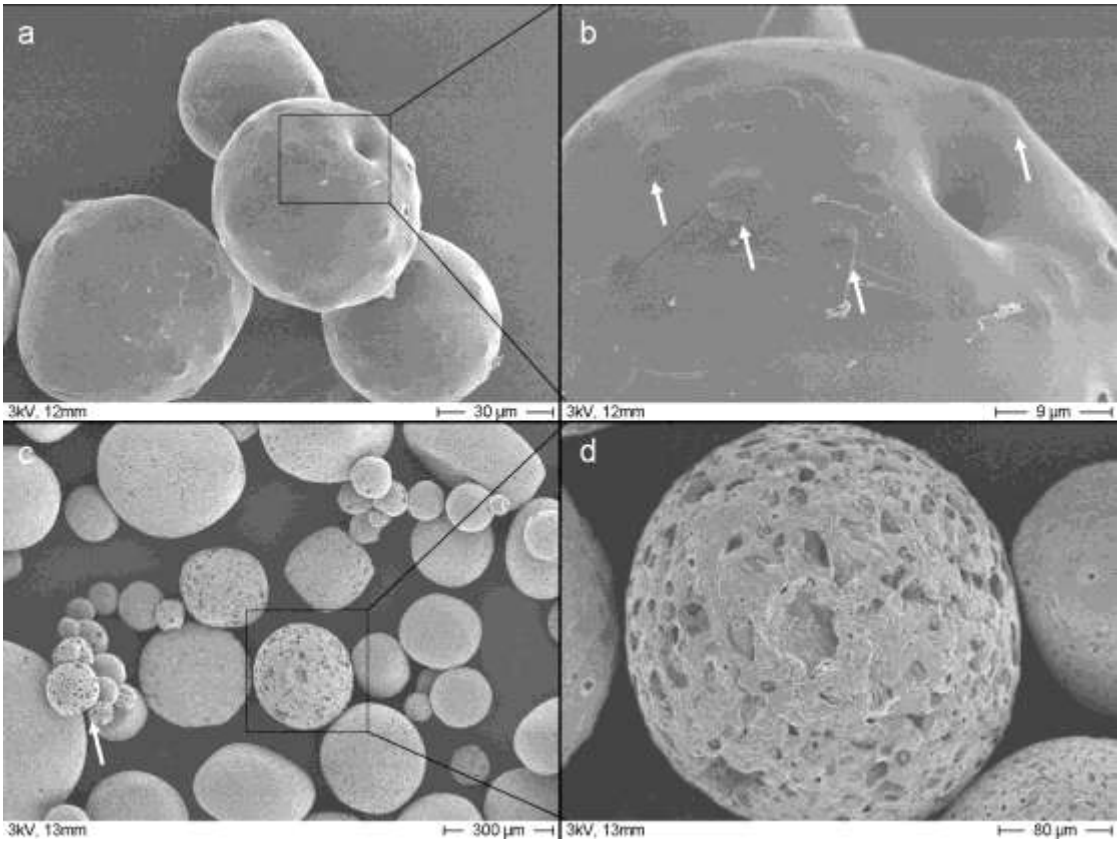

Figure 3.24 SEM micrographs of gas foamed porous MS made at (a, b) 4% NH4HCO3 with O: W2 ratio 8:800 and (c, d) 1% NH4HCO3 with O: W2 ratio 8:100. (b) Pores covered with a thick skin layer are marked by white arrows. (c) Some recovered PLGA mass were partially porous MS marked by white arrows.

In contrast, when the W_2 volume was decreased to 100ml (O:W_2=8:100), some of the recovered PLGA mass were partially porous MS(Figure 3.24c, marked by the white arrow), but most of the PLGA mass had become like large rough particles (Figure 3.24c, d), different from the sponge-like microparticles (Figure 3.19).

3.3.8. Characterization of the skin layer covering the pores

The source of the skin layer was presumably either solidificated PLGA from the PLGA droplets (O) or precipitated PVA from the external solution (W_2). Three candidates, dry PVA, 75:15 PLGA as purchased, and freeze dried covered porous

MS(imaged at Figure 3.17a) were analyzed separately by the ATR-IR. Multiple peaks, including the characteristic peaks of –COC- at 1085 cm^{-1} and –CO- at 1750 cm^{-1}, were found to overlap in the ATR-IR spectra of PLGA and covered porous MS (Figure 3.25). The characteristic peaks of –OH at 3280 cm^{-1} in PVA was not found in the ATR-IR spectra of covered porous MS (Figure 3.25). These data indicates that the source of the skin layer was PLGA itself from the solidification of PLGA droplets, consistent with Bae *et al.*'s report of covered porous MS made by the gas foaming porogen H_2O_2 [110].

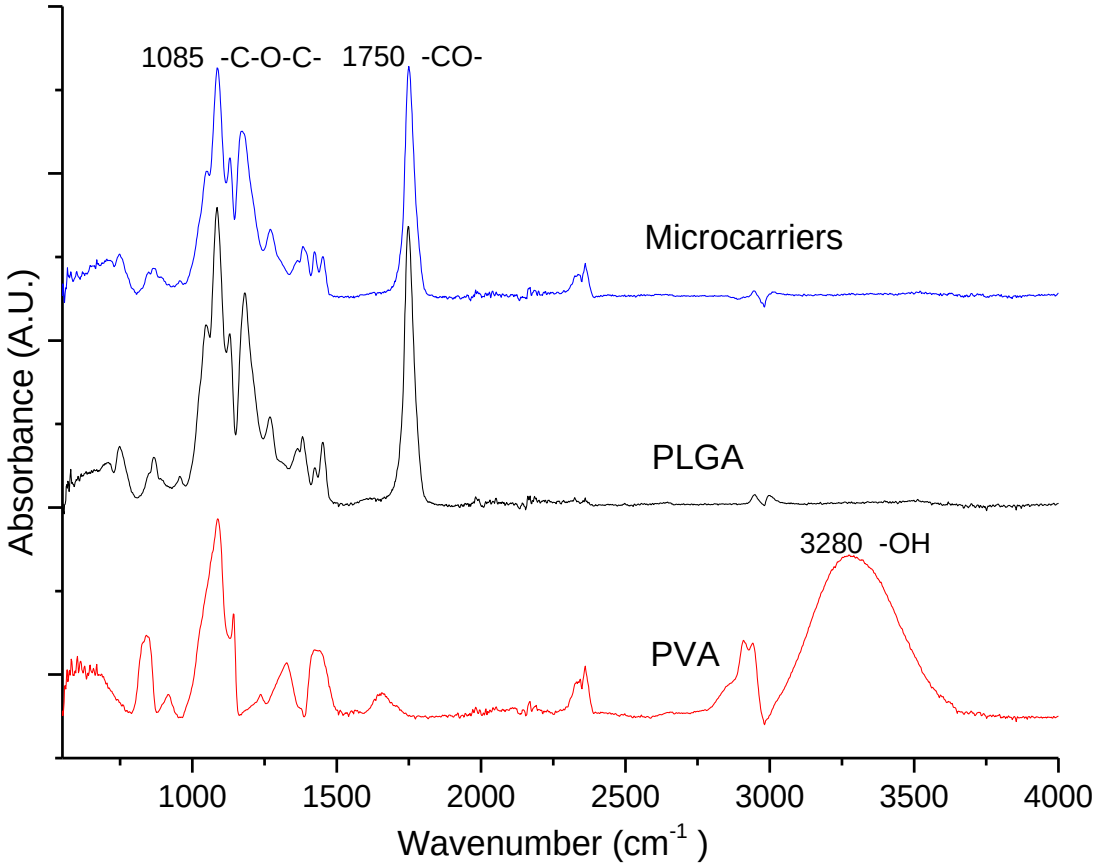

Figure 3.25 Analysis of the skin layer of the covered porous MS using ATR-IR. The multiple peaks were found to overlap in MS and PLGA polymer.

3.3.9. Surface modification of gas foamed porous MS

In order to control the surface open pore size and porosity, gas foamed porous MS

covered by the PLGA skin layer were further immersed in different solutions to remove the skin layer. Various solution types, concentrations and immersion time were investigated to optimize the surface open pore size and porosity.

3.3.9.1. NaOH modification

Since NaOH can hydrolyse the PLGA copolymer into lactide and glycolide, NaOH solution was the first treatment chosen to modify the covered porous MS after confirming the skin layer as PLGA. After 2min immersion in 0.5 mg/ml NaOH (the time was decided based on the experiments discussed later), parts of the PLGA skin layer of covered porous MS (Figure 3.17 a) was hydrolysed into frayed segments (Figure 3.26a). The frayed segments (Figure 3.26a marked by white arrows) indicates that the hydrolysis by NaOH was inadequate to hydrolyze the whole skin layer, but only the thinner parts of the skin layer. The high magnification image of a single microsphere (Figure 3.26) further demonstrated that the hydrolysis process only broke parts of the skin layer while there were still some pores covered by a thin skin layer on the microsphere surface.

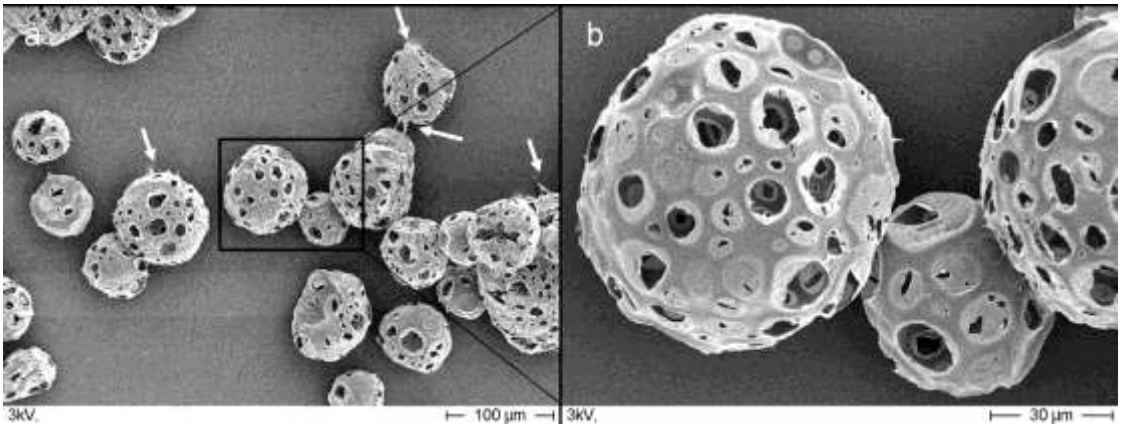

Figure 3.26 SEM micrographs of gas formed porous MS made of 1.6% 75:25 PLGA after immersion in 0.5 mg/ml NOH (a) gross and (b) single morphology. The protruded skin segments after inadequate hydrolysis by NaOH wash are marked by white arrow.

The average open pore size on the MS did not increase significantly (from 7 to 8 µm), but the average open pore porosity (calculated by Equation 3.1) increased significantly from 28% to 32% ($p < 0.05$) after the immersion in 0.5 mg/ml NaOH solution (Figure 3.27).

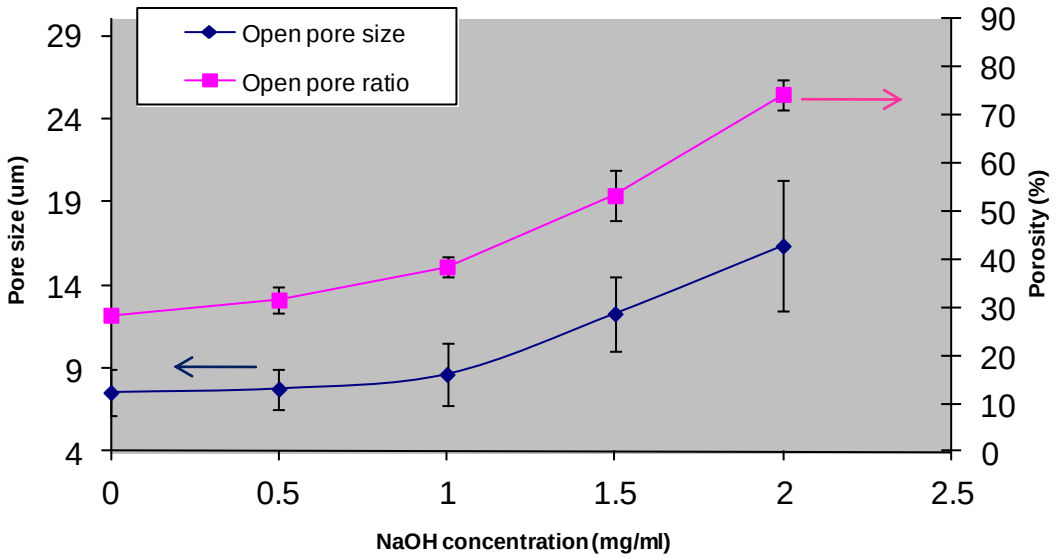

Figure 3.27 The surface open pore size (µm) ● and porosity (%) of the microsphere surface area increased with increasing the NaOH concentration in the wash solution from 0 to 2 mg/ml.

3.3.9.1.1. Effects of NaOH concentration on MS morphology

Increasing the concentration of NaOH solution to 1 mg/ml, caused more of the PLGA skin layer to hydrolyze and be washed away, and left more open pores on the microsphere surface (Figure 3.27). The average open pore size increased from 8 to 9 µm with more variations, and the average porosity increased to 39% (Figure 3.27). Moreover, the remaining skin layer (Figure 3.28d) was thinner and partially broken, compared to those washed by 0.5 mg/ml NaOH (Figure 3.26)

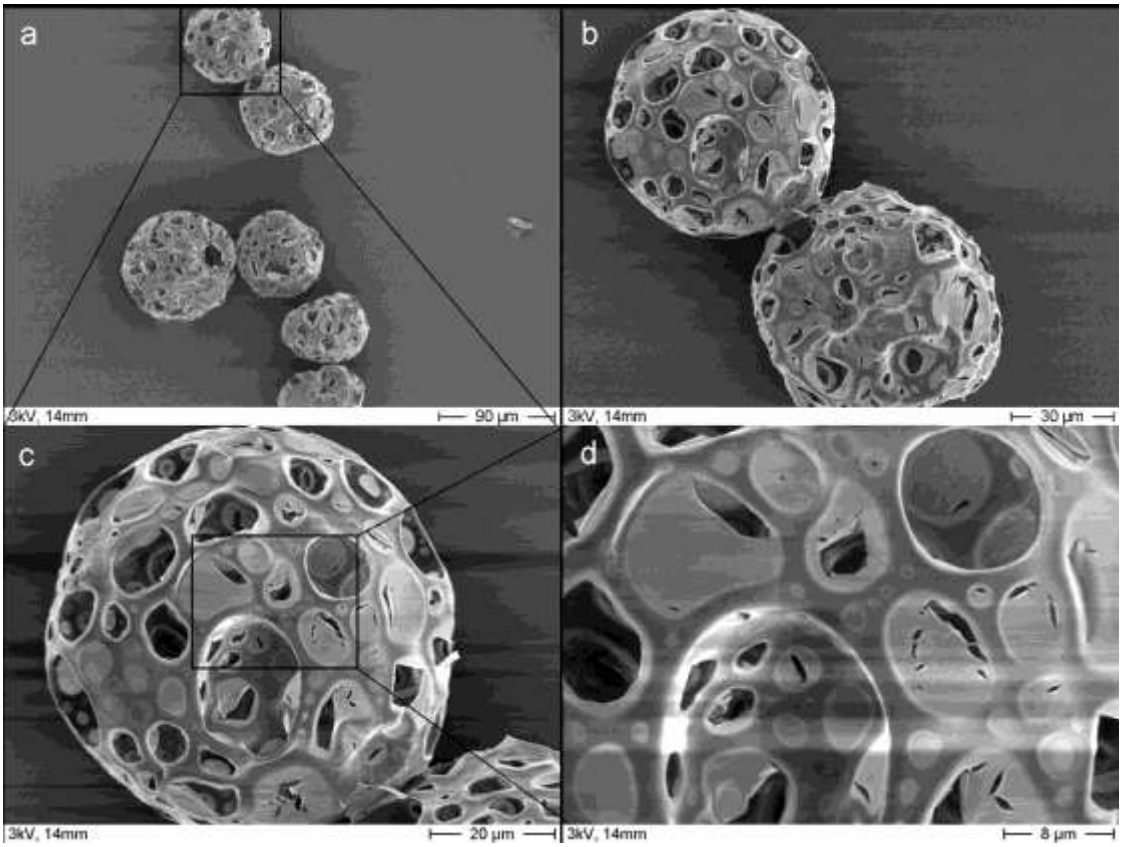

Figure 3.28 SEM micrographs of gas formed porous MS washed by 1mg/ml NaOH: (a) gross, (b and c) single and (d) detailed surface morphology. Part of the skin layers on the surface pore was hydrolysed and washed away. The skin layer which remained was thinner.

Further increasing the NaOH concentration to 1.5 mg/ml, more PLGA skin layer was hydrolysed, creating open porous structures on every microsphere regardless of the microsphere size (Figrure 4.26). The high magnification SEM micrographs (Figrure 4.26c, d) indicate that the PLGA skin layer was almost completely hydrolysed from every pore but there were still some skin layer residues left. Both the average open pore size and porosity increased significantly ($p < 0.05$) to 12 µm and 53% respectively (Figure 3.27).

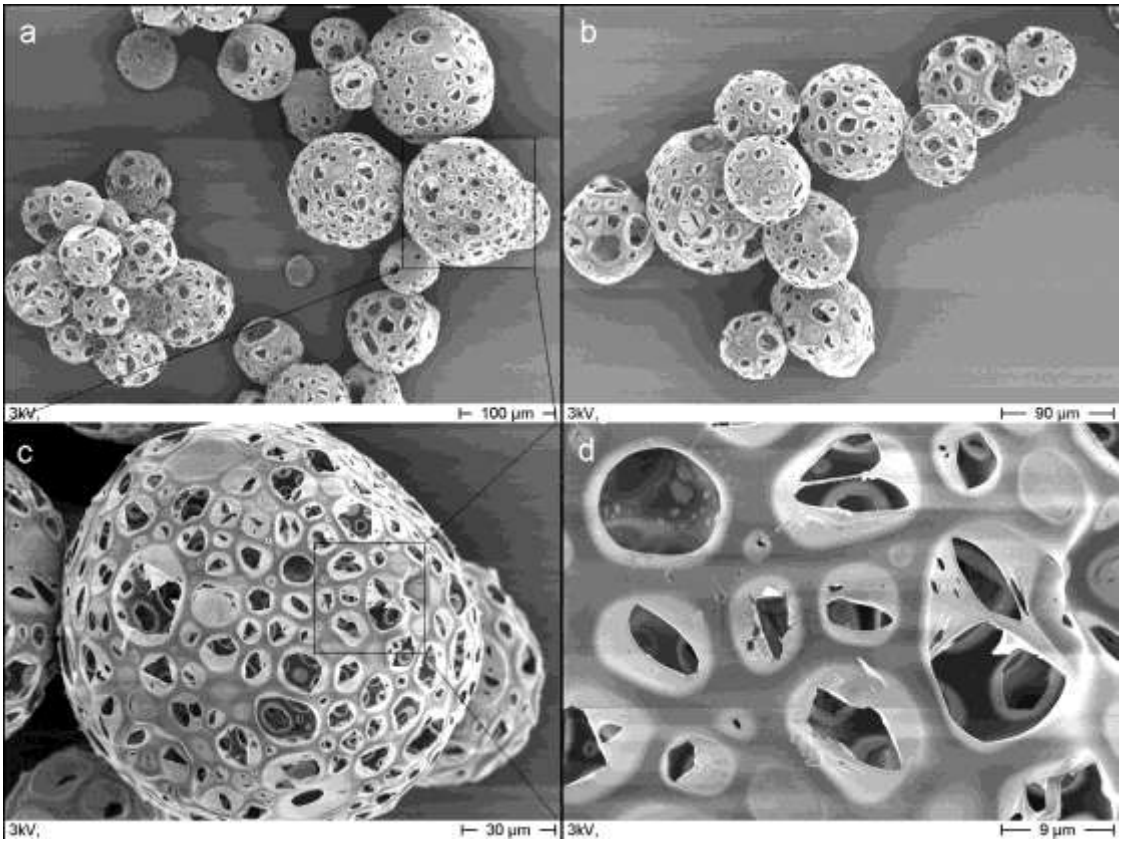

Figure 3.29 SEM micrographs of gas formed porous MS washed by 1.5 mg/ml NaOH: (a, b) gross, (c) single and (d) detailed surface morphology. Most skin layers on the surface pore were hydrolysed and broken, but some skin layer residues remained.

Once increasing the NaOH solution concentration from 1.5 to 2 mg/ml, the skin layer of the MS made of 1.6% 75:25 PLGA, was completely decomposed after 2 min NaOH immersion without destroying the bulk structure of the MS (Figure 3.30). At this concentration, NaOH only hydrolysed the surface PLGA skin layer (thinner than 2 µm, measured from Figure 3.23 b) and created a finely interconnected porous structure (Figure 3.30b). The average open pore size and porosity also greatly increased from 12 to 16 µm and 53% to 75% respectively (Figure 3.27), making these open porous MS more suitable for cell culture than these covered porous MS (Figure 3.17 a).

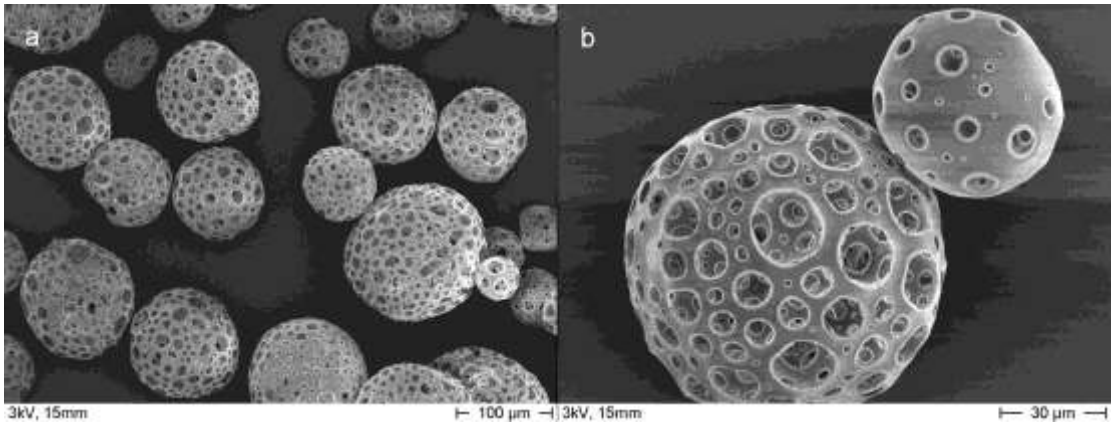

Figure 3.30 SEM micrographs of gas formed porous MS made of 1.6% 75:25 PLGA after immersion in 2 mg/ml NaOH: (a) gross and (b) single morphology. The skin layer was completely hydrolysed and washed away.

3.3.9.1.2. Effects of PLGA concentration on MS morphology

Gas formed porous MS made of 75:25 PLGA were also immersed in 1.5 mg/ml NaOH for 2 min to investigate the effects of PLGA concentration on NaOH modification. Using the same NaOH modification parameters, the PLGA skin layer on MS made with the higher PLGA concentration (2.5%) were partially hydrolysed to create more open pores (Figure 3.31) on the surface than before (Figure 3.17 b), and there were still thin skin residues covering some pres (Figure 3.31c). Moreover, some small pores were even covered by a thick unbroken skin layer, indicating inadequate hydrolysis by NaOH modification (Figure 3.31d). The skin layer of MS made by 2.5% PLGA was thicker and covering more pores (Figure 3.17b) than that made by 1.6% PLGA (Figure 3.17a), and thus more difficult to be completely decomposed by hydrolysis.

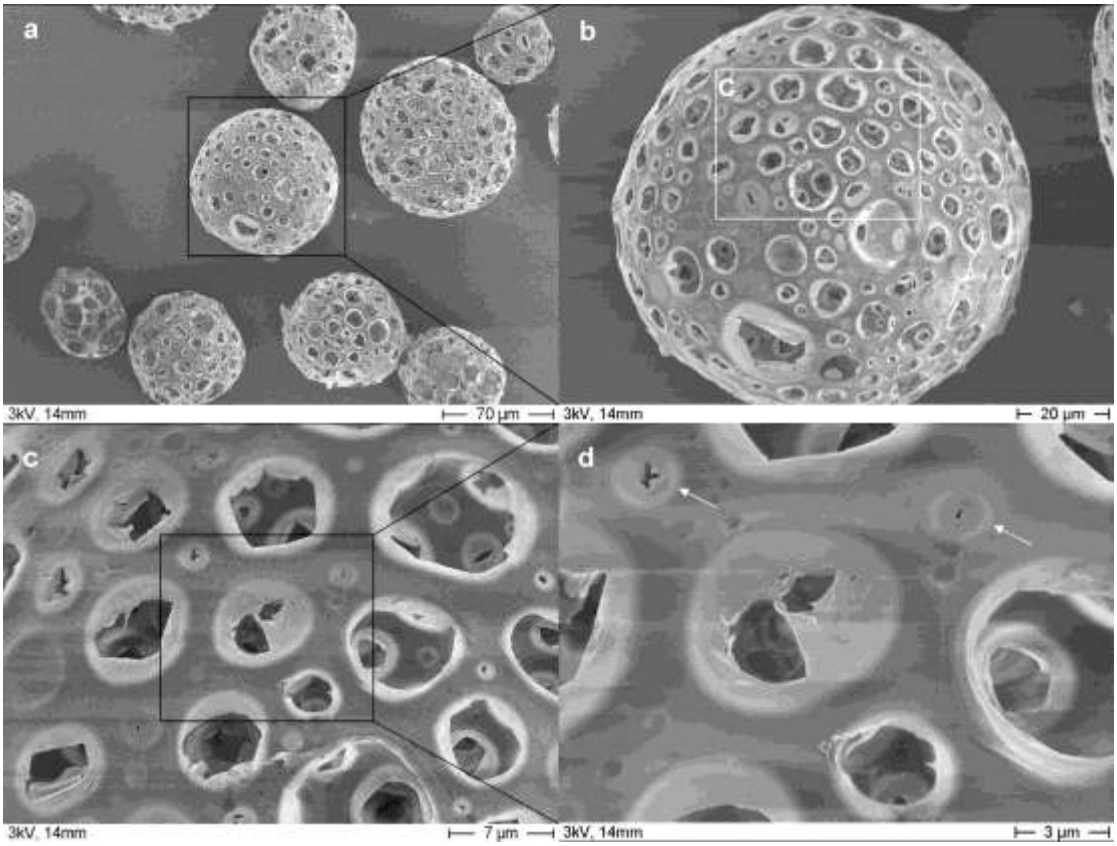

Figure 3.31 SEM micrographs of gas formed porous MS made with higher PLGA concentration (2.5%) washed by 1.5 mg/ml NaOH: (a) gross, (b) single morphology, and (c, d) detailed surface morphology. The unbroken skin layers after inadequate hydrolysis by NaOH wash are marked by white arrows.

However, the thicker skin layer, which had higher resistance for 1.5 mg/ml NaOH than those made by 1.6% PLGA, was also completely hydrolysed by 2 mg/ml NaOH in 2 min (Figure 3.32). No any skin residues were left on the surface pores (Figure 3.32b).

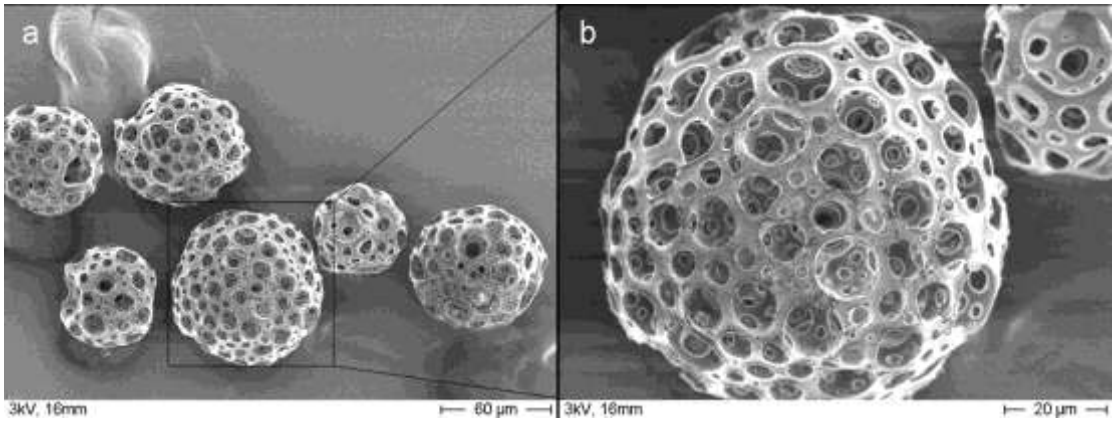

Figure 3.32 SEM micrographs of gas formed porous MS made with 75:25 PLGA concentrations (2.5%) washed by 2 mg/ml NaOH: (a) gross and (b) single morphology.

3.3.9.1.3. Effects of PLGA composition on MS morphology

PLGA composition also affected the microsphere morphology modified by 1.5 mg/ml NaOH solution. The skin layer, on porous MS made of 50:50 PLGA with lower lactide ratio, was easier to be hydrolysed (Figure 3.33) than those made of 75:25 PLGA (Figrure 4.26). The skin layer covering the pores was almost completely hydrolysed to create more open pores with less residual thin skin (Figure 3.33 b), compared with that found on porous MS made of 75:25 PLGA (Figrure 4.26c, d).

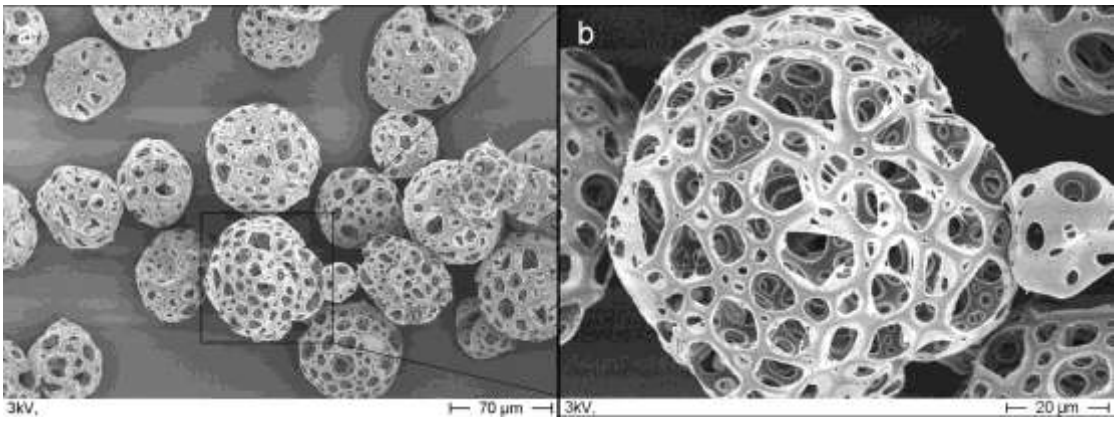

Figure 3.33 SEM micrographs of gas formed porous MS made of 1.6% 50:50 PLGA modified by 1.5 mg/ml NaOH: (a) gross and (b) single morphology. The skin layer on the surface pore was almost completely hydrolysed than that on 75:25 PLGA MS.

The thinner skin layer, on the MS that were made of 1.6% 50:50 PLGA, was also completely decomposed without destroying the bulk structure by 2 minute immersion in 2 mg/ml NaOH (Figure 3.34). All these results determined that 2 minute immersion in 2 mg/ml NaOH was the best treatment to control surface open pore size and porosity.

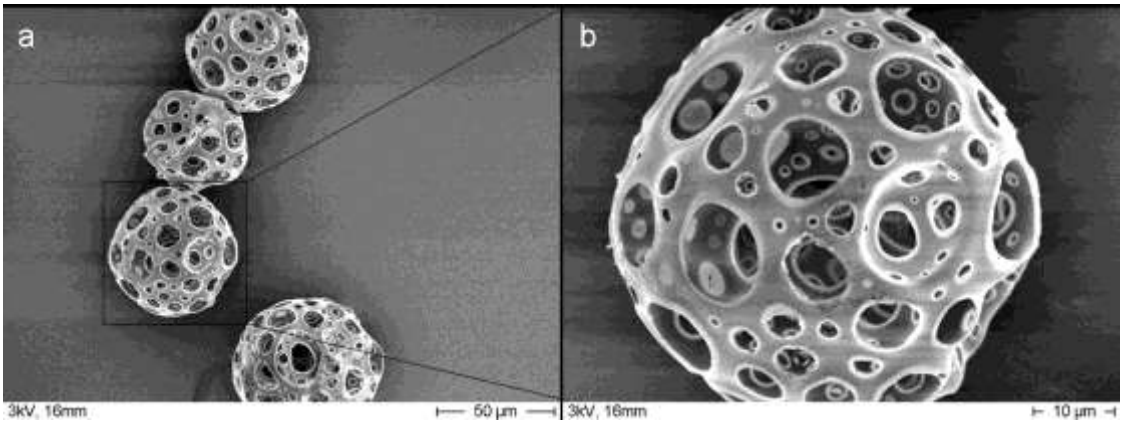

Figure 3.34 SEM micrographs of gas formed porous MS made of 1.6% 50:50 PLGA washed by 2 mg/ml NaOH: (a) gross and (b) single morphology.

3.3.9.1.4. NaOH modification on covered porous MS

Covered porous MS made with O: W_2 ratio as 8:400 with all pores completely covered by the skin layer (Figure 3.23a), were also modified by 2 mg/ml NaOH for 2 minutes. Interestingly, the entire skin layer was also completely hydrolyzed by the NaOH without damaging the MS bulk structure. This indicates that the thickness of the skin layer was not increased too much, although the higher external solution volume induced earlier solidification of the periphery of PLGA droplets prevented the gas bubbles breaking the skin layer. The surface porosity (surface pore areas: total MS surface area) of covered porous MS increased significantly from 0 to 65% after the NaOH modification. The 65% porosity is still significantly lower than that of previously known porous MS (80-99% [109, 112]) which means there are more

regions with high continuity between the pores on the microsphere surface (Figure 3.35).

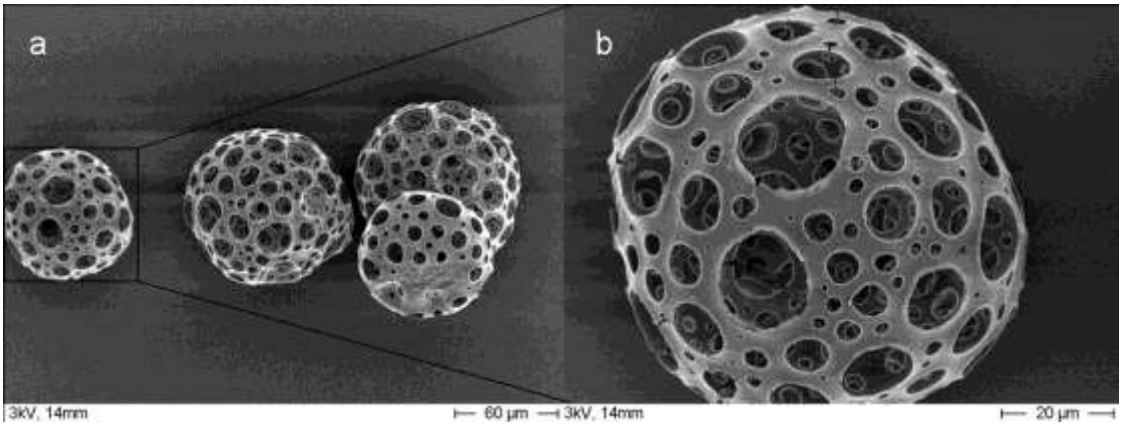

Figure 3.35 SEM micrographs of gas formed porous MS made of 1.6% 75:15 PLGA with O: W_2 ratio as 8:400 washed by 2 mg/ml NaOH: (a) gross and (b) single morphology

3.3.9.1.5. NaOH modification on nonporous MS

Nonporous MS, fabricated at the same condition as the gas foamed porous MS without NH4HCO3 or homogenization, were also immersed in 2 mg/ml NaOH for 2 min as the control group. The microsphere surface was smooth without any pores after NaOH immersion (Figure 3.36), indicating that 2 mg/ml NaOH only hydrolysed a thin surface layer of PLGA MS without generating any pores on the surface.

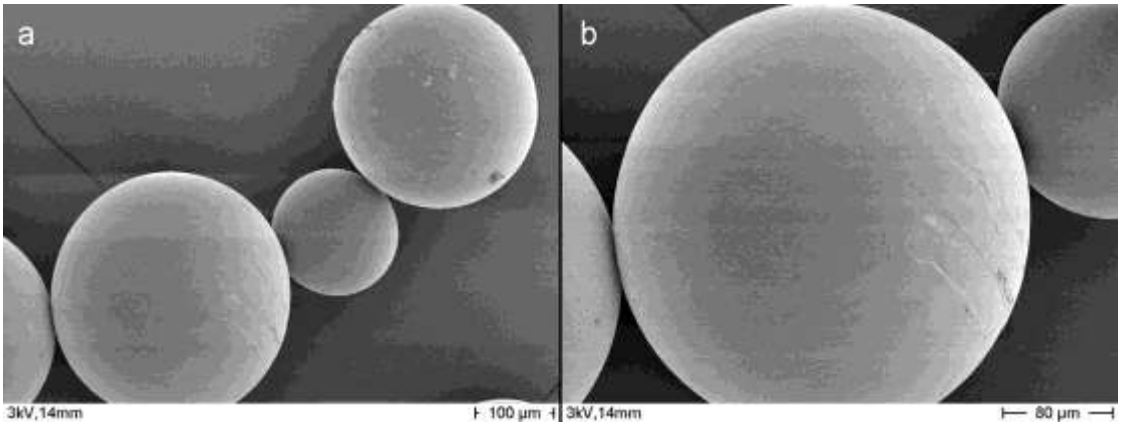

Figure 3.36 SEM micrographs of nonporous MS washed by 2 mg/ml NaOH: (a) gross and (b) single morphology. The microsphere surface was still smooth without any pores.

3.3.9.1.6. Effects of NaOH modification time on MS morphology

The bulk sphere structure of MS was destroyed, if the porous MS made of 1.6% 75:25 PLGA were immersed in 2mg/ml NaOH for a longer period of time, such as 15 min (Figure 3.37). Most MS collapsed into porous fragments (Figure 3.37 a) while only a few maintained the broken sphere structure (Figure 3.37 b).

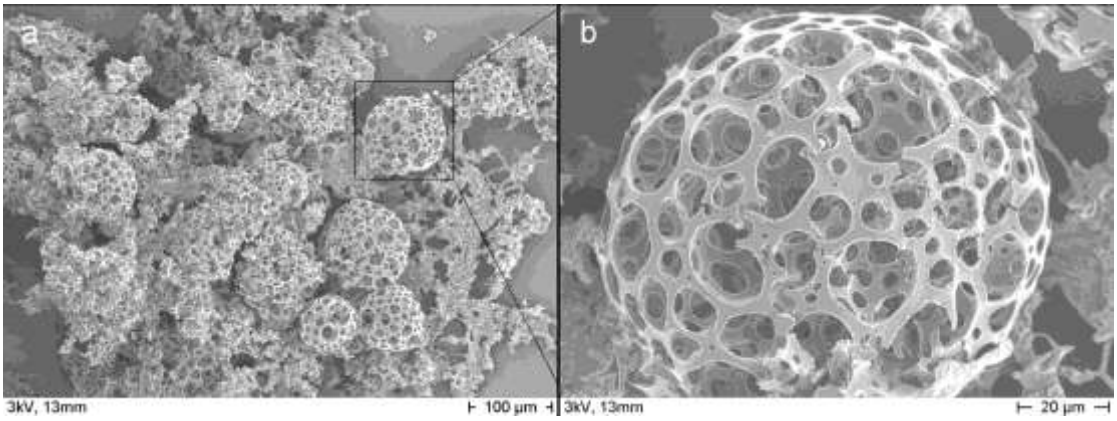

Figure 3.37 SEM micrographs of gas formed porous MS made of 1.6% 75:25 PLGA washed by 2mg/ml NaOH for 15min: (a) gross and (b) single morphology. Most MS collapsed while a few maintained the sphere structure after freeze dried.

3.3.9.2. Mixed solution modification

Since PLGA is hydrophobic, freeze dried PLGA MS were more likely to float on the surface of the NaOH solution. Therefore, the polar solvent ethanol, which can pre-wet and facilitate the dried PLGA MS to disperse homogeneously in the NaOH solution, was added to 2 mg/ml NaOH solution to investigate their function in hydrolysing the PLGA skin layer of covered porous MS. However, the covered porous MS completely collapsed when 50% (v/v) ethanol was added to the NaOH solution (Figure 3.38 a), which indicates that the addition of ethanol enabled NaOH to hydrolyze not only the surface PLGA skin layer but also the bulk sphere structure. By decreasing the ethanol concentration to 25% in the NaOH solution, the covered porous MS partially collapsed (Figure 3.38 b). The bulk sphere structure of the covered porous

microsphere was still partially destroyed when reducing the ethanol concentration to 10% (Figure 3.38 c). Diluted ethanol in the NaOH solution (concentration lower than 10%), is worth being further explored to disperse dried PLGA MS without destroying the sphere structure in future.

Anionic surfactant DSS can also facilitate in dispersing dried PLGA MS homogeneously in the NaOH solution, so a mixed solution of 1% (w/v) DSS and 2 mg/ml NaOH solution was evaluated too to modify the skin layer of covered porous MS. Most covered porous MS were completely collapsed into porous fragments after 2 min immersion in the mixture of 1% DSS with 2 mg/ml NaOH (Figure 3.38 d).

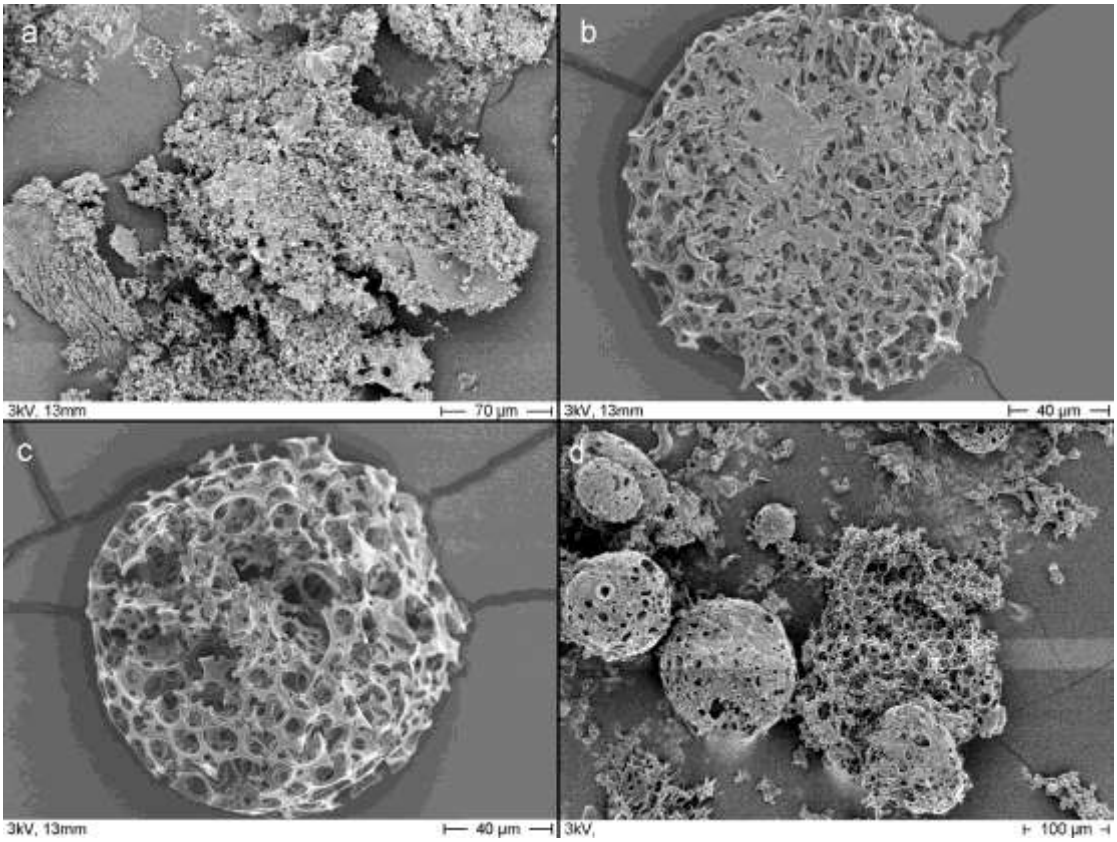

Figure 3.38 SEM micrographs of gas formed porous MS immersed in (a) 2 mg/ml NaOH + 50% ethanol, (b) 2 mg/ml NaOH + 25% ethanol, (c) 2 mg/ml NaOH + 10% ethanol and (d) 2 mg/ml NaOH + 1% DSS after 2 min**.**

3.3.9.3. Acetone modification

PLGA hydrolyzed by NaOH may suffer from an accelerated PLGA degradation in future. Since acetone can dissolve PLGA without inducing accelerated PLGA degradation, 25% (w/w) acetone water solution was also explored to modify the covered porous MS. After 2 min immersion acetone solution, acetone dissolved the surface porous structure of most MS and made them adhere to each other (Figure 3.39 a), although the skin layer was washed away without damaging the bulk sphere structure (Figure 3.39 b). Diluted acetone solution (with water) may be explored as the alternative to 2 mg/ml NaOH to control the surface open pore size and porosity without resulting in an accelerated PLGA degradation.

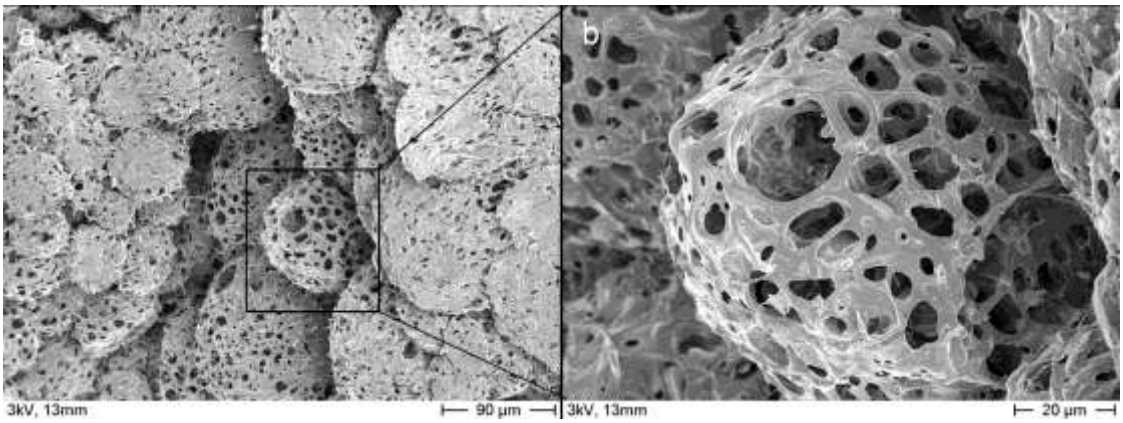

Figure 3.39 SEM micrographs of gas foamed porous MS washed by 25% acetone: (a) gross and (b) single morphology. Acetone washed away some of the skin layer without damaging the sphere structure, but made MS adhere to each other.

3.3.10. Surface modification of pluronic F127-leaching porous MS

Pluronic F127-leaching porous MS were also modified by different wash solutions to adjust the surface open pore size and porosity. Similar to gas formed porous MS, the average open pore size of pluronic F127-leaching porous MS, was increased from 3.5 (Figure 3.12 a, b) to 5 µm after 2 min immersion in 2 mg/ml NaOH (Figure 3.40 a, b).

This indicates that NaOH could hydrolyze the thin PLGA layer on the edge of surface pores to increase the pore size. However, this pore size is still too small for a human cell to penetrate. Moreover, only some MS were porous before the NaOH modification (Figure 3.12 a), but more MS become porous after the NaOH modification (Figure 3.40 a) demonstrating that NaOH hydrolysed some of the thick PLGA skin layer to expose covered pores.

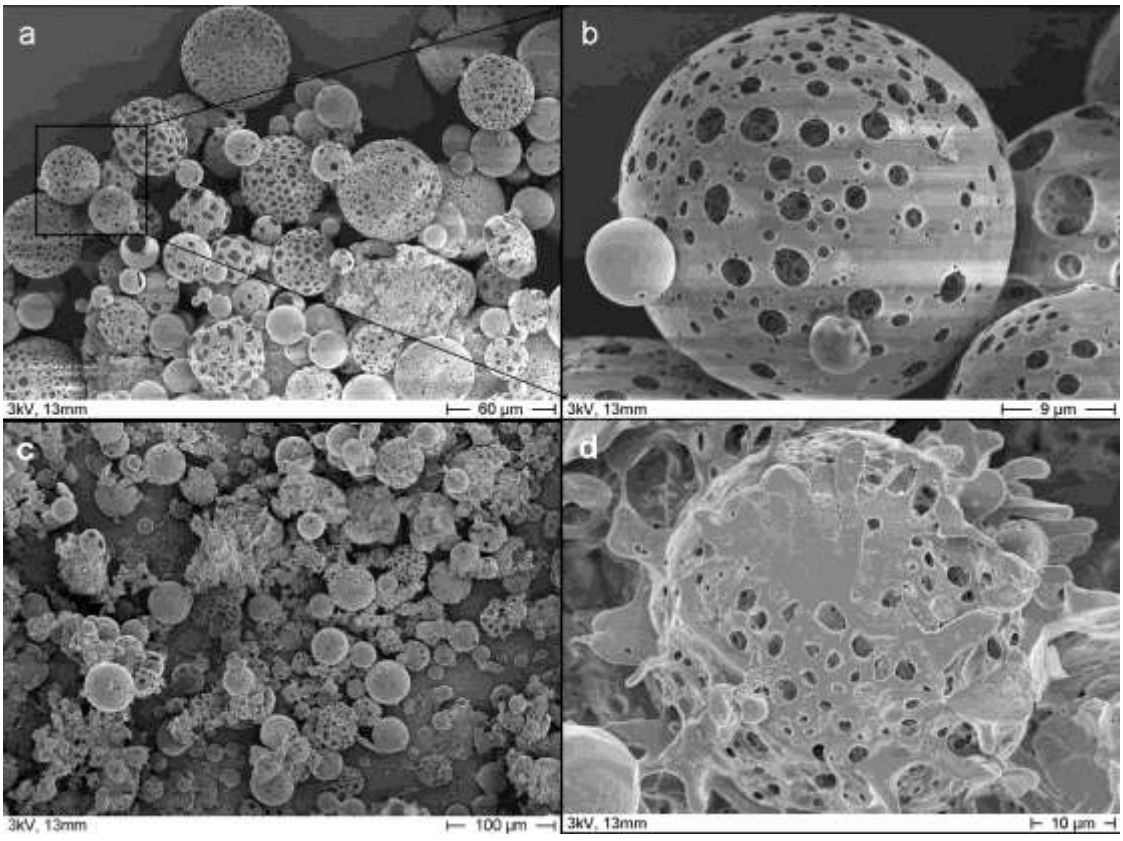

Figure 3.40 SEM micrographs of F127-leaching porous MS washed by (a, b) 2 mg/ml NaOH (c) 2mg/ml NaOH + 10% ethanol, and (d) 25% acetone for 2 min

Although the surface pore size of pluronic F127-leaching MS (3.5 µm) was much smaller than those of gas foamed MS (7 µm), a mixture of 2 mg/ml NaOH with 10% ethanol also made some pluronic F127-leaching porous MS collapse (Figure 3.40 c), indicating that ethanol enabled NaOH to hydrolyze the bulk sphere structure of MS no matter the surface pore size.

25% acetone also dissolved the surface porous structure of pluronic F127-leaching MS and made them stick to each other (Figure 3.40 d).

3.3.11. Surface analysis of NaOH modified MS

The function of NaOH solution in hydrolysing the PLGA skin layer was further confirmed by the change of microsphere surface charge. After 2 min immersion in 2 mg/ml NaOH, the surface charge of gas formed covered porous MS (measured as the zeta potential) decreased from -21.8 to -38.5 mV (Figure 3.41), indicating that more negatively charged functional groups appeared on the microsphere surface after the NaOH modification.

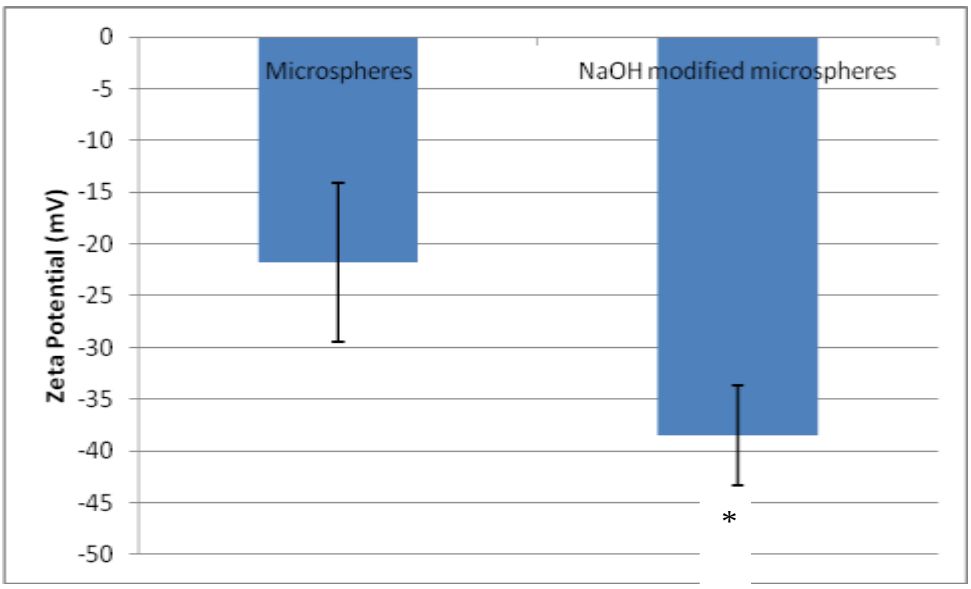

Figure 3.41 Zeta Potential of gas formed porous MS before (-21.8±7.66 mV) and after (-38.5 ±4.88 mV) 2 mg/ml NaOH modification (* significantly different, $p < 0.05$).

3.4. **Discussion**

3.4.1. Porous MS fabricated by osmogen KCl leaching

The osmogen leaching method is derived from the technique in the fabrication of

porous scaffolds [98, 106-108]. The osmogen generates porous structures due to the diffusional mass exchange between polymer oil droplets (discontinuous phase) and the external surfactant solution (continuous phase). In the primary W_1/O emulsion, the sonication dispersed the 1 ml water of 100 mg KCl into the 4 ml DCM of PLGA to form core-shell droplets, aqueous KCl droplets embedded inside the PLGA oil droplets. Once the primary emulsion was poured into the 800 ml external surfactant solution (W_2), the internal KCl water droplets created an osmotic pressure gradient, which attracts the external solution penetrating into the PLGA oil droplets to generate the pores immediately. Some pores were obvious even in the optical micrographs of PLGA oil droplets after being transferred into the PVA surfactant solution (Figure 3.6). After evaporating DCM and being freeze dried, the pores remained on the microsphere surface with diameters approximately 0.5-6 μm (Figure 3.7 a, b) indicating the function of osmogen KCl in generating pores. The smooth and nonporous surface of conventional MS (Figure 3.5) fabricated without any porogens, confirmed the osmogen function on the other hand.

3.4.1.1. Pros and cons of freeze dry and air dry

The same batch of PLGA droplets (Figure 3.6) exhibited different surface roughness and shapes after different dry procedures- freeze dry or air dry (Figure 3.7). In the air dry procedure, the water will remain in the wet PLGA polymer microparticles for a longer time before air drying, which can soften and make the PLGA swell [208]. Once the water was evaporated, the PLGA microparticles will shrink, which made the resultant microparticles with rougher surface and irregular shapes (Figure 3.7 d). Some microparticles even collapsed due to shrinking severely (Figure 3.7 c).

In contrast, for the freeze dry process, wet PLGA microparticles were immediately frozen at −80° C at first, which froze the entrapped water into solid ices and hardened the PLGA polymer preventing the polymer to soften and swell. During the freeze dry period, the ice was sublimated directly without any aqueous phase, which minimized the water influence on the polymer. Therefore, freeze dried MS maintained the structures similar to the orginal droplets without collapsing.

3.4.1.2. Effects of KCl concentration on MS morphology

Excess amount (900 mg) of salt in the inner water phase (W_1) attracted more external solution (W_2) to penetrate into the PLGA oil droplets (O), which resulted in the swelling of the oil droplets. This resulted in the large microparticles with sizes over 400 μm (Figure 3.8). Therefore, the pore size can be increased by increasing KCl concentration.

When the oil phase DCM were extracted into the external solution and evaporated, the oil droplets were hardened and finally precipitated with the PLGA matrix as MS. The penetrated external solution droplets were thus entrapped together with some excess internal droplets (W_1) encapsulated in the MS. After drying, these droplets evaporated, and left pores and excess salt inside and on the microsphere surface (Figure 3.8b). The excess salt left in the polymer matrix by the osmogen method would be troublesome, because the excess salt could influence the *in vitro* cell response to the MS.

3.4.1.3. Effects of anionic surfactants on MS morphology

PLGA MS aggregated together when changing the external solution from nonionic surfactant PVA to anionic surfactant DSS (Figure 3.9). This is because the salt inhibited the DSS ionization. Different from PVA (Figure 3.42), DSS dissolves and ionizes in the aqueous medium to perform its surfactant function. The KCl inhibited DSS dissolving and ionization in the water, which caused the PLGA droplet aggregations in the external emulsion process due to insufficient surfactant to disperse PLGA droplets.

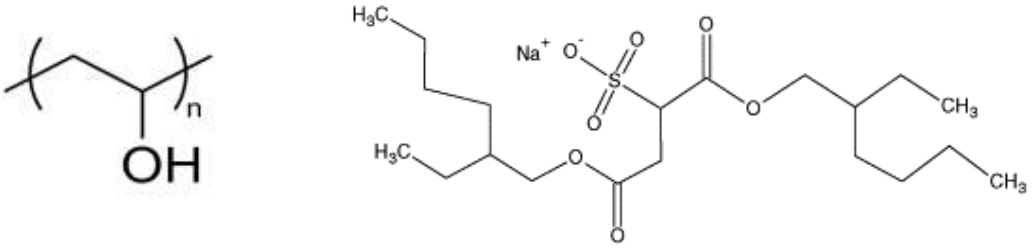

PVA DSS

Figure 3.42 Chemical structures of PVA and DSS

3.4.1.4. KCl effects on DSS dissolution

The inhibition of DSS by KCl was further confirmed by the precipitation of DSS micelle when KCl was added to the DSS solution (Figure 3.10). The DSS micelle size increased with raising DSS concentration, because more DSS molecules were salted out by the KCl inhibition of ionization. In contrast, the PVA solution was clear without any precipitation, after adding KCl.

3.4.2. Porous MS fabricated by extractable porogens

Unlike osmogen, another extractable method based on the mass transformation of the

porogen, was also assessed to fabricate porous MS. The extractable porogen is one kind of polymer soluble in both water and DCM. These water-soluble porogens, as Pluronic F127 and PEG, are mixed with PLGA in the internal oil phase and then thoroughly removed from MS by extensive washing to make pores.

In the O/W emulsion process, Pluronic F127 was firstly dissolved in DCM with PLGA. The mixture was homogenised to get the first oil emulsion with Pluronic F127 distributing in the PLGA oil phase. Once having poured the first oil emulsion into the external surfactant solution, Pluronic F127 was extracted by the excess external solution leaving pores on the unhardened PLGA droplets. These pores were too small to be observed in the optical micrographs (Figure 3.11), but obvious in SEM micrographs (Figure 3.12a, b). However, different from Chung *et al.*'s report where Pluronic F127 resulted in well distributed pores on every microsphere [6, 100, 106], the date in this chapter show Pluronic F127 only induced pores on some MS in this study (Figure 3.12a). It is hypothesized that because the porogen Pluronic F127 was not homogeneously distributed in every PLGA droplet in the primary emulsion, only PLGA droplets with Pluronic F127 embedded generated pores, after the embedded Pluronic F127 were extracted by the external surfactant solution.

3.4.2.1. Effects of anionic surfactants on MS morphology

Compared with the osmogen KCl leaching method, no PLGA MS aggregated when changing the external surfactant solution from PVA to DSS. The is because Pluronic F127 does not inhibit DSS ionization (Figure 3.12c, d). Only some MS presented with well distributed pores on the surface (Figure 3.12c), consistent with those emulsified

in the PVA solution (Figure 3.12a). It would be possible to fabricate negatively charged porous MS by this method with some modification.

3.4.2.2. Effects of homogenization speed on MS morphology

Based on the hypothesis that non-homogeneous distribution of porogen Pluronic F127 in PLGA droplets led to only some MS being porous, higher homogenization speed 24k rpm were applied to improve the Pluronic F127 distribution. Nevertheless, most resultant MS were still nonporous although the average microsphere size decreased (Figure 3.13a), because the higher homogenization speed broke the PLGA droplets into smaller pieces but did not improve the mixture of Pluronic F127 and PLGA in the DCM oil phase.

3.4.2.3. Effects of Pluronic F127: PLGA ratio on MS morphology

Another approach of increasing Pluronic F127: PLGA ratio was tested to improve the Pluronic F127 distribution. More Pluronic F127 was likely to be distributed into each PLGA droplet at higher Pluronic F127: PLGA ratio, but the resultant MS were still nonporous (Figure 3.13b). The may be because the Pluronic F127 and PLGA have different viscosity and dissolution ability in DCM. It is difficult to mix them homogeneously by just increasing the Pluronic F127 ratio.

3.4.2.4. Effects of different PLGA composition on MS morphology

50:50PLGA was used instead of 75:25PLGA to investigate the PLGA composition effects on porous MS. With lower viscosity in DCM than 75:25PLGA, 50:50PLGA is

more likely to be mixed homogeneously with Pluronic F127. Most resultant MS were still nonporous (Figure 3.13c), but there were many pores covered by a thin skin layer on MS (Figure 3.13d). This indicates that 50:50PLGA did not improve the mixture with Pluronic F127, so another extractable porogen or high speed homogenization of the Pluronic F127 and PLGA mixture would be a possible approach to generate more homogeneously porous MS. The skin layer is presumable the 50:50PLGA as reported by Bae *et al*., who fabricated covered porous MS with a skin layer which was confirmed to be PLGA [110].

3.4.2.5. Effects of different extractable porogen on MS morphology

Besides Pluronic F127, another extractable porogen PEG was used to fabricate porous MS with DSS as surfactant. Similar to Pluronic F127, PEG was immediately extracted from the PLGA droplets into the external DSS solution to leave scattered pores on the hardened microsphere surface without any aggregations (Figure 3.14). Moreover, PEG made most resultant MS porous in contrast with Pluronic F127. PEG was more able to be homogeneously mixed with PLGA than Pluronic F127, because PEG used in this study has a smaller molecular weight (Mw 2000) than Pluronic F127 (Mw 12,600), which corresponds to the lower viscosity of PEG in DCM compared with Pluronic F127. With lower viscosity in DCM, PEG is therefore easily distributed more homogenously than Pluronic F127.

However, these pores on PEG based MS (Figure 3.14) were still too small (0.5-3 μm) for cell (10 μm)) penetration. Big pores (10-20μm) may be obtained by increasing the PEG concentration. Therefore, PEG is another potential extractable porogen to make

porous MS with controllable surface pore size.

3.4.3. Porous MS fabricated by gas foaming method

Different from the osmogen and extractable porogen based on the mass transformation of the external solution and porogen to induce porous structure respectively, the gas forming porogen, usually an effervescent chemical, generates pores on the MS by decomposing the porogen to produce the gas bubbles in the PLGA droplets [109]. In the gas foaming method, after pouring the water phase (W_1) with the porogen ammonium bicarbonate (NH_4HCO_3) into the DCM solution of PLGA (O), the high speed homogenization decomposed the NH_4HCO_3 into NH_3 and CO_2 to generate gas bubbles in the PLGA DCM droplets (Figure 3.15a, b). Once transferring this primary W_1/O emulsion into the external surfactant solution (W_2), the oil solvent DCM diffused and evaporated, leading to PLGA droplets, encapsulating the water phase (W_1) and these gas bubbles, into hardened porous MS (Figure 3.15d).

However, there was a thin skin layer covering some pores on the porous MS (Figure 3.15d and Figure 3.23). The skin layer of covered porous MS is similar to Yang *et al.*'s finding on H_2O_2 foamed covered porous MS[99], but different from Chung *et al.*'s reports [88, 102] where there were no skin layers on the porous MS made by the same NH_4HCO_3 derived method. The differences between ours and Chung *et al.*'s NH_4HCO_3 method are that lower homogenization speed (6000rpm) and higher W_2 volume (400ml or 800ml) were used in our study, compared with the 10000rpm homogenization and 200ml W_2 volume used in Chung *et al.*'s study. Therefore, the source of this skin layer was further investigated by ATR-IR later.

Without gas porogen NH_4HCO_3 or homogenization, the resultant MS (Figure 3.16) were similar to the conventional MS with smooth nonporous surface (Figure 3.5a, b), confirming the function of gas forming porogen NH_4HCO_3 to generate pores. As there were no gas bubbles made by the decomposition of NH_4HCO_3 in internal water phase (W_1), the PLGA droplets dispersed in the external PVA solution were inclined to expand as spheres with smooth surface due to the surface tension. As long as the PLGA droplets were soft before completely evaporating the DCM, the PLGA droplets will expand to a smooth sphere structure to minimize the surface potential. Homogenization can only break the PLGA droplets in the primary emulsion into smaller droplets, but can not generate big porous structures. Therefore, the hardened MS were like conventional MS with smooth surface but bigger sizes (Figure 3.16) than those made with gas porogens NH_4HCO_3 (Figure 3.15d).

3.4.3.1. Effect of PLGA concentration on MS morphology

Higher PLGA concentration means there will be more PLGA dissolving in the DCM, which increases the oil phase viscosity. The results in PLGA oil droplets size bigger and thicker than before after dispersing the oil phase in the external surfactant solution. It is also more difficult for the gas bubbles generated by the decomposition of NH_4HCO_3 to break the thicker shells of PLGA oil droplets to form big open pores. Therefore, the size of MS increased but the average open pore size on the surface and porosity decreased ((Figure 3.17 and 3.15) with increasing the PLGA concentration.

3.4.3.2. Effect of NH_4HCO_3 concentration on MS morphology

Kim *et al.* reported that the porous microsphere size and open pore size increased with increasing NH_4HCO_3 concentration [109]. However, in this study the recovered 75:25 PLGA (Mw 80K) mass were no longer microparticles but a porous sponge (Figure 3.19) after increasing the NH_4HCO_3 concentration from 1% to 4%. Yang *et al.* [99] reported a similar microsphere collapse using NH_4HCO_3 as the porogen for pulmonary drug delivery. 50:50 PLGA (Mw 4K) made MS collapse when using high NH_4HCO_3 concentration (10%) in the internal phase [99]. Presumably this is because the excessive effervescence from the NH_4HCO_3 decomposition destroyed the sphere structure of PLGA oil droplets, which induced the breakdown of porous microparticles. Increasing the plasticity of PLGA droplets may prevent this premature collapse of the highly porous structure. The plasticity can be improved by introducing plasticizers such as polyethylene glycol (PEG) [99] or chemicals with plasticizing function like supercritical CO_2 to the PLGA polymer phase [209].

In the high concentration of NH_4HCO_3 (4%), the MS made with higher PLGA concentration (3.8%) also collapsed (Figure 3.20a), but some microparticles were more spherical (Figure 3.20b) than those made at 1.6% PLGA (Figure 3.19b). Some surface pores were still covered by a skin layer (Figure 3.20 1 and 2). The is because the higher PLGA concentration increased the oil phase viscosity inducing thicker and bigger PLGA oil droplets, which made it more difficult for the gas bubbles to completely break the sphere structure. 2% NH_4HCO_3 also broke down the sphere structure of resultant particles made by 3.8% 75:25 PLGA (Figure 3.21a, b), which was due to the same reason of excessive effervescence of NH_4HCO_3.

One interesting phenomenon was that, when doubling the internal phase NH_4HCO_3 (1%) volume from 2.5ml to 5ml, the recovered PLGA mass became even bigger sponge-like particles (Figure 3.21c, d) than those achieved at 2.5ml 2% NH_4HCO_3 (Figure 3.21a, b). This indicates that the higher volume of internal gas porogen solution could lead to bigger resultant PLGA particles with the same amount of gas porogens. The reason is because higher volume of internal phase means more NH_4HCO_3 water droplets will be encapsulated inside each PLGA oil droplet. When the NH_4HCO_3 amount is the same, more NH_4HCO_3 water droplets in PLGA oil droplets can enlarge the oil droplets and soften the resultant PLGA microparticles, facilitating the swelling of PLGA polymer.

3.4.3.3. Effect of PLGA composition on MS morphology

50:50 PLGA has low molecular weight and inherent viscosity in DCM than 75:25 PLGA, which makes it easier for gas bubble to break the skin layer to generate more open pores (Figure 3.22a) than those made with 75:25 PLGA (Figure 3.17a). In contrast, 85:15 PLGA with higher inherent viscosity and molecular weight was stiffer and thus more difficult for gas bubble to completely break the skin layer of resultant MS. Therefore there were fewer open porous pores on the surface of MS made of 85:15 PLGA (Figure 3.22b).

3.4.3.4. Effect of the external solution volume on MS morphology

When decreasing the DCM Oil phase (O) to external surfactant solution (W_2) ratio (O: W2) from 8:200 to 8:400 by doubling the W_2 volume, the surface pores on the porous

MS could be entirely covered by the skin layer (Figure 3.23a). The solidification of PLGA droplets started from the periphery to the inner core after transferring the primary W_1/O emulsion to the external surfactant solution (W_2). Since the solubility of DCM (CH_2Cl_2) in water is about 2% (v/v) at room temperature [210], doubling the W_2 volume led to the earlier solidification onset of the periphery of PLGA droplets, inducing a thick and dense skin layer covering the whole surface of the droplets. The skin layer on the periphery of PLGA droplets promoted the solid (PLGA) - liquid (W_2) separation but slowed down the mass transfer of DCM to the continuous phase (W_2), as the PLGA polymer chains were closer together in the glassy state thus the diffusion of solvent was more difficult. The skin layer also blocked gas bubbles inside the solidificated MS and hence the surface pores were completely covered on the resultant MS (Figure 3.23a). The cross sectional area image (Figure 3.23b) confirmed the interconnected holes and channels in the covered MS.

At higher W_2 volume (800ml), the solidification of the periphery of PLGA droplets occurred even earlier, inducing a thicker and denser skin layer of the PLGA droplets. The hard skin layer was difficult for gas bubbles to expand to make any obvious covered pores on the microsphere surface. Therefore there were only protruded parts covered by a thick skin layer on the microsphere surface (Figure 3.23c, d). Increasing the NH_4HCO_3 concentration to 4%, more gas bubbles were generated in the internal water phase (W_1) which still could not break the dense periphery layer of MS but generated more obviously covered pores (Figure 3.24a, b) rather than protruded parts on the surface (Figure 3.23d). Therefore, NH_4HCO_3 based gas method with higher W_2 volume can also be used to fabricate covered porous MS for more efficient drug

delivery as the H_2O_2 based gas method [110]. The skin layer on the covered porous MS can improve the drug encapsulation efficiency and prevent the drug burst release as reported in the H_2O_2 method [110]. Moreover, the thickness of the skin layer can be increased by increasing the W_2 volume in this NH_4HCO_3 method to achieve higher drug encapsulation efficiency and slower drug release speed.

In contrast, the solidified PLGA mass became big rough particles without surface pores when decreasing the W_2 volume to 100ml (O: W_2=8:100) with 1% NH_4HCO_3 (Figure 3.24c, d). This is because the DCM diffusion to the continuous phase was very slow at this lower W_2 volume, which slowed down the solidification of the periphery of PLGA droplets. Hence the gas bubbles in the PLGA droplets could expand the microdroplets more easily and for a longer time, which resulted in the bigger microparticle sizes (Figure 3.24c, average 260μm in diameter) and the rough surface without the porous structure (Figure 3.24d) due to the long time effervescence.

3.4.4. Characterization of the skin layer

Unlike the study using NH_4HCO_3 to fabricate open porous MS where there was no skin layer [88, 102, 109], a skin layer was observed on the surface of NH_4HCO_3 derived porous MS (Figure 3.17, 3.19 and 3.20) and on Pluronic F127 derived porous MS (Figure 3.13). These skin layers, although partially broken on some pores of the MS (Figure 3.22a), covered the entire surface of most pores on the porous MS. The ATR-IR spectra of covered porous MS were exactly overlapped with that of dry PLGA polymer (Figure 3.25), indicating that there was only PLGA in the covered porous MS. Therefore, the skin layer is undoubtedly PLGA not PVA.

The skin layer was presumably formed during the thermodynamic phase separation at the interface between the dispersed oil phase (PLGA droplets in DCM) and the continuous phase (external surfactant solution) [110]. After transferring the primary W_1/O emulsion to the continuous phase (W_2) for re-emulsification and solvent removal, the DCM solvent of the dispersed oil phase gradually diffused out into the W_2 phase and continuously evaporated. As the polymer concentration in the droplets significantly increased, polymer precipitation occurred at the interface between O and W_2 firstly, and then progressed to the periphery of the droplets. If the gas bubbles were not strong enough to break the precipitated polymer, they would form a thin skin layer covering the resultant MS. On the other hand, the decomposition of NH_4HCO_3 and the release of their resultant NH_3 and CO_2, decreased the internal air pressure of the polymer droplets and thus accelerated the mass transfer of DCM diffusion. This contributed to the early solidification of the droplet periphery, increasing the chance to form a skin layer. The similar formation of skin layer on the porous microsphere was also reported by Bae *et al* [110] on H_2O_2 based porous MS, where H_2O_2 is a gentler effervescent porogen than NH_4HCO_3. In this study, it was concluded that the skin layer was formed because the NH_4HCO_3 concentration was too low to provide gas bubbles strong enough to break the skin layer. Nevertheless, increasing the NH_4HCO_3 concentration did not enable the gas bubbles to break the skin layer (Figure 3.19) but resulted in the microsphere collapse due to the low plasticity of polymer. Therefore, the skin layer was not possible to be completely removed by just modifying the NH_4HCO_3 concentration.

3.4.5. Surface modification

These pore size and porosity (Figure 3.18) were not ideal for cell culture [88], and the residual skin layer may quickly degrade into acidic lactides and glycolides during cell culture which will results in the acidic environment inhibiting cell growth [52-54]. Therefore, NaOH solution, mixtures of NaOH with ethanol or DSS, and acetone solution were investigated to remove the skin layer respectively.

3.4.5.1. NaOH modification

NaOH can hydrolyze the PLGA copolymer into lactide and glycolide. When immersing covered porous PLGA MS into NaOH solution, the PLGA skin layer was completely exposed to NaOH first and thus started decomposition quicker than the internal PLGA bulk. This is the reason why the hydrolysis process can decompose the thin polymer layers without altering the microsphere bulk structure in a short immersion time (Figure 3.26-3.34). As higher NaOH concentration increases the PLGA hydrolysis speed, more of the PLGA skin layer was decomposed when increasing NaOH concentration. Therefore the open pore size and porosity was increased with increasing the NaOH concentration (Figure 3.27).

3.4.5.1.1. Effects of PLGA concentration and composition on MS morphology

As explained before, the thickness of the PLGA skin layer was affected by the PLGA concentration and composition. Increasing the PLGA concentration led to thicker PLGA skin layer, which lead to a longer time to be hydrolysed by NaOH. Hence, only

parts of PLGA skin layer of MS made with higher PLGA concentration was hydrolysed in the same immersion time (Figure 3.31d). On the other hand, the PLGA skin layer of 50:50 PLGA with lower lactide ratio was thinner than that of 75:25 PLGA, and thus it was hydrolysed quicker and more completely (Figure 3.33). The PLGA skin layer, no matter 1.6% or 2.5% 75:25 PLGA, or 1.6% 50:50 PLGA, was completely hydrolysed without altering microsphere bulk properties when the NaOH concentration rose to 2 mg/ml (Figure 3.30, Figure 3.32 and Figure 3.34). The smooth surface of conventional nonporous MS after NaOH modification, demonstrated the function of NaOH in hydrolysing the thin periphery layer without inducting any pores.

3.4.5.1.2. Effects of NaOH modification time on MS morphology

The PLGA hydrolysis is not only affected by the NaOH concentration but also the NaOH modification time. The longer immersion time in the NaOH solution, the more PLGA will be hydrolysed. The is explained why covered porous MS started to collapse after increasing the immersion time from 2 to 15 min (Figure 3.38).

3.4.5.2. Differences between previously discovered and the porous MS fabricated here

Compared with porous MS reported by others (Table 3.1), the notable differences of the porous MS fabricated here were the PLGA skin layer, large pore size and small MS diameter with relatively low surface porosity (30-75%) controlled by the NaOH concentration. In this study, the external solution (W_2) volume was used to control the thickness of the skin layer, which was reported working as a protective barrier in

preventing the initial burst of encapsulated drugs [110]. The inventors of the ammonium bicarbonate gas foaming method did not report any skin layers on their open porous MS [109, 112]. Covered porous MS were previously reported only by using a H_2O_2 gas foaming method [110]. As the release profiles of encapsulated drugs are significantly affected by the external and internal pore structures of biodegradable polymer MS [211], the porous MS with controllable thickness of skin layer can be tailored for a desired sustained drug release.

Large pore sizes on the MS surface can facilitate the diffusion of nutrients and waste compounds, and improves the chances for cells to penetrate inside the MS and to connect with other cells. Small MS diameters eases the injection of MS by needles and improves the efficiency of material utilization.

The skin layer can be hydrolyzed by NaOH to control the surface charge, open pore size and porosity. The surface charge (zeta potential) of MS decreased significantly after the NaOH modification (Figure 3.41). As NaOH hydrolyzed the ester bonds of the PLGA copolymer into polar anionic groups –COOH and –OH on the MS surface, which made the NaOH modified MS more negatively charged (Figure 3.41). These anionic groups make the microsphere more hydrophilic, and enable the microsphere surface interact with other ions for further surface modification.

Table 3.1 Comparisons of our porous MS with known porous MS

	Chemical composition	**Pore former**	**Particle size**	**Pore covered by skin layer**	**Methods to control skin layer thickness**	**Pore size**	**Methods to control pore size**	**Surface porosity**	**Surface modification**
Park et al [112]	75:25 PLGA	NH_4HCO_3	175μm	No	No	25-35μm	NH_4HCO_3	80-99%	Albumin-chemical reaction
Park et al [207]	75:25 PLGA	Hydrophilic polymer	20-80μm	No	No	2-6μm	No	80-99%	Heparin-chemical reaction
Gan et al [111]	PLA	NH_4HCO_3	>200μm	Yes	No	10-20μm	NaOH	90-99%	NaOH
Gan et al [113]	PLA	NH_4HCO_3	>200μm	Yes	No	10-20μm	NaOH	90-99%	NaOH, hydroxyapatite
Bae et al [110]	50:50, 75:25, 85:15PLGA	H_2O_2	150μm	Yes	H_2O_2	5-20μm	H_2O_2	0%	No
MS fabricated here	50:50, 75:25, 85:15PLGA	NH_4HCO_3	30-120μm	Yes	External solution volume	5-40μm	NaOH	30-75%	NaOH

* Fabricated MS are average 175-362μm in diameter but claimed 50-500μm in the patent.

Moreover, the surface open pore size and porosity increased significantly after being modified by NaOH with different concentrations (Figure 3.27). However, the surface porosity of covered porous MS after NaOH modification (65-75%) is lower that that (90-99%) seen in previous studies [109, 112]. This indicates that our MS can provide more continued substrate areas between pores on the surface (as shown on Figure 3.43) for cell adhesion and proliferation, while maintaining enough porous structures for nutrients diffusion [104]. The reason is that the homogenization speed 6,000 rpm used in mixing the W/O emulsion (Figure 3.4) is lower than that 10,000 rpm used in previous studies. As the gas porogen ammonium bicarbonate decomposition is controlled by the homogenization, the lower homogenization speed reduced the amount of gas bubbles generated by the ammonium bicarbonate decomposition and distributed the gas bubbles more separately away from each other. The resulted in the lower porosity and more continued surface areas between pores. Furthermore, the higher W_2 volume in the covered porous MS further reduced the porosity and generated more continued surface areas between pores, because the higher W_2 volume accelerated the PLGA periphery solidification to prevent gas bubble expansion. Rough surfaces can enhance cell differentiation but too higher porosity surfaces without enough continued surfaces inhibit cell adhesion and proliferation as there are no substrate space for cell to adhere and the discontinued surface suppress cell migration and proliferation [104]. The porous MS with controllable porous structure and more continued surface areas between pores can be a dual function device in tissue engineering as drug delivery and injectable cell scaffold.

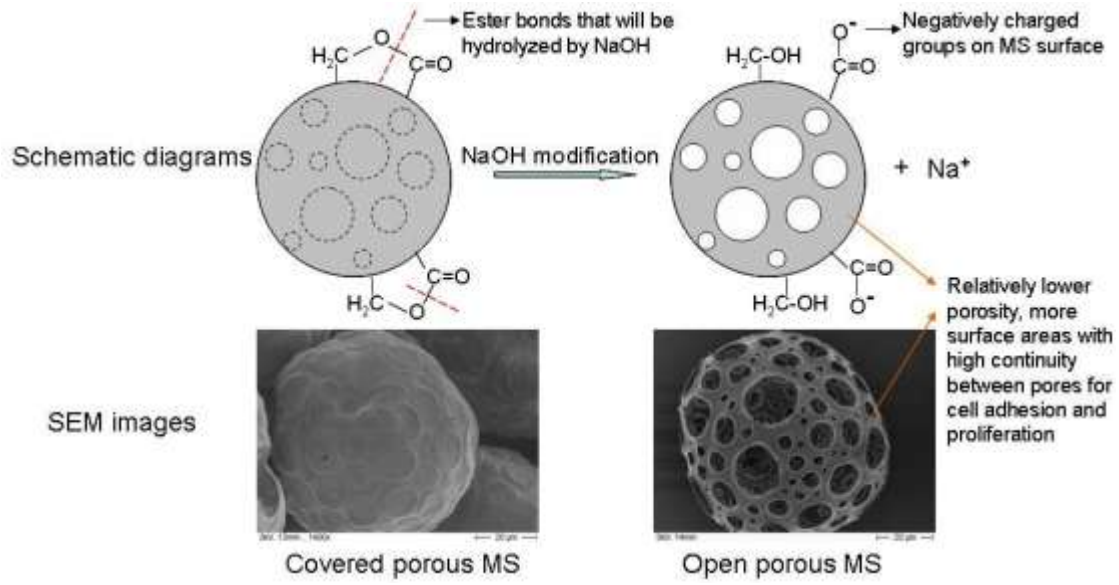

Figure 3.43 Schematic diagrams of covered porous MS modified by NaOH to produce open porous MS. Covered and open pores were represented by dotted and solid circles respectively. The skin layer was hydrolyzed by breaking the ester bonds of PLGA to produce more negatively charged groups on surface. The surface areas with high continuity between pores are marked by red arrows.

3.4.5.3. Mixed solution modification

In order to disperse dried PLGA MS homogeneously in the NaOH solution, the polar solvent ethanol and anionic surfactant DSS were added to the 2 mg/ml NaOH to modify the skin layer of covered porous MS. Due to the hydrophobic nature of PLGA and the air gas in the pores of covered porous MS, the PLGA bulk branches inside the pores of freeze dried PLGA MS might not be exposed to the NaOH as the surface skin layer. The resulted in some MS floating on the NaOH solution surface and the surface skin layer of MS was hydrolysed earlier than the internal bulk PLGA. The additional polar solvent ethanol improved the PLGA dissolvability in the water solution, so NaOH could penetrate into the pores and hydrolyze the internal bulk PLGA. Increasing the ethanol concentration, led to NaOH penetrating quickly into the internal porous structure and more bulk PLGA was hydrolysed. Consequently, the

microsphere bulk structure was broken more completely by increasing the ethanol concentration (Figure 3.38a-c). The hydrophobic functional group of anionic surfactant DSS (Figure 3.42) can conjunct with the hydrophobic PLGA and the hydrophilic functional group of DSS facilitated the microsphere dispersion in NaOH solution. This accelerated the hydrolysis of the microsphere bulk structure, leading to the MS collapse (Figure 3.38d).

3.4.5.4. Acetone modification

Although the 2 mg/ml NaOH only hydrolysed the skin layer without destroying the bulk structure, the NaOH modification resulted in more ionic functional groups on the PLGA, which may have accelerated the PLGA microsphere degradation. Acetone was hence evaluated as the alternative to remove the PLGA skin layer, because it can dissolve PLGA without altering the PLGA microsphere degradation speed. The PLGA skin layer was removed by 25% acetone solution (Figure 3.39b), nevertheless, the periphery structure of PLGA MS was dissolved as well (Figure 3.39a). The is presumably because the acetone concentration is too high so that the periphery layer of PLGA MS is still dissolved in such a short immersion time. Diluted acetone solution may be explored as the potential solution to 2 mg/ml NaOH to control the surface open pore size and porosity.

3.4.6. Surface modification of pluronic F127-leaching porous MS

Similar to gas foamed porous MS, pluronic F127-leaching porous MS presented the same phenomena after being modified by 2 mg/ml NaOH, NaOH with 10% ethanol,

and 25% acetone (Figure 3.40). This indicates that the surface pore and porosity of pluronic F127-leaching porous MS can be increased by surface modification, which makes the pluronic F127 leaching another potential method to produce large open porous MS.

3.5. **Summary**

Salt porogen, extractable porogens as pluronic F127 and PEG, and gas porogen NH_4HCO_3 all produced porous microspheres, but only gas porogen NH_4HCO_3 generated surface pores large than 10μm in diameter on the microspheres. The surface pore size and porosity of gas foamed porous microspheres can be adjusted by the formulation parameters, such as PLGA and NH_4HCO_3 concentrations, PLGA type and O: W2 ratio. However, there was always a thin PLGA skin layer covering some pores on the gas foamed porous microspheres, which could not be avoided by only adjusting the formulation parameters. By adjusting the W_2 volume, the NH_4HCO_3 method can be used to fabricate covered porous MS with controllable skin layer thickness to govern the drug encapsulation efficiency and slower drug release speed. Surface hydrolysis, mixed solutions of NaOH and ethanol, and acetone were introduced to modify the surface properties of the covered porous microspheres. The PLGA skin can be completely removed by the NaOH surface hydrolysis to control the surface pore size and porosity. Porous microspheres with controllable open pore size and porosity are promising multi-function scaffolds combining the advantages of controlled drug delivery and injectable cell carriers.

4. Chapter 4: Heparin coated porous microspheres for controlled protein and cell delivery

4.1. Introduction

Open porous microspheres (MS) functionalized with heparin were investigated as multi-functional injectable scaffolds for growth factor delivery and cell delivery in this chapter. Porous MS can be applied clinically as microcarriers for injectable cell therapy due to facile cell seeding and injection with minimally surgical interference [83, 102]. Cells can partly penetrate into the porous MS to achieve high cell seeding density, and the interconnected channels inside the porous MS can improve the nutrient supply for subsequent cell proliferation and differentiation [83-85]. Figure 4.1 presents the schematic procedures that injectable microspheres may be used for the cell therapy. Cells, especially stem cells are isolated from the donor and seeded onto the porous MS for expansion in the bioreactor. The cell and porous microsphere conjunctions will be injected to the patients for tissue regeneration or repair, after the cells have proliferated to sufficient confluence. In some cases, the stem cells can be differentiated into specific functional mature cells before being injected into the patients.

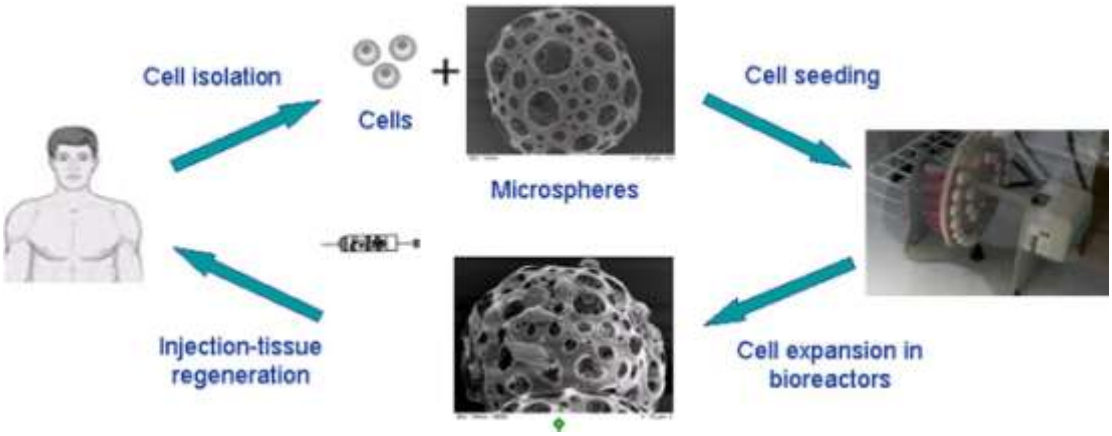

Figure 4.1 A schematic diagram of porous microcarriers for injectable cell therapy

In the injectable cell therapy, it is very important that the ideal porous MS can achieve quick cell adhesion and facilitate cell proliferation and differentiation. However, the PLGA copolymer, used to fabricate porous MS in the last chapter, is hydrophobic in nature [62, 105, 212], which inhibits the initial cell adhesion. Therefore, a surface modification to improve the hydrophilicity is desirable for facilitating the cell adhesion on the PLGA porous MS.

The last chapter described how PLGA porous MS can be fabricated by a water-in-oil-in-water (W/O/W) double emulsion method, which is the most widely used method for encapsulating drugs and protein for controlled delivery [58, 75]. However, since gas foaming porogen NH_4HCO_3 is used in the internal water phase, the foaming process will adversely influence the drug loading efficiency and protein bioactivity [110]. Moreover, the shear stress of the high speed homogenization and a water-oil interface further worsens the stability of loaded protein drugs [57, 78]. Unpredictable and incomplete *in vitro* release with high initial bursts was reported for growth factors loaded PLGA MS [213]. Hence, new drug loading/ encapsulation approaches are required for PLGA porous MS.

Heparin is a sulphated glycosaminoglycan which has been used in various implantable devices for controlled delivery of growth factors [6-8]. Heparin has a binding site for various growth factors due to specific ionic interaction, such as fibroblast growth factor (FGF), heparin-binding epidermal growth factor (HBEGF), and transforming growth factor-b (TGF-b).

Na *et al* coated nonporous MS with linear polyethylenimine (PEI) to load heparin-protein nanoparticles onto the microsphere surface for sustained release [124, 125]. Linear polyethylenimine is positively charged polymer used in cell transformation. The heparin-protein nanoparticles were formed by conjugating growth factors with heparin and poly(l-lysine) (PLL) polyplexes.

Layer-by-layer (LbL) assemble is the most promising approach mimicing the natural polyelectrolyte assembly within ECM [129] to coat heparin on substrate surface. LbL assemble is a repeated sequentially deposition process of oppositely charged polycationic and polyanionic polymers onto a substrate by the ionic interactions [123]. Compared with the covalent chemical methods and other noncovalent approaches, the LbL assemble is a facile method to construct nano-scale bioactive 3D or 2D thin polyelectrolyte films on substrate surface [103].

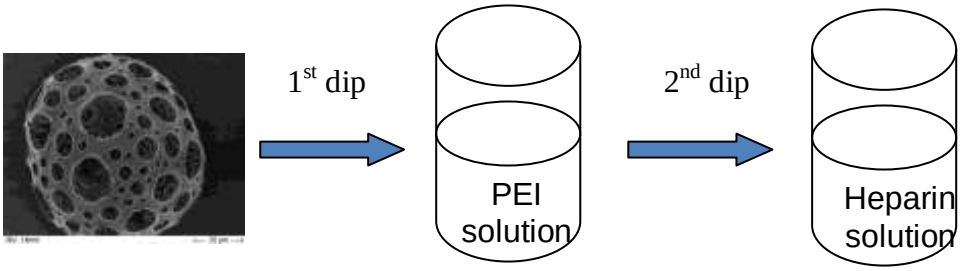

Figure 4.2 A schematic diagram of LbL process to coat heparin on porous MS

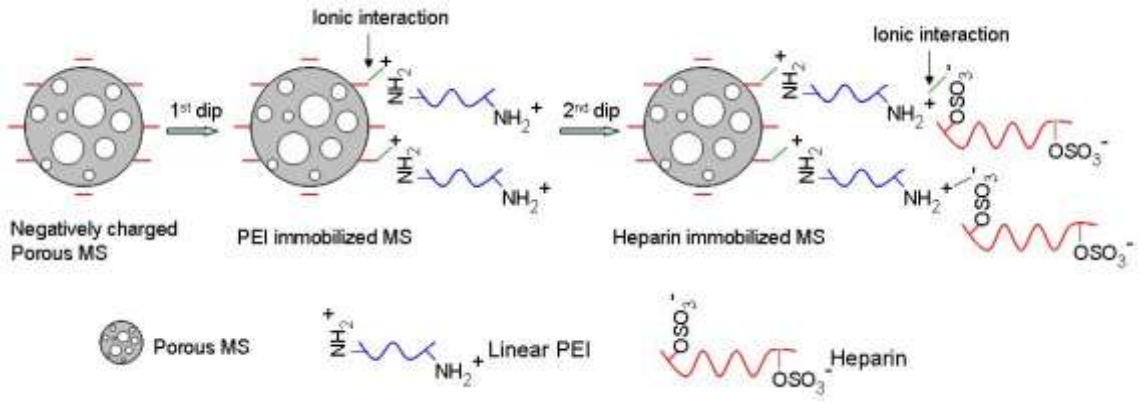

Figure 4.3 Chemical schematics of LbL assembles to coat heparin on porous MS

In this study, the heparin-PLL polyplexes method and LbL assemble method were modified to achieve enhanced protein loading and cell adhesion efficiency on porous MS. In the first method, protein loaded heparin-PLL polyplexes nanoparticles were immobilised on to porous MS fabricated by the extractable Pluronic F127 leaching method, as these porous MS with small open pore size can provide large surface area, compared with the nonporous MS used by Na *et al* [124, 125].

In the second method, a LbL assembly of polyelectrolyte multilayers (PEMs) [126] was used to coat heparin on gas foamed PLGA porous MS for protein delivery, instead of the chemical reaction method using EDC and NHS to conjugate[6]. The LbL assembly is an easy method to sequentially adsorb and alternate polyelectrolytes on the substrate via the ionic interaction [126]. Heparin coated porous MS can combine the advantages of porous structures and controlled protein release from heparin. It is hypothesized that compared with nonporous MS and porous MS, heparin coated porous MS can adsorb protein drugs, and improve cell adhesion and proliferation. The heparin coated porous MS can be innovative microcarriers for drug delivery and cell cultivation in tissue engineering.

4.2. **Materials and Methods**

4.2.1. Materials

PLGA copolymer (75:25 PLGA, Mw 76K, inherent viscosity of 0.57 dL/g; ester-ended) was supplied by Birmingham Polymers Inc. (AL, USA). Pluronic F127 [(PEG)99(PPG)69(PEG)99] (Mw 12,600) was provided by BASF (Germany).

NH_4HCO_3, heparin sodium salt and Poly(l-lysine) (PLL) (Mw 1000-4000 Da) were obtained from Sigma (UK). Linear polyethylenimine (PEI, Mw 2,500) were purchased from Polysciences, Inc (USA). Formaldehyde and toluidine blue were purchased from BDH (VWR, Leicestershire, UK). PBS and alpha modified eagles medium (α-MEM) culture medium were from BioWhittaker (Lonza Wokingham, Berkshire, UK). Fetal Bovine Serum (FBS) was from MB Meldrum Ltd., Buckinghamshire, UK

4.2.2. Fabrication of porous PLGA microspheres

As reported in Chapter 3, two kinds of porous PLGA MS were fabricated by the extractable porogen (Pluronic F127) method and the gas foaming porogen (NH_4HCO_3) method. 75:25 PLGA was mixed with water-soluble polymer Pluronic F127 in dichloromethane (DCM) as the internal oil phase, which was subsequently homogenized in PVA solution. The O/W emulsion was then stirred for 3 hours to evaporate DCM to harden porous MS. For the gas foaming porogen method, NH_4HCO_3 (W_1) was homogenized 6,000 rpm in DCM of PLGA for 3 minutes, and then stirred in the 400 ml external PVA solution for 3h. The MS formed were centrifuged, and then washed 3 times with distilled water.

4.2.3. Preparation of lysozyme-heparin Nanoparticles

Lysozyme was used as the model protein to fabricate lysozyme-heparin nanoparticles. 0.5 mg lysozyme was dissolved with 2.5 mg heparin in 5 ml deionized water. 2.5 mg PLL was subsequently added to the solution to form polyplexes nanoparticles [124,

125]. The nanoparticles were filtered and freeze dried for SEM observation. The zeta potential of pure heparin solution, heparin-PLL polyplexes without lysozyme, and lysozyme- heparin nanoparticles were measured at 25 °C by Zetasizer Nano (Malvern Instruments, U.K.). The size of lysozyme- heparin nanoparticles was also measured by Zetasizer Nano.

4.2.4. Loading lysozyme-heparin nanoparticles onto porous MS

Pluronic F127 based porous MS, freshly fabricated without freeze drying, were stirred in 1 mg/ml linear PEI solution for 1h, filtered and then washed with deionized water. The PEI coated porous MS were gently stirred in the solution of fresh lysozyme-heparin nanoparticles overnight to adsorb the nanoparticles onto the microsphere surface. The lysozyme-heparin nanoparticles loaded MS were then filtered and freeze dried for SEM observation.

4.2.5. Surface modification of the gas foamed covered porous MS

Since a thin PLGA skin layer covered the surface pores of gas foamed porous MS, the covered porous MS were modified in 2 mg/ml NaOH solution for 2 minutes to produce open porous MS as reported in Chapter 3.

4.2.6. Layer-by-layer heparin coating on gas foamed open porous MS

A simple layer-by-layer (LbL) assembly approach was used to coat heparin on gas foamed open porous MS, which is easier and more cost efficient than the previous chemical method (Figure 4.2) [6]. Heparin coating was achieved by dipping open

porous MS into the positively charged PEI solution for 1 hour with gently stirring. The resultant MS were then filtered and washed with deionized water, before dipping in the heparin solution for another 1 hour. In order to evaluate the influence of PEI and heparin concentration on the microsphere surface charge, a batch of open porous MS were dipped into 1 mg/ml, 3 mg/ml and 5 mg/ml PEI solution respectively. The recovered MS from 5 mg/ml PEI solution were subsequently immersed in 5 mg/ml, 10 mg/ml and 15 mg/ml heparin solution respectively. The surface charges of resultant MS were measured at 25 °C by Zetasizer Nano. The heparin coated MS for further investigations and cell experiments were all dipped in 5 mg/ml PEI and 15 mg/ml heparin solution.

4.2.7. Contact angle measurement

The static water contact angle is an indication of surface energy and relative hydrophilicity of the modified polymer surface. In order to evaluate the effects of NaOH modification, PEI and heparin coating on the PLGA copolymer, contact angles were measured on the prepared PLGA film surfaces at 25ºC. PLGA film has the same smooth surface as the continuous unoccupied surface between pores on porous MS. PLGA films were fabricated by placing 500 μl DCM of 0.5 mg PLGA in models and air dried. Some of the hardened films were subsequently immersed in 2 mg/ml NaOH, 5 mg/ml PEI solution and 15 mg/ml heparin solution for 2 minutes respectively. These films were then washed by deionized water and dried by an air dryer. A drop of distilled water (50 μl) was added on the surface of all original and modified PLGA films on a horizontal bench. Images of the droplets were immediately taken by camera at 0 and 2 minutes later. The angle between the horizontal plane and the tangent to the

drop at the point of contact with the substrate was measured by analyzing the images using Image J. Results were obtained by averaging the results of three measurements.

4.2.8. Determination of heparin coating by Alcian Blue staining

The heparin coating on the open porous MS was determined by using Alcian Blue staining to visually confirm the heparin binding onto the MS [214]. Alcian Blue is a cationic dye used for selective staining of glycosaminoglycans [214]. Heparin coated MS and original porous MS as the control, were immersed in 3% (v/v) acetic acid for 3 minutes and subsequently in 1% Alcian Blue stain for 30 minutes. The MS were then washed 3 times with nonionic water, and photographed using a digital camera and optical microscopy (Zeiss, UK).

4.2.9. Microcharacterization of microspheres

4.2.9.1. Scanning electron microscopy

The surface morphology of lysozyme-heparin nanoparticles and porous MS were examined by scanning electron microscopy (SEM; JEOL JSM 840F) at an accelerating voltage of 3 kV. All MS were freeze dried, and pre-coated with 3nm Pt.

4.2.9.2. Surface charge measurement

The zeta-potentials (surface charges) of polyplexes, nanoparticles and MS were examined at 25°C using Zetasizer Nano (Malvern Instruments, U.K.). The samples were prepared with deionized water to ensure the low ionic strength environment. All results were three replicates of 30 zeta runs for each sample.

4.2.9.3. ATR-IR spectroscopy

Attenuated total reflection infrared (ATR-IR) spectroscopy (Spectrum 2000, Perkin Elmer Ltd., UK) was performed on the freeze dried MS to determine the appearances of heparin coating and proteins loaded on the MS.

4.2.9.4. Energy-dispersive X-ray spectrometry (EDX)

EDX was carried out on environmental scanning electron microscopy (ESEM; Zeiss's EVO LS 15) with an INCA EDX at 10 kV to analyse the surface element of MS.

4.2.10. Incorporation of lactoferrin on heparin coated open porous MS

Lactoferrin is an iron containing glycoprotein extracted from milk with multiple functions. As an anabolic reagent, lactoferrin can promote bone cell proliferation and differentiation [215]. Therefore lactoferrin is investigated as the model protein to test the protein adsorption and release functions of heparin coated open porous MS. Fresh heparin coated open porous MS (10 mg) were immersed in a tube of 8 ml PBS solution containing 500 μg/ml lactoferrin rolling at 20 rpm for 4 hours. The tube was previously washed by PBS solution of 500 μg/ml lactoferrin to avoid the system error of lactoferrin adsorbed on the tube. The MS were then washed with distilled water for cell culture or freeze dried for ART-IR spectroscopy.

4.2.11. Lactoferrin adsorption efficiency

The amount of lactoferrin left in the supernatant was measured by BCA protein assay kit (Pierce, IL) following the manufacturer’s protocol. The UV-vis absorptions of a

series of lactoferrin solutions with known concentrations were measured at 570 nm to produce the standard curve of UV-vis absorptions against the lactoferrin concentrations. Three parallel experiments were carried and results were presented as means and standard deviations. The protein loading efficiency was calculated as:

$$\text{Efficiency} = (1 - Ls/Lt) \quad \text{- Equation 4.1}$$

Where *Ls* is the lactoferrin left in the supernatant after MS immersion and measured by BCA assay; *Lt* is the total lactoferrin in the PBS before MS immersion

4.2.12. Sterilization of MS for cell culture

The glasses, stirrer and pipettes were sterilized by autoclaving (120°C, 20 minutes). DSS, PEI, and heparin solutions were all filtered through a 0.2 μm filter. Freshly nonporous and open porous MS were sterilized in 70% EaOH at 4ºC for 1 hour, and then washed three times with distilled water and PBS. The sterilized open porous MS were then immersed in filtered PEI and heparin solutions sequentially for 1 hour each to achieve PEI and heparin coating. All MS were re-suspended in the cell culture medium at 4ºC for 1 hour before seeding cells.

4.2.13. Cell culture

The human mesenchymal stem cells (hMSC) were supplied by Lonza, UK (16057-1 Cat PT-2501 LOT No. 7F3915). Mouse bone marrow mononuclear cells (MMC) were harvested from female mouse (C57BL/6) euthanized by 4% isofluorane in CO_2 [216]. The human osteoblast-like MG63 cell line was defrosted from stock as previously reported [104]. All cells were cultured in α-MEM supplemented with 10% FBS,

penicillin (100 units/ml) and streptomycin (100 μg/ml) in T75 flasks (Falcon, BD biosciences, UK) using a humidified incubator (Heraeus instruments 6000) gassed with 5%CO_2 in air at 37^{o}C. The culture medium was replaced every 2 days. Once grown to 70-80% confluency, cells were detached by the enzymatic dissociation using 0.25% trypsin-EDTA for 5 minutes at 37 ^{o}C. The trypsinization was stopped by adding α-MEM with 10% FBS. Cells were collected by centrifugation for 3 minutes at 1000 rpm. Cell pellets were re-suspended in the culture medium and the cell numbers were counted using disposable counting chambers (Fast Read 102, ISL, Paignton, UK) before transferring to new flasks for sub-culture or being seeded onto MS.

4.2.14. Preliminary cell viability on heparin coated open porous MS

The hMSC were used to evaluate the cell viability on heparin coated open porous MS (Porous-heparin MS) without loading growth factors. 1000 cells were seeded with Porous-heparin MS and 20 μL cell culture medium in each well in 60 well Terasaki plates (Greiner Bio-One, UK). Cells dropped down to the bottom of Terasaki plates with MS as a single layer firstly. By turning the Terasaki plates upside down, cells were forced to gather on MS (Figure 4.3). Gas foamed open porous MS (Porous MS, modified by 2 mg/ml NaOH) were used as the control group with the same cell seeding method. The viability of hMSC on the MS was assessed by the Live & Dead^{TM} stain (Invitrogen, UK) according to the manufacturer's protocol. After 24 hour cultures, the culture medium was discarded and MS with cells were stained by 0.1% (v/v) calcien AM and 0.1% (v/v) ethidium homodimer-1 dyes in PBS. Calcein AM fluoresces green when cleaved by intracellular esterases in viable cells. Dead

cells fluoresce red as the increased membrane permeability allows take up of the ethidium homodimer dye. After 30 minutes at 37°C in the incubator, cells were rinsed twice by PBS to remove any dye and then imaged using confocal microscopy (Carl-Ziess LSM710, Zeiss, UK).

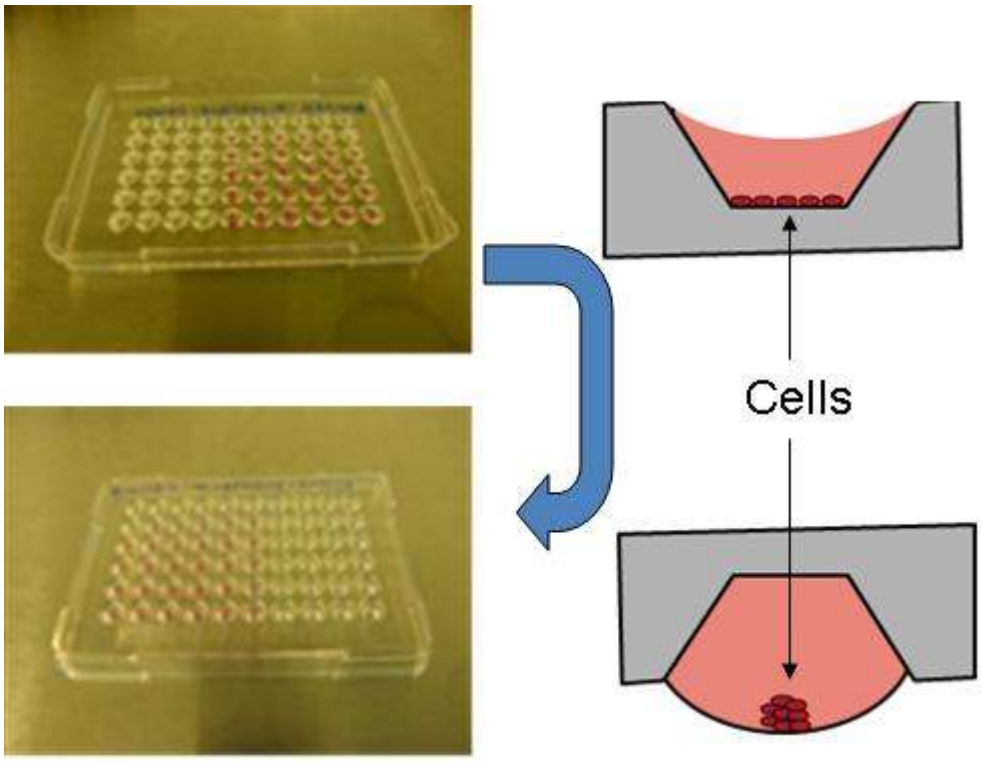

Figure 4.4 A schematic diagram of upside down culture using Terasaki plates

4.2.15. Cell seeding

In order to further evaluate the cell responses of the heparin coated MS, mouse MMC were seeded onto nonporous MS (nonporous MS), Porous MS, and Porous-heparin MS in a 2 ml tube (Cryo.s^{TM} ubes, Cat No. 126263-2DG, Greiner Bio-One, UK) at rotating conditions (60 rpm) with 3.5×10^5 cell/ml. After 1 day rotating incubation, the cells and MS were transferred into new tubes for further rolling culture. 3.5×10^5 cells were seeded in new tubes as the control. The culture medium was replaced every 2

days.

The osteoblast-like MG-63 cells were used to assess the effects of lactoferrin-loaded and heparin-coated MS (lactoferrin-porous MS) on cell differentiation [104]. MG63 cells (1.0×10^4 cell/ml) were firstly seeded onto 2 ml tubes (as the control), nonporous MS, Porous MS, Porous-heparin MS, and lactoferrin-porous MS in tubes at the same rotating conditions (60 rpm). After 6h rotating culture in the incubator, the cells and MS were transferred into 48 well plates for further culture. The culture medium was replaced every 2 days.

The cell attachment efficiency of the MS is the percentage of cells attached onto the MS at the first 24 hour or 6 hour rotating culture. The is calculated by the following equation:

$$\text{Efficiency} = Na / Nt \quad \text{- Equation 4.2}$$

Where *Na* is the cell number adhered on MS after the initial rotating culture and measured by the Alamar Blue™ assay; *Nt* is the totally seeded cell number and counted using disposable counting chambers before seeding.

4.2.16. Cell proliferation

Cell proliferation was assessed with Alamar Blue™ assay (BioSource Europe, Nivelles, Belgium). At pre-designed time (1 and 4 days), the culture medium was replaced with serum free α-MEM with 5% Alamar Blue™ solution and the cells were incubated at 37 °C for 2 hours with 5% CO_2 and 100% humidity. The Relative

Fluorescent Unit (RFU) of cell-degraded Alamar Blue™ solution is measured by a SPECTRAmax GEMINI microplate spectrofluorimeter (Molecular Devices, Berks, UK) at an excitation wavelength of 530 nm and an emission wavelength 590 nm, with a cut-off at 570 nm. The RFU was converted to cell numbers based on the standard curve of fresh cells with known cell numbers (counted using disposable counting chambers).

4.2.17. Cell viability

After 4 day culture, the Live & Dead™ stain (Invitrogen, UK) was used to assess the viability of mouse MMC on MS and imaged using fluorescent microscopy (Olympus DP70 with Olympus U-RFL-T, Olympus Optical, Co. Ltd, Japan).

4.2.18. SEM analysis

After 4 day culture, the cell morphology was analysed by SEM (JSM 840F). Cells adhered to MS were prepared using a previously published protocol [217]. Specimens were fixed in 4% glutaraldehyde with 0.1M PBS for 24 h, then washed twice in PBS for 5 minute. The specimens were serially dehydrated in 40%, 70%, 80%, 90%, 95% and 100% ethanol solutions for 15 minutes each, infiltrated in 50% (v/v) hexamethyldisilazane in ethanol and 100% hexamethyldisilazane each for 30 minutes. Finally, the specimens were washed with fresh 100% hexamethyldisilazane again and left in a fuming cabinet to air dry. The dried specimens were coated with platinum and analysed by SEM (JSM 840F).

4.2.19. Alkaline phosphatase staining

The presence of the enzyme alkaline phosphatase (ALP) is used to measure osteogenic differentiation. The ALP in the MG63 after 15 day culture on MS was stained by 0.25% naphthol AS-MX phosphate alkaline solution. The nuclei of all cells were stained as blue fluorescence by Hoechst 33342 kit (DAPI).

4.2.20. Statistical analysis

Data was evaluated by one way analysis of variance (ANOVA) in combination with Fisher's test and was considered as statistically significant for $p < 0.05$.

4.3. **Results**

4.3.1. Lysozyme-heparin nanoparticles

The zeta potentials of pure heparin solution, heparin-PLL polyplexes without lysozyme, and lysozyme-heparin nanoparticles were presented in Figure 4.5. Pure heparin is negatively charged and PLL is a positive charged protein. They formed nearly neutral polyplexes if using the same amount of heparin and PLL [124, 125]. After loading the model protein lysozyme to the polyplexes of heparin and PLL, the resultant lysozyme-heparin nanoparticles were also approximately neutral, as the positively charged lysozyme only took up a small fraction of the polyplexes.

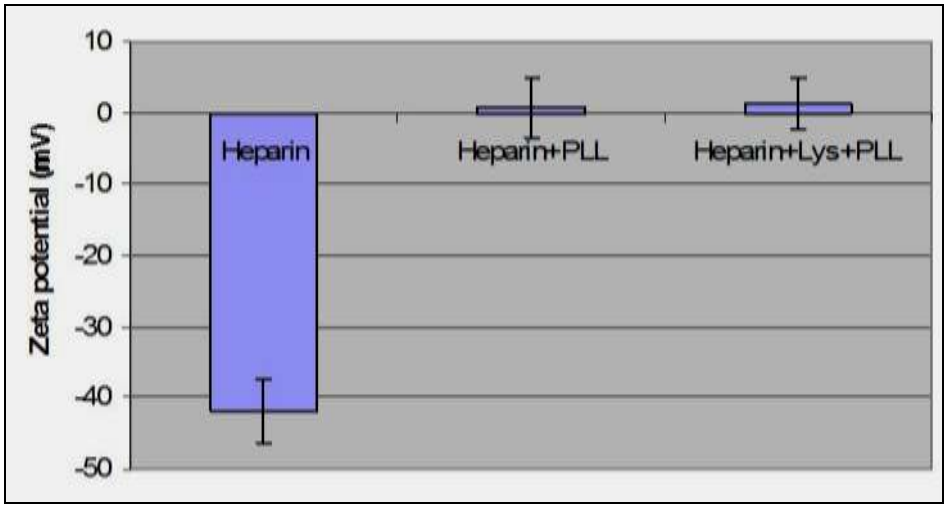

Figure 4.5 Zeta potential of pure heparin solution, heparin-PLL polyplexes without lysozyme, and lysozyme-heparin nanoparticles (Heparin+Lys+PLL).

The average diameter of the lysozyme-heparin nanoparticles was 258.9±69.1 nm (Figure 4.6), bigger than Na *et al*'s protein-heparin nanoparticles using the similar heparin-PLL polyplexes [124, 125].

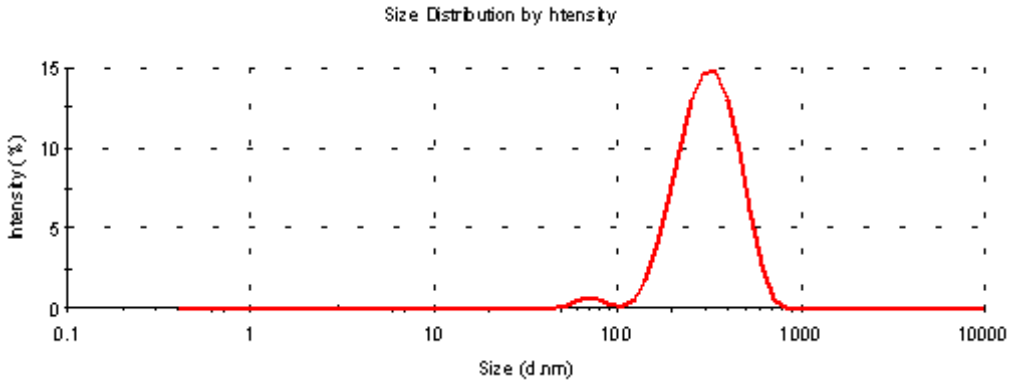

Figure 4.6 The size distribution by intensity of lysozyme-heparin nanoparticles. Their average diameter was 258.9±69.1 nm.

The freeze dried lysozyme-heparin nanoparticles were irregular white particles and aggregated together due to the electrostatic interactions (Figure 4.7 a).

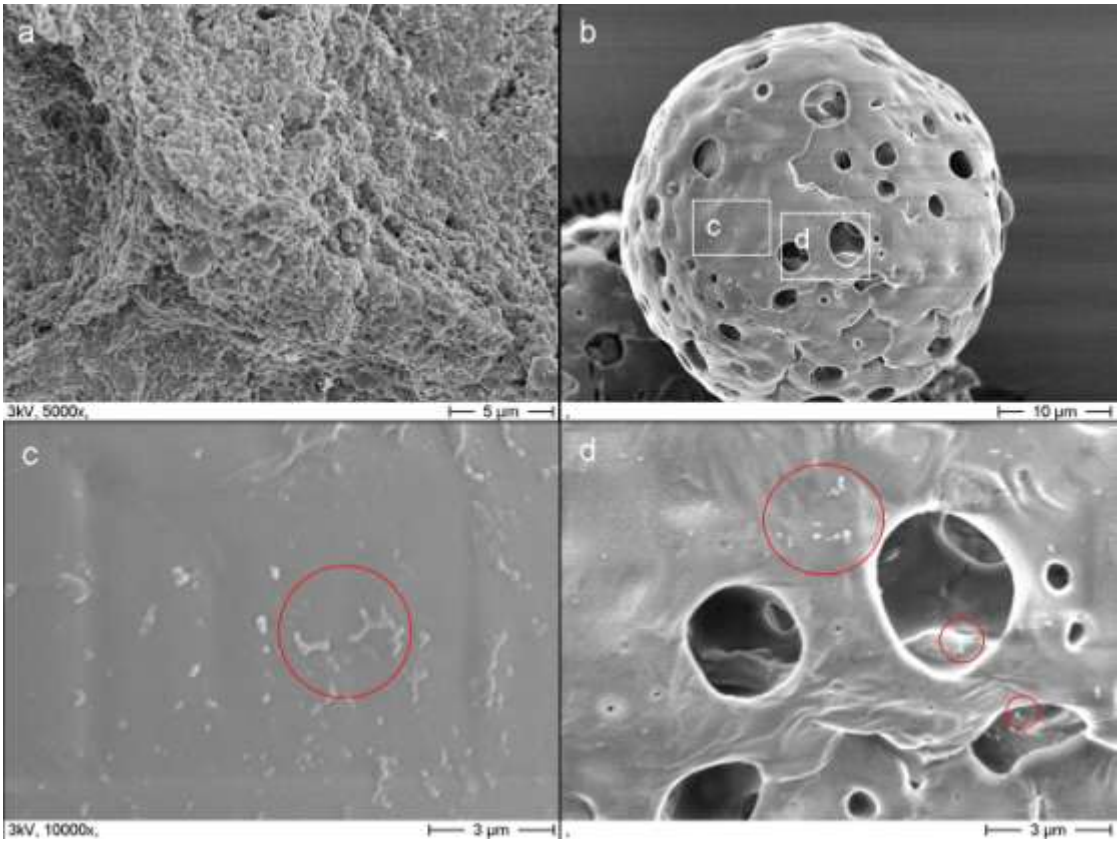

Figure 4.7 SEM micrographs of (a) aggregations of freeze dried lysozyme-heparin nanoparticles, (b) Pluronic F127-leaching porous MS coated with lysozyme-heparin nanoparticles, and their detailed surface (c, d): (c) nanoparticles immobilized on the microsphere surface, and (d) nanoparticles immobilized on the microsphere surface and inside the pores (some marked with red circles).

4.3.2. Lysozyme-heparin nanoparticles loaded porous MS

After dipping in PEI solution, the lysozyme-heparin nanoparticles were successfully immobilized onto pluronic F127-leaching porous MS (Figure 4.7 b). The detailed SEM micrographs demonstrate that the lysozyme-heparin nanoparticles were not only immobilized on the microsphere surface (Figure 4.7 c), but also inside the surface pores (Figure 4.7 d).

However, the lysozyme loading efficiency cannot be measured in our lab because there was no lysozyme specific ELISA kit. The lysozyme was conjugated with PLL

(another protein), and the available BCA kit in our lab can only measure the total protein amount. As there was not enough funding to purchase a lysozyme specific ELISA kit to measure the loaded lysozyme amount, the work of lysozyme-heparin nanoparticles was hence suspended. The second modified method, a simple layer-by-layer (LbL) assembly approach was continued.

4.3.3. Layer-by-layer (LbL) heparin coating on open porous MS

The new layer-by-layer (LbL) heparin coating via ionic immobilization is simple and highly efficient. The LbL process is confirmed by the change of surface charge (measured as the zeta potential) on the gas formed porous MS (

Figure 4.8). The gas formed porous MS presented negatively charged surface due to the functional groups –COOH and –COH. After the NaOH modification, the surface charge of MS decreased from -21.8 to -38.5 mV, indicating that ester bonds of PLGA on the microsphere surface were hydrolysed to ionic –COOH and –COH groups. After 1 hour dipping in the 1 mg/ml PEI solution, the negatively charged MS became positively charged, indicating that the positively charged PEI successfully conjugated onto the microsphere surface via ionic immobilization. The is further confirmed by the increase of the microsphere surface charge with increasing the PEI concentration from 1 mg/ml to 5 mg/ml. With 1 hour immersion in the 5 mg/ml heparin, the positively charged MS with PEI coating became negatively charged again, which demonstrates the negative heparin was immobilized on the microsphere surface via charge interactions. The surface charge was also enhanced by increasing the heparin concentration as PEI.

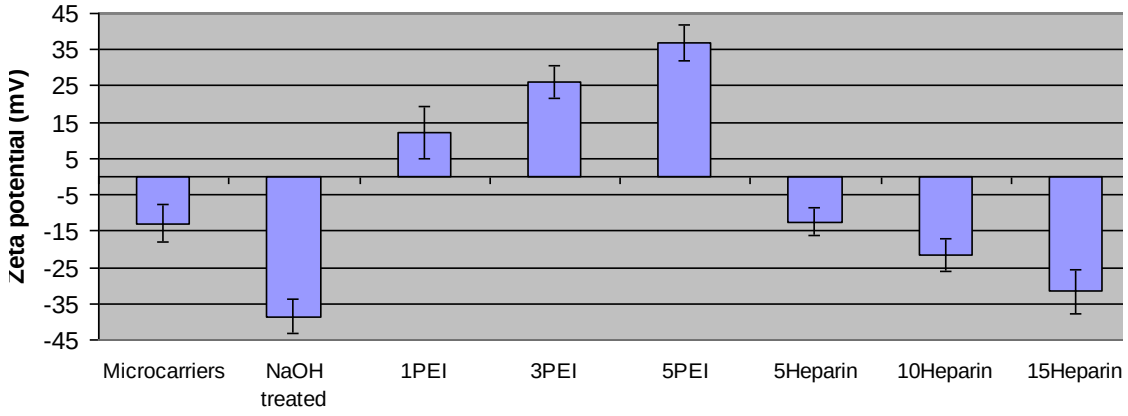

Figure 4.8 Zeta Potential of gas formed MS before (-21.8±7.66 mV) and after (-38.5 ±4.88 mV) 2 mg/ml NaOH modification, after 1 mg/ml PEI (1PEI), 3 mg/ml PEI (3PEI), 5 mg/ml PEI (5PEI) coated (+37.1±4.96), and after 5 mg/ml heparin (5Heparin), 10 mg/ml heparin (10Heparin), and 15 mg/ml heparin coated (-31.7±5.99).

4.3.4. Contact angles measurement

PLGA films are made of the same materials PLGA by the same DCM evaporation method as the gas foamed porous MS before NaOH modification, so the PLGA films have the same surface as the continuous surface between pores on the porous MS. As it is difficult to observe the contact angles on the relative small continuous surface between pores, PLGA films were used for the contact angle measurements mimicing the continuous surface between pores. The contact angle measurements on the surfaces of control group- PLGA films alone, NaOH, PEI and heparin modified PLGA films (Figure 4.9 and 5.9) are an indication of the relative hydrophilicity of these surfaces. More hydrophilic surfaces ordinarily have smaller water contact angles, corresponding to more flat water droplets. The contact angles on the surfaces of control PLGA films, NaOH, PEI and heparin modified PLGA films changed accordingly. The NaOH hydrolysed films (Figure 4.9 b) all had more flat water droplets than those found on the control PLGA films (Figure 4.9 a), suggesting that the surfaces became more hydrophilic after the first modification. When the NaOH

hydrolysed films were coated with PEI (5 mg/ml solution), the water droplets became even more flat (Figure 4.9 c), implying a further improvement of the surface hydrophilicity. After the further modification with heparin, the contact angles of the water droplets increased (Figure 4.9 d), but they were still smaller than the control (Figure 4.9a) and NaOH hydrolysed films (Figure 4.9b). The heparin coated PLGA films are thus expected to have a better cell compatibility and adhesion, compared with the originally control PLGA films. The contact angel measurement demonstrates that the surface hydrophilicity of the modified PLGA films was in this older: PEI coated > Heparin coated > NaOH hydrolysed > originally control films.

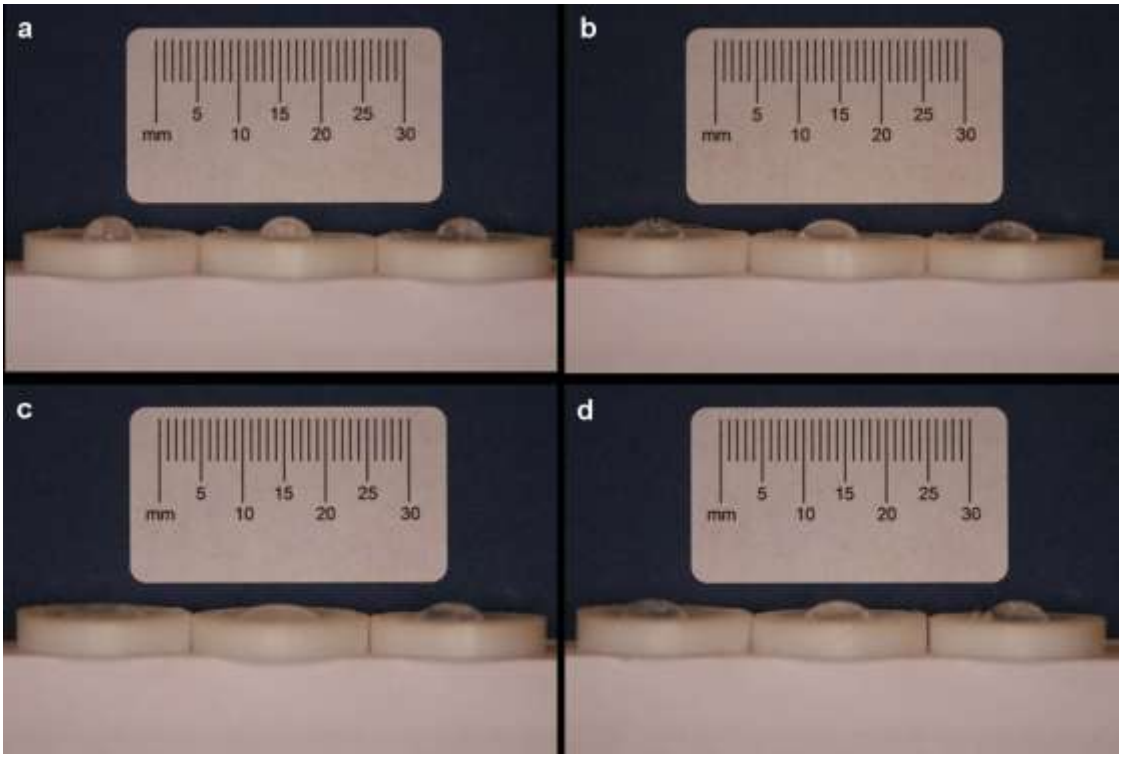

Figure 4.9 Digital images of static distilled water droplets (50µl) on (a) control PLGA films, (b) NaOH hydrolysed PLGA films, (c) PEI coated PLGA films and (d) heparin coated PLGA films for contact angle measurements. More flat droplets corresponding to smaller contact angles, indicates a more hydrophilic surface.

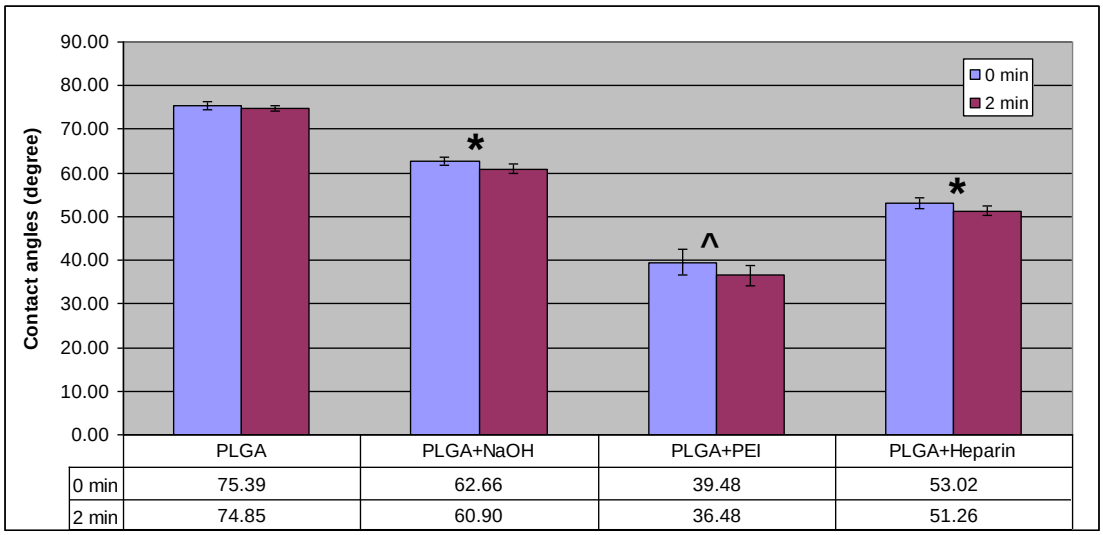

	PLGA	PLGA+NaOH	PLGA+PEI	PLGA+Heparin
0 min	75.39	62.66	39.48	53.02
2 min	74.85	60.90	36.48	51.26

Figure 4.10 Contact angles measured of above static distilled water droplets on Control- PLGA films alone, NaOH hydrolysed (PLGA + NaOH), PEI coated (PLGA + PEI) and Heparin coated PLGA films (PLGA + Heparin) after 0 and 2 minutes. (*significant decrease compared with Control; ^ significant decrease compared with Control and Heparin coated $p < 0.05$)

4.3.5. Determination of heparin coating by Alcian Blue staining

The heparin coating on the porous MS is further confirmed by Alcian Blue staining (Figure 4.11). Heparin can react with alcian blue to form a blue complex, while the PLGA does not react. The results indicate that heparin is immobilized onto the porous MS and maintains its activity.

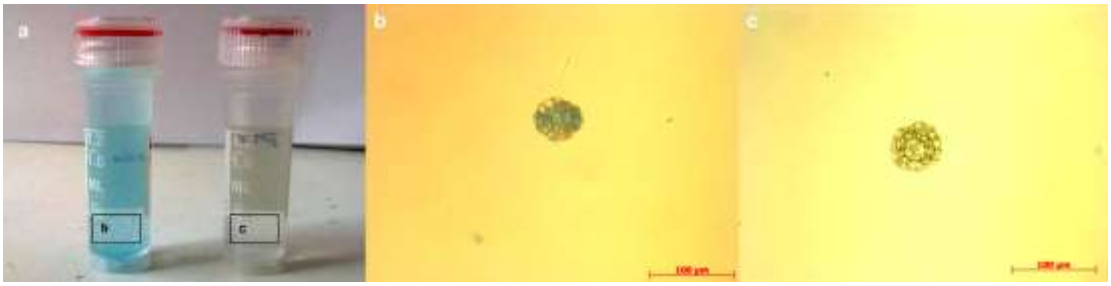

Figure 4.11 Images of porous MS after Alcian Blue staining (a) optical images of (b) heparin coated and (c) control MS (NaOH modified without immersion in heparin. Heparin, stained blue, was only found on (b) the heparin coated MS.

4.3.6. Characterisation of microsphere

4.3.6.1. ATR-IR spectra

The typical hydroxyl bending (1610 cm^{-1}) of heparin and -NH_2 stretching (1565 cm^{-1}) of PEI, are both probed only on the heparin coated MS (

Figure 4.12), which is the evidence for successful heparin and PEI immobilizations on the MS.

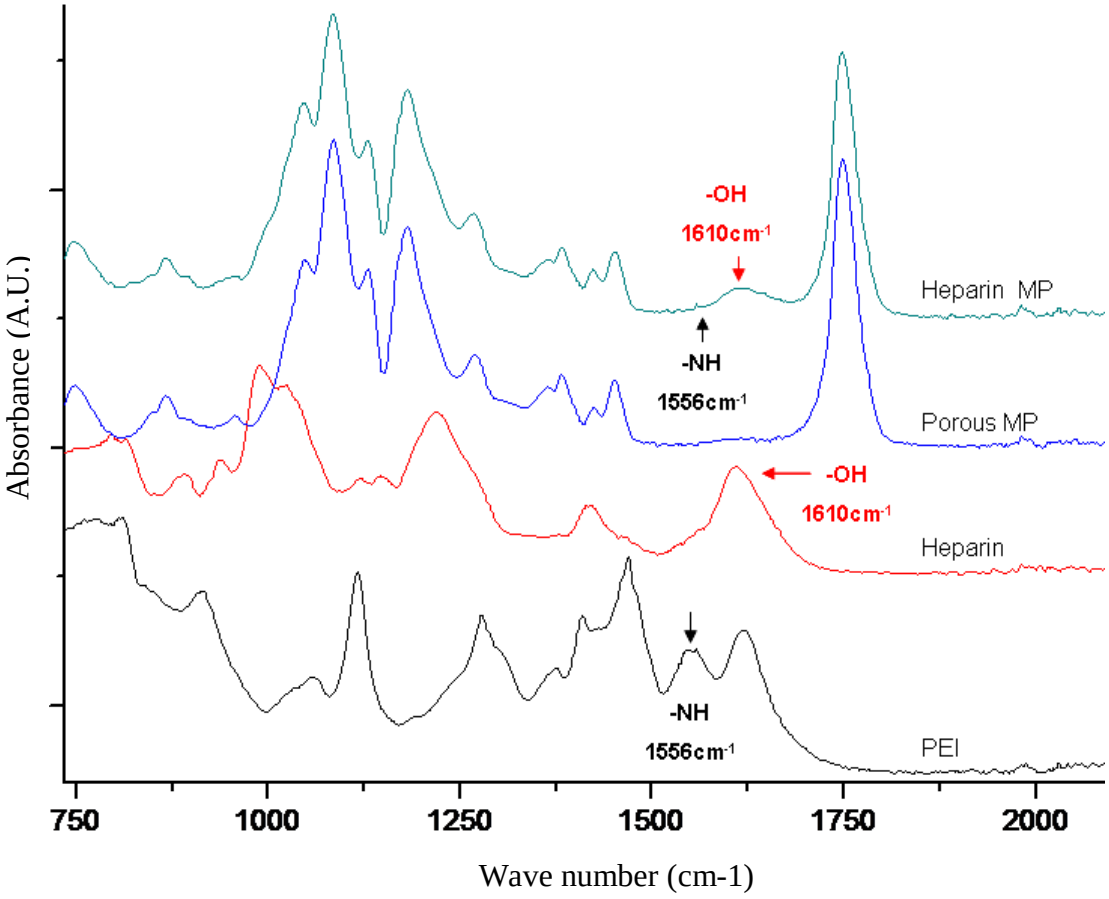

Figure 4.12 ATR-IR spectra of PEI and Heparin powders, original porous MS (Porous MS) and heparin coated MS (Heparin MS). The characteristic absorptions of hydroxyl bending (1610 cm^{-1}) of heparin and -NH_2 stretching (1565 cm^{-1}) of PEI, were both detected only in the heparin coated MS.

4.3.6.2. EDX

The characteristic element of heparin, S, is detected in the EDX spectrum of the heparin coated microsphere (Figure 4.13), implying the sound immobilization of

heparin on the microsphere surface.

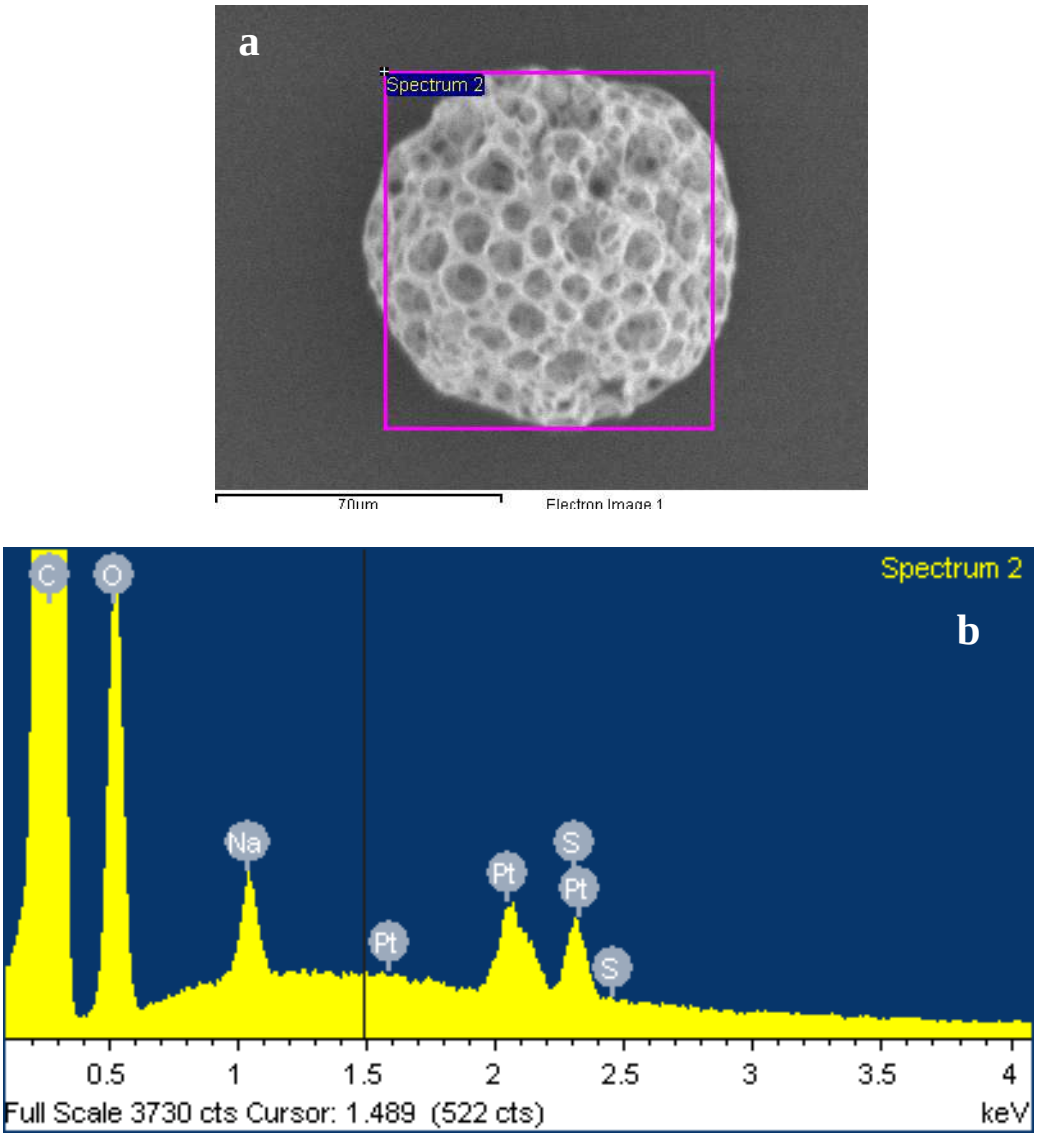

Figure 4.13 (a) SEM micrograph of the heparin coated microsphere for EDX analysis; (b) EDX spectrum of the heparin coated microsphere. The characteristic element-S of heparin is found present in the EDX spectrum, indicating the well immobilization of heparin on the microsphere surface.

4.3.7. Lactoferrin adsorption efficiency

The model protein lactoferrin was loaded onto the heparin coated MS by a simple and gentle dipping method. After 4 hour immersion in the lactoferrin solution, the MS

were harvested by centrifuge. The amount of lactoferrin left in the supernatant was measured by the BCA protein assay kit, comparing with the standard curve (Figure 4.14). There was 380.9 µg/ml lactoferrin remained in the supernatant 8 ml PBS solution after 4 hour immersion for adsorbing lactoferrin on MS. Therefore, the lactoferrin left in the supernatant, which were not adsorbed by the heparin coated MS, was 3047.2 µg (= 380.9 µg/ml * 8 ml). According to the Equation 4.1, the loading efficiency of lactoferrin is 23.82% (= 1 - 3047.2/4000) of the total lactoferrin used.

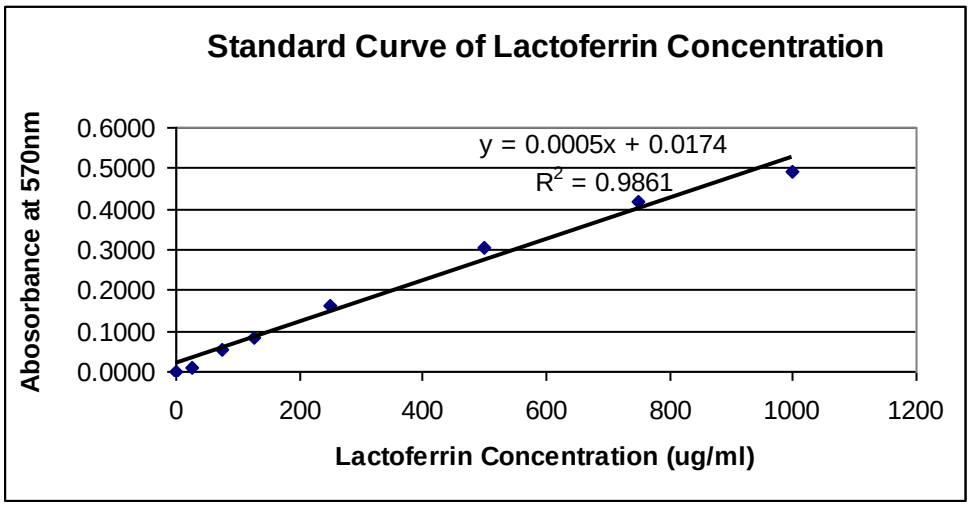

Figure 4.14 Standard curve of lactoferrin concentration measured by BCA assay

4.3.8. hMSC viability on Porous-heparin MS

After 24 hour seeding with hMSC, the confocal micrographs were shown no dead cells and only viable cells on the Porous-heparin MS (Figure 4.15b, d). In contrast, there were only dead cells on Porous-MS (Figure 4.15b, d). The porous structure of both kinds of MS was obvious in the optical micrographs.

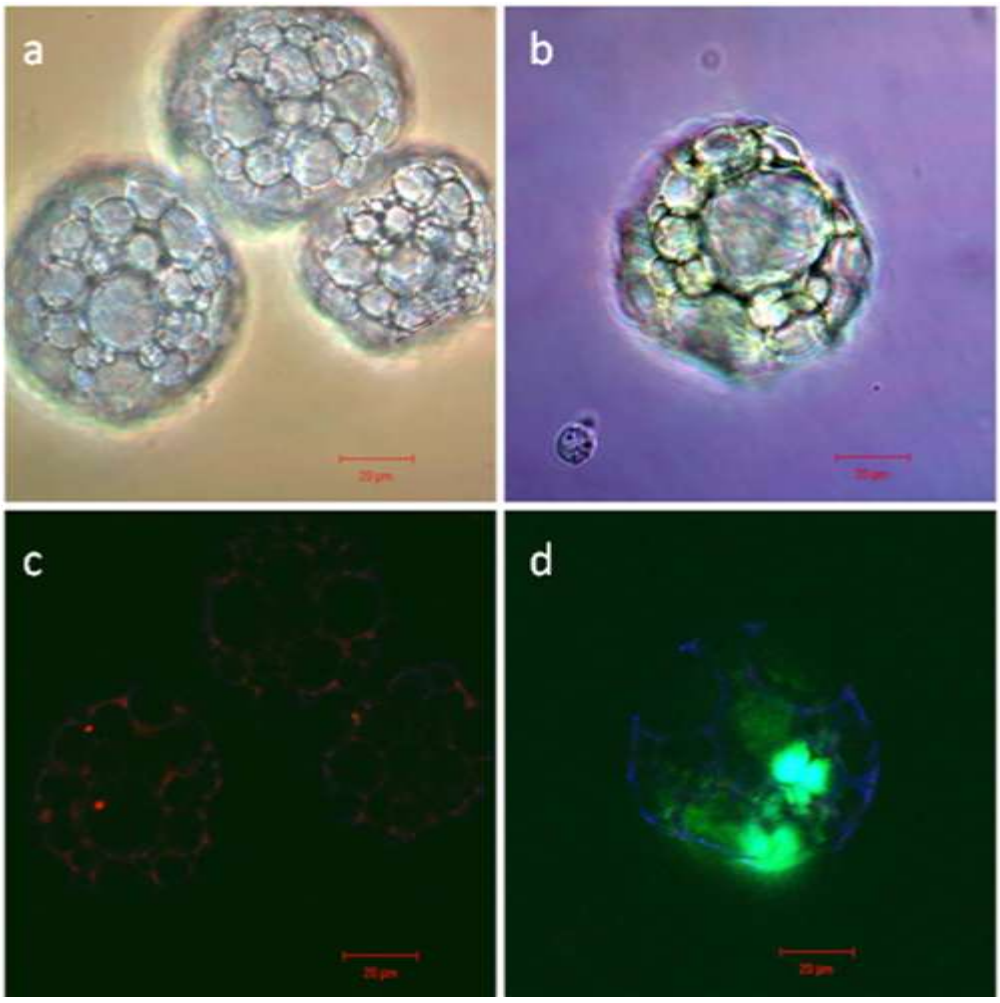

Figure 4.15 Confocal micrographs of hMSC on Porous MS (a, c) and Porous-heparin MS (b, d) after 24 hour culture.

4.3.9. Response of mouse MMC on heparin coated MS

4.3.9.1. MMC attachment efficiency

Since the viable, namely viable, cell number is proportional to the absorbance in Alamar blue assay, the standard curve of cell number is achieved by comparing the results of cell counting with the absorbance in Alamar blue assay, as shown in Figure 4.16. The resultant equation to calculate cell number ($y \times 10^4$) based on the Alamar blue absorbance (x), with $R^2 = 0.9781$, is as follows:

$$y = 0.0171\ x + 2.3187 \quad \text{-- Equation 4.3}$$

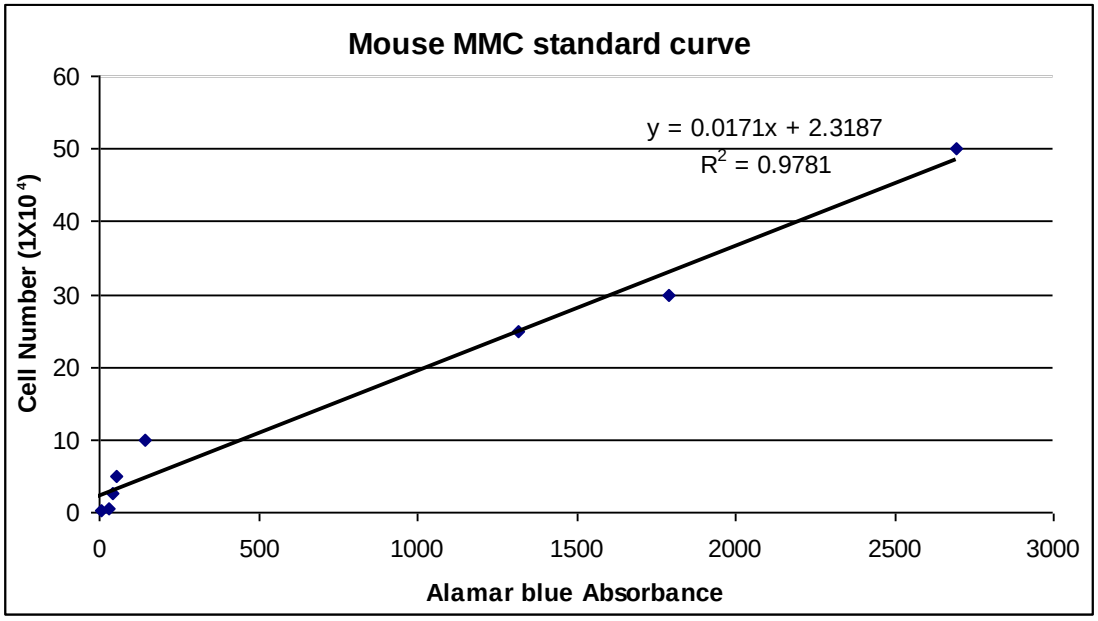

Figure 4.16 Standard curve of MMC number with absorbance in Alamar blue assay

The cell attachment efficiency, viability and proliferation on MS were thus evaluated by the viable cell numbers using Alamar BlueTM assay and Equation 4.3. Approximately 3.5×105 cells/tube was initially seeded on the control (tubes only), nonporous MS (MS), porous MS and heparin coated porous MS (Porous-heparin MS). After 24h rolling incubation, the heparin coated MS maintained the highest viable cell numbers on the MS (Figure 4.18), namely the highest cell adhesion efficiency (Figure 4.17). The MMC adhesion efficiency of porous MS is also higher than nonporous MS, and it is further enhanced by the heparin coating (Figure 4.17).

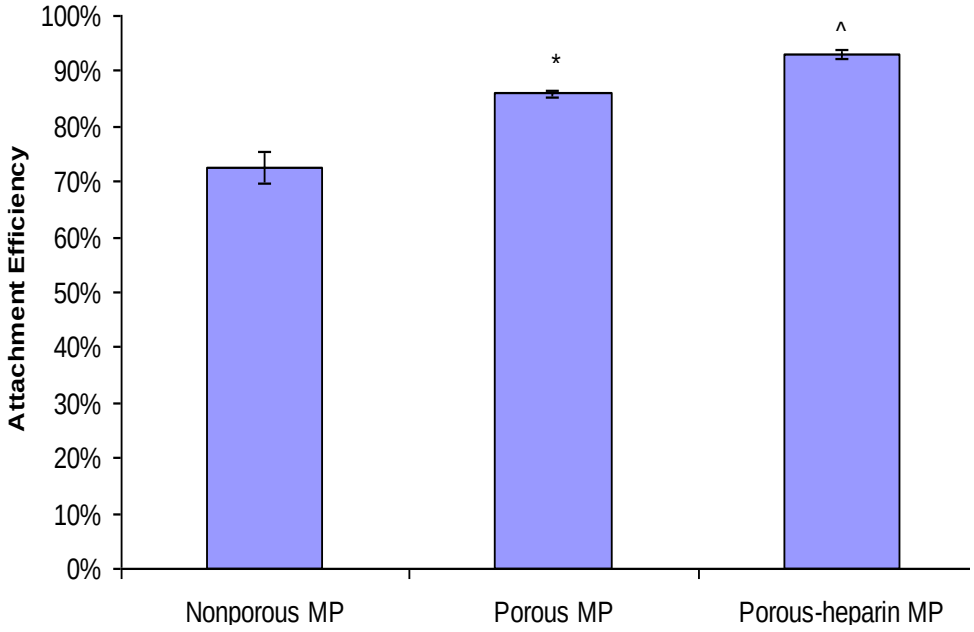

Figure 4.17 Mouse MMC attachment efficiencies after 1 day rolling culture on MS examined by Alamar Blue Assay (* significant increase compared with Nonporous; ^ significant increase compared with Nonporous and Porous MS $p < 0.05$)

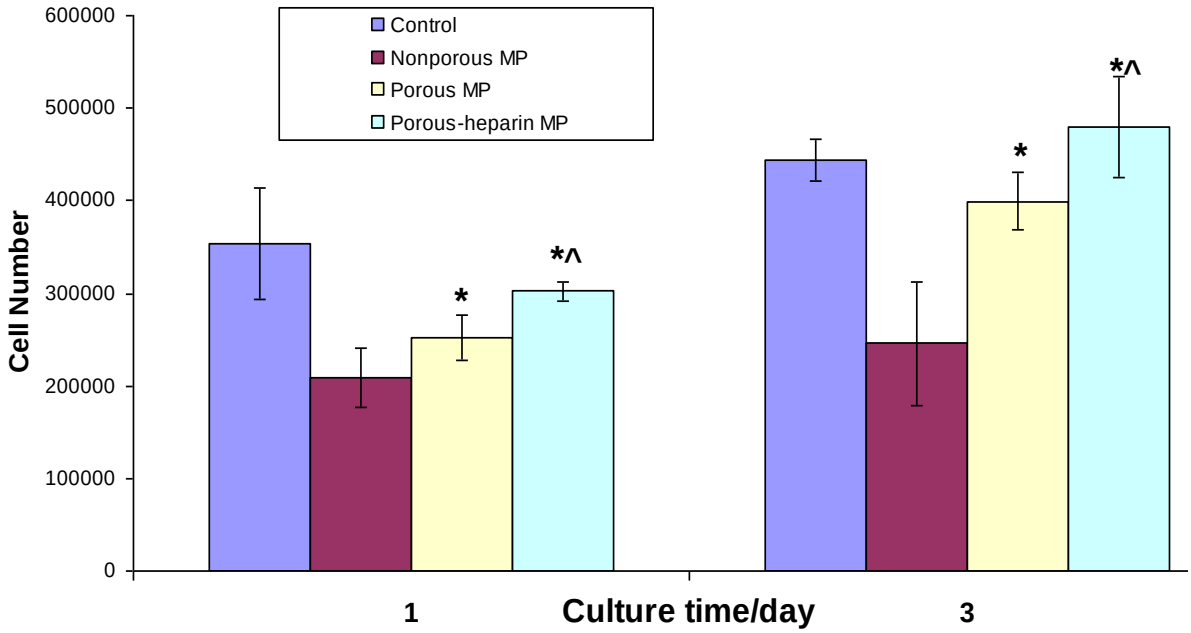

Figure 4.18 Mouse MMC proliferations after 1 and 3 day rolling culture on MS examined by Alamar Blue Assay (* significant increase compared with Nonporous; ^ significant increase compared with Porous MS $p < 0.05$)

4.3.9.2. MMC proliferation

After transferring the MS with attached cells to new tubes for a further 3 day rotating

culture, there was a significant increase ($p < 0.05$) in the viable cell number for porous MS and heparin coated MS compared with the number of attached cells after 1 day rotating culture (Figure 4.18). After 3 day rotating culture, the viable cells on porous MS are still significant more than that on nonporous MS, and significant less than that on heparin coated MS ($p < 0.05$). This indicates that porous MS are more favourable for MMC adhesion and proliferation than nonporous MS and heparin

4.3.9.3. MMC viability

After 3 day rotating culture, the cell viability was assessed by Live & Dead^{TM} staining. Living cells were stained with fluorescent green by calcien AM, while fluorescent red colour indicated damaged or dead cells stained by ethidium homodimer-1. Cells cultured with nonporous, porous and heparin coated porous MS were all almost stained green, implying that most cells were alive after 3 day rotating culture (Figure 4.19). The demonstrates that all three kinds of MS were non-toxic.

Only a few viable cells (bright green spots, marked by blue arrows in Figure 4.19 a) were attached to the surface of nonporous MS (big spheres in Figure 4.19 a), indicating that nonporous MS showed a low cell adhesion. Many viable cells did not adhered onto the nonporous MS (bright green spots, marked by pink arrows in Figure 4.19 a).

In contrast, more viable cells adhered onto the porous MS (small light green spheres, marked by blue arrows in Figure 4.19 b, c), and even penetrated inside the porous MS (Figure 4.19 c). The is the reason why some bright green spots (viable cells) were not

clear in the optical micrograph (Figure 4.19 c), because they were actually presented inside the porous MS. The also demonstrates that porous MS have better cell adhesion than nonporous MS.

The most viable cells were observed on the heparin coated MS in Figure 4.19 (d, e). The viable cells (bright green spots) on one heparin coated microsphere (small light green spheres in Figure 4.19 e) were more than these on the porous MS (Figure 4.19 c).

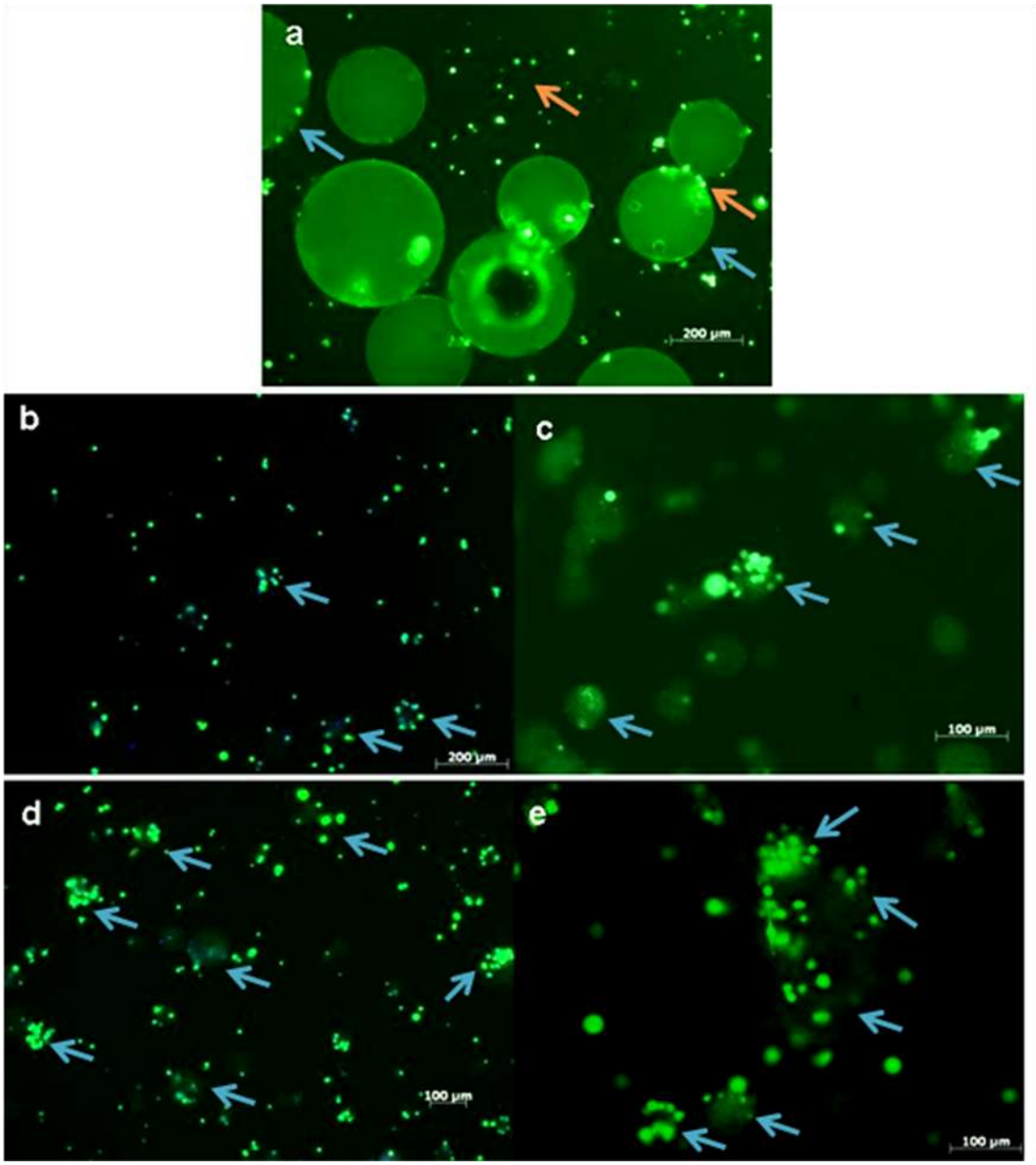

Figure 4.19 The fluorescence images of mouse MMC attached on (a) Nonporous MS, (b, c) Porous MS, (d, e) Porous-heparin MS examined by Live & Dead^{TM} staining after 3 day rolling culture. (a, b, d) × 10 magnification. (c, e) × 20 magnification of (b) and (d). The bright green spots represented the viable cells stained by green fluorescent dye. Living cells, which did not adhere onto non porous MS- big light green spheres in (a), are marked by pink arrows. Living cells adhered onto and inside porous MS- small light green spheres in (b-e), are marked by blue arrows.

4.3.9.4. MMC morphology

The better cell adhesion and proliferation abilities of the heparin coated MS are

further evidenced by the SEM images of MMC (Figure 4.20-5.20). The cell morphologies were different along the microsphere surface structure. Although nonporous MS were bigger in diameter (Figure 4.20, around 200µm in diameter), there were more MMC present on the Porous MS (Figure 4.21) and Porous-heparin MS (Figure 4.22-5.20), suggesting the enhanced cell proliferation. On the smooth surface of nonporous MS, the footprints of detached cells were found (Figure 4.20), indicating week cell affinity on nonporous MS. In contrast, no footprints of detached cells were observed on the Porous MS (Figure 4.21) and Porous-heparin MS (Figure 4.22-5.20). Three of four MMC on nonporous MS formed spherical shapes (Figure 4.20b), although there were plenty of spaces for cell spreading.

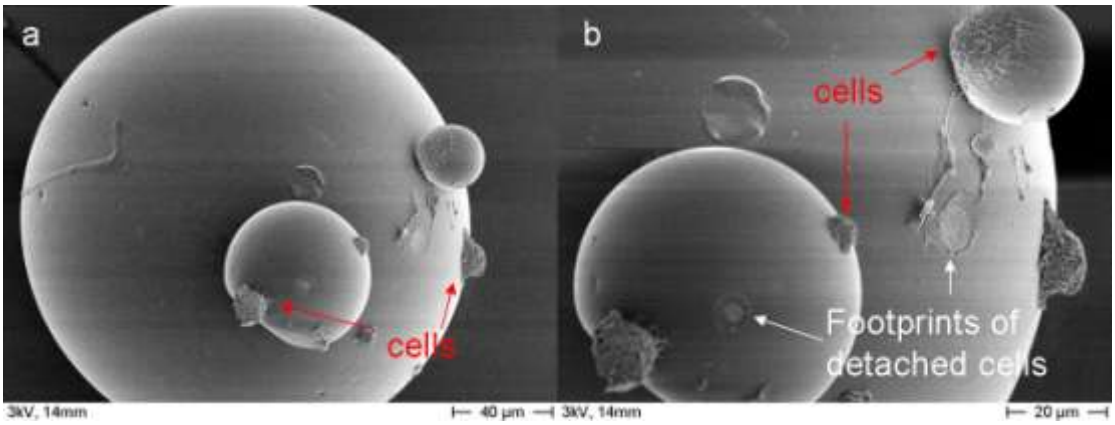

Figure 4.20 SEM images of mouse MMC on Nonporous MS at (a) low magnification and (b) high magnification. Cells are marked with red arrows and footprints of detached cells are marked with white arrows

In comparison, there were more MMC attached on the surface (Figure 4.21c, d) and even inside of the porous MS (Figure 4.21a, b). Although the porous microsphere (Figure 4.21a, around 80µm in diameter) was much smaller than the nonporous porous MS (Figure 4.20a), and the surface pores were bigger than cell bodies, there were more spherical MMC adhered onto the narrow frames between pores on the porous MS (Figure 4.21a). Some MMC connected with other cells on the porous

microsphere surface (Figure 4.21d) and inside the pores (Figure 4.21b), demonstrating the porous structure facilitated the cell interactions.

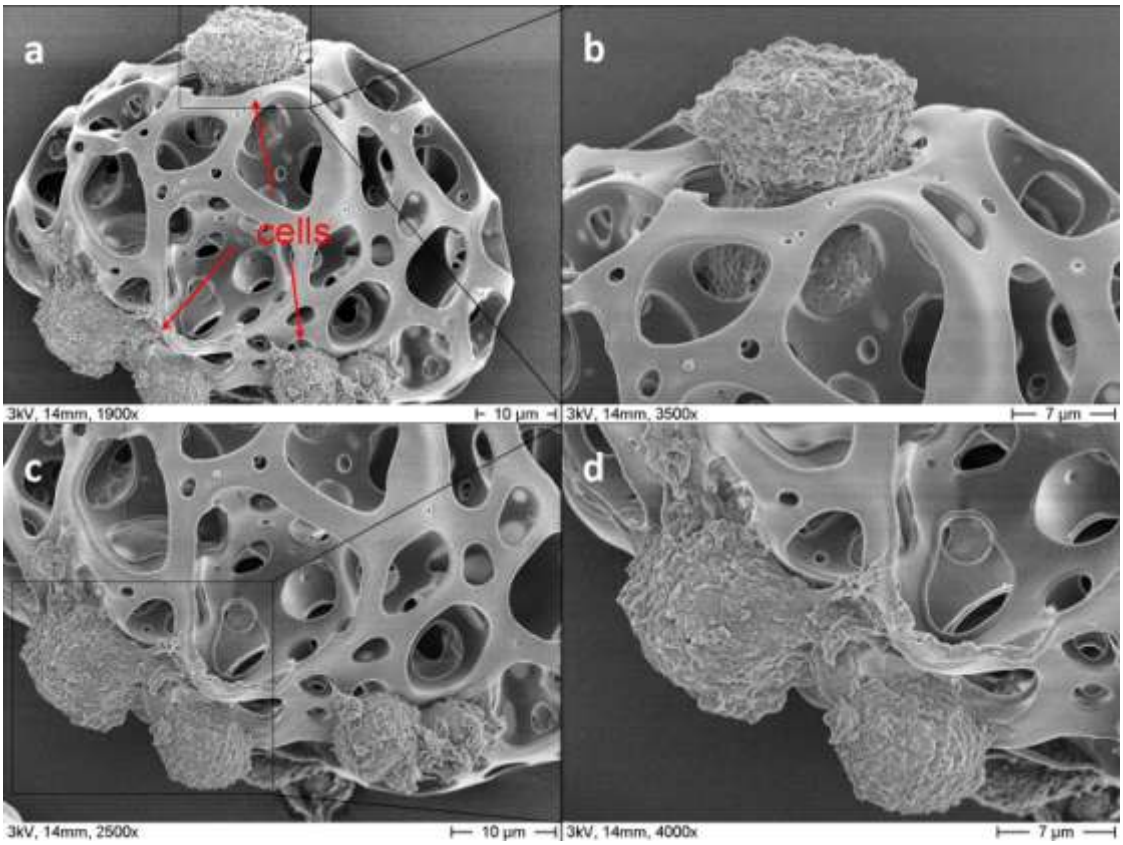

Figure 4.21 SEM images of mouse MMC on Porous MS for (a) overall and (b, c, d) detailed morphologies. Cells are marked with red arrows.

The heparin coating on porous MS further improved the cell adhesions and proliferation, attracting more MMC onto the surface (Figure 4.22a, b) and inside the MS (Figure 4.22c-f). Moreover, the heparin coating on porous MS demonstrated significant effects on cell morphology after the cell adhesion (Figure 4.21f and Figure 4.23). Some MMC on the Porous-heparin MS spread inside the internal channels (Figure 4.21f) and along the surface of MS (Figure 4.23), and were longer and flatter than that on the nonporous (Figure 4.20) and porous MS (Figure 4.21). Cell filopodias were seen stretched out along the microsphere surface (Figure 4.21b, e and Figure 4.23b). The elongated cytoplasmic processes provided the contact with other cells and

the attachment to substrate (Figure 4.21f and Figure 4.23b). The MMC on nonporous MS (Figure 4.20) and porous MS (Figure 4.21), however, were all remaining round. The influences of heparin coated MS on cell differentiation were further assessed by the use of human osteoblast-like MG63 cells.

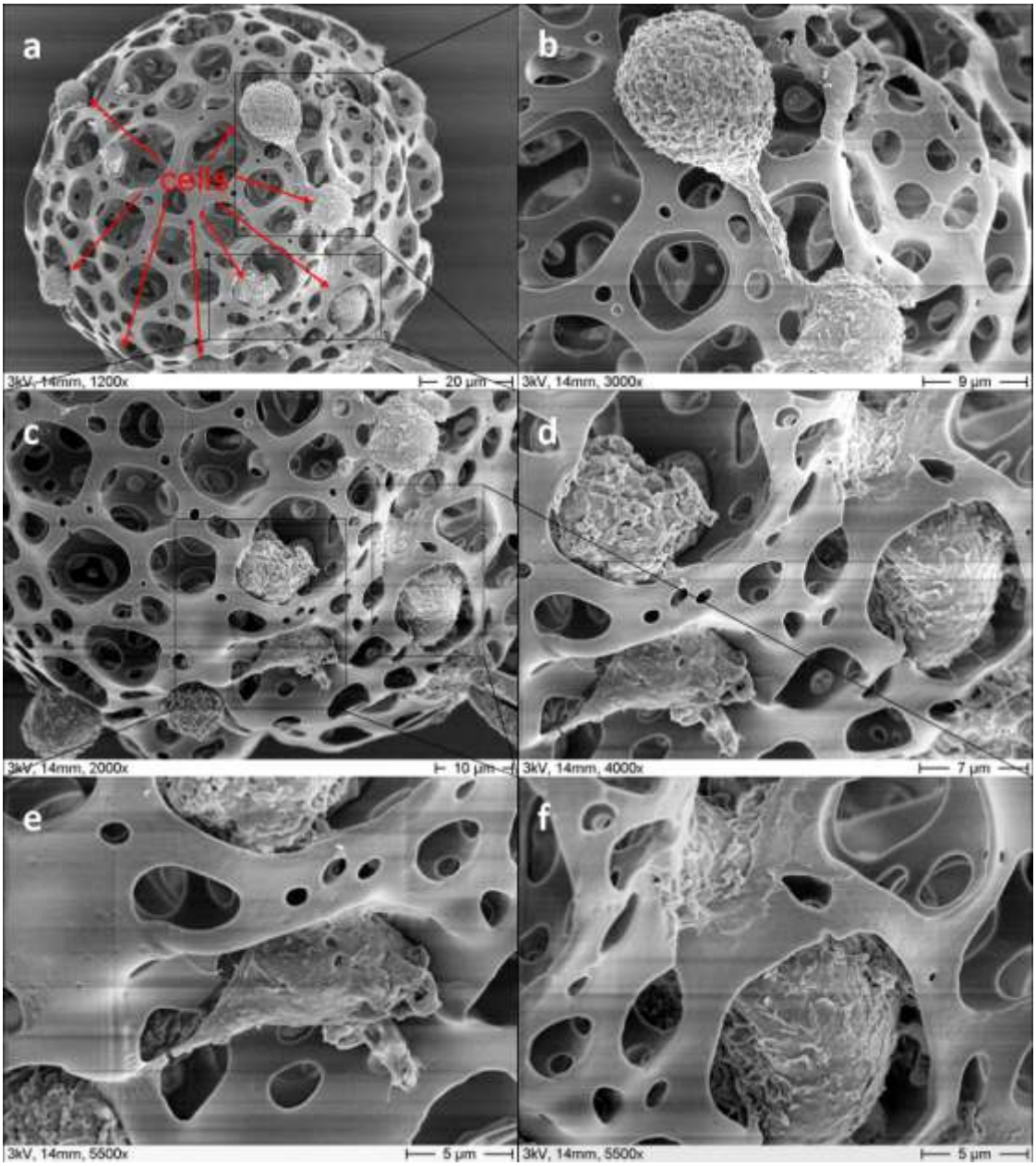

Figure 4.22 SEM images of mouse MMC on Porous-heparin MS for (a) overall and (b-f) detailed morphologies; (d-f) were high magnifications of (c). Cells are marked with red arrows.

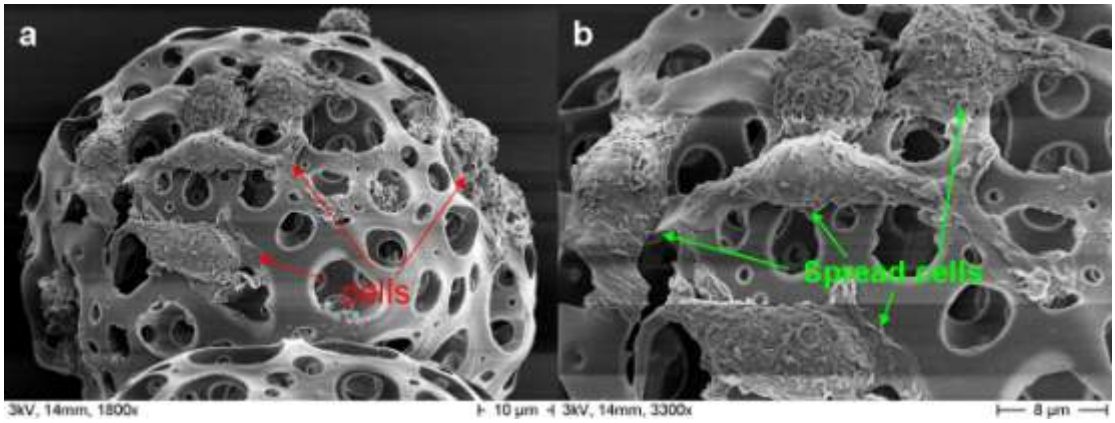

Figure 4.23 SEM images of mouse MMC on Porous-heparin MS. Cells are marked with red arrows, and spread cells are marked with green arrows.

4.3.10. The effects of Porous-heparin MS on cell differentiation

The model protein lactoferrin was loaded onto the heparin coated MS (Lactoferrin-porous MS) by the simple dipping method. The functions of Lactoferrin-porous MS on protein delivery and cell differentiation were assessed by human osteoblast-like MG63 cell line [104]. Nonporous, Porous, and Porous-heparin MS were evaluated to compare with Lactoferrin-porous MS.

4.3.10.1. MG63 adhesion efficiency

Approximately 1.0×10^4 cells/tube MG63 were initially seeded on the 2ml control (tubes), nonporous MS (MS), porous MS, heparin coated porous MS (Porous-heparin MS), and lactoferrin loaded heparin coated porous MS (Lactoferrin-porous MS) in 2 ml tubes. After 3 hour rotating culture (60rpm) in the tubes, the MG63 adhesions on MS were assessed by the optical microscopy (Figure 4.24). With the control group cells grown on the tissue culture plates, MG63 just adhered onto the plates (Figure 4.24 a). For the nonporous MS, almost no cells adhered onto the MS (Figure 4.24 b).

However, cells had already adhered onto the porous MS (Figure 4.24 c), indicating the porous MS were more favourable for quick cell adhesions than nonporous MS. Even more cells had adhered onto the Porous-heparin MS and Lactoferrin-porous MS (Figure 4.24 d, e), implying the further enriched cell adhesion ability.

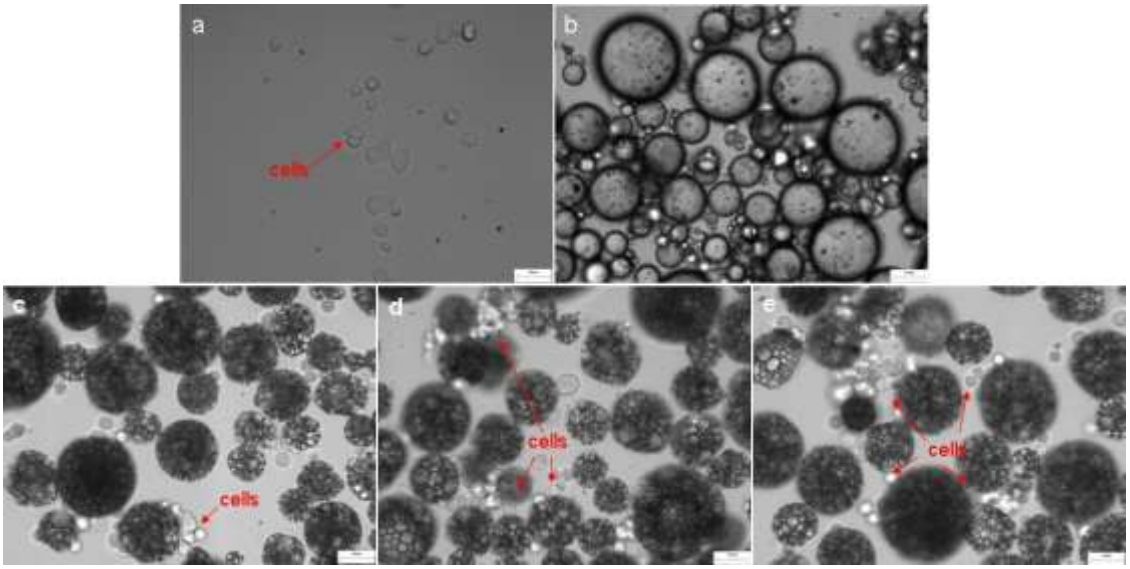

Figure 4.24 Optical microscopic images of MG63 cells after 3h seeding on (a) tissue culture plate, (b) Nonporous MS, (c) Porous MS, (d) Porous-heparin MS, and (e) Lactoferrin-porous MS. Cells are marked with red arrows.

The MG63 cell numbers were also estimated by using the Alamar Blue^{TM} assay. The standard curve of cell number (Figure 4.25), gives the following equation to convert relative fluorescent units (RFUs, x) into cell number (y) ($R^2 = 0.9917$).

$$y = 9.8535x - 1961.6 \quad \text{-- Equation 4.4}$$

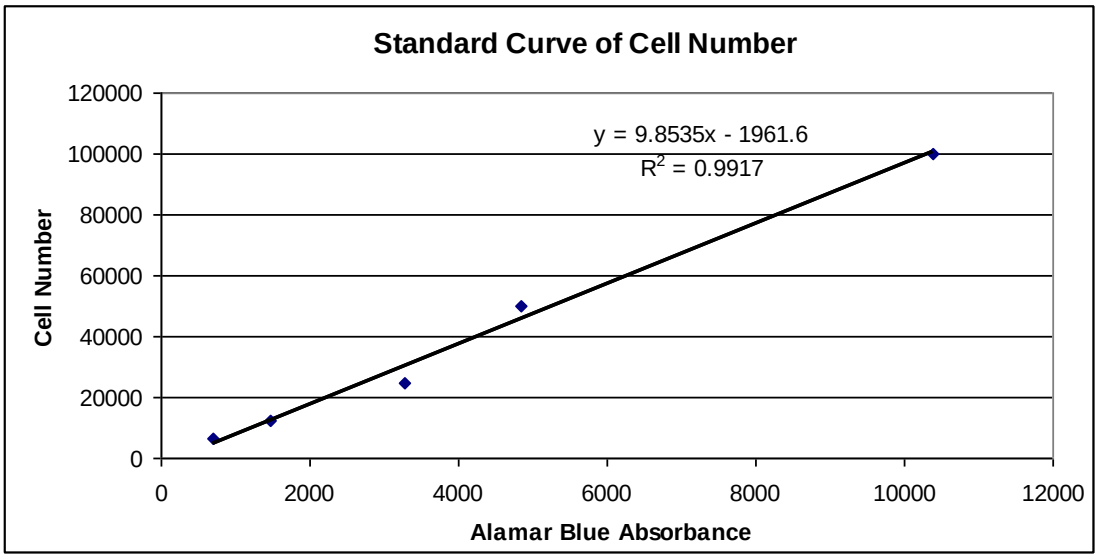

Figure 4.25 Standard curve of MG63 number with RFUs in Alamar Blue™ assay

After 6 hour rolling incubation at 60 rpm, the viability of the viable cells adhered to the MS were assessed by Alamar Blue assay to quantify the cell adhesion ability of MS. The number of viable cells on the MS increased in the following order: Nonporous < Porous < Lactoferrin-porous < Porous-heparin (Figure 4.26). The demonstrates that the MG63 cells significantly preferred to adhere to the Porous MS, compared with Nonporous MS. Interestingly, the heparin coating further significantly improved the number of MG63 cells binding to the Porous-heparin MS, but the numbers were reduced slightly (albeit not significantly) after loading lactoferrin onto the Porous-porous MS. The sequence of MG63 adhesion efficiency on different MS was consistent with that of mouse MMC, with Porous-heparin MS maintaining the highest adhesion efficiency (Figure 4.27).

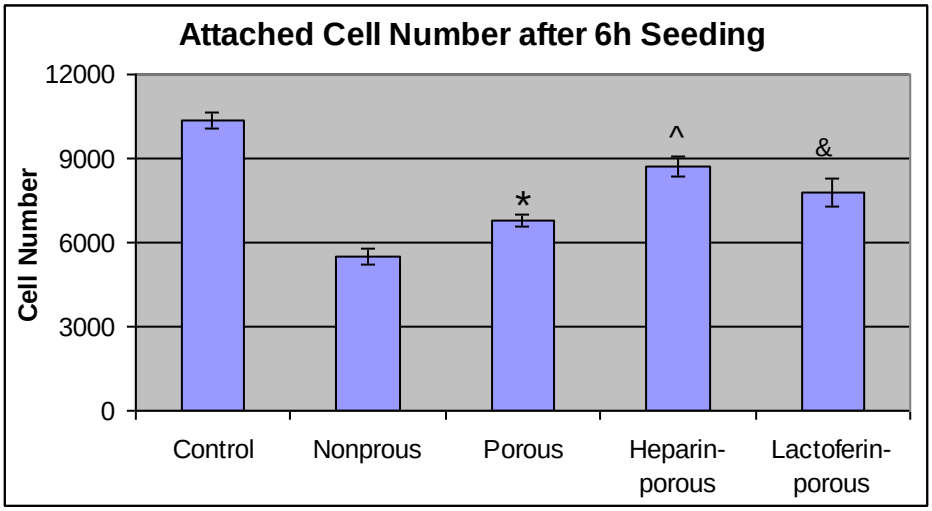

Figure 4.26 Adhered viable MG-63 cells after 6h culture on MS in centrifuge tubes (* significant increase compared with Nonporous $p < 0.05$, ^ significant increase compared with Nonporous and Porous $p < 0.01$, & significant increase compared with Nonporous $p < 0.01$ and no significant difference compared with Porous-heparin and Porous)

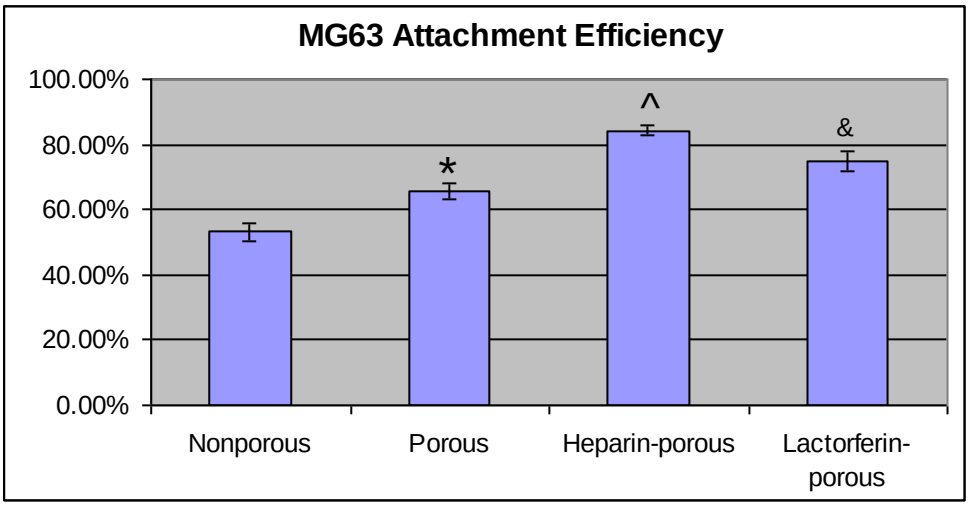

Figure 4.27 Adhesion efficiency of viable MG-63 cells after 6h culture on MS in centrifuge tubes (* significant increase compared with Nonporous $p < 0.05$, ^ significant increase compared with Nonporous and Porous $p < 0.01$, & significant increase compared with Nonporous $p < 0.01$ and no significant difference compared with Porous-heparin and Porous)

4.3.10.2. MG63 proliferation

After transferring the MS with attached cells from the tubes to the tissue culture plates for further 4 day culture, the viable cells on all MS significantly increased creating an

new order: Nonporous < Porous < Porous-heparin < Lactoferrin-porous (Figure 4.28). The was in accordance with that of mouse MMC: the viable cells on porous MS were significant more than that on nonporous MS, and less than that on heparin coated MS. The demonstrates that cells favour Porous MS for proliferation, compared with Nonporous MS, and the heparin coating further enhanced the cell proliferation.

Intriguingly, although the initial number of viable cells on Lactoferrin-porous MS was less than that on Porous-heparin MS after 6h rotating culture, the total number of viable cells on Lactoferrin-porous MS increased greatly and became more significant that on Porous-heparin MS. This indicates that the lactoferrin loading on the MS, initially reduced the MG63 adhesion efficiency, but greatly improved the cell proliferation later.

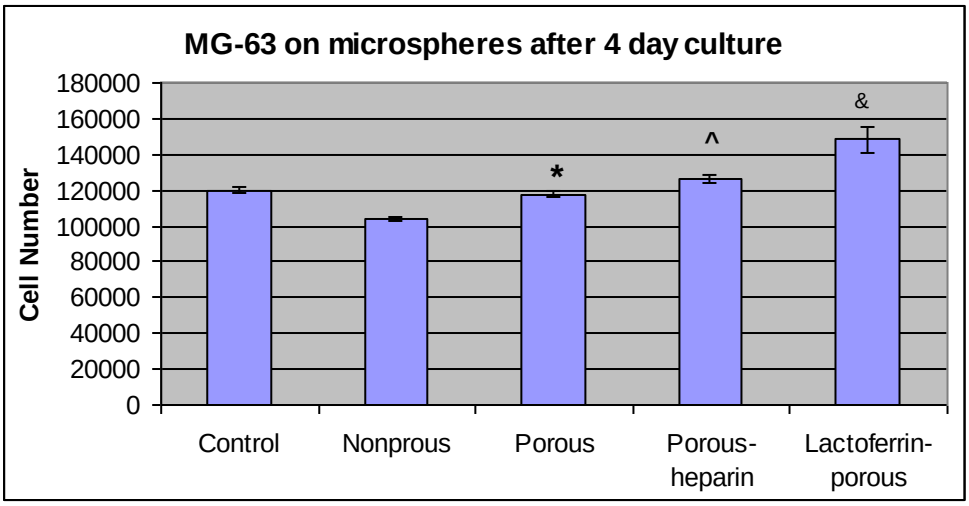

Figure 4.28 Proliferation of MG-63 cells after 4 Day culture on MS in 48 Well TC Plates examined by Alamar Blue Assay (* significant increase compared with Nonporous $p < 0.05$; ^ significant increase compared with Nonporous $p < 0.01$; & significant increase compared with Nonporous and Porous $p < 0.01$ and Porous-heparin $p < 0.05$)

4.3.10.3. MG63 differentiation

The functions of Lactoferrin-porous MS and Porous-heparin MS on MG63 differentiation were assessed by ALP cytochemical staining after 15 day cultures. The MG63 cells were first seeded onto MS with rotating culture for 6h, and then the MS with attached cells were transferred to the tissue culture plates for further 15 day culture.

ALP is an early marker of osteogenic differentiation, which is stained red in the ALP staining assay (marked with red circles on Figure 4.29). The positive areas of ALP staining were more pronounced in the following order: Lactoferrin-porous > Porous-heparin > Porous > Non-porous, which indicated that the heparin coating improved the osteogenic differentiation of MG63, compared with Porous and Nonporous MS. The loaded protein lactoferrin further promoted the osteogenic differentiation by more expression of ALP.

Moreover, ALP positive cells were seen closer to Lactoferrin-porous MS and along the MS array (Figure 4.29g). The suggested the combination of lactoferrin and heparin coated porous MS increased the ALP production of cells, especially the cells on and around the lactoferrin loaded MS.

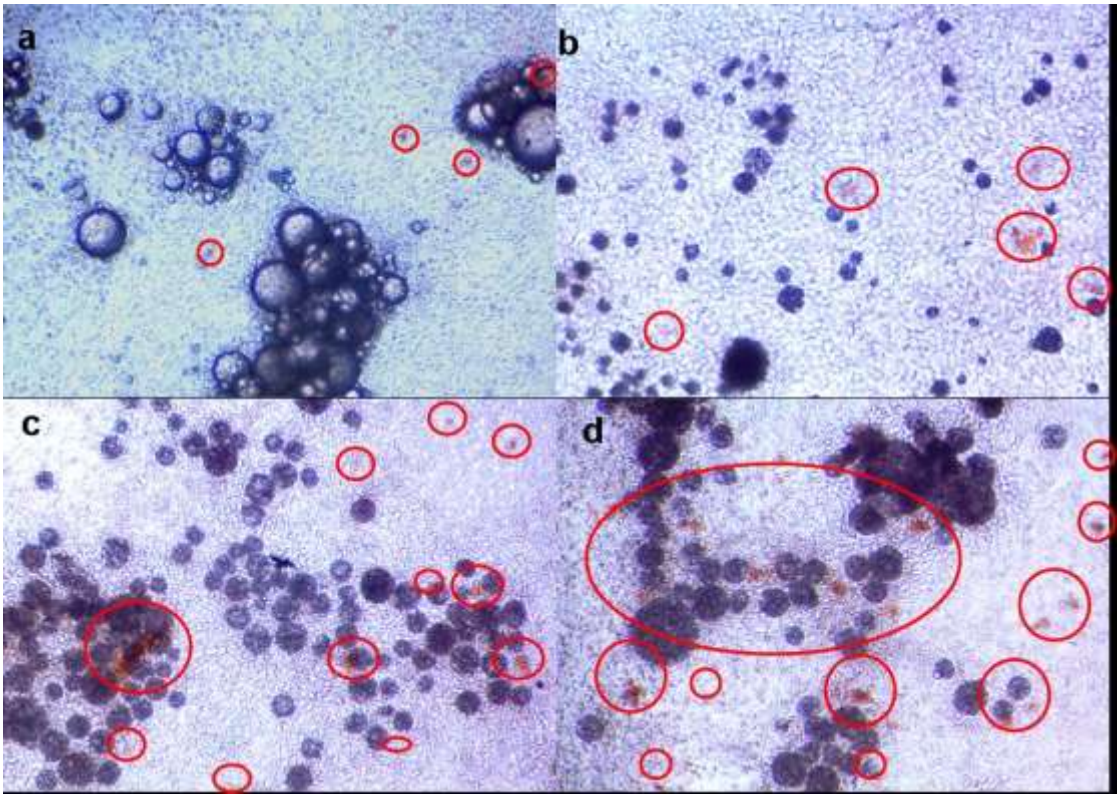

Figure 4.29 ALP Staining images (×20 magnification) of MG63 15 days on (a) Nonporous, (c) Porous, (e) Porous-heparin, and (g) Lactoferrin-porous MS; Red circles show ALP positive areas representing more differentiated phenotype.

4.4. **Discussion**

4.4.1. Lysozyme-heparin nanoparticles immobilized on polymer-leaching porous MS

Heparin is a negatively charged sulphated glycosaminoglycan (negative zeta potential in Figure 4.5) [129], which formed polyplexes with the positively charged PLL due to the ionic interactions. Model protein lysozyme was successfully loaded onto to the polyplexes to form lysozyme-heparin nanoparticles (Figure 4.7 a), because the -OSO_3- groups of heparin can bind specifically with the lysine and arginine groups of the protein [114]. The polyplexes can also protect the conjugated lysozyme from the shear stress and a water-oil interface [117, 124, 125]. Highly positively charged PEI

polymer was localized onto the porous MS by the ionic interactions between PEI and the surface-exposed negative groups of PLGA (–COOH and –OH). The lysozyme-heparin nanoparticles were subsequently immobilized onto the PEI coated MS, both on the surface and inside the pores (Figure 4.7) because of the ionic interactions between PEI and heparin. The ratio of heparin to PEI can be adjusted to achieve highly negatively charged polyplexes, which will promote the nanoparticles immobilization on the PEI coated MS. These nanoparticles on the MS improved the surface roughness and are expected to act as sites for protein delivery and cell adhesions [124, 125]

4.4.2. Layer-by-layer heparin coating on gas foamed porous MS

Due to the lack of lysozyme specific ELISA kit in our group to test the lysozyme loading efficiency, the above PLL-heparin polyplexes method was replaced by the layer-by-layer (LbL) assemble to coat MS and load proteins Compared with the convent chemical methods [6-8] the LbL assemble of heparin coating via ionic interactions [123] is facile and highly efficient.

The LbL assemble of heparin coating is a two step process (Figure 4.2). Firstly, similar to the lysozyme-heparin nanoparticles loading process, the positively charged PEI was localized onto the porous MS by the ionic interactions with the negatively charged PLGA MS. Son *et al* [218] reported similar PEI coating on nonporous PLGA MS, but their MS needed to be treated with O_2 plasma to enhance the surface charge so that the PEI molecules can approach and interact easily with the PLGA surface. In this study, a more facile and cost effective method, NaOH dipping, was used instead

of the O_2 plasma to modify the microsphere surface. NaOH modification enhanced the negative charges of MS (Figure 4.8) by hydrolysing the ester bonds of PLGA, which provided more –COOH and –OH groups on the MS surface for more efficient PEI immobilization. Moreover, the NaOH modification also improved the surface hydrophilicity, which is confirmed by the contract angle measurement (Figure 4.9 and 5.9). After the NaOH modification, the MS were dipped into the PEI solution to obtain a positively charged PEI coating (Figure 4.8) via the charge interaction, which was confirmed by the ATR-IR for the PEI presence on the MS (Figure 4.11).

Secondly, the PEI coated MS were immersed in the heparin solution for a quick heparin coating due to the ionic interaction between negatively charged heparin and positively charged PEI. The heparin coating on the MS was confirmed by ATR-IR (Figure 4.11), EDX (Figure 4.13) and Alcian Blue assay (Figure 4.11).

Interestingly, after coating the NaOH hydrolyzed PLGA films with PEI, the microsphere surface became more hydrophilic, even more than when further coating with heparin (Figure 4.9 and 5.9). This is possible due to the higher zeta potential of PEI coated films than those further coated with heparin (Figure 4.8). As PEI is only used for cell and DNA transfer [219], the second heparin coating was designed to bring in the combination of growth factor delivery [220] with cell delivery [10].

As the LbL process is gentle, the PEI and heparin solution used for coating MS can be re-utilized for repeated LbL assemble to get a highly charged 3D multi-layer polyelectrolyte films on MS to improve surface charge and roughness. Almodovar *et*

al [221, 222] recently reported similar 3D polyelectrolyte multilayer coating on chitosan nanofibers by the LbL assemble of N,N,N-Trimethyl chitosan and heparin. The effective LbL process enhanced the surface charge and hydrophilicity of porous MS, which, in turn, was expected to improve cell affinity on MS [29].

4.4.3. Protein absorption ability of heparin coated MS

The lactoferrin was bound to the heparin moieties immobilized on the microsphere surface due to the special binding between the $-OSO^3-$ groups of heparin and the lysine and arginine groups of the protein [114]. Since the lactoferrin loading process is simple and gentle, the unloaded lactoferrin in the supernatant is still bioactive, and can be re-used for lactoferrin loading on fresh MS. Due to the same binding interaction between heparin and proteins, the lactoferrin release profiles from Porous-heparin MS can be expected to be similar to that of bFGF released from heparinized PLGA MS, which is a sustained manner with reduced initial burst over 30 days [207]. Heparin is a negatively charged glycosaminoglycan (Figure 1.7) rich on the cell membrane and ECM which can regulate various protein binding and release [129]. The lactoferrin binding and release from the heparin coated MS mimicked the natural binding mechanism of protein in the ECM, so this can avoid many disadvantages of conventional growth factor delivery methods, such as growth factor damage or degradation during the fabrication, low loading efficiency and unpredictable release profile [52-54].

4.4.4. Improved cell adhesion, proliferation and spreading on Porous-heparin MS

The preliminary study of hMSC adhesion demonstrates cells favoured the Porous-heparin MS than the PLGA Porous MS (Figure 4.15), consistent with previous studies [10]. Although Nonporous MS were bigger in diameter, they attracted the fewest MMC cells and had the lowest viable cell numbers after 3 day culture. Moreover, most cells on Nonporous and Porous MS without heparin coating were rounded and spread slightly (Figure 4.20 and 5.20). The reason is that the hydrophilic nature of PLGA, suppress the ECM protein interactions with the MS surface [29], which makes PLGA inherently less cell-adhesive [66, 67].

The NaOH hydrolyzed PLGA Porous MS presented higher MMC adhesion efficiency than PLGA Nonporous MS (Figure 4.17), due to the enhanced surface charge (Figure 4.8) and hydrophilicity (Figure 4.9 and 5.9). The is because NaOH hydrolyzed the ester bonds of PLGA copolymer to induce more charged $–COO^-$ groups exposed on the Porous MS surface (Figure 4.29). Furthermore, compared to the previously known porous MS [109], the Porous MS in this study have lower surface porosity and more continued surface areas between the pores (marked on Figure 4.29) for cell adhesion and proliferation. Lee *et al* reported that the polycarbonate membrane with small micropores of 0.2-1.0 μm in diameter attracted more MG63 cells to adhere, spread well and show spindle-shape; however the polycarbonate membrane with larger micropores (5-8 μm), attracted only a few cells with more spherical cell shape and fewer filopodias and lamellapodia, because the discontinued surface with pores bigger than one cell body suppressed the cell spreading and proliferation [104]. As the

continued flat regions between the pores on our Porous MS are bigger than one cell body, while those continued regions on previously known porous MS are much smaller than one cell [109], our Porous MS are hence more cell-adhesive than those reported previously. On the other hand, although the pores on our Porous MS are also bigger than one cell body, the drawbacks of Lee *et al's* polycarbonate membrane [104] were avoided because our Porous MS are 3D structured spheres with bigger continued regions between pores, where cells can penetrate inside the pores to adhere on the insider continued regions.

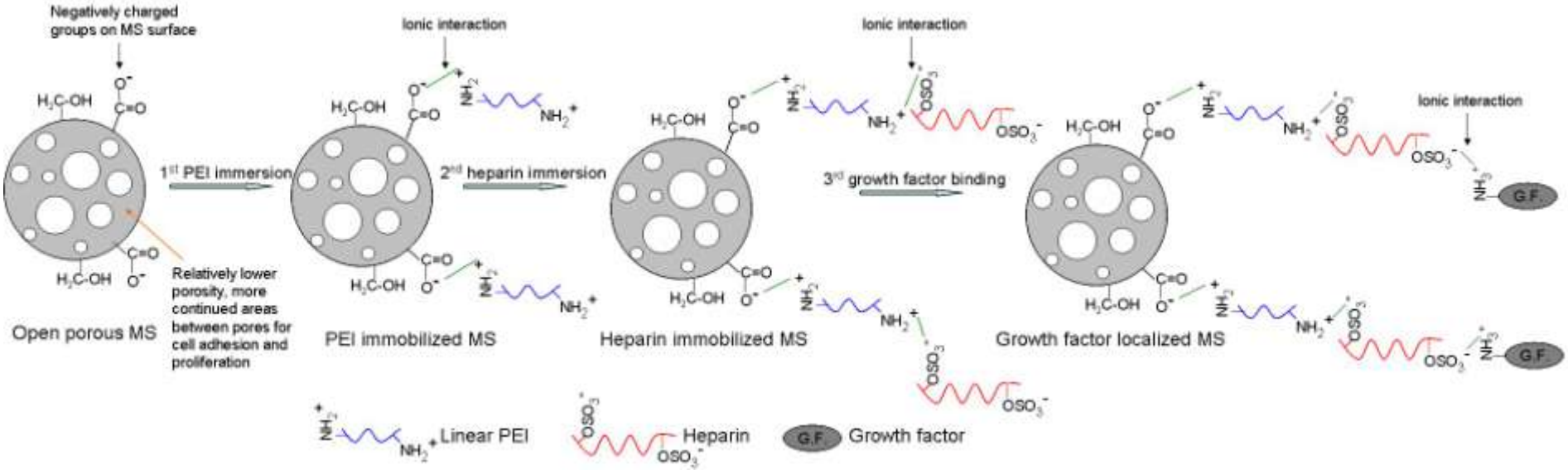

Figure 4.30 A schematic diagram of heparin LbL assemble on porous MS for growth factor delivery

The cell adhesion was further enhanced by the LbL immobilized heparin coating (demonstrated on Figure 4.29), which can facilitate a quick cell expansion as cell-adhesive substrates [10, 220]. After 3 day culture, more viable cells were detected on Porous-heparin MS (Figure 4.18 and 5.18), implying that the Porous-heparin MS favour cell proliferation. It has been reported that the higher cell adhesion facilitates the following cell proliferation and differentiation [223]. The improvement in cell attachment, spreading and proliferation of Porous-heparin MS was further confirmed by the SEM images (Figure 4.20-5.22). More spindle-shape cells spread flatly across the surface and inside the pores of Porous-heparin MP, and their filopodium and lamellipodium presented well adherent with the microsphere surface and other cells. However, only spherical-shape cells randomly adhered onto the Nonporous MP and porous MP. The initial cell shape after adhesion, especially well-spread cell shape, has been reported promoting the future cell growth, gene expression and extracellular matrix metabolism [104].

As the heparin coating further improved the surface charge (Figure 4.8) and hydrophilicity (Figure 4.9 and 5.9) than the NaOH hydrolyzed Porous MS, these surface chemical properties improved the cell adhesion, spreading and proliferation [29, 105, 206]. Moreover, as ECM component, heparin has specific $–SO_3^-$ ionic binding with the $–NH_3^+$ groups of various growth factors [114] (as shown on Figure 4.29), so the Porous-heparin MS can incorporate growth factors from the cell culture medium, fetal bovine serum (FBS) as reported to promote cell proliferation [129]. Various proteins and proteoglycans are contained in the FBS [224], which can modulate the cell adhesion and growth By localizing growth factors from FBS at the

interface between cell and Porous-heparin MS, heparin coating on porous MS amplified the growth factor bioactivity locally and hence modulated the cellular functions, mimicing the natural process in the ECM [123, 129, 224]. Heparin has been reported working as a vehicle to sequester and increase the protein concentration on the substrate surface to stimulate cell proliferation [10].

4.4.5. Improved cell differentiation by Porous-heparin MS loaded with lactoferrin

Porous-heparin MS enhanced the MG63 expression of ALP, an early marker of osteogenic differentiation, because the heparin coating on the MS surface significantly enhanced cell adhesion and spreading, which will facilitate the following cell differentiation [223]. Many evidence exists that heparin can support cell adhesion and differentiation due to its specific binding to growth factors in the regulation of the osteoblast cell line [115] and osteogenic differentiation [10, 120]. The improved growth and differentiation of bone marrow stroma, the native hMSC niche, has been reported by the selective colocalization of cytokines and ECM components from heparin [120]. Furthermore, heparin localized growth factor from FBS on the cell-MS interfaces, which, in turn, can stimulate cell differentiation [10, 224]

The promoted initial cell adhesion by heparin coating was hedged after loading the lactoferrin on the surface (Figure 4.27). This is presumable because the loaded lactoferrin reduces the surface charges and blocks contact between the heparin and cells. However, the significant increase of cell on lactoferrin-porous MS after 3 day culture, made the total viable cell more than that on Porous-heparin MS. As the

lactoferrin can promote cell proliferation and differentiation as a growth factor [215], this indicates that the heparin coating successfully bound and released the lactoferrin from the Lactoferrin-porous MS. The cell differentiation, assessed by the ALP staining, was also further promoted by the lactoferrin-porous MS compared with Porous-heparin MS, which further confirms the binding and release of lactoferrin from the heparin coating.

Compared with previously know porous MS (Table 4.1), the porous MS in this study was heparin functionalized by a facile LbL assemble, which makes the porous MS promising for the combination of drug delivery and injectable cell therapy. With lower porosity and more continued surface areas between pores, the Porous-heparin MS can achieve better cell adhesion and proliferation than previously know porous MS [104]. These novel low porosity Porous-heparin MS have great commercial potentials as microcarriers for cell expansion, drug delivery devices and injectable cell scaffolds for regenerative medicine.

Table 4.1 Comparisons of the applications of our MS with previous studies.

	Chemical composition	**Pore former**	**Surface porosity**	**Surface modification**	**Drug delivery**	**Cell delivery**	**Cell type exemplified**	**Cell differentiation**
Park et al [112]	75:25 PLGA	NH_4HCO_3	80-99%	Amine	No	Yes	Chondrocytes	N/A
Park et al [207]	75:25 PLGA	Fluronic F127	80-99%	Heparin-chemical reaction	Yes	No	In-vivo angiogenesis	N/A
Gan et al [111]	PLA	NH_4HCO_3	90-99%	NaOH	No	Yes	No	N/A
Gan et al [113]	PLA	NH_4HCO_3	90-99%	NaOH	No	Yes	MG63	N/A
Bae et al [110]	50:50, 75:25, 85:15 PLGA	H_2O_2	0	No	Yes	No	No	N/A
Our MS	50:50, 75:25, 85:15 PLGA	NH_4HCO_3	65-75%	NaOH, heparin immersion	Yes	Yes	Mouse bone cells, MG63, hMSC	Enhanced

(N/A: not available)

4.5. **Summary**

Besides controlling the surface pore size and porosity, the NaOH hydrolysis modification of MS also increased the surface carboxylic acid and hydroxyl groups to facilitate the PEI localization on MS. Heparin was subsequently immobilized onto MS by the LbL assemble due to ionic interactions with positively charged PEI. Heparin coating improved the MS surface hydrophilicity and cell cell response. Open Porous MS with more continued surface areas between pores, attracted more mouse MMC to the surface and inside pores, compared with Nonporous MS. The cell cell response was further enhanced by the heparin coating, which improved MMC adhesion and proliferation. The model protein lactoferrin was successfully loaded onto the heparin coated porous MS, which promoted the MG63 cell proliferation and differentiation by higher expression of ALP. The heparin coated porous MS will have great potential to be used as injectable scaffolds for cell delivery and controlled growth factor release due to the specific protein binding of heparin.

5. Chapter 5: Conclusions

The purpose of this thesis is to develop multi-functional biomedical devices which can be used for drug delivery and as injectable cell scaffolds in tissue engineering to improve the current bone disease therapy.

FDA approved anionic surfactant DSS successfully emulsified highly negatively charged PLGA microspheres instead of the toxic SDS [57] to induce fast HA precipitation. The fast HA precipitation by the constant composition method created continuous and complete HA nanocrystal coating on the PLGA microspheres, regardless of the size and morphology of the microsphere substrates (single microsphere or microsphere aggregations). However, the HA precipitation could be suppressed if the drug, which can inhibit HA nucleation, is leaked during the HA coating process. The encapsulation efficiency of antibiotic drug inside the PLGA core was over 60% with a typically triphasic in vitro release lasting over 21 days. The HA coating shell could further release the second protein drug lysozyme, and also improved the osteoblast cell attachment and proliferation, which makes the HA coated microspheres attractive device for dual drug delivery.

However, as the HA coated microspheres are smaller than one single cell, the PLGA was further evaluated to fabricate big porous microspheres for injectable cell delivery. Three different methods using salt porogen, extractable porogens and gas porogen were compared to fabricate porous microspheres. Only the gas porogen NH4HCO3

generated pores bigger than 10μm in diameter on the microsphere surface, therefore the gas porogen method is further investigated. By adjusting the external solution volume, completely covered porous microspheres can be fabricated with controllable PLGA skin layer thickness. This skin layer was reported governing the drug encapsulation efficiency and the initial drug burst release. The PLGA skin can be completely hydrolysed by the NaOH modification, which can control the surface open pore size and porosity.

As PLGA is hydrophobic and non cell-adhesive [29, 66], heparin, a negatively charged glycosaminoglycan of extracellular matrix (ECM) components, was immobilized on the above NaOH modified porous microspheres by a facile layer-by-layer (LbL) assemble in order to improve the cell cell response [224]. The NaOH modification did not only increase the surface open pore size and porosity, but also increased the negative surface charges of microspheres, which in turn facilitated the LbL assemble. Heparin coating improved the microsphere surface charges, hydrophilicity and cell cell response. Due to the ionic interactions with proteins, growth factor-like protein lactoferrin was localized on the heparin coated porous microspheres for controlled drug delivery. The lactoferrin bound heparin microspheres enhanced the cell differentiation by higher expression of ALP. Therefore, the novel heparin coated porous microspheres have great commercial potential as injectable cell scaffolds for cell delivery and controlled growth factor delivery in the regenerative medicine. The heparin coating on porous microspheres can mimic the natural ECM component to bind and release growth factors to regulate cell functions in a porous structure, which is similar to the ECM structures.

6. Chapter 6: Future work

Due to the time constraints, some aspects of this thesis were not comprehensively developed, and the following work can be conducted in future:

Large HA coated nonporous PLGA microspheres

In Chapter 2, HA nanocrystals were successfully grown on drug loaded nonporous PLGA microspheres by a modified constant composition method in 3 hours, but the HA coated microspheres, average 3-9 μm in diameter, are too small for cell adhesion and subsequent migration [104, 206]. Therefore, the fabrication of large HA coated microspheres (50-200 μm) for cell adhesion is interesting work for future. Based on the review in Chapter 1 and experiments in Chapter 3, the S/O/W method without homogenization may be a suitable approach to fabricate microspheres with diameter around 50-200 μm, which can be coated by HA with the same constant composition method to produce large HA coated microspheres. The model protein lysozyme, which was used to test the protein absorption of outer HA shell in Chapter 2, can be further tested for its *in-vitro* release profile to prove the concepts of dual drug delivery from both the inner PLGA core and the outer HA shell. Lysozyme can also be changed to other proteins or growth factors which can facilitate cell proliferation and differentiation, such as lactoferrin and BMP-2. Besides absorbing growth factors on the outer HA shell, growth factors can also be co-precipitated into the HA shell during the HA precipitation process in the constant composition method [152], [153, 154]. Comprehensive *in-vitro* evaluation (such as cell differentiation and morphology) and *in-vivo* histological assessments are the next steps for the application of large HA

coated microspheres as bone-specific dual drug delivery.

Microspheres based scaffolds with controllable HA gradient and drug release

Chapter 2 has also shown that the enough amount of anionic surfactant DSS (Figure 2.8) is critical to provide enough ionized $-SO_3^-$ as the nucleation sites on microsphere surface to capture Ca^{2+} ion for HA overgrowth in the constant composition method [57]. Without using anionic surfactant, there were no HA nanocrystals grown on PLGA microspheres emulsified by conventional nonionic surfactant PVA [50]. Therefore, scaffolds with controllable HA gradient and drug release can be fabricated by pre-designed mixture of DSS emulsified microspheres with PVA emulsified microspheres, and then coating HA on the microspheres based scaffolds by the constant composition method. HA will only grow on DSS emulsified microspheres in the scaffolds to provide HA gradient controlled by the locations of DSS emulsified microspheres. Drug release functions of the scaffolds can be achieved by physically encapsulating drugs in the microspheres, absorbing growth factors onto the HA gradient coating, or co-precipitating growth factors into the HA coating during the constant composition method. Microspheres can be mixed and bonded to each other to form scaffolds with controllable mechanical property by ethanol immersion with pressure, melting with pressure, liquid CO_2, or solvent evaporation. The microspheres based scaffolds with controllable HA gradient and drug release will be promosing implantable devices for bone-cartilage interface tissue repair and regeneration.

Porous microspheres fabricated by other porogens

In Chapter 3, PEG has shown promising results as porogens to fabricate porous microspheres (Figure 3.14) but more investigations are needed to optimize the PEG: PLGA ratio to increase the pore sizes.

Comprehensive evaluation of the heparin coated porous microspheres

In Chapter 4, the heparin coating on porous microspheres by the LbL assemble has been qualitatively verified by the Alcian Blue staining [214]. The first step of future work can be to quantify the heparin amount bounded onto the microspheres and hence to calculate heparin loading efficiency of the LbL assemble. Heparin coating on microspheres can be quantified by analysing the un-bonded heparin left in the heparin solution after the 2nd dip in the LbL assemble (Figure 4.2), which can be measured by heparin-specific UV-VIS absorbance at 505 nm. The *in-vitro* release profile of model protein lactoferrin on heparin coated porous MS also need to be quantified, although the release profile has been discussed with possiblle similarity to bFGF release from heparinized MS over 30 days [207]. As only 2 polyelectrolyte layers (one is PEI and the other one is heparin) were coated onto the porous microspheres by the LbL assemble, there is no visiable polyelectrolyte film on porous microspheres. Almodovar *et al* [221, 222] recently reported 3D polyelectrolyte film coating on chitosan nanofibers by the LbL assemble of 15 cycle repeated immersion in N,N,N-Trimethyl chitosan and heparin sequentially. There is therefore the potential to grow a visiable nano-scale 3D polyelectrolyte film on microspheres by more repeated immersion in PEI and heparin, which will improve microsphere surface charge and roughness to regulate cell response. Only a qualitatively ALP staining has been used

to prove that lactoferrin loaded Porous-heparin microspheres enhanced cell differentiation, therefore a quantitative ALP assay can be further performed to confirm the positive influence of loaded lactoferrin. After comprehensive *in-vitro* evaluation, *in-vivo* histological assessments are the next steps for the evaluation of heparin coated porous microspheres.

Bone-targeteting heparin coated porous microspheres

As bisphosphonates have strong specific binding to bone mineral and bisphosphonates, can conjugate with heparin by ionic interactions, the incorporation of bisphosphonate with heparin can fabricate multi-functional injectable cell scaffolds with bone targeting and drug delivery function.

Iron oxide nanoparticles can be further physically encapsulated into the heparin coated porous microspheres, so that the microsphere distribution in the body can be controlled by the external magnetites. This can bestow heparin coated porous microspheres with controllable site-specific drug and cell delivery for more accurate localized therapy.

HA coated porous PLGA microsphere

As PEI and heparin are more expensive than HA, and HA is osteoconductive, coating HA on porous microspheres can produce another drug deliverying injectable scaffolds, being used as an alternative to heparin coated porous microspheres specifically for bone tissue repair. Since the pore former NH_4HCO_3 can work as KCl to inhibit

anionic surfactant DSS ionization (Figure 3.10), the anionic surfactant cannot be used to fabricate porous microspheres based on NH_4HCO_3 gas foamed method. Therefore, the fast constant composition method cannot be used directly to coat HA on gas foamed porous microspheres. A combination of ×5 SBF (ionic concentration 5 times as the standard SBF) and the constant composition method may overcome this problem. ×5 SBF may be used to grow amorphous CaP globes on porous microspheres firstly in 30 minutes, and then the amorphous CaP globes can act as the nucleation sites instead of $-SO_3^-$ from DSS, to induce rapid HA overgrowth in the constant composition method. This proposed combination method avoids the usage of anionic surfactant, and can be developed as a fast universal method to precipitate highly crystallised HA on any surface.

Commericialization of heparin coated porous microspheres

As the main purpose of this thesis is to develop biodegradable microspheres for drug and cell delivery to improve the current thearpy, the commericialization of the research results is one important part of the future work. The world market size for tissue engineering and cell transplant is blooming, and is expected to rise to around $15 billion and $6 billion respectively in 2013. In 2010, a collagen-HA-ECM scaffold was launched in the European market as bone implant by Orthomimetics Ltd (spin-out from Dept of Materials, Cambridge Univeristy, acquired by TiGENIX in 2009 by EUR 16 million). Considering the long development time for drug dlivery and cell transplant devices, heparin coated porous microspheres developed in this thesis, can be firstly commercialized as cell culture/expansion microcarriers for research institutes or pharmaceutical companies. This is an easy entrance market without the

need for clnincal trial, where the current available products are all nonporous or sub-micron porous microcarriers. The heparin coated porous microspheres have bigger pores than products in the market, which can promote cell proliferation and differentiation. The only challenge is that the PLGA used in this thesis is expensive and biodegradable, so the material of the porous microspheres need be changed to cheaper and more stable polymers yet safe in an *in-vivo* environment, such as polystyrene and polycaprolactone. Once heparin coated porous microspheres can be scaled up as a microcarrier product in the market, this will generate cash and attact more investments to further develop these microspheres as drug delivery device (without cells) or injectable cell scaffolds for tissue repair.

Reference

[1] X. Luan, PhD Thesis, Freien Universitat Berlin, (2005).
[2] F. Rose, R.O.C. Oreffo, Biochem. Biophys. Res. Commun., 292 (2002) 1-7.
[3] G.L. Flynn, Pharmaceutical technology, 6 (1982) 33-39.
[4] V.V. Ranade, M.A. Hollinger, Drug delivery systems, CRC Press, 2003.
[5] V. Luginbuehl, L. Meinel, H.P. Merkle, B. Gander, Eur. J. Pharm. Biopharm., 58 (2004) 197-208.
[6] H.J. Chung, H.K. Kim, J.J. Yoon, T.G. Park, Pharmaceutical research, 23 (2006) 1835-1841.
[7] A. Perets, Y. Baruch, F. Weisbuch, G. Shoshany, G. Neufeld, S. Cohen, J. Biomed. Mater. Res. Part A, 65A (2003) 489-497.
[8] G.C.M. Steffens, C. Yao, P. Prevel, M. Markowicz, P. Schenck, E.M. Noah, N. Pallua, Tissue Eng., 10 (2004) 1502-1509.
[9] D.S.W. Benoit, K.S. Anseth, Acta Biomater., 1 (2005) 461-470.
[10] D.S.W. Benoit, A.R. Durney, K.S. Anseth, Biomaterials, 28 (2007) 66-77.
[11] F. Barrere, C.M. van der Valk, G. Meijer, R.A.J. Dalmeijer, K. de Groot, P. Layrolle, J. Biomed. Mater. Res. Part B, 67B (2003) 655-665.
[12] P. Kasten, R. Luginbuhl, M. van Griensven, T. Barkhausen, C. Krettek, M. Bohner, U. Bosch, Biomaterials, 24 (2003) 2593-2603.
[13] Y.F. Chou, J.C.Y. Dunn, B.M. Wu, J. Biomed. Mater. Res. Part B, 75B (2005) 81-90.
[14] S. Radin, J.T. Campbell, P. Ducheyne, J.M. Cuckler, Biomaterials, 18 (1997) 777-782.
[15] M. Stigter, J. Bezemer, K. de Groot, P. Layrolle, Journal Of Controlled Release, 99 (2004) 127-137.
[16] J. Vaughan, The Physiology of Bone, 3rd ed ed., Clarendon Press, Oxford, 1981.
[17] L.G.R. John P. Bilezikian, Gideon A. Rodan, Principle of bone biology, second edition ed., Academic Press, 2002.
[18] J.E. Shea, S.C. Miller, Advanced Drug Delivery Reviews, 57 (2005) 945.
[19] P. Ducy, T. Schinke, G. Karsenty, Science, 289 (2000) 1501-1504.
[20] S.L. Teitelbaum, Science, 289 (2000) 1504-1508.
[21] H.K. Vaananen, H. Zhao, M. Mulari, J.M. Halleen, Journal Of Cell Science, 113 (2000) 377-381.
[22] K. Vaananen, Advanced Drug Delivery Reviews, 57 (2005) 959.
[23] V. Everts, J.M. Delaisse, W. Korper, D.C. Jansen, W. Tigchelaar-Gutter, P. Saftig, W. Beertsen, Journal Of Bone And Mineral Research, 17 (2002) 77-90.
[24] F.R. Bringhurst, Journal of Musculoskeletal & Neuronal Interactions, 2 (2002) 245-251.
[25] M. Vallet-Regi, J.M. Gonzalez-Calbet, Progress in Solid State Chemistry, 32 (2004) 1-31.
[26] R.Z. LeGeros, Clin. Orthop. Rel. Res., (2002) 81-98.
[27] J.T. Lin, J.M. Lane, Clin. Orthop. Rel. Res., (2004) 126-134.
[28] G.O.A. Qing Yang, Drug Development and Industrial Pharmacy,, (2000).
[29] T.A. Einhorn, Clin. Orthop. Rel. Res., (1998) S7-S21.
[30] H. Hirabayashi, J. Fujisaki, Clin. Pharmacokinet., 42 (2003) 1319-1330.
[31] N. Goyal, M. Gupta, K. Joshi, O.N. Nagi, J. Mol. Histol., 41 193-197.
[32] F. Goldblatt, D.A. Isenberg, Clinical And Experimental Immunology, 140 (2005) 195-204.

[33] G.S.P. Gary S. Firestein, and Frank A. Wollheim, Rheumatoid Arthritis: Frontiers in pathogenesis and treatment, 1st edition ed., Oxford University Press, 2000.
[34] A.J.S.a.J.E. Pearson, Arthritis Research, 4 (2002) S265-S272.
[35] I. Onsten, A. Nordqvist, A.S. Carlsson, J. Besjakov, S. Shott, Journal Of Bone And Joint Surgery-British Volume, 80B (1998) 417-425.
[36] S. Itoh, M. Matubara, T. Kawauchi, H. Nakamura, S. Yukitake, S. Ichinose, K. Shinomiya, J. Mater. Sci.-Mater. Med., 12 (2001) 575-581.
[37] D.R. Sumner, T.M. Turner, A.F. Purchio, W.R. Gombotz, R.M. Urban, J.O. Galante, J. Bone Joint Surg.-Am. Vol., 77A (1995) 1135-1147.
[38] A.J. Salgado, O.P. Coutinho, R.L. Reis, Macromol. Biosci., 4 (2004) 743-765.
[39] U. Joosten, A. Joist, T. Frebel, B. Brandt, S. Diederichs, C. von Eiff, Biomaterials, 25 (2004) 4287-4295.
[40] A.K. Jain, R. Panchagnula, Int. J. Pharm., 206 (2000) 1-12.
[41] A.D. Hanssen, Clin. Orthop. Rel. Res., 437 (2005) 91-96.
[42] Z. Ruszczak, W. Friess, Advanced Drug Delivery Reviews, 55 (2003) 1679-1698.
[43] C. Soundrapandian, S. Datta, B. Sa, Critical reviews in therapeutic drug carrier systems, 24 (2007) 493-545.
[44] S.M.K. Louis V. Avioli, Metabolic bone disease, Third edition ed., Academic Press, 1998.
[45] N. Saito, N. Murakami, J. Takahashi, H. Horiuchi, H. Ota, H. Kato, T. Okada, K. Nozaki, K. Takaoka, Advanced Drug Delivery Reviews, 57 (2005) 1037-1048.
[46] F. Rose, Q.P. Hou, R.O.C. Oreffo, J. Pharm. Pharmacol., 56 (2004) 415-427.
[47] C.A. Simmons, E. Alsberg, S. Hsiong, W.J. Kim, D.J. Mooney, Bone, 35 (2004) 562-569.
[48] L. Jongpoiboonkit, T. Franklin-Ford, W.L. Murphy, Adv. Mater., 21 (2009) 1960-1963.
[49] X. Shi, Y. Wang, R.R. Varshney, L. Ren, F. Zhang, D.A. Wang, Biomaterials, 30 (2009) 3996-4005.
[50] Q. Xu, A. Crossley, J. Czernuszka, Journal of pharmaceutical sciences, 98 (2009) 2377-2389.
[51] K. Garvin, C. Feschuk, Clin. Orthop. Rel. Res., (2005) 105-110.
[52] S. Takada, Y. Yamagata, M. Misaki, K. Taira, T. Kurokawa, Journal of Controlled Release, 88 (2003) 229-242.
[53] A. Lamprecht, H.R. Torres, U. Schafer, C.M. Lehr, Journal of Controlled Release, 69 (2000) 445-454.
[54] T. Morita, Y. Sakamura, Y. Horikiri, T. Suzuki, H. Yoshino, Journal of Controlled Release, 69 (2000) 435-444.
[55] U. Joosten, A. Joist, G. Gosheger, U. Liljenqvist, B. Brandt, C. von Eiff, Biomaterials, 26 (2005) 5251-5258.
[56] H.W. Kim, J.C. Knowles, H.E. Kim, J. Mater. Sci.-Mater. Med., 16 (2005) 189-195.
[57] Q. Xu, J.T. Czernuszka, J Control Release, 127 (2008) 146-153.
[58] R. Jalil, J.R. Nixon, Journal of Microencapsulation, 7 (1990) 297-325.
[59] X. Wu, In: Wise et al., editors. Encyclopedic Handbook of Biomaterials and Bioengineering. New York: Marcel Dekker, 1995. p. 1015}54., (1995).
[60] I.J. Oh, J.Y. Oh, K.C. Lee, Archives of Pharmacal Research (Seoul), 16 (1993) 312-317.
[61] H. Kranz, N. Ubrich, P. Maincent, R. Bodmeier, Journal of Pharmaceutical Sciences, 89 (2000) 1558-1566.

[62] J.M. Anderson, M.S. Shive, Advanced Drug Delivery Reviews, 28 (1997) 5-24.
[63] Y. Matsusue, T. Yamamuro, M. Oka, Y. Shikinami, S.H. Hyon, Y. Ikada, Journal of Biomedical Materials Research, 26 (1992) 1553-1567.
[64] K.A. Athanasiou, G.G. Niederauer, C.M. Agrawal, Biomaterials, 17 (1996) 93-102.
[65] J. Klompmaker, R.P.H. Veth, H.W.B. Jansen, H.K.L. Nielsen, J.H. deGroot, A.J. Pennings, R. Kuijer, Biomaterials, 17 (1996) 1685-1691.
[66] L. Feng, J.D. Andrade, Journal of Biomedical Materials Research, 28 (1994) 735-743.
[67] D.L. Elbert, J.A. Hubbell, Annual Review of Materials Science, 26 (1996) 365-394.
[68] S.M. Li, H. Garreau, M. Vert, Journal of Materials Science-Materials in Medicine, 1 (1990) 123-130.
[69] S.M. Li, H. Garreau, M. Vert, Journal of Materials Science-Materials in Medicine, 1 (1990) 131-139.
[70] C.G. Pitt, M.M. Gratzl, G.L. Kimmel, J. Surles, A. Schindler, Biomaterials, 2 (1981) 215-220.
[71] A.M. Reed, D.K. Gilding, Polymer, 22 (1981) 494-498.
[72] M. Vert, S. Li, H. Garreau, J. Mauduit, M. Boustta, G. Schwach, R. Engel, J. Coudane, Angewandte Makromolekulare Chemie, 247 (1997) 239-253.
[73] R.A. Miller, J.M. Brady, D.E. Cutright, Journal of Biomedical Materials Research, 11 (1977) 711-719.
[74] H. Jeffery, Int. J. Pharm. 1991, 77, 169., (1991).
[75] W. XS., In: Wise et al., editors. Encyclopedic handbook of biomaterials and bioengineering. New York: Marcel Dekker, 1995. p. 1151}200., (1995).
[76] R. Arshady, Journal of Controlled Release, 17 (1991) 1-21.
[77] V. Lassalle, M.L. Ferreira, Macromolecular Bioscience, 7 (2007) 767-783.
[78] S. Putney, Biotechnol. 1998, 16, 153., (1998).
[79] J. Siepmann, N. Faisant, J.P. Benoit, Pharm. Res., 19 (2002) 1885-1893.
[80] C. Zandonella, Nature, 421 (2003) 884-886.
[81] S.S. Kim, S.J. Gwak, C.Y. Choi, B.S. Kim, J. Biomed. Mater. Res. Part B, 75B (2005) 369-377.
[82] R. Langer, J.P. Vacanti, Science, 260 (1993) 920-926.
[83] X.H. Liu, X.B. Jin, P.X. Ma, Nat. Mater., 10 (2011) 398-406.
[84] Y. Martin, M. Eldardiri, D.J. Lawrence-Watt, J.R. Sharpe, Tissue Eng. Part B-Rev., 17 (2011) 71-80.
[85] J.Y. Liu, J. Hafner, G. Dragieva, B. Seifert, G. Burg, Wound Repair Regen., 12 (2004) 148-156.
[86] C.J. Detzel, A.L. Larkin, P. Rajagopalan, Tissue Eng. Part B-Rev., 17 101-113.
[87] M. Frohlich, W.L. Grayson, L.Q. Wan, D. Marolt, M. Drobnic, G. Vunjak-Novakovic, Current stem cell research & therapy, 3 (2008) 254-264.
[88] H.J. Chung, I.K. Kim, T.G. Kim, T.G. Park, Tissue engineering, 14 (2008) 607-615.
[89] J.R. Smythies, Nature, 216 (1967) 1176-&.
[90] A.L. van Wezel, Developments in biological standardization, 37 (1976) 143-147.
[91] GE Healthcare Biosciences AB, www.gelifesciences.com/aptrix/upp01077.nsf/contents/products?openDocument&parentid=666921&moduleid=167175 (2009).
[92] A.M. Fernandes, T.G. Fernandes, M.M. Diogo, C.L. da Silva, D. Henrique,

J.M.S. Cabral, J. Biotechnol., 132 (2007) 227-236.
[93] L. Boo, L. Selvaratnam, C.C. Tai, T.S. Ahmad, T. Kamarul, J. Mater. Sci.-Mater. Med., 22 (2011) 1343-1356.
[94] Y. Yang, F.M.V. Rossi, E.E. Putnins, Biomaterials, 28 (2007) 3110-3120.
[95] R. Ahmadi, N. Mordan, A. Forbes, R.M. Day, Acta Biomater., 7 (2011) 1542-1549.
[96] D.A. Edwards, J. Hanes, G. Caponetti, J. Hrkach, A. BenJebria, M.L. Eskew, J. Mintzes, D. Deaver, N. Lotan, R. Langer, Science, 276 (1997) 1868-1871.
[97] A. Rawat, Q.H. Majumder, F. Ahsan, J Control Release, 128 (2008) 224-232.
[98] F. Ungaro, R. d'Emmanuele di Villa Bianca, C. Giovino, A. Miro, R. Sorrentino, F. Quaglia, M.I. La Rotonda, Journal of Controlled Release, 135 (2009) 25-34.
[99] Y. Yang, N. Bajaj, P. Xu, K. Ohn, M.D. Tsifansky, Y. Yeo, Biomaterials, 30 (2009) 1947-1953.
[100] H. Kim, H. Park, J. Lee, T.H. Kim, E.S. Lee, K.T. Oh, K.C. Lee, Y.S. Youn, Biomaterials, 32 (2011) 1685-1693.
[101] H. Kim, H. Park, J. Lee, T.H. Kim, E.S. Lee, K.T. Oh, K.C. Lee, Y.S. Youn, Biomaterials, 32 1685-1693.
[102] H.J. Chung, T.G. Park, Tissue engineering, 15 (2009) 1391-1400.
[103] H.J. Chung, T.G. Park, Adv. Drug Deliv. Rev., 59 (2007) 249-262.
[104] S.J. Lee, J.S. Choi, K.S. Park, G. Khang, Y.M. Lee, H.B. Lee, Biomaterials, 25 (2004) 4699-4707.
[105] S.J. Lee, G. Khang, Y.M. Lee, H.B. Lee, J. Colloid Interface Sci., 259 (2003) 228-235.
[106] A.R. Ahmed, R. Bodmeier, Eur J Pharm Biopharm, 71 (2009) 264-270.
[107] E.S. Lee, M.J. Kwon, H. Lee, K. Na, J.J. Kim, Eur. J. Pharm. Sci., 29 (2006) 435-441.
[108] H. Kim, J. Lee, T.H. Kim, E.S. Lee, K.T. Oh, D.H. Lee, E.S. Park, Y.H. Bae, K.C. Lee, Y.S. Youn, Pharmaceutical research, 28 (2011) 2008-2019.
[109] T.K. Kim, J.J. Yoon, D.S. Lee, T.G. Park, Biomaterials, 27 (2006) 152-159.
[110] S.E. Bae, J.S. Son, K. Park, D.K. Han, J Control Release, 133 (2009) 37-43.
[111] X.D. Shi, L. Sun, J. Jiang, X.L. Zhang, W.J. Ding, Z.H. Gan, Macromol. Biosci., 9 (2009) 1211-1218.
[112] H.J. Chung, I.K. Kim, T.G. Kim, T.G. Park, Tissue Eng. Part A, 14 (2008) 607-615.
[113] S. Xudong, J. Jian, S. Lei, G. Zhihua, Colloids Surf. B, Biointerfaces, 85 73-8080.
[114] M. Rusnati, D. Coltrini, P. Caccia, P. Dellera, G. Zoppetti, P. Oreste, B. Valsasina, M. Presta, Biochem. Biophys. Res. Commun., 203 (1994) 450-458.
[115] A.C. Rapraeger, A. Krufka, B.B. Olwin, Science, 252 (1991) 1705-1708.
[116] H. Lin, Y. Zhaol, W.J. Sun, B. Chen, J. Zhang, W.X. Zhao, Z.F. Xiao, J.W. Dai, Biomaterials, 29 (2008) 1189-1197.
[117] J. Sudhalter, J. Folkman, C.M. Svahn, K. Bergendal, P.A. Damore, J. Biol. Chem., 264 (1989) 6892-6897.
[118] J.J. Yoon, H.J. Chung, H.J. Lee, T.G. Park, J. Biomed. Mater. Res. Part A, 79A (2006) 934-942.
[119] D.S.W. Benoit, S.D. Collins, K.S. Anseth, Adv. Funct. Mater., 17 (2007) 2085-2093.
[120] P. Gupta, C.D. Pan, M.S. Nelson, M. Reyes, Blood, 100 (2002) 525A-525A.
[121] A.P. Zhu, M. Zhang, J. Wu, J. Shen, Biomaterials, 23 (2002) 4657-4665.

[122] S. Murugesan, J. Xie, R.J. Linhardt, Curr. Top. Med. Chem., 8 (2008) 80-100.
[123] C.M. Jewell, D.M. Lynn, Adv. Drug Deliv. Rev., 60 (2008) 979-999.
[124] K.S. Na K, Park K, Kim K, Woo DG, Kwon IC, Chung HM, Park KH, J Am Chem Soc, 129(18) (2007) 5788-5789.
[125] K.P. Ji Sun Park, Dae Gyun Woo, Han Na Yang, Hyung-Min Chung, Keun-Hong Park Small, 4 (2008) 1950-1955.
[126] C.J. Detzel, A.L. Larkin, P. Rajagopalan, Tissue Eng. Part B-Rev., 17 (2011) 101-113.
[127] M. Ishihara, M. Sato, H. Hattori, Y. Saito, H. Yura, K. Ono, K. Masuoka, M. Kikuchi, K. Fujikawa, A. Kurita, J. Biomed. Mater. Res., 56 (2001) 536-544.
[128] S.H. Oh, T.H. Kim, J.H. Lee, Biomaterials, 32 8254-8260.
[129] O. Guillame-Gentil, O. Semenov, A.S. Roca, T. Groth, R. Zahn, J. Voros, M. Zenobi-Wong, Adv. Mater., 22 5443-5462.
[130] L. Liu, S.R. Guo, J. Chang, C.Q. Ning, C.M. Dong, D.Y. Yan, J. Biomed. Mater. Res. Part B, 87B (2008) 244-250.
[131] Z.M. Liu, Q.Y. Gu, Z.K. Xu, T. Groth, Macromol. Biosci., 10 1043-1054.
[132] M.J. Olszta, X.G. Cheng, S.S. Jee, R. Kumar, Y.Y. Kim, M.J. Kaufman, E.P. Douglas, L.B. Gower, Mater. Sci. Eng. R-Rep., 58 (2007) 77-116.
[133] F.Z. Cui, Y. Li, J. Ge, Materials Science & Engineering R-Reports, 57 (2007) 1-27.
[134] M. Kikuchi, T. Ikoma, S. Itoh, H.N. Matsumoto, Y. Koyama, K. Takakuda, K. Shinomiya, J. Tanaka, Compos. Sci. Technol., 64 (2004) 819-825.
[135] L.M. Sun, C.C. Berndt, K.A. Gross, A. Kucuk, J. Biomed. Mater. Res., 58 (2001) 570-592.
[136] A.T. Wong, in: Department of Materials, University of Oxford, Oxford, 1993.
[137] J.C. Heughebaert, G.H. Nancollas, Journal of Physical Chemistry 88 (1984) 2478-2481.
[138] J.F. Derooij, J.C. Heughebaert, G.H. Nancollas, Journal of colloid and interface science, 100 (1984) 350-358.
[139] J. Christoffersen, M.R. Christoffersen, W. Kibalczyc, F.A. Andersen, J. Cryst. Growth, 94 (1989) 767-777.
[140] A.T.C. Wong, J.T. Czernuszka, Colloids and Surfaces a-Physicochemical and Engineering Aspects, 78 (1993) 245-253.
[141] J.W. Zhang, G.H. Nancollas, J. Cryst. Growth, 125 (1992) 251-269.
[142] A.T.C. Wong, J.T. Czernuszka, Colloid Surf. A-Physicochem. Eng. Asp., 103 (1995) 23-36.
[143] P.G. Koutsoukos, Z. Amjad, M.B. Tomson, G.H. Nancollas, Journal of the American Chemical Society, 102 (1980) 1553-1557.
[144] A. Veis, The chemistry and biology of mineralized connective tissues. , Elsevier, 1981.
[145] Y.Z. Yang, K.H. Kim, J.L. Ong, Biomaterials, 26 (2005) 327-337.
[146] I. Zhitomirsky, Adv. Colloid Interface Sci., 97 (2002) 277.
[147] R.Y. Zhang, P.X. Ma, Macromolecular Bioscience, 4 (2004) 100-111.
[148] W.L. Murphy, D.H. Kohn, D.J. Mooney, J. Biomed. Mater. Res., 50 (2000) 50-58.
[149] Q. Xu, J.T. Czernuszka, J Control Release, 127 (2008) 146-153.
[150] Y. Chen, A.F.T. Mak, J.S. Li, M. Wang, A.W.T. Shum, J. Biomed. Mater. Res. Part B, 73B (2005) 68-76.
[151] R.Y. Zhang, P.X. Ma, J. Biomed. Mater. Res., 45 (1999) 285-293.

[152] J.D. Kretlow, A.G. Mikos, Tissue Engineering, 13 (2007) 927-938.
[153] D. Tadic, T. Welzel, P. Seidel, E. Wust, E. Dingeldein, M. Epple, Materialwiss. Werkstofftech., 35 (2004) 1001-1005.
[154] M.P. Ginebra, T. Traykova, J.A. Planell, Journal of Controlled Release, 113 (2006) 102-110.
[155] M. Singh, J. Kazzaz, M. Ugozzoli, J. Chesko, D.T. O'Hagan, Expert Opin. Biol. Ther., 4 (2004) 483-491.
[156] J. Kazzaz, J. Neidleman, M. Singh, G. Ott, D.T. O'Hagan, Journal of Controlled Release, 67 (2000) 347-356.
[157] M. Singh, J. Kazzaz, J. Chesko, E. Soenawan, M. Ugozzoli, M. Giuliani, M. Pizza, R. Rappouli, D.T. O'Hagan, J. Pharm. Sci., 93 (2004) 273-282.
[158] J. Chesko, J. Kazzaz, M. Ugozzoli, D.T. O'Hagan, M. Singh, J. Pharm. Sci., 94 (2005) 2510-2519.
[159] M. Singh, J. Chesko, J. Kazzaz, M. Ugozzoli, E. Kan, I. Srivastava, D.T. O'Hagan, Pharm. Res., 21 (2004) 2148-2152.
[160] D.T. O'Hagan, R. Rappuoli, Pharm. Res., 21 (2004) 1519-1530.
[161] H.Y. Li, J. Chang, Compos. Sci. Technol., 65 (2005) 2226-2232.
[162] J. Siepmann, K. Elkharraz, F. Siepmann, D. Klose, Biomacromolecules, 6 (2005) 2312-2319.
[163] T. Miyazaki, C. Ohtsuki, Y. Akioka, M. Tanihara, J. Nakao, Y. Sakaguchi, S. Konagaya, J. Mater. Sci.-Mater. Med., 14 (2003) 569-574.
[164] M. Kawashita, M. Nakao, M. Minoda, H.M. Kim, T. Beppu, T. Miyamoto, T. Kokubo, T. Nakamura, Biomaterials, 24 (2003) 2477-2484.
[165] M. Tanahashi, T. Matsuda, J. Biomed. Mater. Res., 34 (1997) 305-315.
[166] T. Kawai, C. Ohtsuki, M. Kamitakahara, T. Miyazaki, M. Tanihara, Y. Sakaguchi, S. Konagaya, Biomaterials, 25 (2004) 4529-4534.
[167] A. Oyane, M. Minoda, T. Miyamoto, R. Takahashi, K. Nakanishi, H.M. Kim, T. Kokubo, T. Nakamura, J. Biomed. Mater. Res., 47 (1999) 367-373.
[168] Q. Xu, DPhil thesis, University of Oxford, 2008.
[169] Inactive ingredient database, USFDA, Center for drug ecaluation and research, 2003.
[170] S.D. Putney, P.A. Burke, Nature Biotechnology, 16 (1998) 153-157.
[171] N. Faisant, J. Akiki, F. Siepmann, J.P. Benoit, J. Siepmann, International Journal of Pharmaceutics, 314 (2006) 189-197.
[172] B.L. Bales, L. Messina, A. Vidal, M. Peric, O.R. Nascimento, Journal of Physical Chemistry B, 102 (1998) 10347-10358.
[173] M.B. Tomson, G.H. Nancollas, Science, 200 (1978) 1059-1060.
[174] P.D. Delmas, Current Opinion In Rheumatology, 17 (2005) 462-466.
[175] G. Rodan, A. Reszka, E. Golub, R. Rizzoli, Current Medical Research And Opinion, 20 (2004) 1291-1300.
[176] E. Boanini, M. Gazzano, K. Rubini, A. Bigi, Advanced Materials, 19 (2007) 2499.
[177] Q. Xu, Y. Tanaka, J.T. Czernuszka, Biomaterials, 28 (2007) 2687-2694.
[178] S.P.a.R.Z.L. J.D.B. Featherstone, Caries Res, 18 (1984) 63-66.
[179] A. Dion, M. Langman, G. Hall, M. Filiaggi, Biomaterials, 26 (2005) 7276-7285.
[180] L. Tang, C. Zhao, Y. Xiong, C. Pan, A. Wang, Orthopedics, 32 (2009) 324.
[181] L.N. Luong, S.I. Hong, R.J. Patel, M.E. Outslay, D.H. Kohn, Biomaterials, 27 (2006) 1175-1186.
[182] H. Fleisch, Expert Opin. Ther. Patents, 11 (2001) 1371-1381.

[183] G.S. Lee, J.H. Park, U.S. Shin, H.W. Kim, Acta Biomater., 7 3178-3186.
[184] F. Barrere, C.A. van Blitterswijk, K. de Groot, P. Layrolle, Biomaterials, 23 (2002) 1921-1930.
[185] S.Y. Lin, M.J. Li, W.T. Cheng, Spectr.-Int. J., 21 (2007) 1-30.
[186] A. Geze, I. Chourpa, F. Boury, J.P. Benoit, P. Dubois, Analyst, 124 (1999) 37-42.
[187] V. Maquet, A.R. Boccaccini, L. Pravata, I. Notingher, R. Jerome, Biomaterials, 25 (2004) 4185-4194.
[188] V. Maquet, A.R. Boccaccini, L. Pravata, I. Notingher, R. Jerome, J. Biomed. Mater. Res. Part A, 66A (2003) 335-346.
[189] X.Y. Yuan, A.F.T. Mak, J.L. Li, J. Biomed. Mater. Res., 57 (2001) 140-150.
[190] C. Du, F.Z. Cui, W. Zhang, Q.L. Feng, X.D. Zhu, K. de Groot, J. Biomed. Mater. Res., 50 (2000) 518-527.
[191] M. Tanahashi, T. Yao, T. Kokubo, M. Minoda, T. Miyamoto, T. Nakamura, T. Yamamuro, J. Am. Ceram. Soc., 77 (1994) 2805-2808.
[192] F. Miyaji, H.-M. Kim, S. Handa, T. Kokubo, T. Nakamura, Biomaterials, 20 (1999) 913-919.
[193] E. Dalas, J.K. Kallitsis, P.G. Koutsoukos, Langmuir, 7 (1991) 1822-1826.
[194] P.G. Koutsoukos, G.H. Nancollas, Colloids and Surfaces, 28 (1987) 95-108.
[195] J. Kim, I.S. Kim, T.H. Cho, K.B. Lee, S.J. Hwang, G. Tae, I. Noh, S.H. Lee, Y. Park, K. Sun, Biomaterials, 28 (2007) 1830-1837.
[196] F.M. Chen, Y.M. Zhao, R. Zhang, T. Jin, H.H. Sun, Z.F. Wu, Y. Jin, Journal of Controlled Release, 121 (2007) 81-90.
[197] L.S. Ferreira, S. Gerecht, J. Fuller, H.F. Shieh, G. Vunjak-Novakovic, R. Langer, Biomaterials, 28 (2007) 2706-2717.
[198] N. Spanos, P.G. Koutsoukos, Journal of Materials Science, 36 (2001) 573-578.
[199] H.T. Schmidt, B.L. Gray, P.A. Wingert, A.E. Ostafin, Chem. Mat., 16 (2004) 4942-4947.
[200] J. Ryu, S.H. Ku, H. Lee, C.B. Park, Adv. Funct. Mater., 20 (2010) 2132-2139.
[201] N. Spanos, V. Deimede, P.G. Koutsoukos, Biomaterials, 23 (2002) 947-953.
[202] G. Wu, Y.L. Liu, T. Iizuka, E.B. Hunziker, Tissue Eng. Part C-Methods, 16 (2010) 1255-1265.
[203] M. Jarcho, Clin. Orthop. Rel. Res., (1981) 259-278.
[204] L.L. Hench, J. Wilson, Science, 226 (1984) 630-636.
[205] L.L. Hench, J. Am. Ceram. Soc., 74 (1991) 1487-1510.
[206] J.H. Lee, H.W. Jung, I.K. Kang, H.B. Lee, Biomaterials, 15 (1994) 705-711.
[207] H.K. Kim, H.J. Chung, T.G. Park, J Control Release, 112 (2006) 167-174.
[208] J. Wang, B.A. Wang, S.P. Schwendeman, J. Control. Release, 82 (2002) 289-307.
[209] K. Koushik, U.B. Kompella, Pharm. Res., 21 (2004) 524-535.
[210] R. Jeyanthi, B.C. Thanoo, R.C. Metha, P.P. DeLuca, Journal of Controlled Release, 38 (1996) 235-244.
[211] H.K. Kim, H.J. Chung, T.G. Park, J. Control. Release, 112 (2006) 167-174.
[212] R.A. Jain, Biomaterials, 21 (2000) 2475-2490.
[213] M. van de Weert, W.E. Hennink, W. Jiskoot, Pharm. Res., 17 (2000) 1159-1167.
[214] T. Vankuppevelt, J.H. Veerkamp, Microsc. Res. Tech., 28 (1994) 125-140.
[215] Y. Takayama, K. Mizumachi, J. Biosci. Bioeng., 107 (2009) 191-195.
[216] X.L. Shi, Y.D. Qiu, X.Y. Wu, T. Xie, Z.H. Zhu, L.L. Chen, L. Li, Y.T. Ding, Hepatol. Res., 31 (2005) 223-231.

[217] Z.D. Xia, Y.Z. Huang, L.E. Adamopoulos, A. Walpole, J.T. Triffitt, Z.F. Cui, J. Biomed. Mater. Res. Part A, 79A (2006) 582-590.
[218] J.S. Son, M. Appleford, J.L. Ong, J.C. Wenke, J.M. Kim, S.H. Choi, D.S. Oh, J. Control. Release, 153 133-140.
[219] S. Brunner, E. Furtbauer, T. Sauer, M. Kursa, E. Wagner, Mol. Ther., 5 (2002) 80-86.
[220] O. Jeon, S.J. Song, S.W. Kang, A.J. Putnam, B.S. Kim, Biomaterials, 28 (2007) 2763-2771.
[221] J. Almodovar, M.J. Kipper, Macromol. Biosci., 11 (2011) 72-76.
[222] J. Almodovar, L.W. Place, J. Gogolski, K. Erickson, M.J. Kipper, Biomacromolecules, 12 2755-2765.
[223] J. Folkman, A. Moscona, Nature, 273 (1978) 345-349.
[224] G.A. Hudalla, J.T. Koepsel, W.L. Murphy, Adv. Mater., 23 5415.